Escola de Camins
Escola Tècnica Superior d'Enginyeria de Camins, Canals i Ports
UPC BARCELONATECH

Numerical analysis on stainless steel diamond bird-beak joints subjected to compressive and tensile forces

Treball realitzat per:

Enric Rovira Canellas

Dirigit per:

Rolando Antonio Chacón Flores

Màster en:

Enginyeria de Camins, Canals i Ports de Barcelona

Barcelona, 11/06/2018

DECA - Departament d'Enginyeria Civil i Ambiental

TREBALL FINAL DE MÀSTER

Preface

I would like to thank my family for all the support they have given to me along the time I have dedicated to this thesis. In addition, I would like to mention both my hometown friends as well as my university friends and collegues for their help and support. To all of them, my sincere gratitude. Finally, I would like to thank Professor Rolando Antonio Chacón Flores for giving me the opportunity to work on this thesis.

This work was developed in the frame of the Project BIA2016-75678-R, AEI/FEDER, UE "*Comportamiento estructural de pórticos de acero inoxidable. Seguridad frente a acciones accidentales de sismo y fuego*", funded from the MINECO (Spain).

"*Numerical analysis on stainless steel diamond bird-beak joints subjected to compressive and tensile forces*" is the result and summary of all my years as a student at UPC and is the last step of this incredible and unforgettable life stage.

Enric Rovira Canellas

Table of Contents

Abstract

The diamond bird-beak is a joint configuration for RHS construction and is achieved by rotating the chord and the brace of a traditional joint through 45º along their longitudinal axes. The main objective of the current thesis is to study diamond bird-beak X-type (DBBX) joints of stainless steel material under compression loading as well as tensile loading by means of a parametric analysis.

Variation of two dimensionless parameters are considered within the parametric study: $\beta = b_1/b_0$ (relation between brace width and chord width) and $2\gamma = b_0/t_0$ (relation between chord width and chord thickness), which leads to a total amount of 32 models i. e. 16 models subjected to compression loading as well as same 16 models subjected to tensile loading.

Results are analysed in terms of design resistance dependance of both parameters i.e. F_u-β and F_u-2γ; as well as load-displacement curves. Comparisons are also made with actual European Normative formulation EN 1993-1-8 [3] as well as J.S. Owen et. al. (2001) formulation achieved in their article [6]. Finally, results of a stainless steel DBB X-type joint obtained in this thesis are compared to results of a carbon steel DBB X-type joint of same geometrical dimensions.

Keywords: rectangular hollow sections, diamond bird-beak joint, stainless steel, tensile loading, compression loading, design resistance, failure mode

List of figures and tables

List of figures

List of tables

List of abbreviations and symbols

In the present thesis, SI-units are used. Unless stated otherwise in the equations, dimensions are given in mm, cross sections in mm^2, section modulus in mm^3, moment of inertia in mm^4 and stresses, strengths and moduli of elasticity in N/mm^2. For the sake of simplicity, loads are given in kN.

Symbol	Description	Units
a	Throat weld thickness	mm
A_0	Cross-sectional area	mm^2
b_0	Width of chord member	mm
b_1	Width of brace member	mm
DBB	Diamond bird-beak joint	-
E	Young's modulus	N/mm^2
f_u	Ultimate tensile strength	N/mm^2
f_y	Yield strength	N/mm^2
G	Shear modulus	N/mm^2
L_0	Length of chord member	mm
t_0	Thickness of chord member	mm
t_1	Thickness of brace member	mm
α	Dimensionless parameter $2L_0/b_0$	-
β	Dimensionless parameter b_1/b_0	-
2γ	Dimensionless parameter b_0/t_0	-
ε_{max}	Maximum elongation	-
ε_u	Fracture elongation	-
ν	Poisson's ratio	-

1. INTRODUCTION

Design is an interactive process between the functional and architectural requirements and the strength and fabrication aspects. Although the manufacturing costs of hollow sections are higher than those for other sections, leading to higher unit material cost, economical applications are achieved in many fields.

One of the constraints initially hampering the application of hollow sections was the design of the joints. However, nowadays design recommendations exist for all basic types of joints, and further research evidence is available for many special types of joints.

Three different designations for structural applications of tubular shaped profiles are circular hollow sections (CHS), rectangular hollow sections (RHS) and square hollow sections (SHS). Hollow sections may be produced either seamless or welded.

In the particular case of this thesis, diamond bird-beak X-type joints are analysed, which are a joint configuration for RHS construction and is achieved by rotating the chord and the brace of a traditional joint through 45º along their longitudinal axes.

1.1 SCOPE OF WORK AND BACKGROUND

Much attention has been focused recently on the relative cost, aesthetic appeal, strength and stiffness of various types of connection used in both open-section and tubular shaped profiles. Rectangular and square hollow sections (RHS and SHS, respectively) represent nowadays a vast source of structural alternatives for several structural purposes.

Bird-beak joint is an innovative type of tubular constructions composed of square hollow sections. The main difference between this type of joint in comparison to the conventional SHS-to-SHS welded joints where the chord walls are parallel or perpendicular to the brace walls is the angles between chord and brace walls of a bird-beak joint are oblique. In fact, diamond bird-beak joint is generated by simply rotating the members of a conventional SHS joint at 45º about their longitudinal axes.

Although the literature background is not as wide as in the case of conventional tubular joints, efforts have been carried out in order to acknowledge performance of beak-bird joints. Thus, several studies and articles have been devoted to the ultimate resistance of carbon steel bird-beak square hollow section X-joints including J.S. Owen et. al. [6] and A. Peña and R. Chacón [7] studying these joints subjected to compressive and tensile forces; and Yu Chen et. al. studying in-plane and out-of-plane bending[8,9]. T-joint configurations under tensile and compressive loading are studied as well in both articles by Yu Chen et. al. [13] and by L. Tong et. al. [10].

Moreover, further literature studies bird-beak SHS joints as T configuration by means of numerical and finite element analysis in order to approach stress concentration factors of these joints such as B. Cheng et. al.[12] and L. Tong et. al. [11].

This thesis is based on European Normatives: EN 1993 Design of steel structures. The most important parts of the normative that are used in this thesis are "EN 1993-1-1: General rules and rules for buildings" [1], "EN 1993-1-4: General rules– Supplementary rules for stainless steel" [2], "EN 1993-1-8: Design of joints" [3] and "EN 1993-1-9: Fatigue" [4].

Among the literature mentioned, "*The influence of member orientation on the resistance of cross joints in square RHS construction*" by J.S. Owen et. al. [6] is of high importance for the current thesis, thus validation of the numerical analysis within ABAQUS will be compared to experimental joint studied in this article. Furthermore, parametric analysis results modelled by finite element method of a stainless steel joint is compared to formulation of design resistances achieved by J.S. Owen as well as EN-1993-1-8 [3] formulation.

Finally, stainless steel results are compared to identical geometrical joints of carbon steel by A. Peña and R. Chacón, which their results are published in the article "*Structural analysis of diamond bird-beak joints subjected to compressive and tensile forces*" [7].

Since most of the existing literature regarding diamond bird-beak joints are focused on structural carbon steel, present thesis is an attempt to approach these joints but considering stainless steel instead, thus slightly differences to mentioned bibliography are expected.

1.2 GENERAL OBJECTIVES

The main objective of the present thesis is to analyse a stainless steel diamond bird-beak joint in X configuration by means of the finite element method using ABAQUS software.

The analysis will be carried out as a parametric study, where variation of dimensionless geometric parameters $\beta = b_1/b_0$ (relation between brace width and chord width) and $2\gamma = b_0/t_0$ (relation between chord width and chord thickness) will be of high importance. Thus, a total amount of 16 models will be modelled and studied in order to analyse variations in terms of ultimate design resistance of the joint. Those

16 models will be studied under tensile loading as well as compression loading, therefore a total amount of 32 models are analysed.

1.3 SPECIFIC OBJECTIVES OF THE PRESENT THESIS

Specific objectives of the current thesis are listed below:

- Study of stainless steel diamond bird-beak X-type joints subjected to compressive loading by means of a parametric study that consists of a variation of dimensionless parameters β and 2γ. Results of desin resistances will be compared to EN 1993-1-8 [3] and J.S. Owen formulations [6] and widely discussed.

- Study of stainless steel diamond bird-beak X-type joints subjected to tensile loading by means of a parametric study conducted by a variation of the same parameters β and 2γ. As in the compressive loading case, design resistances results will be compared with mentioned bibliography and widely discussed.

- Load-displacement curves for both tensile and compression results are analysed for all 32 models in order to explain and discuss failures modes dependance on geometrical characteristics.

- Comparison of the obtained results in terms of load-displacement curves to similar models studied in carbon steel by A. Peña and R. Chacón [7]. It is expected to achieve higher ultimate resistances in stainless steel models due to their higher ductility.

Since this thesis is a study of a stainless steel joint, results may not be as close as expected to J.S. Owen results. Furthermore, European Normative formulation is set for a traditional RHS joint, thus diamond bird-beak configuration might lead to slightly differences as well. However, it is expected to find realistic and consistent results and a similar performance of the stainless steel joint in comparison to conventional structural steel joint results, but with higher ultimate resistance.

2. STATE OF THE ART

This thesis is based on two main topics: stainless steel and diamond bird-beak joints. On the one hand, stainless steel is excellent due to its high ductility properties and, on the other hand, diamond bird-beak joints have better resistance properties than the traditional rectangular and square hollow sections (i.e. RHS and SHS, respectively)

Rectangular and square hollow sections represent nowadays a vast source of structural alternatives due to their wide advantages against traditional open profiles. Specifically, diamond bird-beak RHS X-joints are deemed as being a type of welded X-joint between steel rectangular hollow sections in which both the chord as well as the brace are rotated 45º around their longitudinal axes, as it is represented in *Figure 1*. The most relevant structural advantages are clear for elements under torsion as well as buckling due to compression. However, RHS and SHS profiles are not considered the best option to resist flexural behaviour.

The applications of structural hollow sections nearly cover all fields. Hollow sections may be used because of the beauty of their shape or to express lightness, while in other cases their geometrical properties determine their application. For instance, in buildings and halls, hollow sections are mainly used for column and lattice girders or space frames for roofs. Several applications may be considered as well for bridges construction. Also, there are a few aspects which make hollow sections increasingly suitable for hydraulic structures, such as barriers.

Combination of both stainless steel and diamond bird-beak joints shall result in a join with good performance under axial loading. This paragraph will focus on the main characteristics of both main topics of this thesis i.e. stainless steel and diamond bird-beak configuration joint, and state the most important theoretical aspects in order to be able to analise results in an appropriate and accurate way.

Theoretical aspects of both topics are mainly based on European Normative framework and, in particular, "EN 1993-1-4: General rules–Supplementary rules for stainless steel" [2], which gives a detailed normative on stainless steel, and "EN 1993-1-8: Design of joints" [3], which details normatives and formulations for a vast source of joints. Since this thesis is focused on hollow section joints, paragraph 7 of EN 1993-1-8 is of high importance for this thesis.

Finally, a paragraph of the timeline of articles analysing diamond bird-beak joints is described in order to place the present thesis in the overall history of these types of joints. For the high importance for this thesis, J. S. Owen's article [6] is described and most relevant conclusions are explained in order to set limiting values of dimensionless parameters β and 2γ.

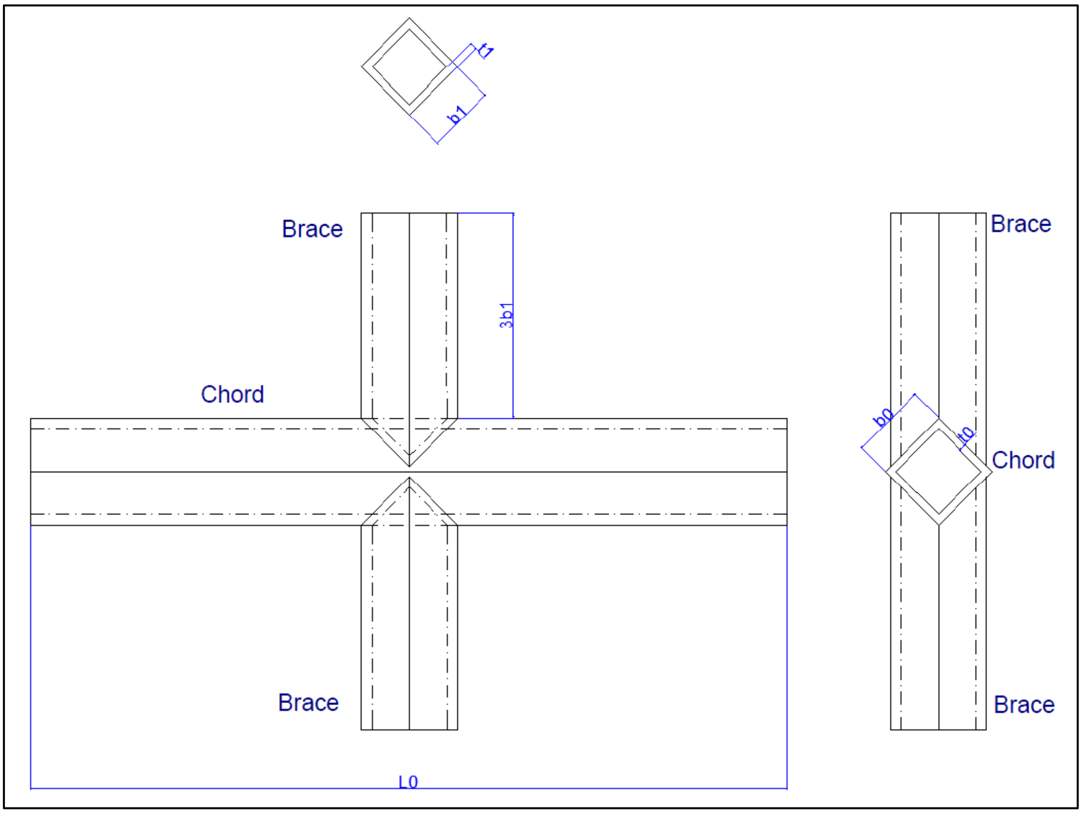

Figure 1 *Diamond bird-beak X-type joint representation*

2.1 CROSS SECTION CLASSIFICATION

Sections are classified depending on their moment-rotation characteristics. The role of cross section classification is to identify the extent to which the resistance and rotation capacity of cross sections is limited by its local buckling resistance.

Four classes of steel cross-sections are defined as follows, according to EN1993-1-1 [1]:

Class 1: Plastic	Class 1 cross-sections are those which can form a plastic hinge with the rotation capacity required from plastic analysis without reduction of the resistance
Class 2: Compact	Class 2 cross-sections are those which can develop their plastic moment resistance, but have limited rotation capacity because of local buckling
Class 3: Semi-compact	Class 3 cross-sections are those in which the stress in the extreme compression fibre of the steel member assuming an elastic distribution of stresses can reach the yield strength, but local buckling is liable to prevent development of the plastic moment resistance
Class 4: Slender	Class 4 cross-sections are those in which local buckling will occur before the attainment of yield stress in one or more parts of the cross-section

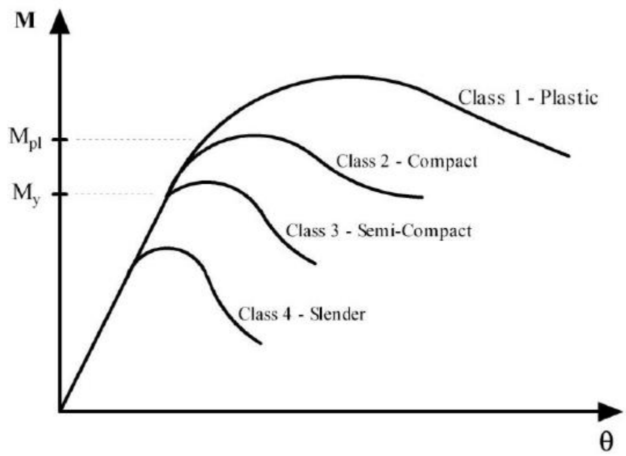

Figure 2 *Theoretical moment-curvature curves for different classes of steel cross-sections*[1]

1 Font: https://www.researchgate.net/figure/Cross-section-classification-according-to-Eurocode-3_fig3_265167619

The classification of a cross-section depends on the width to thickness ratio of parts subject to compression. It should be noted that Class 4 joints would not be realistic, so yield strength would not be reached and therefore limiting the elastic capacity of the joint. Moment-rotation characteristics are displayed in *Figure 2*. In the particular case of tubular cross-sections, *Table 1* will be used in order to classify stainless steel cross-sections in each case.

Therefore, first steps and calculations of the current thesis will be focused to determine which class is considered to be each model taking into account *Table 1* formulation according to EN 1993-1-8.

Tubular sections

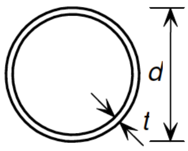

Class	Section in bending Up to 240 CHS	Section in compression
1	$d/t \leq 50\varepsilon^2$	$d/t \leq 50\varepsilon^2$
2	$d/t \leq 70\varepsilon^2$	$d/t \leq 70\varepsilon^2$
3	$d/t \leq 280\varepsilon^2$ **NOTE:** For $d > 240$ mm and $d/t > 280\varepsilon^2$ see EN 1993-1-6.	$d/t \leq 90\varepsilon^2$ **NOTE:** For $d/t > 90\varepsilon^2$ see EN 1993-1-6.

$\varepsilon = \left[\frac{235}{f_y}\frac{E}{210\,000}\right]^{0,5}$	Grade	1.4301	1.4401	1.4462
	f_y (N/mm^2)	210	220	460
	ε	1,03	1,01	0,698

Table 1 *Maximum width-to-thickness ratios for compression parts for stainless steel (EN 1993-1-4 Table 5.2 [2])*

2.2 INTRODUCTION TO STAINLESS STEEL

Stainless steel was invented by Harry Brearley at the beginning of 20th century. It is a steel alloy with a minimum of 10.5% chromium content by mass. Some stainless steel types contain other elements, which nickel is the most common among them. It is notable for its corrosion resistance, which increases with increasing chromium content, and it does not readily corrode, rust or stain with water as ordinary steel does. Those properties make it an ideal material for many applications where both strength of steel and corrosion resistance is required.

However, it is not fully stain-proof in low-oxigen, high-salinity or poor air-circulation environments. Basically, quemical composition of stainless steel differs from carbon steel by the amount of chromium present. There are various grades and surface finishes of stainless steel to suit the environment the alloy must resist. Thus, there are over 150 grades of stainless steel of which 15 are most commonly used.

Furthermore, stainless steel are classified into four main families: ferritic, austenitic, martensitic and duplex. Among them, austenitic and duplex stainless steel are the most commonly used in structural design.

Ferritic stainless steel	Only chromium is present. They have a ferrite microstructure and are magnetic, similar to carbon steel.
Austenitic stainless steel	The largest family of stainless steels. They possess an austenitic microstructure, which is achieved by alloying with sufficient nickel, which allows the austenite structure of iron to be stabilized. This crystal structure makes such steels virtually non-magnetic and less brittle at low temperatures
Martensitic stainless steel	More carbon is added in order to achieve greater hardness and strength. They are hardened by heat treatment.
Duplex stainless steel	Also called ausenitic-ferritic stainless steel due to their mixed microstructure of austenite and ferrite. It provides improved resistance to chloride stress corrosion cracking in comparison to austenitic stainless steels

Stress-strain behaviour is also slightly different between carbon steel and stainless steel. The most important difference is visible in stress-strain curve, theoretically displayed in *Figure 3*. On the one hand, carbon steel has a linear behaviour until yiled stress is achieved followed by an almost constant and planar line before strain hardening occurs. On the other hand, stainless steel has a more rounded curve and yield stress is not well-defined. Furthermore, it shall be noted that stainless steel can absorb considerable impacts before fracture occurs thanks to excellent ductility, specially austenitic stainless steel, and its hardening properties by deformation.

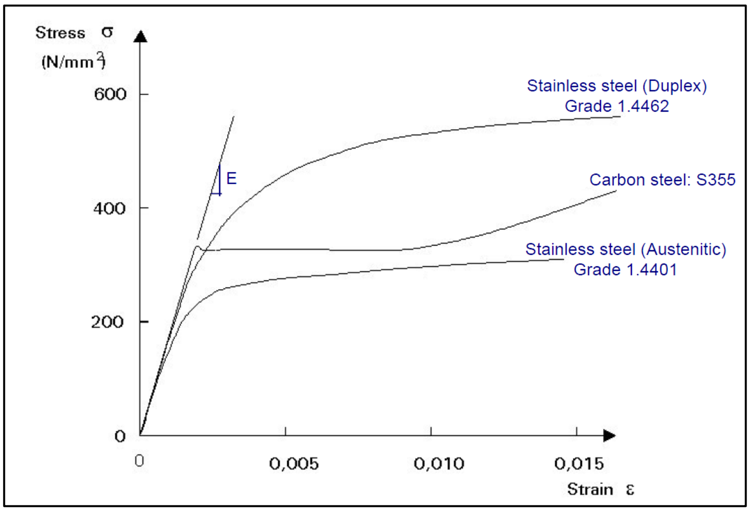

Figure 3 *Theoretical constitutive equations of carbon steel and stainless steel*

2.3 MATERIAL PROPERTIES

2.3.1 Mechanical properties of stainless steel

The most important mechanical properties for steel material, and in particular for stainless steel, are shown in the stress-strain curve.

Theoretical stress-strain curve for stainless steel material is displayed in *Figure 4*. It is visible that, in the case of stainless steel, yield stress is not achieved within the elastic phase.

- **σ_u** Ultimate tensile strength (f_u)
- **$\sigma_{0.2}$** Yield strength (f_y)
- **E** Young's modulus
- **ε_f** maximum elongation
- **ε_u** fracture elongation

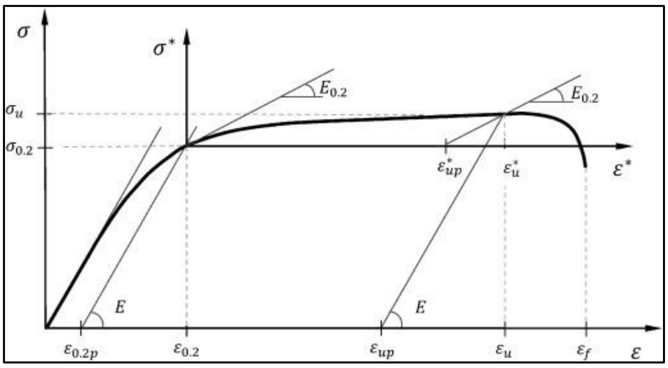

Figure 4 *Theoretical stress-strain curve for structural stainless steel*[2]

[2] Font: I. ARRAYAGO, E. REAL, L. GARDENER. "*Description of stress-strain curves for stainless steel alloys*" [17]

Table 2 shows nominal values of the yield strength f_y and the ultimate tensile strength f_u for structural stainless steels according to EN 1993-1-4 [2].

Following values of the material coefficients may be assumed for the global analysis and in determining the resistance of members and cross-sections:

- Modulus of elasticity E:

$E = 200000\ N/mm^2$	For the austenitic and austenitic-ferritic grades in *Table 2* excluding grades 1.4539, 1.4529 and 1.4547
$E = 195000\ N/mm^2$	For the austenitic grades 1.4539, 1.4529 and 1.4547
$E = 220000\ N/mm^2$	For the ferritic grades in Table 2

- Shear modulus G, where:

$$G = \frac{E}{2(1+\nu)} \qquad \textbf{\textit{Eq. 1}}$$

- Poisson's ratio in elastic stage, ν=0.3.

Type of stainless steel	Grade	Product form							
		Cold rolled strip		Hot rolled strip		Hot rolled plate		Bars, rods and sections	
		Nominal thickness t							
		$t \leq 6$ mm		$t \leq 12$ mm		$t \leq 75$ mm		$t \leq 250$ mm	
		f_y N/mm²	f_u N/mm²	f_y N/mm²	f_u N/mm²	f_y N/mm²	f_u N/mm²	f_y N/mm²	f_u N/mm²
Ferritic steels	1.4003	280	450	280	450	250[3]	450[3]	260[4]	450[4]
	1.4016	260	450	240	450	240[3]	430[3]	240[4]	400[4]
	1.4512	210	380	210	380	-	-	-	-
Austenitic steels	1.4306	220	520	200	520	200	500	180	460
	1.4307							175	450
	1.4541							190	500
	1.4301	230	540	210	520	210	520		
	1.4401	240	530	220	530	220	520	200	500
	1.4404								
	1.4539							230	530
	1.4571		540		540			200	500
	1.4432	240	550	220	550	220	520		
	1.4435								
	1.4311	290	550	270	550	270	550	270	550
	1.4406	300	580	280	580	280	580	280	580
	1.4439	290		270		270			
	1.4529	300	650	300	650	300	650		
	1.4547	320	650	300	650	300	650	300	650
	1.4318	350	650	330	650	330	630	-	-
Austenitic -ferritic steels	1.4362	420	600	400	600	400	630	400[2]	600[2]
	1.4462	480	660	460	660	460	640	450	650

1) The nominal values of f_y and f_u given in this table may be used in design without taking special account of anisotropy or strain hardening effects.
2) $t \leq 160$ mm
3) $t \leq 25$ mm
4) $t \leq 100$ mm

Table 2 *Nominal values of the yield strength fy and the ultimate tensile strength f_u for structural stainless steels (EN 1993-1-4 Table 2.1 [2])*

2.3.2 Fracture toughness

The austenitic and austenitic-ferritic stainless steels in *Table 2* may be assumed to be adequately tough and not susceptible to brittle fracture for service temperatures down to -40º.

2.3.3 Ductility

Ductility is a measure of material's ability to undergo significant plastic deformation before rupture, which may be expressed as percent elongation from a tensile test.

In the particular case of steel, minimum ductility is required that should be expressed in terms of limits for:

- Ratio f_u/f_y
- The elongation at failure on a gauge length of 5.65 $\sqrt{A_0}$ (where A_0 is the original cross-sectional area)
- Ultimate strain

According to EN 1993-1-1 [1], following limiting values are recommended:

$f_u/f_y \geq 1.10$	$\varepsilon_u \geq 0.15$	$\varepsilon_u \geq 15\varepsilon_y$

In accordance to EN 1993-1-4 [2], the ductility requirements also apply to stainless steel. Steels conforming with one of the steel grades listed in *Table 2* should be accepted as satisfying these requirements.

2.3.4 Durability

Durability is the ability of a product to perform its required function over a lengthy period under normal conditions of use without excessive expenditure or maintenance.

Durability for carbon steel is widely explained in EN 1993-1-1 [1], so current paragraph will focus in the main differences between using stainless steels and using carbon steels.

The principal difference between these types of steel is that for carbon steels, protection from environmental effects, and hence life expectancy, can be dealt separately from structural design. On the other hand, for stainless steel, life expectancy is not determined by subsequent protective treatments, but by the initial selection of materials, the design process and the fabrication procedures, and by their suitability for the environmental conditions.

Stainless steels are generally very resistant to corrosion and they will perform satisfactorily in most environments. The limit of corrosion resistance for a given stainless steel depends on its alloying elements, which means that each grade has a slightly different response when exposed to a corrosive environment.

2.3.5 Fatigue

Structural members shall be designed for fatigue such that there is an acceptable level of probability that their performance will be satisfactory throughout their design life. Fatigue assessments should be undertaken using either damage tolerant method or safe life method.

On the one hand, the damage tolerant method should provide an acceptable reliability that a structure will perform satisfactorily for its design life, provided that a prescribed inspection and maintenance regime for detecting and correcting fatigue damage is implemented throughout the design life of the structure.

On the other hand, the safe life method should provide an acceptable level of reliability that a structure will perform satisfactorily for its design life without the need for regular in-service inspection for fatigue damage.

The assessment methods given in EN 1993-1-9 [4] are applicable to all grades of structural steels and stainless steels.

2.3.6 Properties of the materials for the present thesis

Stainless steel used in the current thesis is an austenitic elasto-plastic material with the stress-strain curve displayed in *Figure 5* obtained by means of the CodeSkulptor web site (www.codeskulptor.org). Refer to "*Appendix F. STAINLESS STEEL CODE*" to check the overall code for stainless steel.

$$E = 200000\ N/mm^2$$

$$\upsilon = 0.3$$

$$\gamma = 78.5\ kN/m^3$$

$$f_y = 280\ N/mm^2$$

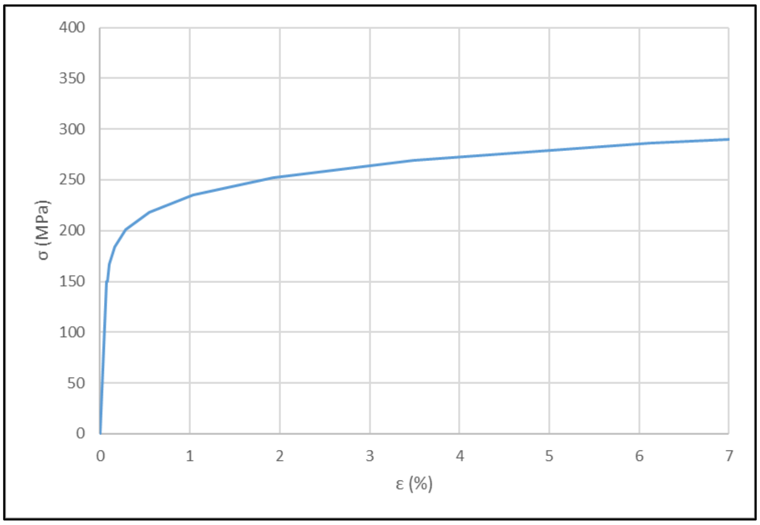

Figure 5 *Austenitic stainless steel stress-strain curve*

2.4 JOINTS AND STRUCTURAL ELEMENTS

2.4.1 Basis of design

All joints shall have a design resistance such that the structure is capable of satisfying all the basic design requirements (EN 1993-1-1 [1] and EN 1993-1-8 [3]).

The partial safety factors γ_M for joints are given EN 1993-1-8 [3] and listed in *Table 3*:

Resistance of members and cross-sections	γ_{M0} , γ_{M1} and γ_{M2} see EN 1993-1-1
Resistance of bolts	γ_{M2}
Resistance of rivets	
Resistance of pins	
Resistance of welds	
Resistance of plates in bearing	
Slip resistance - at ultimate limit state (Category C) - at serviceability limit state (Category B)	 γ_{M3} $\gamma_{M3,ser}$
Bearing resistance of an injection bolt	γ_{M4}
Resistance of joints in hollow section lattice girder	γ_{M5}
Resistance of pins at serviceability limit state	$\gamma_{M6,ser}$
Preload of high strength bolts	γ_{M7}
Resistance of concrete	γ_c see EN 1992

Table 3 *Partial safety factors for joints (EN 1993-1-8 Table 2.1 [3])*

Recommended values given in EN 1993-1-1 [1] are as follows:

$$\gamma_{M0} = 1.0$$

$$\gamma_{M1} = 1.0$$

$$\gamma_{M2} = 1.25$$

Recommended values given in EN 1993-1-8 [3] for joints are as follows:

$$\gamma_{M3} = 1.25 \qquad \gamma_{M5} = 1.0$$

$$\gamma_{M3,ser} = 1.1 \qquad \gamma_{M6,ser} = 1.0$$

$$\gamma_{M4} = 1.0 \qquad \gamma_{M7} = 1.1$$

2.4.2 Introduction to joints and structural elements

Every joint should be designed in order to resist forecasted loads; level of safety should be adequate; have a good behaviour in terms of serviceability and ultimate states, and should be ease and safety in terms of fabrication and execution.

Several joints as a whole set should be considered as a structural truss. Trusses may be either planar (axes of the joints are within the same geometrical plan) or spatial (axes of the joints are not within the same geometrical plan). The main elements of a structural truss are:

Chord	It is the main beam of the truss, which has continuity along the joint into consideration.
Diagonal	Secondary element, which starts and/or ends at the joint node and has an angle with the chord member different to 90º.
Brace	Secondary beam, which starts and/or ends at the joint node. The main difference with a diagonal member is that it is set at 90º with the chord member.

There are basically two types of joints or connections: bolted joints and welded joints. Since the current thesis is focused on welded joints between RHS brace member and RHS chord member, those will be explained in the following paragraph. Refer to EN 1993-1-8 [3] for further information about bolted joints.

2.4.3 General aspects for welded joints

The explanation of welded joints described in this paragraph apply to weldable structural steels conforming to EN 1993-1-1 [1] and to material thickness of 4 mm and over.

The most common weld types are fillet welds, fillet weld all round, butt welds and flare groove welds. Butt welds may either be full penetration or partial penetration. Also, both fillet welds all round and plug welds may either be in circular holes or in elongated holes.

FILLED WELDS	Filled welds may be used for connecting parts where the fusion faces form an angle between 60º and 120º. Angles smaller than 60º are also permitted, but in such cases the weld should be considered to be a partial penetriation butt weld. Fillet welds finishing at the ends or sides of parts should be returned coninuously, full size, around the corner for a distance of at least twice the leg length of the weld.
FILLET WELDS ALL ROUND	Fillet welds all round, comprising fillet welds in circular or elongated holes, may be used only to transmit shear or to prevent the buckling or separation of lapped parts.
BUTT WELDS	Butt welds can be either full penetration or partial penetration welds. On the one hand, a full penetration butt weld is defined as a weld that has complete penetration and fusion of weld and parent metal throughout the thickness of the joint. On the other hand, a partial penetration butt weld is defined as a weld that has joint penetration which is less than the full thickness of the parent material.
PLUG WELDS	Plug welds may be used to transmit shear, to prevent the buckling or separation of lapped parts and to inter-connect the components of built-up members. However, they should not be used to resist externally applied tension.
FLARE GROOVE WELDS	This type is used for hollow section joints and will be explained in the hollow section paragraph "*2.5 HOLLOW SECTION JOINTS*", thus they are used in this thesis for DBB X-type joints.

2.5 HOLLOW SECTION JOINTS

2.5.1 Scope and field of application of hollow section joints

Several assumptions should be taken into account in order to analyse hollow section joints within the European Normative framework. The most important and relevant assumptions are listed below. Each assumption is taken into account in the present thesis.

- For hot finished hollow sections and cold-formed hollow sections, the nominal yield strength of the final product should not exceed 460 N/mm^2. For products with a nominal yield strength higher than 355 N/mm^2, the static design resistances should be reduced by a factor of 0.9. Since this thesis analyses a stainless steel with a yield stress of 280 N/mm^2, this assumption is achieved.
- The nominal wall thickness of hollow sections should not be less than 2.5 mm. For this thesis, minimum nominal wall thickness of any element is 5 mm.
- The nominal wall thickness of a hollow section chord should not be greater than 25 mm unless special measures have been taken to ensure that the through thickness properties of the material will be adequate. For this thesis, maximum nominal wall thickness of the chord is 15 mm.
- The compression elements of the members should satisfy the requirements for Class 1 or Class 2 for the condition of pure bending. As it is stated in paragraph "*3.4.3 Classification of cross-sections*", all models of the current thesis are Class 1.

2.5.2 Truss and joint configurations

Various types of trusses are used in practice. Trusses made of hollow sections should be designed in such a way that the number of joints and, thus, fabrication is minimised. Depending on the type of truss, various types of joints are used i.e. X, T, Y, N, K or KT.

The types of joints in hollow section joints are shown in *Figure 6*.

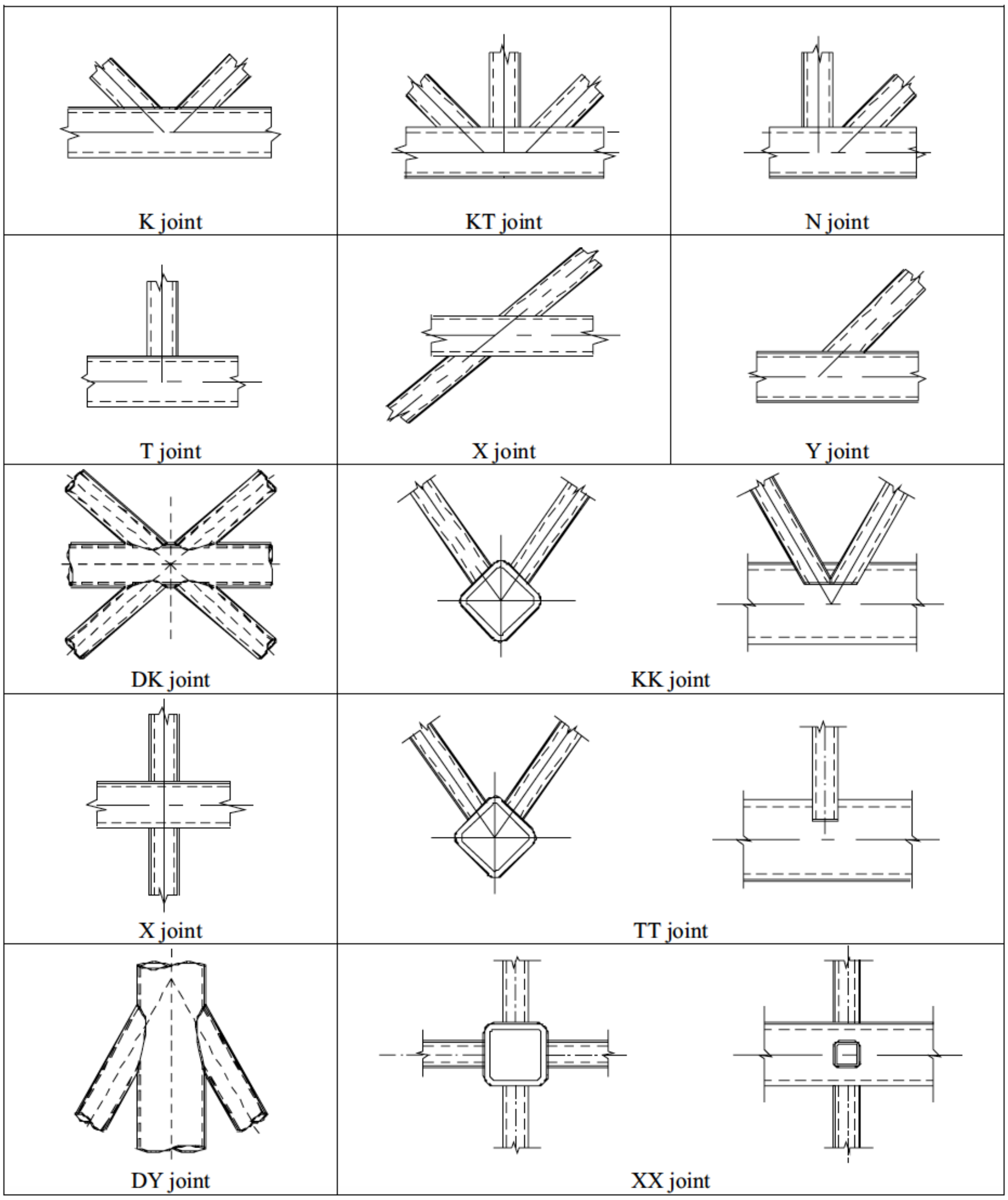

Figure 6 *Types of joints in hollow section lattice girders (EN 1993-1-8 Figure 7.1 [3])*

Dimensions of a hollow section joint with sigle brace member are displayed in *Figure 7*. For the current thesis, a diamond bird-beak X (DBBX) joint will be analysed, which is a type of welded X-joints between SHS in which both the chord as well as the brace are rotated 45º around their longitudinal axes. Furthermore, θ angle between brace and chord is 90º.

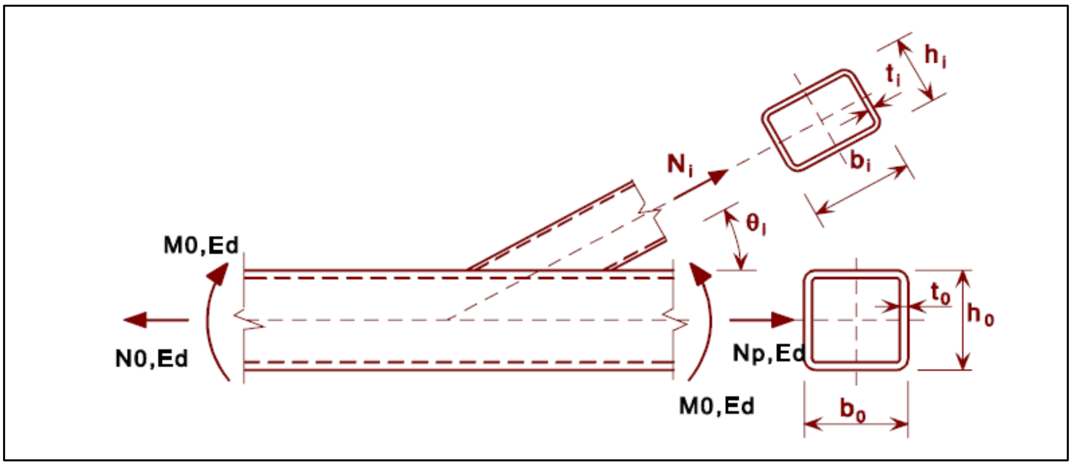

Figure 7 *Dimensions and other parameters at aa hollow section lattice girder joint (EN 1993-1-8 Figure 1.4 [3])*

2.5.3 Mechanical properties of hollow sections

Hollow sections are made of similar steel as used for other steel sections, thus there is no difference when considering mechanical properties. Current thesis will take into account mechanical properties of stainless steel mentioned in paragraph "*2.3.1 Mechanical properties of stainless steel*".

2.5.4 Geometric properties of hollow sections

Geometric properties may be considered taking into account load conditions acting in the hollow section. For instance, geometric properties may be different for members under tensile loading, compression loading, bending, shear, internal pressure and/or a combination of previous loadings.

Since current thesis will be focused on the results of a diamond bird-beak X-type joint under tension loading as well as compression, those will be explained afterwards.

TENSION

The design capacity $N_{t,Rd}$ of a member under tensile loading depends on the cross sectional area and the design yield strength, and is independent of the sectional shape. Thus, there is no advantage nor disadvantage in using hollow sections from the point of view of the amount of material requiered. The design capacity is given by:

$$N_{t,Rd} = A \cdot f_{yd} \quad \textbf{Eq. 2}$$

In the case of a cross sections weakened by bolt holes or slots, the net cross sections should be reduced as follows:

$$N_{t,Rd} = \frac{A \cdot f_u}{\gamma_{M2}} \cdot 0.9 \qquad \textbf{\textit{Eq. 3}}$$

COMPRESSION

For centrally loaded members in compression, the critical buckling load depends on the slenderness λ and the section shape. The slenderness λ is given by the ratio of the buckling length and the radius of gyration:

$$\lambda = \frac{l_b}{i} \qquad \textbf{\textit{Eq. 4}}$$

It should be noted that gyration's radius of a hollow section is generally much higher than for the weak axis of an open section. For a given length, this difference results in a lower slenderness for hollow sections and thus a lower mass when compared with open sections.

2.5.5 Failure modes for hollow section joints

On the one hand, behaviour for tubular joints under loading conditions is controlled by geometry of the joint and, on the other hand, by loading structural conditions of the overall structure.

The design joint resistances of connections between hollow sections and of connections between hollow sections and open sections, should be based on the following failure modes as applicable:

Mode (a)	Chord face failure (plastic failure of the chord face) or chord plastification (plastic failure of the chord cross-section)
Mode (b)	Chord side wall failure (or chord web failure) by yielding, crushing or instability (crippling or buckling of the chord side wall or chord web) under the compression brace member
Mode (c)	Chord shear failure
Mode (d)	Punching shear failure of a hollow section chord wall (crack initiation leading to rupture of the brace members from the chord member)
Mode (e)	Brace failure with reduced effective width (cracking in the welds or in the brace members)
Mode (f)	Local buckling failure of a brace member or of a hollow section chord member at the joint location

Figure 8 shows failure modes for RHS joints. Although the resistance of a joint with properly formed welds is generally higher under tension than under compression, the

design resistance of a joint is generally based on the resistance of the brace in compression to avoid the possible excessive local deformation or reduced rotation capacity or deformation capacity with which might otherwise occur.

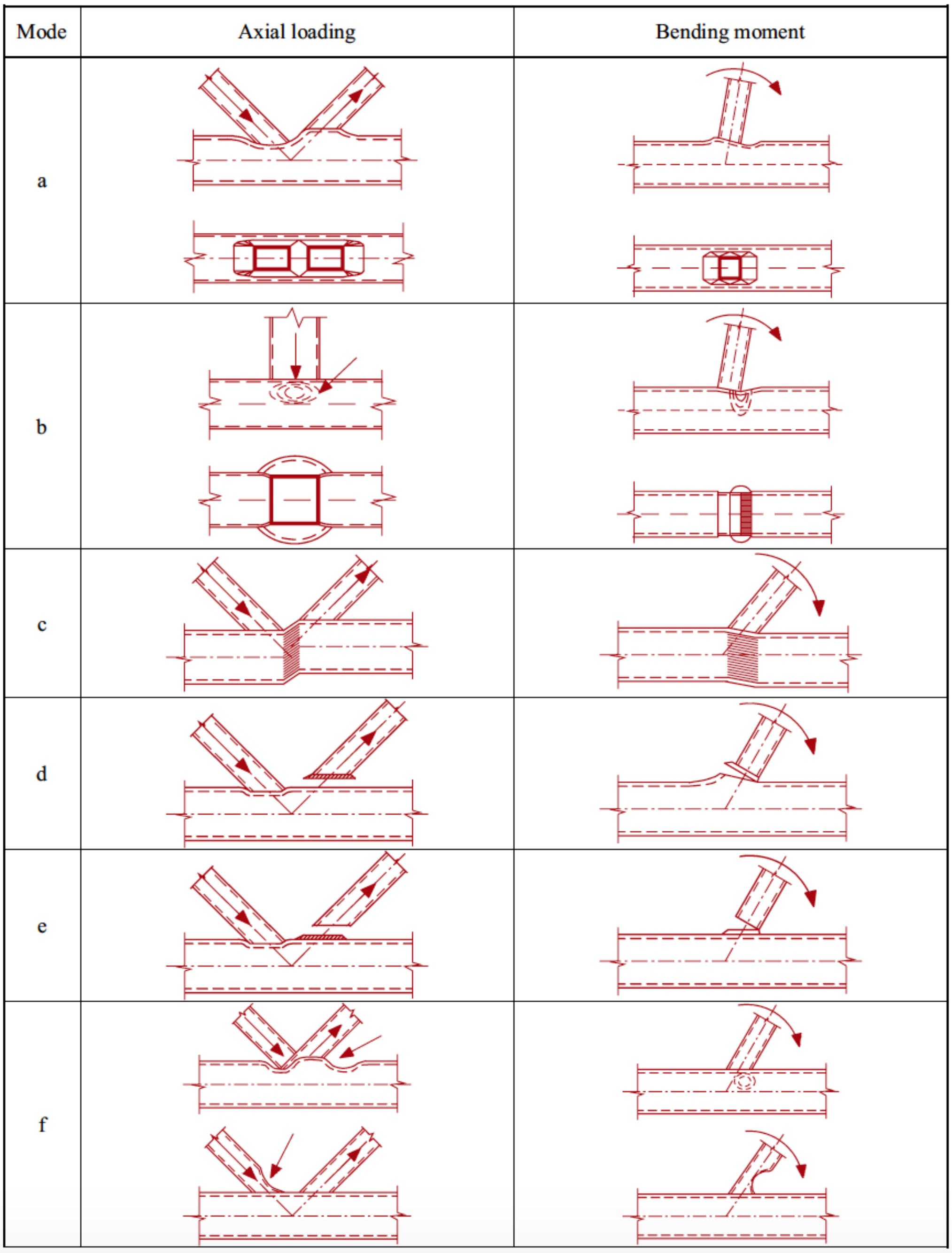

Figure 8 *Failure modes for joints between RHS brace members and RHS chord members (EN 1993-1-8 Figure 7.3 [3])*

2.5.6 Welded joints for hollow section joints

The welds connecting the brace members to the chords shall be designed to have sufficient resistance to allow for non-uniform stress-distributions and sufficient deformation capacity to allow for redistribution of bending moments.

In welded joints, the connection should normally be formed around the entire perimeter of the hollow section by means of a butt weld, a fillet weld, or a combination of the two.

The design resistance of the weld, per unit length of perimeter of a brace member, should not normally be less than the design resistance of the cross-section of that member per unit length of perimeter.

For rectangular structural hollow sections, as they are those used in the current thesis, the design throat thickness of flare groove welds is defined according to *Figure 9*:

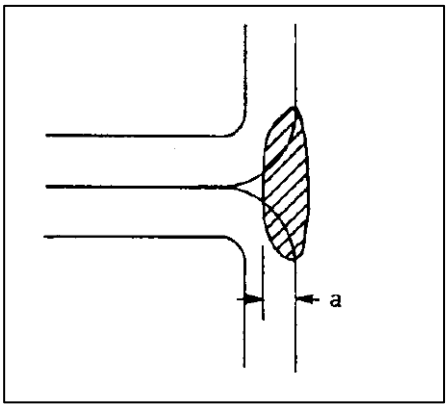

Figure 9 *Design throat thickness of flare groove welds in rectangular structural hollow sections (EN 1993-1-8 Fig 7.5 [3])*

To avoid weld failure it is recommended to design the welds to be stronger than the connected brace members.

This thesis will take into consideration that fillet weld connection is stronger enough to avoid weld failure among the joint. Thus, weld will not be modelled within ABAQUS.

2.5.7 Range of validity of joints

The range of validity for the geometry of the joints is given in the table below. On the one hand, for joints within the range of validity, only the design criteria covered in this table need to be considered and the design resistance of a connection should be taken as the minimum value for all applicable criteria. On the other hand, for joints outside the range of validity, all the criteria for uniplanar joints should be considered. In addition, the secondary moments in the joints caused by their rotational stiffness should be taken into account.

<table>
<tr><th rowspan="3">Type of joint</th><th colspan="6">Joint parameters [i = 1 or 2, j = overlapped brace]</th></tr>
<tr><th rowspan="2">b_i/b_0
or
d_i/b_0</th><th colspan="2">b_i/t_i and h_i/t_i or d_i/t_i</th><th rowspan="2">h_0/b_0
and
h_i/b_i</th><th rowspan="2">b_0/t_0
and
h_0/t_0</th><th rowspan="2">Gap or overlap

b_i/b_j</th></tr>
<tr><th>Compression</th><th>Tension</th></tr>
<tr><td>T, Y or X</td><td>$b_i/b_0 \geq 0,25$</td><td rowspan="2">$b_i/t_i \leq 35$
and
$h_i/t_i \leq 35$
and
Class 2</td><td rowspan="3">b_i/t_i
≤ 35
and
h_i/t_i
≤ 35</td><td rowspan="3">$\geq 0,5$
but
$\leq 2,0$</td><td>≤ 35
and
Class 2</td><td>–</td></tr>
<tr><td>K gap
N gap</td><td>$b_i/b_0 \geq 0,35$
and
$\geq 0,1 + 0,01\, b_0/t_0$</td><td>$\leq 35$
and
Class 2</td><td>$g/b_0 \geq 0,5(1-\beta)$
but $\leq 1,5(1-\beta)$ 1)
and as a minimum
$g \geq t_1 + t_2$</td></tr>
<tr><td>K overlap
N overlap</td><td>$b_i/b_0 \geq 0,25$</td><td>Class 1</td><td>Class 2</td><td>$\lambda_{ov} \geq 25\%$
but $\lambda_{ov} \leq 100\%$ 2)
and $b_i/b_j \geq 0,75$</td></tr>
<tr><td>Circular brace member</td><td>$d_i/b_0 \geq 0,4$
but $\leq 0,8$</td><td>Class 1</td><td>d_i/t_i
≤ 50</td><td colspan="3">As above but with d_i replacing b_i and d_j replacing b_j.</td></tr>
<tr><td colspan="7">1) If $g/b_0 > 1,5(1-\beta)$ and $g/b_0 > t_1 + t_2$ treat the joint as two separate T or Y joints.
2) The overlap may be increased to enable the toe of the overlapped brace to be welded to the chord.</td></tr>
</table>

Table 4 *Range of validity for welded joints between RHS brace members and RHS chord members (EN 1993-1-8 Table 7.8 [3])*

<table>
<tr><th>Type of brace</th><th>Type of joint</th><th colspan="2">Joint parameters</th></tr>
<tr><td rowspan="2">Square hollow section</td><td>T, Y or X</td><td>$b_i/b_0 \leq 0,85$</td><td>$b_0/t_0 \geq 10$</td></tr>
<tr><td>K gap or N gap</td><td>$0,6 \leq \dfrac{b_1 + b_2}{2b_1} \leq 1,3$</td><td>$b_0/t_0 \geq 15$</td></tr>
<tr><td rowspan="2">Circular hollow section</td><td>T, Y or X</td><td></td><td>$b_0/t_0 \geq 10$</td></tr>
<tr><td>K gap or N gap</td><td>$0,6 \leq \dfrac{d_1 + d_2}{2d_1} \leq 1,3$</td><td>$b_0/t_0 \geq 15$</td></tr>
</table>

Table 5 *Additional conditions for welded joints between RHS brace members and RHS chord members (EN 1993-1-8 Table 7.9 [3])*

2.5.8 Design resistances

Considering uniplanar joints between RHS brace members and RHS chords, two different types of joints may be considered: unreinforced joints and reinforced joints. Design axial resistances of welded T, X and Y joints between RHS braces and RHS chords as well as design resistance moments of welded joints between RHS brace members and RHS chords accordinng to EN 1993-1-8 [3] are displayed in *Table 6* and *Table 7,* respectively. Note that current thesis will only be focused on the unreinforced joints.

Brace member connections subjected to combined bending and axial force should satisfy the following requirement:

$$\frac{N_{i,Ed}}{N_{i,Rd}} + \frac{M_{ip,i,Ed}}{M_{ip,i,Rd}} + \frac{M_{op,i,Ed}}{M_{op,i,Rd}} \leq 1 \qquad \textbf{\textit{Eq. 5}}$$

Where:

$M_{ip,i,Rd}$ is the design in-plane moment resistance
$M_{ip,i,Ed}$ is the design in plane internal moment
$M_{op,i,Rd}$ is the design out-of-plane moment resistance
$M_{op,i,Ed}$ is the design out-of-plane internal moment

Since analysis of the models of this thesis is only for joints subjected to axial loads, desgn resistance moments in *Table 7* are not taken into account.

<table>
<tr><th>Type of joint</th><th colspan="2">Design resistance [$i = 1$]</th></tr>
<tr><td rowspan="8">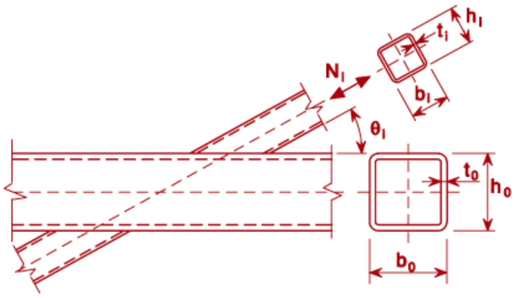
</td><td>Chord face failure</td><td>$\beta \leq 0{,}85$</td></tr>
<tr><td colspan="2">$N_{i,Rd} = \dfrac{k_n f_{y0} t_0^2}{(1-\beta)\sin\theta_1}\left(\dfrac{2\eta}{\sin\theta_1} + 4\sqrt{1-\beta}\right) / \gamma_{M5}$</td></tr>
<tr><td>Chord side wall buckling [1)]</td><td>$\beta = 1{,}0$ [2)]</td></tr>
<tr><td colspan="2">$N_{i,Rd} = \dfrac{f_b t_0}{\sin\theta_i}\left(\dfrac{2h_i}{\sin\theta_1} + 10t_0\right) / \gamma_{M5}$</td></tr>
<tr><td>Brace failure</td><td>$\beta \geq 0{,}85$</td></tr>
<tr><td colspan="2">$N_{i,Rd} = f_{yi} t_i (2h_i - 4t_i + 2b_{eff}) / \gamma_{M5}$</td></tr>
<tr><td>Punching shear</td><td>$0{,}85 \leq \beta \leq (1 - 1/\gamma)$</td></tr>
<tr><td colspan="2">$N_{i,Rd} = \dfrac{f_{y0} t_0}{\sqrt{3}\sin\theta_1}\left(\dfrac{2h_i}{\sin\theta_1} + 2b_{e,p}\right) / \gamma_{M5}$</td></tr>
<tr><td colspan="3">1) For X joints with $\theta < 90°$ use the smaller of this value and the design shear resistance of the chord side walls given for K and N gap joints in Table 7.12.
2) For $0{,}85 \leq \beta \leq 1{,}0$ use linear interpolation between the value for chord face failure at $\beta = 0{,}85$ and the governing value for chord side wall failure at $\beta = 1{,}0$ (side wall buckling or chord shear).</td></tr>
<tr><td colspan="3">For circular braces, multiply the above resistances by $\pi/4$, replace b_1 and h_1 by d_1 and replace b_2 and h_2 by d_2.</td></tr>
<tr><td rowspan="3">For tension:
$f_b = f_{y0}$

For compression:
$f_b = \chi f_{y0}$ (T and Y joints)
$f_b = 0{,}8\, \chi f_{y0} \sin\theta_i$ (X joints)

where χ is the reduction factor for flexural buckling obtained from EN 1993-1-1 using the relevant buckling curve and a normalized slenderness $\bar{\lambda}$ determined from:
$\bar{\lambda} = 3{,}46 \dfrac{\left(\dfrac{h_0}{t_0} - 2\right)\sqrt{\dfrac{1}{\sin\theta_i}}}{\pi\sqrt{\dfrac{E}{f_{y0}}}}$</td><td colspan="2">$b_{eff} = \dfrac{10}{b_0/t_0}\dfrac{f_{y0} t_0}{f_{yi} t_i} b_i$ but $b_{eff} \leq b_i$</td></tr>
<tr><td colspan="2">$b_{e,p} = \dfrac{10}{b_0 t_0} b_i$ but $b_{e,p} \leq b_i$</td></tr>
<tr><td colspan="2">For $n > 0$ (compression): $k_n = 1{,}3 - \dfrac{0{,}4n}{\beta}$ but $k_n \leq 1{,}0$
For $n \leq 0$ (tension): $k_n = 1{,}0$</td></tr>
</table>

Table 6 *Design axial resistances of welded T, X and Y joints between RHS braces and RHS chords (EN 1993-1-8 Table 7.11 [3])*

T and X joints	Design resistance
In-plane moments ($\theta = 90°$)	Chord face failure $\beta \le 0,85$
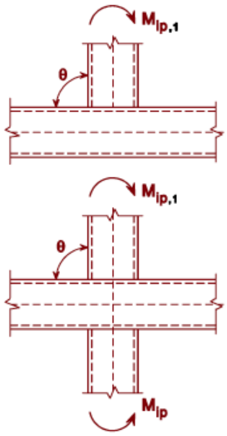	$M_{ip,1,Rd} = k_n f_{y0} t_0^2 h_1 \left(\frac{1}{2\eta} + \frac{2}{\sqrt{1-\beta}} + \frac{\eta}{1-\beta} \right) / \gamma_{M5}$
	Chord side wall crushing $0,85 \le \beta \le 1,0$
	$M_{ip,1,Rd} = 0,5 f_{yk} t_0 (h_1 + 5t_0)^2 / \gamma_{M5}$ $f_{yk} = f_{y0}$ for T joints $f_{yk} = 0,8 f_{y0}$ for X joints
	Brace failure $0,85 \le \beta \le 1,0$
	$M_{ip,1,Rd} = f_{y1} \left(W_{pl,1} - (1 - b_{eff} / b_1) b_1 h_1 t_1 \right) / \gamma_{M5}$
Out-of-plane moments ($\theta = 90°$)	Chord face failure $\beta \le 0,85$
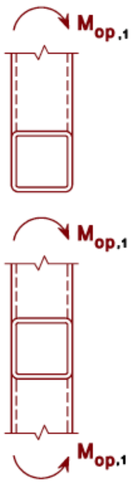	$M_{op,1,Rd} = k_n f_{y0} t_0^2 \left(\frac{h_1 (1+\beta)}{2(1-\beta)} + \sqrt{\frac{2 b_0 b_1 (1+\beta)}{1-\beta}} \right) / \gamma_{M5}$
	Chord side wall crushing $0,85 \le \beta \le 1,0$
	$M_{op,1,Rd} = f_{yk} t_0 (b_0 - t_0)(h_1 + 5t_0) / \gamma_{M5}$ $f_{yk} = f_{y0}$ for T joints $f_{yk} = 0,8 f_{y0}$ for X joints
	Chord distortional failure (T joints only) *)
	$M_{op,1,Rd} = 2 f_{y0} t_0 \left(h_1 t_0 + \sqrt{b_0 h_0 t_0 (b_0 + h_0)} \right) / \gamma_{M5}$
	Brace failure $0,85 \le \beta \le 1,0$
	$M_{op,1,Rd} = f_{y1} \left(W_{pl,1} - 0,5(1 - b_{eff} / b_1)^2 b_1^2 t_1 \right) / \gamma_{M5}$
Parameters b_{eff} and k_n	
$b_{eff} = \frac{10}{b_0 / t_0} \frac{f_{y0} t_0}{f_{y1} t_1} b_1$ but $b_{eff} \le b_1$	For $n > 0$ (compression): $k_n = 1,3 - \frac{0,4n}{\beta}$ but $k_n \le 1,0$ For $n \le 0$ (tension): $k_n = 1,0$
*) This criterion does not apply where chord distortional failure is prevented by other means.	

Table 7 *Design resistance moments of welded joints between RHS brace members and RHS chords (EN 1993-1-8 Table 7.14 [3])*

2.6 DIAMOND BIRD-BEAK JOINT: TIMELINE AND BRIEF HISTORY

This paragraph is focused in placing this thesis within the overall history of studies of diamond bird-beak joints. For instance, diamond bird-beak history is short and not many articles have been carried out to study this particular joint.

In 2001, J.S. Owen et. al. were pioneers on the topic of diamond bird-beak joints with their article titled "*The influence of member orientation on the resistance of cross joints in square RHS construction*" [6]. The main conclusion of their study was achieving an analytical formulation for a diamond bird-beak joint which was really accurate in comparison to normative formulations for a traditional square hollow section joints. Since formulation obtained by J.S. Owen is of high importance fort his thesis, conclusions of their article are explained in "*2.7 DBB JOINT IN LITERATURE: J.S. OWEN'S ANALYTICAL FORMULATION*".

Few years later, in 2007, A. D. Christitsas et. al. conducted a study to analyse conventional and square bird-beak joints subjected to in-plane bending by means of the finite element method. Conclusions were written in an article titled "*FEM analysis of conventional and square bird-beak SHS joint subject to in-plane bending moment—experimental study*" [18].

In 2014, A. PEÑA and R. CHACÓN conducted a parametric analysis varying parameters β and 2γ of a carbon steel diamond bird-beak joint and sumarised their conclusions in an article titled "*Structural analysis of diamond bird-beak joints subjected to compressive and tensile forces*" [7] in order to verify J.S. Owen's formulations.

It was not until 2014 that diamond bird-beak joints were widely studied, specially by chinese researchers. L. TONG, Y. FU, Y. LIU, D. YAN and X. L. ZHAO studied stress concentration factors in their article "Stress concentration factors of diamond bird-beak SHS T-joints under brace loading" [19]. For instance, stress concentration factors were largely studied in several articles in 2015 such as "Finite element analysis and formulae for stress concentration factors of diamond bird-beak SHS T-joints" by L. TONG et. al. [11], "Numerical investigation on stress concentration factors of square bird-beak SHS T-joints subject to axial forces" by B. CHENG et. al. [12], "Stress concentration factors of negative large eccentricity tubular N-joints under axial compressive loading in vertical brace" by J. YANG [15]. In 2018, stress concentration factors are still a subject of discussion in "*SCF of bird-beak SHS X-joints under asymmetrical brace axial forces*" by B. CHENG [20].

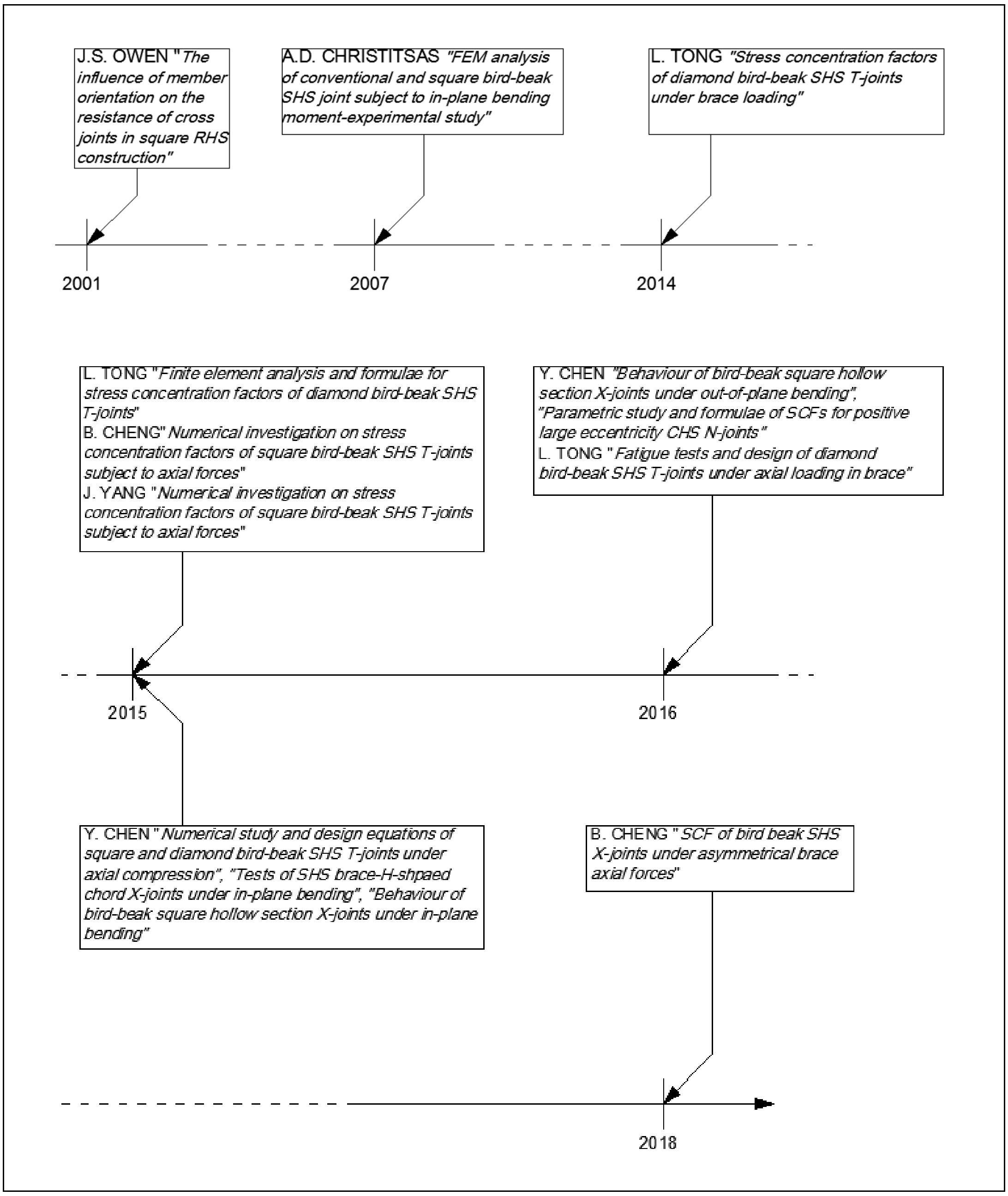

Figure 10 *Diamond bird-beak joints timeline*

Among all the chinese researchers, Y. CHEN stands out for focusing in acknowledging the behaviour of diamond bird-beak joints uner in-plane bending and out-of-plane bending in articles titled "*Behaviour of bird-beak square hollow section X-joints under in-plane bending*" [9] and "*Behaviour of bird-beak square hollow section X-joints under out-of-plane bending*" [8], respectively. Furthermore, J. CHEN et. al. conducted a numerical study titled "*Numerical study and design equations of square and diamond bird-beak SHS T-joints under axial compression*" [13] and an article "*Tests of SHS brace-H-shpaed chord X-joints under in-plane bending*" [16].

Y. CHEN was also interested in stress concentration factors. For instance, they studied stress concentration factors for positive large eccentricity of circular hollow sections and published their conclusions in an article titled "*Parametric study and formulae of SCFs for positive large eccentricity CHS N-joints*" [14] and was part of the team of "*Stress concentration factors of negative large eccentricity tubular N-joints under axial compressive loading in vertical brace*" by J. YANG [15], mentioned before.

Mentioned articles are all the literature that discusses and analyses diamond bird-beak joints since J.S. Owen introduces this topic in 2001. It shall be noted that all of them have in common that they have analysed diamond bird-beak joints in carbon steel. Therefore stainless steel diamond bird-beak joints, which are the central topic of this thesis, are yet to be discussed.

2.7 DBB JOINT IN LITERATURE: J.S. OWEN'S ANALYTICAL FORMULATION

The analytical solution achieved by J.S. Owen et al. (2001) in the article titled "*The influence of member orientation on the resistance of cross joints in square RHS construction*" [6] is based on a diamond bird-beak (DBB) joint under compression load by means of the variation of the following dimensionless geometric parameters:

$$\alpha = 2\frac{L_0}{b_0} \qquad \beta = \frac{b_1}{b_0} \qquad 2\gamma = \frac{b_0}{t_0}$$

The most relevant geometric parameters are shown in *Figure 11*.

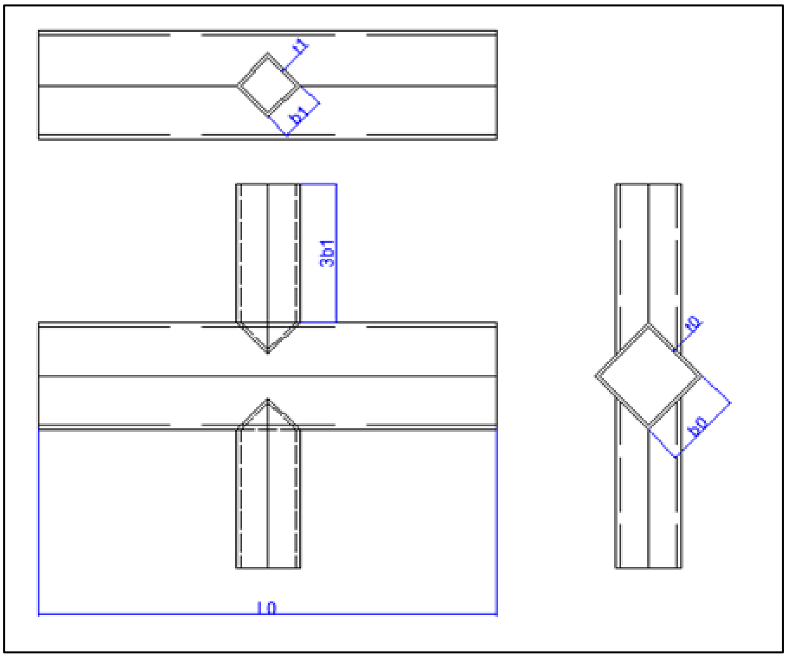

Figure 11 *Geometric parameters for a hollow section DDB X joint*

In accordance to J.S. Owen et al., previous parameters are limited within the following values:

$$5.3 < \alpha < 80 \qquad 0.2 < \beta < 0.9 \qquad 9.4 < 2\gamma < 35$$

The parameter α refers to the releation between chord length and half of its width. Four cases were considered for the chord end boundary conditions in order to find joint capacity dependance on chord length ratio (α):

- Case 1: All nodes at the end of the chord are restrained in all degrees of freedom (incluiding londitudinal)
- Case 2: All nodes at the end of the chord are restrained, in all but the longitudinal degree of freedom
- Case 3: All nodes at the end of the chord are free to move longitudinally and to rotate about the three axes but are not allowed to displace transversely.
- Case 4: Free ends (no restraint applied)

The study carried out by J.S. Owen et al. concluded that for α≥40, joint capacity results for DDB joints are effectively constant with chord length and is independent of the restraints at the end of the chord, as it is visible in *Figure 12*.

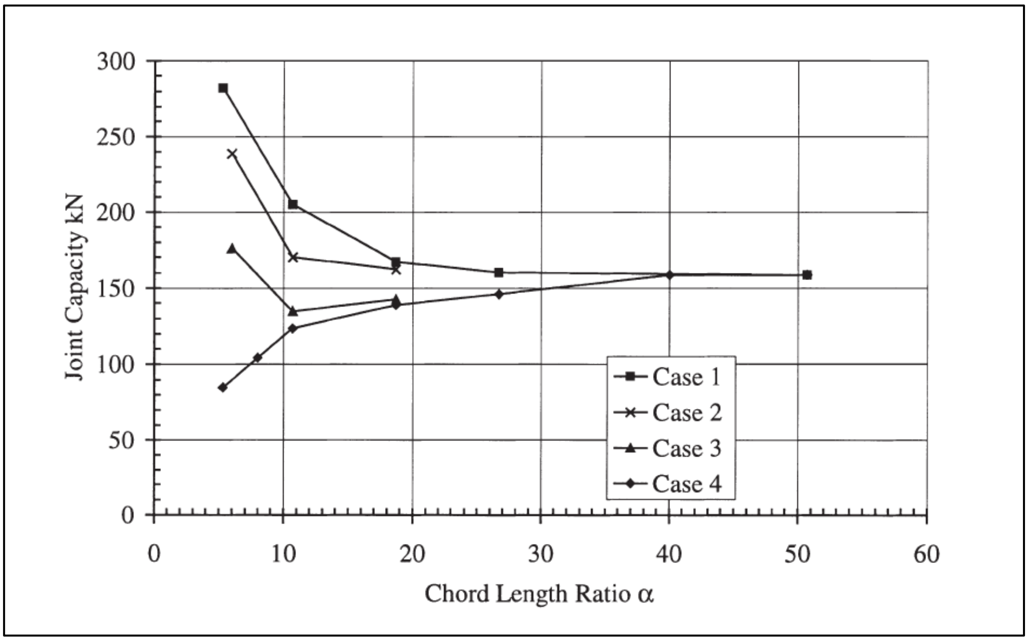

Figure 12 *Effect of length and end restraint on joint capacity (β=0.6, b_0=150 mm, t_0=6.3 mm, f_y=275 N/mm^2) extracted of the study of J.S. Owen et al.[6]*

Diamond bird-beak X joint used in J.S. Owen et. al. study has following geometric parameters:

$L_0 = 520\ mm$	$b_0 = 150\ mm$	$t_0 = 6.2\ mm$
$L_1 = 3 \cdot b_1$	$b_1 = 90\ mm$	$t_1 = 6.25\ mm$
$\alpha = 6.933$	$\beta = 0.6$	$2\gamma = 23.8$

As well as following material properties:

$$E = 206000\ N/mm^2$$

$$\upsilon = 0.3$$

$$\gamma = 78.5\ kN/m^3$$

Taking into account those parameters, J.S. Owen et. al. displayed load-displacement graph curves for a diamond bird-beak joint (*Figure 13*).

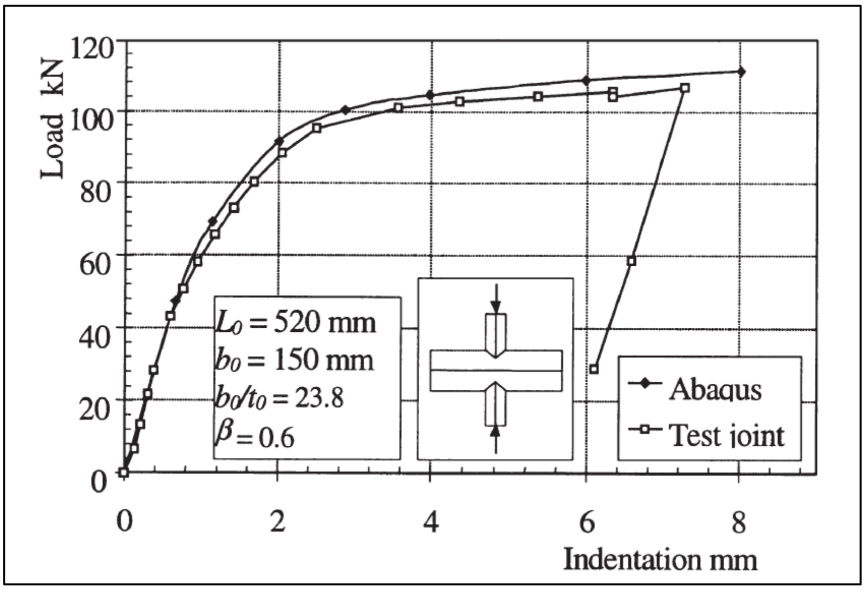

Figure 13 *Load-displacement curve for a diamond bird-beak joint by J.S. Owen et. al. [6]*

Assuming α=40 and f_y=275 N/mm², the conclusion of the study derives to the following analytical formulation:

$$F_{u1} = \frac{f_{y0}}{1000}\left(\frac{f_{y0}}{275}\right)^{0.8} \frac{(6.06 - 5.6\beta + 11.4\beta^2)(0.6 + 1.97\sqrt{\beta})t_0^2}{\frac{t_0}{b_0}(6.06 - 5.6\beta + 11.4\beta^2) + \frac{1}{3}(0.6 + 1.97\sqrt{\beta})} \qquad \textbf{Eq. 6}$$

Previous formulation is only dependent of dimensionless parameters β and 2γ, as well as chord thickness (t_0), chord width (b_0) and yield strength f_y.

2.8 ASSUMPTIONS FOR THE PRESENT THESIS

Once state of the art has been set as the most important tools for the present thesis, some assumptions might be taken into account in order to carry out this thesis and analyse results as accurate as possible.

1) Material used in this thesis is a stainless steel with f_y=280 N/mm^2 and E=200000 N/mm^2. Since comparisons of modelled results are made for formulations of carbon steel joints, several differences might be expected, specially by means of ductility performance of the joint.
2) Joint studied in this thesis is a Diamond Bird-beak X-type joint, which as stated before both the chord as well as the brace are rotated 45º around their longitudinal axes. Therefore, formulation for traditional SHS and RHS from European Normative might not be enough accurate for the specific purpose of this thesis. It might be expected some differences from obtained results to European Normative as well, but results should be at the safety side.
3) Different design resistances are described in EN 1993-1-8 for the particular case of $\beta \geq 0{,}85$, which leads to different failure modes of the joint. For the present thesis, design resistance for $\beta \geq 0{,}9$ is considered as the minimum of different failure modes i.e. minimum value between chord face failure, chord side wall buckling, brace failure and punching shear. However, minimum value of the design resistance might not be the actual failure mode of the modelled joint.
4) Loading is applied as boundary conditions in order to set an axial displacement in the top brace of -20 mm in the case of compression analysis and 20 mm in the case of tensile analysis, whereas bottom end brace is fixed. Therefore, eccentricity is not studied because axial load is applied trhoughout the longitudinal axes of the brace and, thus, in-plane moment as well as out-of-plane moment are not taken into account in this analysis.
5) Chord length is considered to be 3000 mm, whereas chord width is set as a fixed value of 150 mm. Therefore, dimensionless parameter α is 40 and, as J.S. Owen concluded in *The influence of member orientation on the resistance of cross joints in square RHS construction*" [6], for $\alpha \geq 40$ joint capacity results for DDB joints are effectively constant with chord length and is independent of the restraints at the end of the chord. Thus, parametric analysis is only dependent on the variation of parameters β and 2γ.

3. THE FINITE ELEMENT METHOD

3.1 INTRODUCTION TO STRUCTURAL ANALYSIS AND FEM

The structural analysis is the determination of the effects of loads on physical structures and their components. It employs the fields of applied mechanics, materials science and applied mathematics to compute a structure's deformations, internal forces, stresses, support reactions, accelerations and stability.

To perform an accurate analysis, the results of such an analysis typically include support reactions, stresses and displacements. This information is then compared to criteria that indicate the conditions of failure. There are three approaches to the analysis: the mechanics of materials approach, the elasticity theory approach and the finite element approach. The first two make use of analytical formulations, whereas the finite element approach is actually a numerical method for solving differential equations generated by theories of mechanics such as elasticity theory and strength of materials.

For the current thesis, finite element method (FEM) will be used by means of ABAQUS software, which is explained in the following paragraph.

3.2 ABAQUS SOFTWARE

3.2.1 Introduction

Abaqus/CAE is a complete Abaqus environment that provides a simple, consistent interface for creating, submitting, monitoring and evaluating results from Abaqus/Standard and Abaqus/Explicit simulations, which will we further described below. Abaqus/CAE is divided into modules, where each module defines a logical aspect of the modelling process such asdefining the geometry, defining the material properties, generating the mesh, among other aspects.

Basically, Abaqus is a software based on the finite element method (FEM) which main goal is to solve science and engineering problems of a wide range of disciplines. This software allows obtaining a complete solution of virtual tests by means of a realistic simulation, which largely reduces computational cost as well as time.

Abaqus is composed off of four different softwares, where every each is specifically and suitable for different types of problems: ABAQUS/CAE, ABAQUS/Standard, ABAQUS/Explicit and ABAQUS/CFD.

Abaqus/CAE and Abaqus/Standard have been used for the analytical study of the current thesis, thus they are the suitable option to model and visualize results for plastic behaviour of the diamond bird-beak joint.

3.2.2 Software modules

Abaqus/CAE is divided into functional units called modules. Each module contains only those tools that are relevant to a specific portion of the modelling task. The following list of the modules available within Abaqus/CAE briefly describes the modelling tasks one can perform in each module. Refer to "*Abaqus/CAE User's Manual version 6.12*" for further information about each module.

Part module	Create individual parts by sketching or importing their geometry.
Property module	Create section and material definitions and assign them to regions of parts.
Assembly module	Create and assemble part instances.
Step module	Create and define the analysis steps and associated output requests.
Interaction module	Specify the interactions, such as contact, between regions of a model.
Load module	Specify loads, boundary conditions, and fields.
Mesh module	Create finite element mesh.
Optimization module	Create and configure an optimization task.
Job module	Submit a job for analysis and monitor its progress.
Visualization module	View analysis results and selected model data.
Sketch module	Create two-dimensional sketches.

3.3 SCOPE OF THE PROBLEM

In order to approach the study of the stainless steel joint as accurate as possible, several models will be analysed, which every each of them will be slightly different in terms of geometry.

For the current thesis, 16 different models will be analysed which their geometrical parameters are different. They will be named as shown below for the sake of simplicity, where DBB stands for Diamond Bird-Beak, X stands for welded X-type joint and SS stands for Stainless Steel:

$$DBBX\_i\_SS;\ i = \{01, \ldots, 16\}$$

Previous models will be analysed under compression as well as under tension, which results in 32 models in total.

First of all, it is needed to calibrate the numerical model in order to verify that Abaqus software is used accurately. Thus, first step will be modelling a DDB X-type joint taking into account J.S. Owen et al. study and compare the numerical finite element approach obtained with their results. It is expected to obtain close results in comparison with those of J.S. Owen et al.

Assuming that the calibration of the model is correct, following steps will be focused in repeating and analysing systematically the different models described before.

Finally, once all the calculations have been obtained, results will be displayed in three different graphs: design resistance dependence on β parameter, design resistance dependence on 2γ parameter and load-displacement curves.

$$F_u - \beta \qquad F_u - 2\gamma \qquad P - \delta$$

3.4 NUMERICAL METHOD RELEVANT ASPECTS

3.4.1 Geometrical models to study

As mentioned in the previous paragraph, parametric analysis is carried out for a total amount of 32 models.

Figure 14 displays the most important geometric parameters that define all the models.

Taking into account the limiting values for parameters β and 2γ stated by J.S. Owen, geometric parameters for each model are defined in *Table 8*.

$$0.2 < \beta < 0.9 \qquad 9.4 < 2\gamma < 35$$

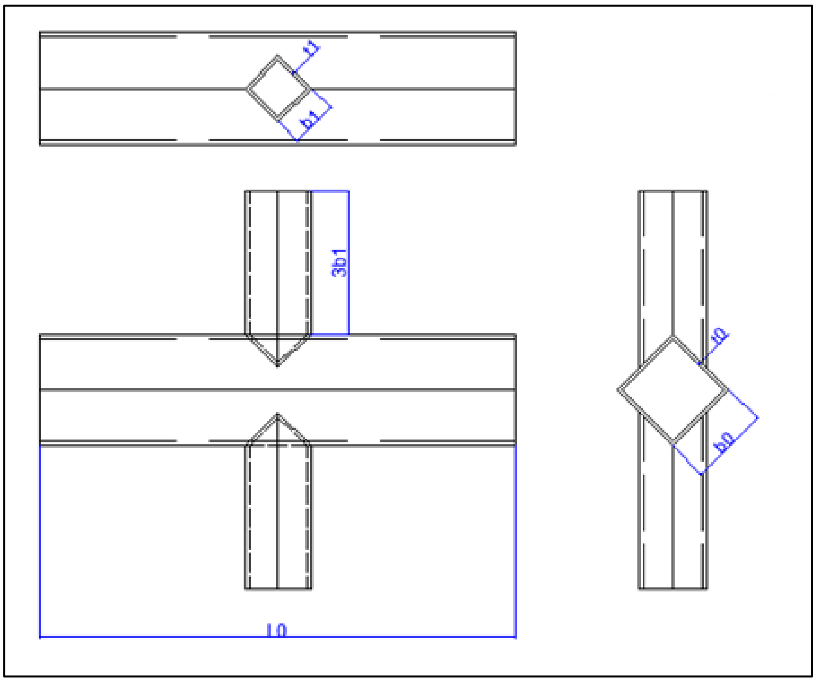

Figure 14 *Geometric parameters for a hollow section DDB X joint*

JOINT	fy	Geometric parameters					2γ	β
		Chord			Brace			
		L_0	b_0	t_0	b_1	t_1		
DBBX_01_SS	280	3000	150	15	30	15	10	0.2
DBBX_02_SS	280	3000	150	15	60	15	10	0.4
DBBX_03_SS	280	3000	150	15	90	15	10	0.6
DBBX_04_SS	280	3000	150	15	135	15	10	0.9
DBBX_05_SS	280	3000	150	10	30	10	15	0.2
DBBX_06_SS	280	3000	150	10	60	10	15	0.4
DBBX_07_SS	280	3000	150	10	90	10	15	0.6
DBBX_08_SS	280	3000	150	10	135	10	15	0.9
DBBX_09_SS	280	3000	150	6	30	6	25	0.2
DBBX_10_SS	280	3000	150	6	60	6	25	0.4
DBBX_11_SS	280	3000	150	6	90	6	25	0.6
DBBX_12_SS	280	3000	150	6	135	6	25	0.9
DBBX_13_SS	280	3000	150	5	30	5	30	0.2
DBBX_14_SS	280	3000	150	5	60	5	30	0.4
DBBX_15_SS	280	3000	150	5	90	5	30	0.6
DBBX_16_SS	280	3000	150	5	135	5	30	0.9

Table 8 *Geometric parameters for each DBB X joint model*

3.4.2 Loads and boundary conditions

The loads applied to the DBB joint are compression and tension, which are set to the cross-section of the braces.

Previous loads are set as boundary conditions by means of an imposed displacement of the top brace end, whereas bottom brace end is fixed. Throughout of the displacement calculation, software calculates structure reactions on the bottom brace end.

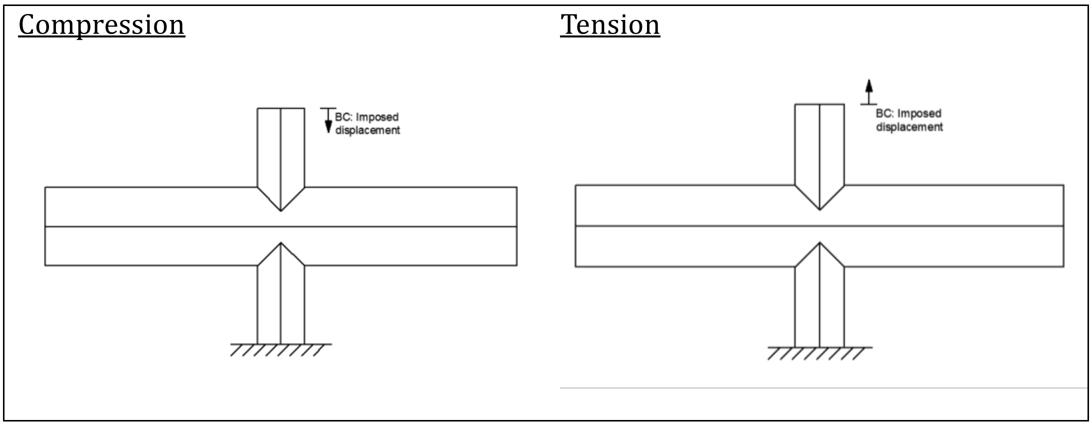

Figure 15 *Schematic representation of boundary conditions for analysis of the models*

The main reason to submit the displacement calculation is that it allows achieving better convergence results as well as load-deformation complete curve.

In conclusion, boundary conditions at the ends of the braces are restrained in any direction with the exception of the longitudinal direction of the top brace, which is allowed to move freely.

3.4.3 Classification of cross-sections

Local effects of instability are checked by the cross-section classification, explained in *Table 1*. Taking into account this classification, chord and bracings may be classified in order to foresee possible local instability during analysis.

All the chords and bracings for the different models are Class 1, which should not lead to local instability effects.

It should be noted that Class 4 joints would not be realistic, so yield strength would not be reached and therefore limiting the elastic capacity of the joint.

JOINT	Class	
	Chord	Brace
DBBX_01_SS	Class 1	Class 1
DBBX_02_SS	Class 1	Class 1
DBBX_03_SS	Class 1	Class 1
DBBX_04_SS	Class 1	Class 1
DBBX_05_SS	Class 1	Class 1
DBBX_06_SS	Class 1	Class 1
DBBX_07_SS	Class 1	Class 1
DBBX_08_SS	Class 1	Class 1
DBBX_09_SS	Class 1	Class 1
DBBX_10_SS	Class 1	Class 1
DBBX_11_SS	Class 1	Class 1
DBBX_12_SS	Class 1	Class 1
DBBX_13_SS	Class 1	Class 1
DBBX_14_SS	Class 1	Class 1
DBBX_15_SS	Class 1	Class 1
DBBX_16_SS	Class 1	Class 1

Table 9 *Classification of chord and bracings for DDB X joint of the different models according to EN 1993-1-4*

3.4.4 Classification of FEM types

The finite element type used in order to model the DBB X-joint is the shell type, which thickness is largely smaller than other two dimensions and normal tensions along thickness direction are negligible.

There are two different types of shell elements.

- Thick shell elements, which are based on Reissner-Mindlin theory. This theory stated that those elements are needed in cases where cross-sectional flexibility is significant, so second order interpolation is required.
- Thin shell elements, which are based on Kirchhoff theory. This theory stated that those elements are used when cross-sectional flexibility is negligible.

Number of nodes of the element determines interpolation order needed to stablish section shell behaviour. On the one hand, elements that have all the nodes at the vertices of the element uses linear interpolation, thus they are called linear elements or first order elements. On the other hand, elements that have intermediate nodes uses quadratic interpolation and they are called quadratic elements or second order elements. Triangular elements as well as tetrahedral uses second order interpolation

ABAQUS may use several numerical techniques in order to solve integration in each element. However, Gauss integration is the most commonly used. The software evaluates the material for each integration point for each element. Furthermore, the integration may either be complete or reduced. The main difference between both integration methods is that the reduced integration reduces computational cost.

For the current thesis, S4R shell elements has been used, which are square elements with 4 nodes of reduced integration and linear interpolation. These elements are used because they has better convergence in comparison with triangular as well as tetrahedron elements. Refer to "*Abaqus/CAE User's Manual version 6.12*" for further information about different types of FEM analysis.

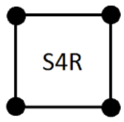

Figure 16 *Representation of square element with 4 nodes of reduced integration (S4R)*

Cross-section behaviour of a shell may be studied either by Simpson integration or Gauss quadrature. Despite the fact that Gauss quadrature is more accurate that Simpson integration method, Simpson has been the choice, so it allows to analyse results in the surface of the shell. Furthermore, five points of integration has been used throughout the thickness of the shell.

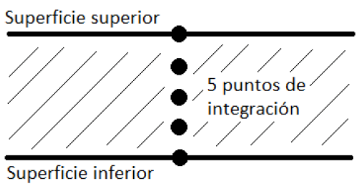

Figure 17 *Representation of the five integration points throughout shell thickness in order to carry out Simpson integration method*

3.4.5 Convergence analysis

It is important to carry out a convergence analysis before the analytical parametric study in order to find the best mesh size that allows finding an accurate solution as close as possible to reality with a minimum computational cost.

3.5 STUDY TO CALIBRATE THE NUMERICAL MODEL

3.5.1 Characteristics of the joint to validate

Before the parametric study of the stainless steel joint is carried out, it would be of high importance to validate the model in order to assure the results. This validation will be carried out considering the geometric and material properties of a known joint i.e. Owen et. al.'s DBBX-joint will be analysed, thus the results are reliable. This model joint will be used to test several mesh sizes in order to achieve the convergence analysis.

3.5.2 Joint model procedure

Current paragraph will be focused on widely explaining the joint model procedure using the finite elements method within the Abaqus software. This explanation and all the procedure steps should be considered as guidelines for the parametric study of the stainless steel joint. Repeating sistematically the procedure that is explained in this paragraph will lead to modelling the total amount of 32 models.

Diamond bird-beak X joint used in Owen et. al. study has following geometric parameters:

$L_0 = 520\ mm$	$b_0 = 150\ mm$	$t_0 = 6.2\ mm$
$L_1 = 3 \cdot b_1$	$b_1 = 90\ mm$	$t_1 = 6.25\ mm$
$\alpha = 6.933$	$2\gamma = 23.8$	$\beta = 0.6$

As well as following material properties for carbon steel:

$$E = 206000\ N/mm^2$$

$$\upsilon = 0.3$$

$$\gamma = 78.5\ kN/m^3$$

3.5.2.1 Creation of different parts (Part module)

First of all, parts should be defined within "Part module". It should be created a part for the chord as well as a part for the brace with dimensions displayed in *Figure 18*. Since each brace is composed off of four faces with the same geometry, only one face will be created within the part module, thus they will be copied within Assembly module. The same procedure is applied to the chord.

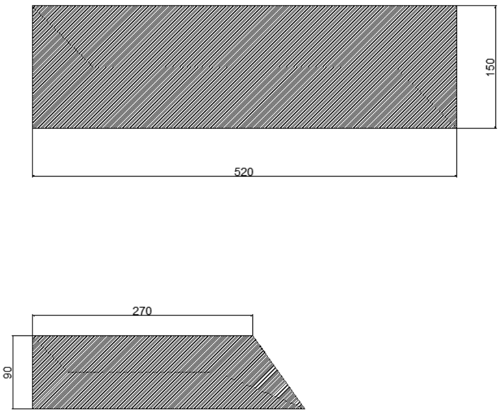

Figure 18 *Geometry of the chord and brace parts*

Each part is defined as 3D modelling space, deformable type and shell planar shape.

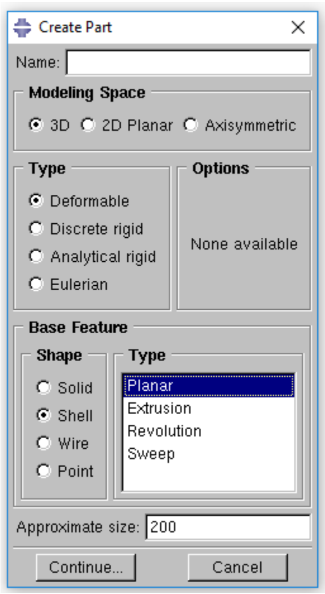

Figure 19 *"Create part" dropdown window*

3.5.2.2 Material properties assignment (Property module)

Defining material properties should be carried out within "Property module". The material properties are defined in Owen et. al.'s experimental study.

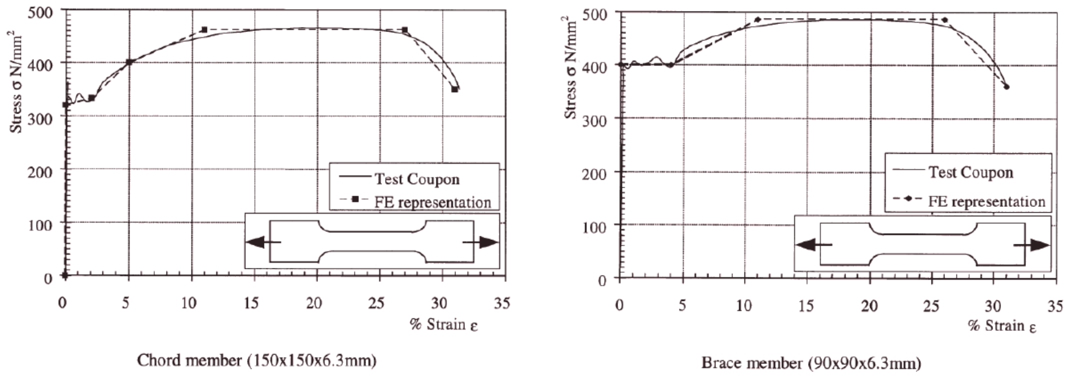

Figure 20 *Material properties for carbon steel (J. S. Owen et. al.)*

In order to define material properties within Abaqus, density, elasticity and plasticity should be introduced in Property module dropdown window for both chord part (*Figure 21*) and brace part (*Figure 22*).

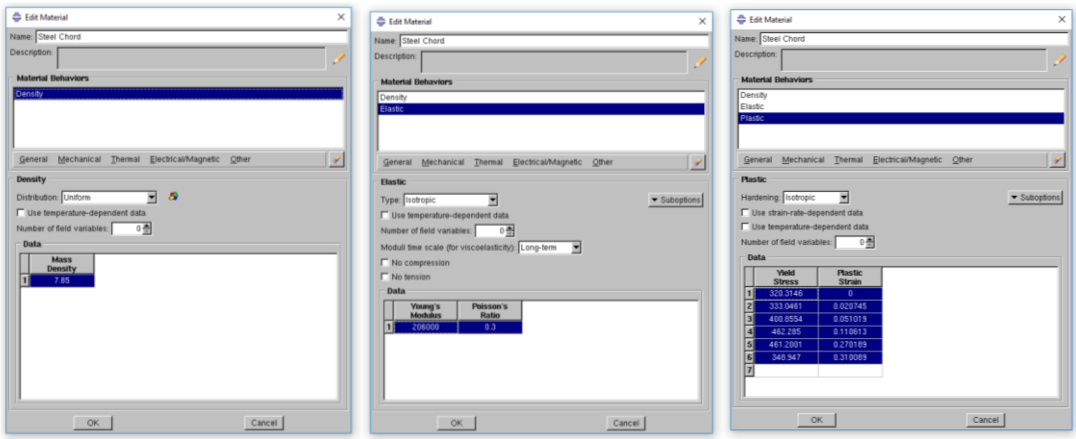

Figure 21 *"Material properties" dropdown window for chord*

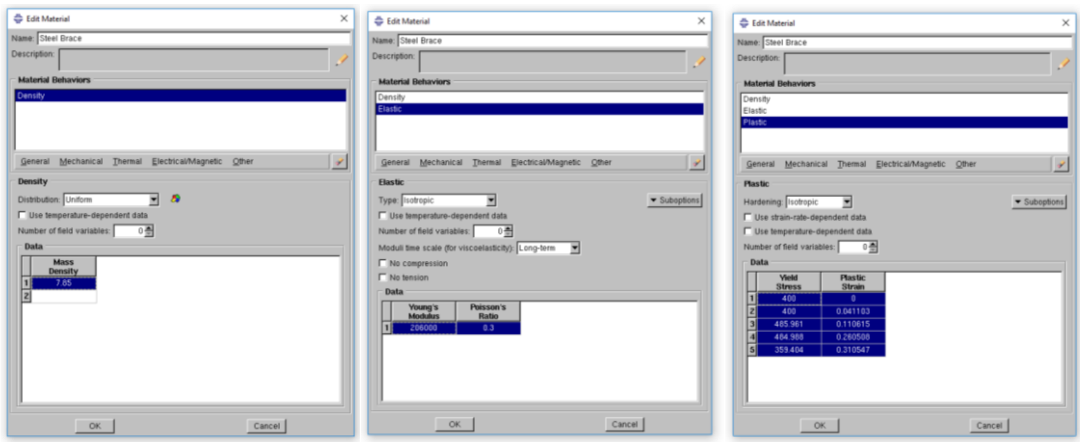

Figure 22 *"Material properties" dropdown window for brace*

Once the material properties have been defined, it is time to create and define the different sections. Section thickness is equal to 6.2 mm for chord member and 6.25 for brace member.

Section would be a continuum and homogeneous shell. Simpson's method with 5 points of integration through thickness will be used.

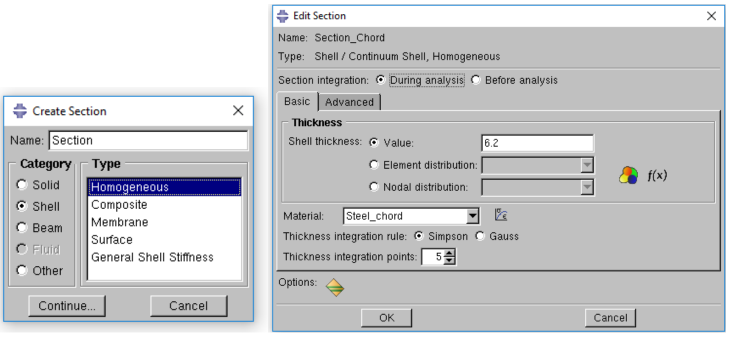

Figure 23 *"Section edition" dropdown window within Abaqus for chord part*

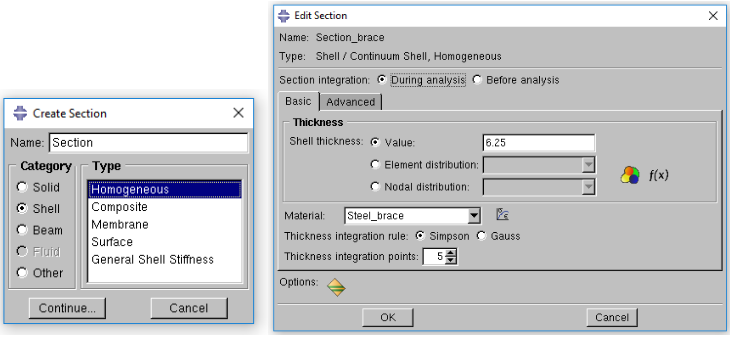

Figure 24 *"Section edition" dropdown window within Abaqus for brace part*

Sections should be assigned to each part that have been created previously.

3.5.2.3 Part assembly procedure (Assembly module)

Next step within the modelling procedure is to assembly and merge the parts created previously. Assembly is carried out throughout displacement and rotation of the parts within a global coordinate system.

Assembly of joint model is shown in *Figure 25*.

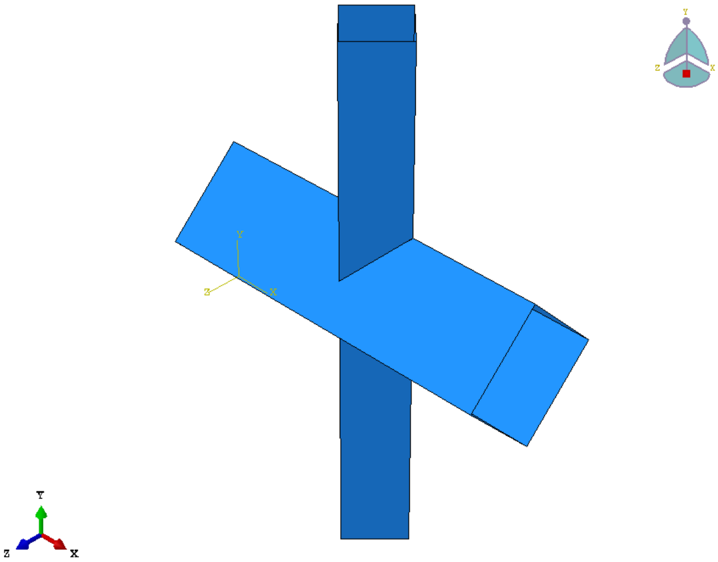

Figure 25 *Assembly and merge procedure of the joint (Assembly module)*

3.5.2.4 Step definition (Step module)

Step module is used to set the different steps of the model calculation.

First of all, a new "Static, Riks" step is created, which allows to apply loading under arc-length control.

On the one hand, *"Nlgeom"* option is set as on in order to set the analysis as a second order calculation. On the other hand, incrementation is set as automatic with a maximum number of 300 increments. Initial, minimum and maximum arc length increment sizes are 0,05, 1E-05 and 1, respectively.

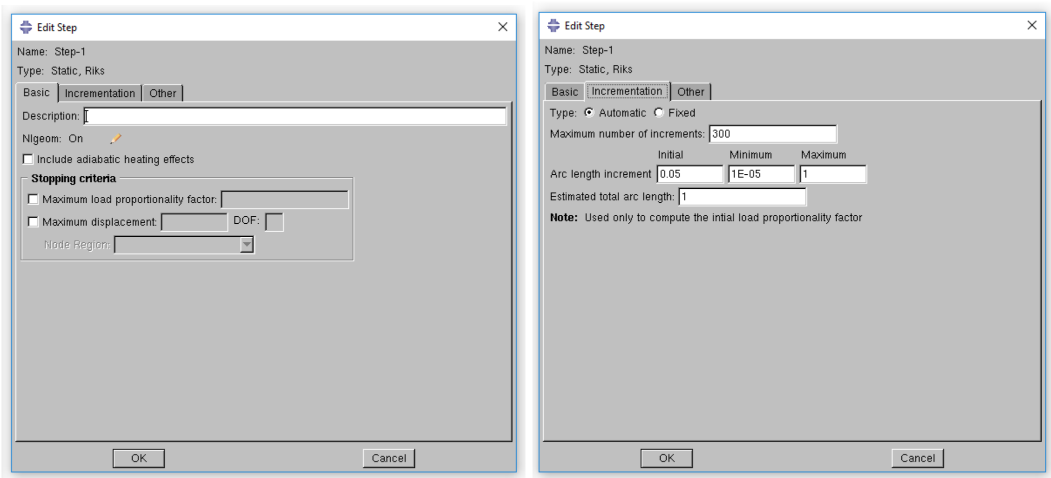

Figure 26 *"Step definition" dropdown list within Abaqus*

Note that for some models of the parametric analysis (DBBX_04_SS, DBBX_07_SS, DBBX_08_SS and DBBX_12_SS subjected to compression loading), minimum arc length have been reduced to 1E-08 in order to avoid convergence errors.

3.5.2.5 Loads and boundary conditions (Load module)

Loading is applied as boundary conditions in order to set an axial displacement in the top brace whereas bottom brace is fixed. Thus, two boundary conditions should be created i.e. one boundary condition for top brace and one boundary condition for bottom brace.

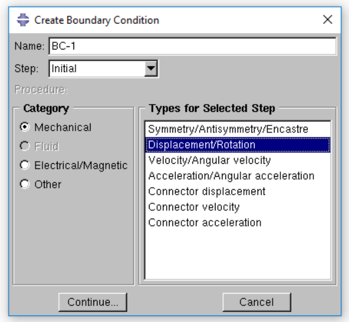

Figure 27 *"Create boundary condition" dropdown list within Abaqus*

Top boundary condition (BC-1) is set as a vertical displacement to -20 mm in order to model compression loading. Bottom boundary condition (BC-2) is set as a fixed support.

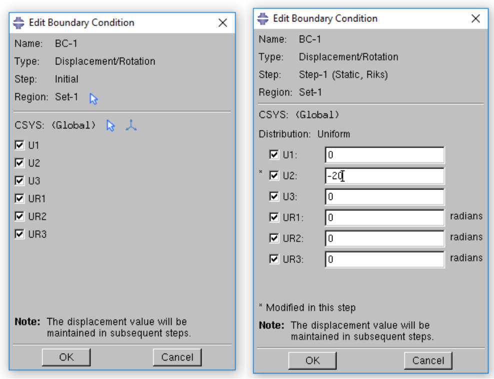

Figure 28 *"Edit boundary condition" dropdown list for BC-1 within Abaqus*

Note that for parametric analysis, vertical displacement is set to 20 mm instead of -20 mm in order to model tensile loading.

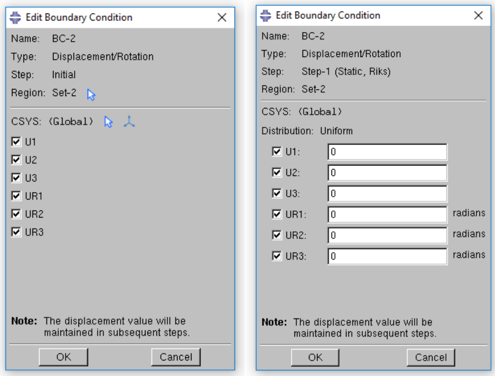

Figure 29 *"Edit boundary condition" dropdown list for BC-2 within Abaqus*

Boundary conditions are displayed in *Figure 30*:

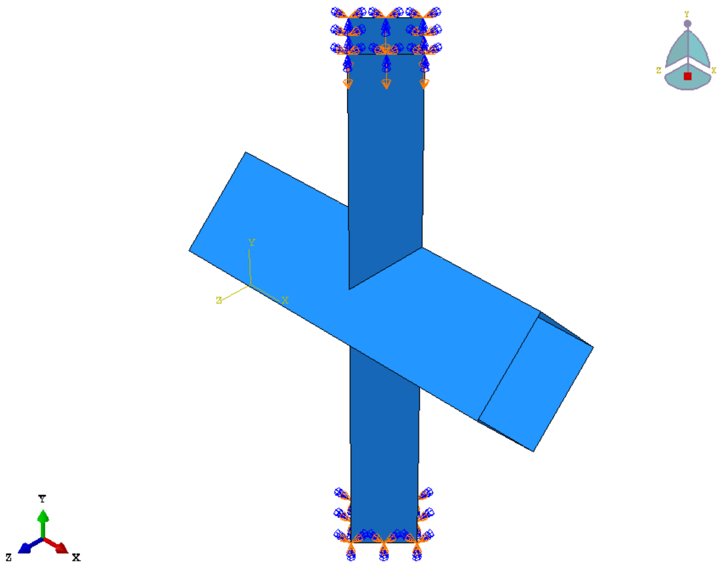

Figure 30 *Graphical representation of boundary conditions*

3.5.2.6 Mesh creation (mesh module)

Last step of modelling procedure is to define the mesh and seed the part. As an example, mesh size of 5 mm is displayed in *Figure 32*. A convergence analysis will be conducted in order to define and optimize the best mesh size for the purpose of the current thesis.

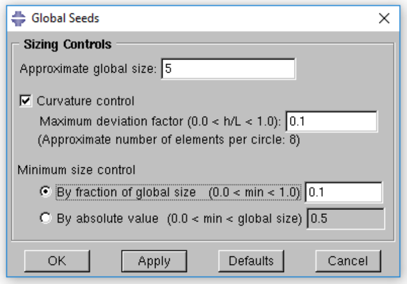

Figure 31 *"Global seeds" dropdown list to set mesh size within Abaqus*

For the current thesis, S4R shell elements has been used, which are square elements with 4 nodes of reduced integration and linear interpolation. These elements are used because they has better convergence in comparison with triangular as well as tetrahedron elements.

Graphical representation of the meshed part is displayed in *Figure 32*:

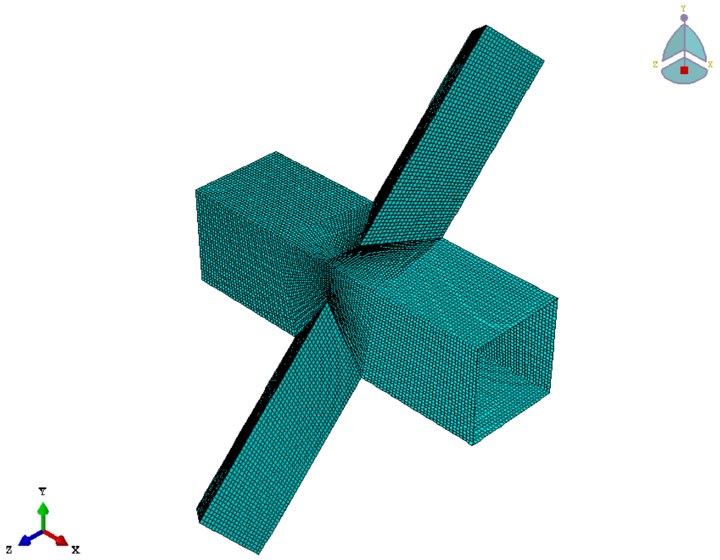

Figure 32 *Graphical representation of a mesh size of 5 mm*

It is of high importance to define which nodes or elements are those of results will be obtained and analysed (Model > Assembly > Sets). Reactions are obtained as the sum of forces from all the nodes of the bottom brace fixed end, whereas displacements are obtained from a node in the top brace end and from a node within the plane of symmetry of the chord.

3.5.2.7 Calculation (job module)

Job module is used in order to create and submit the job for calculation, which default options are set.

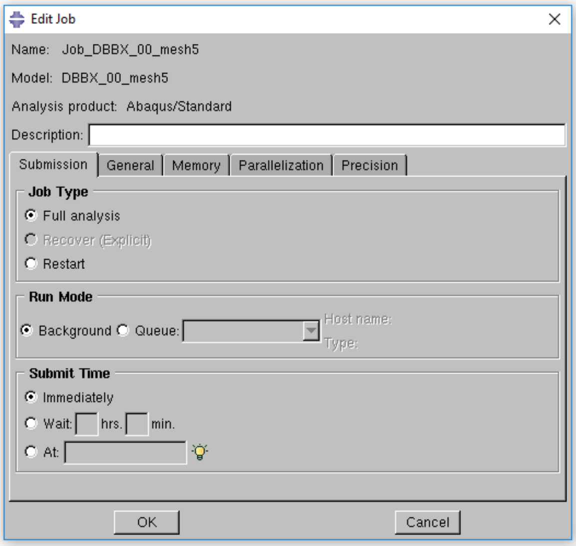

Figure 33 *"Edit job" dropdown list*

3.5.2.8 Results

Finally, after calculation of the model has been completed, results should be exported from Abaqus by means of (X,Y) data. On the one hand, reactions at bottom brace are exported and, on the other hand, displacements of top brace are obtained as well. Those values should be processed within MS Excel in order to obtain Load-Displacement curves. Overall reaction load will be the sum of the loads in each node.

3.5.3 Convergence analysis

Convergence analysis has been carried out in the joint explained previously in order to define the optime mesh size in terms of calculation time as well as number of elements. This analysis is of high importance in order to obtain as close to reality as possible results with the minimum computational cost.

Mesh density has been set as structured and homogeneous along the joint. Mesh sizes rangs from 2 mm to 20 mm:

Mesh size =20 mm	Mesh size =15 mm	Mesh size =10 mm
Mesh size =5 mm	Mesh size =3 mm	Mesh size =2 mm

Results for the convergence analysis are shown in *Figure 34*, where displacement results have been considered at a node in the top brace.

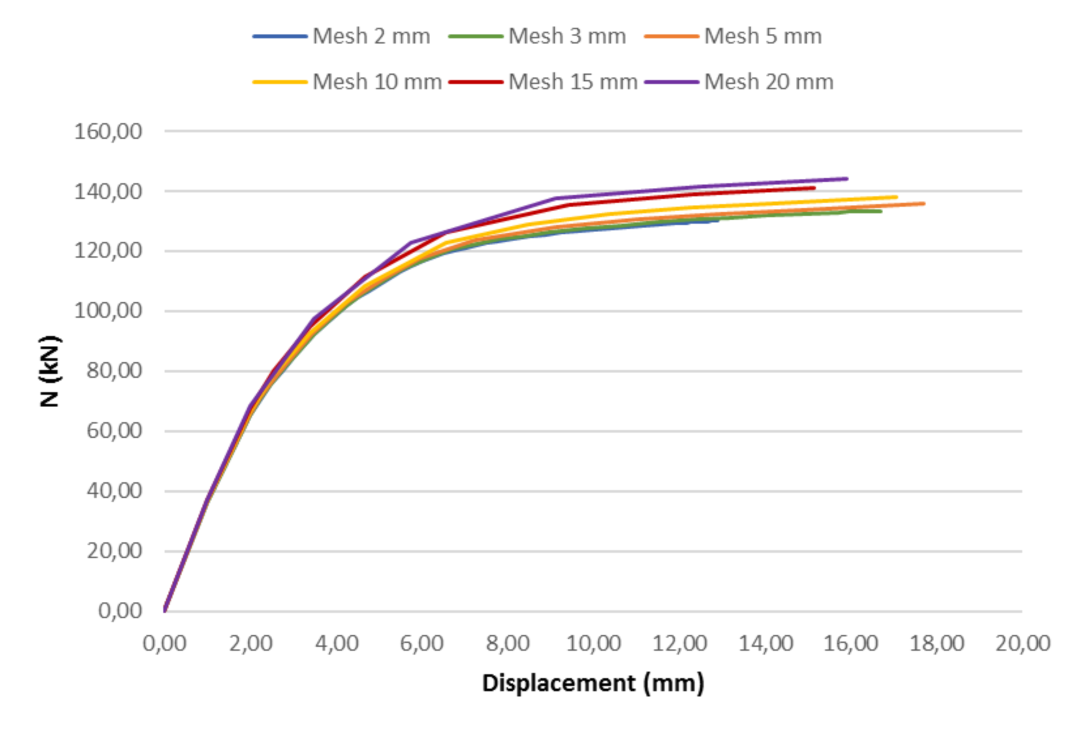

Figure 34 *Load-deformation curves for different mesh sizes*

As it is visible in *Figure 34*, elastic behaviour is independent of mesh size, whereas plastic behaviour is strongly linked to mesh size.

In order to choose the optimum mesh size to carry out calculation of all the models, mesh size of 2 mm is considered to be equal to reality. Calculation time and reaction load for 7 mm of displacement are compared for the different meshes.

Table 10 summarises calculation CPU time within ABAQUS, reaction load at 7 mm for each mesh size and relative error with respect to mesh size of 2 mm.

Mesh size (mm)	Number of elements	Time CPU (s)	Load (kN) (at 7 mm)	Difference (kN)	Relative difference (%)
2	176683	70887	120.8014	-	0.00%
3	77617	23256	121.2852	0.4838	0.40%
5	27990	3098.8	123.0032	2.2018	1.82%
10	7192	2134	124.5703	3.7689	3.12%
15	2936	846.88	127.5204	6.719	5.56%
20	1881	552.11	130.7149	9.9135	8.21%

Table 10 *Summary of convergence analysis*

Convergence analysis is displayed in *Figure 35*, which is visible that solution converges as mesh size decreases.

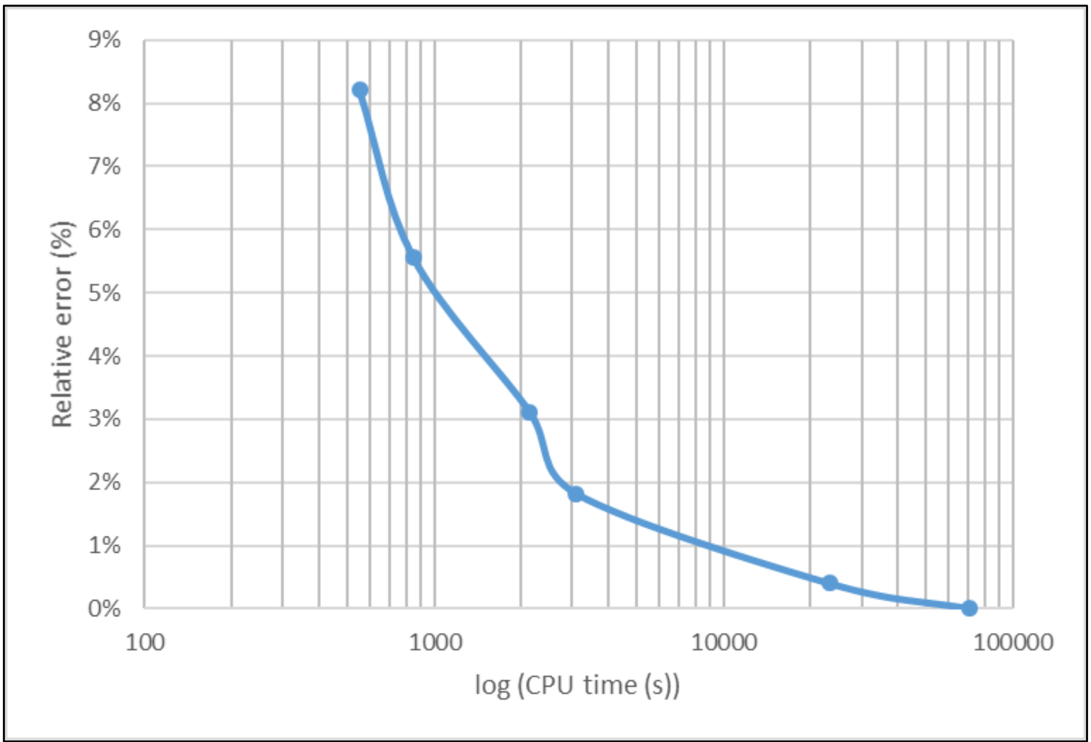

Figure 35 *Graphical representation of relative error of reaction load to calculation CPU time in logaritmic scale*

For the purpose of the present thesis, a mesh size of 5 mm would be appriopriate. Thus, its relative error is less than 2%, which shall be assumed to be adequate for the calculations and purpose of this thesis.

3.5.4 Validation of the numerical model in comparison to the analytical formulation

Loading-deformation curves shows that as deformation increases, load increases as well. *Figure 36* displays a graph that compares results obtained in ABAQUS to those of the study of J.S. Owen. Validation has been conducted for a carbon steel diamond bird-beak joint because literature results were reliable.

Displacement results have been considered in a node within the plane of symmetry of the chord.

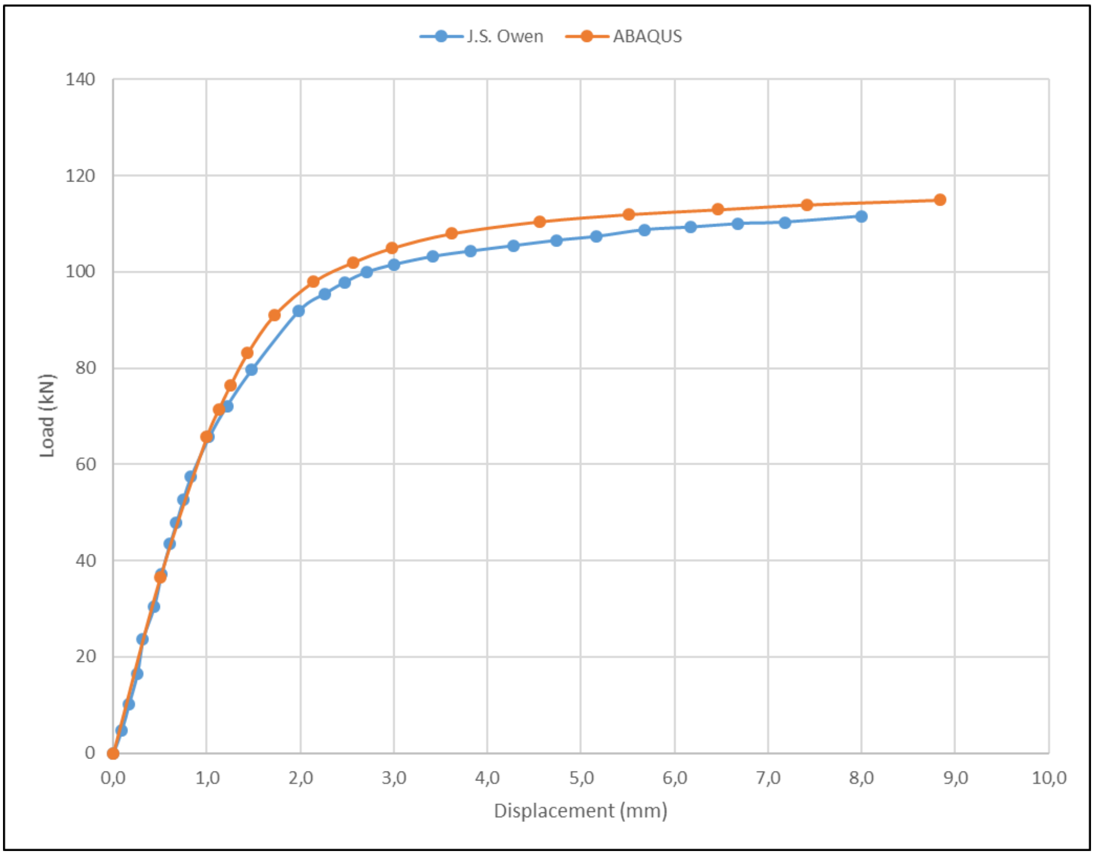

Figure 36 *Loading-deformation curves obtained from ABAQUS in comparison to J.S. Owen study*

As expected, obtained results are almost identical as those obtained by Owen. Thus, finite element procedure to study diamond bird-beak joints should be considered as appropriate.

This validation has been carried out for a carbon steel diamond bird-beak joint, whereas this thesis is based on analysing stainless steel joints. The only procedure step that will differ from the validation explained in this paragraph is "*3.5.2.2 Material properties assignment (Property module)*", where stainless steel material properties should be introduced.

4. PARAMETRIC STUDY OF DBB-X JOINTS

4.1 INTRODUCTION

Present paragraph develops a parametric study in order to compare 16 models of a planar diamond bird-beak joint with sligthly different geometric parameters under compression as well as the same 16 models under tensile loading.

4.2 GEOMETRIC PARAMETER VARIATION

As said before, variation of the geometric dimensions will be carried out. Those dimensions are related as follows:

$$\alpha = 2\frac{L_0}{b_0} \qquad \beta = \frac{b_1}{b_0} \qquad 2\gamma = \frac{b_0}{t_0}$$

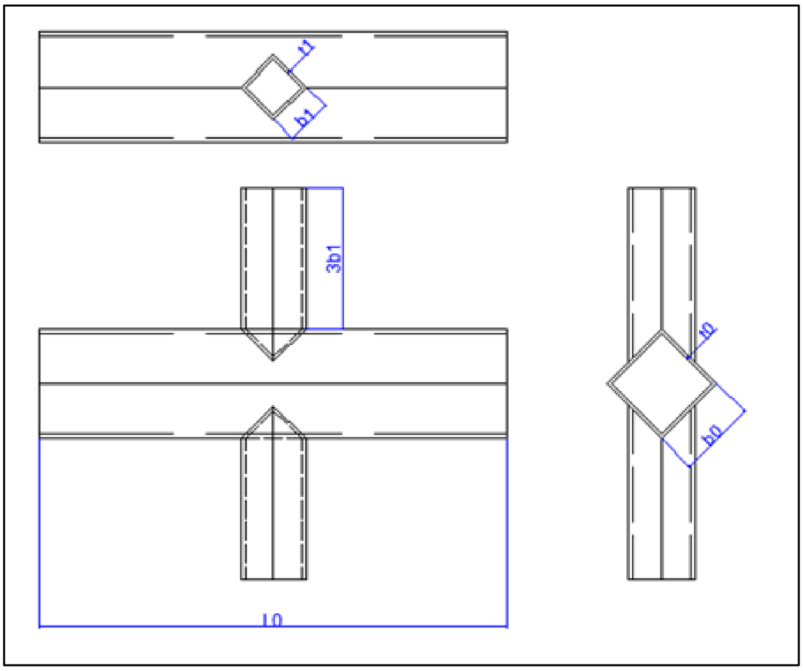

Figure 37 *Geometric parameters for a hollow section DDB X joint*

As stated in J.S. Owen article, for α≥40, joint capacity results for DDB joints are effectively constant with chord length and is independent of the restraints at the end of the chord. Since for the present thesis α=40, parametric analysis is carried out with the variation of parameters β and 2γ.

This thesis is an attempt to cover as many models as possible with the variation of those parameters.

4.2.1 PARAMETER β

The relationship between chord width and brace width is defined as β.

$$\beta = \frac{b_1}{b_0} \qquad \textbf{Eq. 7}$$

As stated in Owen et. al., parameter β ranges from 0.2 to 0.9.

In the particular case of this thesis, β is taken as 0.2, 0.4, 0.6 and 0.9, which have been obtained from mantaining constant chord width and varying brace width for the values 30 mm, 60 mm, 90mm and 135 mm, respectively.

4.2.2 PARAMETER 2γ

The relationship between chord width and chord thickness is defined as the parameter 2γ.

$$2\gamma = \frac{b_0}{t_0} \qquad \textbf{Eq. 8}$$

As before, in the Owen et. al.'s Article it is ranged between 9.4 to 35.3.

In this thesis, 2γ values are: 10, 15, 25 and 30, which are obtained from varying thickness for values 15 mm, 10 mm, 6 mm and 5 mm, respectively.

4.2.3 SUMMARY

Table 11 summarises all the models:

		β			
		0,2	**0,4**	**0,6**	**0,9**
2γ	**10**	DBBX_01_SS	DBBX_02_SS	DBBX_03_SS	DBBX_04_SS
	15	DBBX_05_SS	DBBX_06_SS	DBBX_07_SS	DBBX_08_SS
	25	DBBX_09_SS	DBBX_10_SS	DBBX_11_SS	DBBX_12_SS
	30	DBBX_13_SS	DBBX_14_SS	DBBX_15_SS	DBBX_16_SS

Table 11 *Geometric parameters assigned to each model*

4.3 RESULTS

Parameteric analysis derives to a large amount of data wich shall be treated appropriately and accurately within MS Excel in order to obtain Load-Displacement curves. Overall reaction load will be the sum of the loads in each node. Design ultimate resistance for each model are listed in *Table 12*. Refer to "*Appendix C. VON MISES*" for images of Von Mises stresses for each model for both compression and tensile and refer to "*Appendix D. PARAMETRIC RESULTS*" for the overall Load-displacement data for each model as well as their graphical curves.

JOINT	Compression (kN)	Tension (kN)
DBBX_01_SS	706,12	1162,76
DBBX_02_SS	829,57	1157,29
DBBX_03_SS	2484,84	3486,48
DBBX_04_SS	1854,58	4001,41
DBBX_05_SS	380,17	775,18
DBBX_06_SS	406,93	1547,74
DBBX_07_SS	1562,32	2324,73
DBBX_08_SS	854,18	2682,92
DBBX_09_SS	146,11	465,31
DBBX_10_SS	163,95	929,17
DBBX_11_SS	747,25	1394,78
DBBX_12_SS	786,52	1742,20
DBBX_13_SS	105,65	387,74
DBBX_14_SS	118,02	774,99
DBBX_15_SS	544,64	1162,10
DBBX_16_SS	564,18	1408,86

Table 12 *Design resistance for each model subjected to compression loading and tensile loading*

Results obtained throughout this thesis will be deeply and largely analysed in the following paragraph "*5. ANALYSIS OF RESULTS*".

5. ANALYSIS OF RESULTS

Results obtained after parametric analysis of all the models is concluded are compared and discussed from different perspectives. On the one hand, they are compared to EN 1993-1-8 [3] formulation as well as J.S. Owen [6] formulation for both compression and tensile loading. This comparison is done in terms of design resistance dependance on parameter β, design resistance dependance on parameter 2γ and in terms of load-displacement curves. On the other hand, stainless steel geometric models are compared to carbon steel identical models, which were studied by A. Peña and R. Chacón [7] in order to discuss advantages of stainless steel against carbon steel.

5.1 DESIGN RESISTANCES

As mentioned before, once the parametric study is completed, obtained results are compared to those obtained thorughout European Normative EN 1993-1-8 [3] as well as J.S. Owen et. al. [6] formulations.

On the one hand, European Normative gives a formulation for axial resistance for a traditional welded X joint between RHS brace and RHS chord. Since the thesis is based on an analysis of a diamond bird-beak joint, several differences are expected from ABAQUS results. On the other hand, J.S. Owen analysed a diamond bird-beak joint of carbon steel subjected to compression loading. Thus, differences are expected for tensile analysis. Furthermore, slightly differences may be obtained for compression analysis due to material studied in this thesis is stainless steel, which is more ductile than carbon steel joint analysed by J.S. Owen.

Comparison procedure will be carried out by means of design value of the resistance of the joint dependance on the parameters β and 2γ.

5.1.1 Design resistances according to EN 1993-1-8

Following formulations are taken into account from Eurocode EN 1993-1-8 [3] in order to set the design value of the resistance of the hollow section joint. Minimum design resistance among the following will be taken into account as the most restrictive design resistance.

Although the resistance of a joint with properly formed welds is generally higher under tension than under compression, it should be noted that the design resistance of a joint is generally based on the resistance of the brace in compression to avoid the possible excessive local deformation or reduced rotation capacity or deformation capacity with which might otherwise occur. Therefore, design resistance of the modelled joint subjected to tensile loading might lead to different failure mode than the theoretical failure mode of the normative.

- Chord face failure β ≤ 0.85

$$N_{1,Rd} = \frac{\frac{k_n f_{y0} t_0^2}{(1-\beta)\sin\theta_1}\left(\frac{2\eta}{\sin\theta_1} + 4\sqrt{1-\beta}\right)}{\gamma_{M5}} \qquad \textbf{\textit{Eq. 9}}$$

- Chord side wall buckling β = 1.0

$$N_{1,Rd} = \frac{\frac{f_b t_0}{\sin\theta_1}\left(\frac{2h_i}{\sin\theta_1} + 10t_0\right)}{\gamma_{M5}} \qquad \textbf{\textit{Eq. 10}}$$

- Brace failure β ≥ 0.85

$$N_{1,Rd} = \frac{f_{y1} t_1 (2h_1 - 4t_1 + 2b_{eff})}{\gamma_{M5}} \qquad \textbf{\textit{Eq. 11}}$$

- Punching shear 0.85 ≤β ≤ (1-1/γ)

$$N_{1,Rd} = \frac{\frac{f_{y0} t_0}{\sqrt{3}\sin\theta_1}\left(\frac{2h_1}{\sin\theta_1} + 2b_{e,p}\right)}{\gamma_{M5}} \qquad \textbf{\textit{Eq. 12}}$$

Since chord face failure is only allowed for β≤0.85, linear interpolation between the value for chord face failure at β=0.85 and the governing value for chord side wall buckling failure at β=1.0 should be considered for higher values of β, as it is stated in EN 1993-1-8 [3]. *Table 13* displays linear interpolation to find chord face failure for β=0.9.

	DBBX_04_SS		DBBX_08_SS		DBBX_12_SS		DBBX_16_SS	
β	**$N_{i,Rd,TENS}$ (kN)**	**$N_{i,Rd,COMP}$ (kN)**	**$N_{i,Rd,TENS}$ (kN)**	**$N_{i,Rd,COMP}$ (kN)**	**$N_{i,Rd,TENS}$ (kN)**	**$N_{i,Rd,COMP}$ (kN)**	**$N_{i,Rd,TENS}$ (kN)**	**$N_{i,Rd,COMP}$ (kN)**
0,2	376,24	376,24	167,22	167,22	301,00	60,20	459,85	41,80
0,4	577,33	577,33	256,59	256,59	554,24	92,37	769,77	64,15
0,6	965,45	965,45	429,09	429,09	1081,30	154,47	1394,53	107,27
0,85	4325,32	2162,66	2594,37	1297,18	3735,89	466,99	4540,14	324,30
0,9	**3471,55**	**1865,13**	**2074,91**	**1071,99**	**2675,39**	**385,24**	**3176,09**	**263,98**
1	1764,00	1270,08	1036,00	621,60	554,40	221,76	448,00	143,36

Table 13 *Linear interpolation to find chord face failure for β higher than 0.85*

Several assumptions shall be taken into account in order to calculate design resistance.

- Node joint is only subjected to axial load i.e. tensile loading and compression loading depending each case. Thus, bending moment influence shall be excluded from calculations.
- θ_1 angle of the braces is 90º, thus $\sin(\theta_1)=1$.
- Resistance of joints in hollow section lattice girder is $\gamma_{M5}=1$
- Since no axial load is trasmitted throughout the chord, n value is 0. Thus, k_n is 1.

Design resistance for each model is considered to be the minimum design axial resitance among all of the failure modes. *Table 14* displays design axial resistance in accordance to En 1993-1-8 [3] formulation. All the values for the different failures modes are attached in "*Appendix B. DESIGN RESISTANCES*".

JOINT	Design of axial resistances			
	Tension (kN)		Compression (kN)	
	$N_{i,Rd,TENS}$	Failure mode	$N_{i,Rd,COMP}$	Failure mode
DBBX_01_SS	376.24	Chord face failure	376.24	Chord face failure
DBBX_02_SS	577.33	Chord face failure	577.33	Chord face failure
DBBX_03_SS	965.45	Chord face failure	965.45	Chord face failure
DBBX_04_SS	1309.43	Punching shear	1270.08	Chord side wall buckling
DBBX_05_SS	167.22	Chord face failure	167.22	Chord face failure
DBBX_06_SS	256.59	Chord face failure	256.59	Chord face failure
DBBX_07_SS	429.09	Chord face failure	429.09	Chord face failure
DBBX_08_SS	727.46	Punching shear	621.60	Chord side wall buckling
DBBX_09_SS	60.20	Chord face failure	60.20	Chord face failure
DBBX_10_SS	92.37	Chord face failure	92.37	Chord face failure
DBBX_11_SS	154.47	Chord face failure	154.47	Chord face failure
DBBX_12_SS	366.64	Punching shear	221.76	Chord side wall buckling
DBBX_13_SS	41.80	Chord face failure	41.80	Chord face failure
DBBX_14_SS	64.15	Chord face failure	64.15	Chord face failure
DBBX_15_SS	107.27	Chord face failure	107.27	Chord face failure
DBBX_16_SS	290.98	Punching shear	143.36	Chord side wall buckling

Table 14 *Design resistance values for each model taking into account EN 1993-1-8*

5.1.2 Design resistances according to J.S. Owen

Design resistances according to J.S. Owen are obtained from following formulation:

$$F_{u1} = \frac{f_{y0}}{1000}\left(\frac{f_{y0}}{275}\right)^{0.8} \frac{(6.06 - 5.6\beta + 11.4\beta^2)(0.6 + 1.97\sqrt{\beta})t_0^2}{\frac{t_0}{b_0}(6.06 - 5.6\beta + 11.4\beta^2) + \frac{1}{3}(0.6 + 1.97\sqrt{\beta})} \qquad \textbf{\textit{Eq. 13}}$$

Table 15 displays design axial resistance in accordance to J.S. Owen formulation.

JOINT	F_{u1} (kN)
DBBX_01_SS	494.33
DBBX_02_SS	564.45
DBBX_03_SS	665.58
DBBX_04_SS	875.41
DBBX_05_SS	266.01
DBBX_06_SS	298.47
DBBX_07_SS	353.54
DBBX_08_SS	477.34

JOINT	F_{u1} (kN)
DBBX_09_SS	115.184
DBBX_10_SS	126.675
DBBX_11_SS	150.818
DBBX_12_SS	209.947
DBBX_13_SS	84.261
DBBX_14_SS	92.089
DBBX_15_SS	109.813
DBBX_16_SS	154.354

Table 15 *Design resistance values for each model taking into account J.S. Owen formulation*

5.1.3 Comparison of design resistances

It shall be of high importance to study the relative difference between different formulations in terms of percentages. Those percentages are calculated as follows:

$$Relative\ difference\ (\%)_{EN} = \frac{ABAQUS - EN}{EN} \cdot 100 \qquad \textbf{Eq. 14}$$

$$Relative\ difference\ (\%)_{Owen} = \frac{ABAQUS - J.S.Owen}{J.S.Owen} \cdot 100 \qquad \textbf{Eq. 15}$$

If design resistance obtained from ABAQUS modelization is larger than those of formulations previously mentioned, relative difference is positive and safety side is met. Otherwise, if design resistance from ABAQUS is lower than those values of formulations previously mentioned, relative difference is negative and insafety side is met. It is expected that most of the models are at the safety side.

Results for design resistances for ABAQUS, EN 1993-1-8 formulation and J.S. Owen et. al. Formulation for each model subjected to compression loading are listed in *Table 16*, whereas design resistances for each models subjected to axial tensile loading are listed in *Table 17*.

Results for models under compression loading will be discussed and analysed in "*5.3 ANALYSIS OF RESULTS: COMPRESSION LOADING*", whereas results for models subjected to tensile loading will be discussed in "*5.4 ANALYSIS OF RESULTS: TENSIILE LOADING*".

JOINT	Compression (kN)		
	ABAQUS	EN 1993-1-8	J.S. Owen
DBBX_01_SS	706,12	376,24	494,33
DBBX_02_SS	829,57	577,33	564,45
DBBX_03_SS	2484,84	965,45	665,58
DBBX_04_SS	1854,58	1270,08	875,41
DBBX_05_SS	380,17	167,22	266,01
DBBX_06_SS	406,93	256,59	298,47
DBBX_07_SS	1562,32	429,09	353,54
DBBX_08_SS	854,18	621,60	477,34
DBBX_09_SS	146,11	60,20	115,18
DBBX_10_SS	163,95	92,37	126,68
DBBX_11_SS	747,25	154,47	150,82
DBBX_12_SS	786,52	221,76	209,95
DBBX_13_SS	105,65	41,80	84,26
DBBX_14_SS	118,02	64,15	92,09
DBBX_15_SS	544,64	107,27	109,81
DBBX_16_SS	564,18	143,36	154,35

Table 16 *Comparison of design axial resistances under compression loading*

JOINT	Tension (kN)		
	ABAQUS	EN 1993-1-8	J.S. Owen
DBBX_01_SS	1162.76	376.24	494.33
DBBX_02_SS	1157.29	577.33	564.45
DBBX_03_SS	3486.48	965.45	665.58
DBBX_04_SS	4001.41	1309.43	875.41
DBBX_05_SS	775.18	167.22	266.01
DBBX_06_SS	1547.74	256.59	298.47
DBBX_07_SS	2324.73	429.09	353.54
DBBX_08_SS	2682.92	727.46	477.34
DBBX_09_SS	465.31	60.20	115.18
DBBX_10_SS	929.17	92.37	126.68
DBBX_11_SS	1394.78	154.47	150.82
DBBX_12_SS	1742.20	366.64	209.95
DBBX_13_SS	387.74	41.80	84.26
DBBX_14_SS	774.99	64.15	92.09
DBBX_15_SS	1162.10	107.27	109.81
DBBX_16_SS	1408.86	290.98	154.35

Table 17 *Comparison of design axial resistances under tensile loading*

5.2 ANALYSIS OF RESULTS: COMPRESSION LOADING

As stated in previous paragraphs, compression results will be analysed form different points of view:

1) Overview analysis and summary of obtained results under compression loading
2) Analysis of F_u-β curves of obtained results in the current thesis and comparison to EN 1993-1-8 [3] formulation as well as J.S. Owen empirically formulation in terms of the overall performance and relative error between different formulations with respect to ABAQUS results
3) Idem as previous point for F_u-2γ curve.
4) Analysis of Load-displacement curves of obtained results in this thesis for both β dependance as well as 2γ dependance and failure modes under compression loading

5.2.1 Design resistance dependance on β and 2γ under compression loading

Design resistance dependance on β and 2γ is displayed in *Table 18*. On the one hand, dependance on β parameter shall be read along rows i.e. for a fixed value of parameter 2γ. On the other hand, dependance on 2γ parameter shall be read along columns i.e. for a fixed value of parameter β.

		β			
		0,2	**0,4**	**0,6**	**0,9**
2γ	**10**	DBBX_01_SS 706.12 kN	DBBX_02_SS 829.57 kN	DBBX_03_SS 2484.84 kN	DBBX_04_SS 1854,58 kN
	15	DBBX_05_SS 380.17 kN	DBBX_06_SS 406.93 kN	DBBX_07_SS 1562.32 kN	DBBX_08_SS 854,18 kN
	25	DBBX_09_SS 146.11 kN	DBBX_10_SS 163.95 kN	DBBX_11_SS 747.25 kN	DBBX_12_SS 786,52
	30	DBBX_13_SS 105.65 kN	DBBX_14_SS 118.02 kN	DBBX_15_SS 544.64 kN	DBBX_16_SS 564.18 kN

Table 18 *Summary of the combined analysis for parameters β and 2γ under compression loading*

As it is visible in *Table 18*, if β increases, which means brace width increases as well, design resistance of the joint is higher. On the contrary, if 2γ increases, which means thickness of the brace decreases, design resistance of the joint is lower. Results are almost consistent for all the models. However, for the particular cases of {β=0,9; 2γ=10} and {β=0,9;2γ=15} results are not consistent with the overall analysis, thus design resistances are lower than results for β=0,6. A summary of perfomance variation of parameter β is visible in *Figure 38*, whereas performance of parameter 2γ for all models is displayed in *Figure 39*.

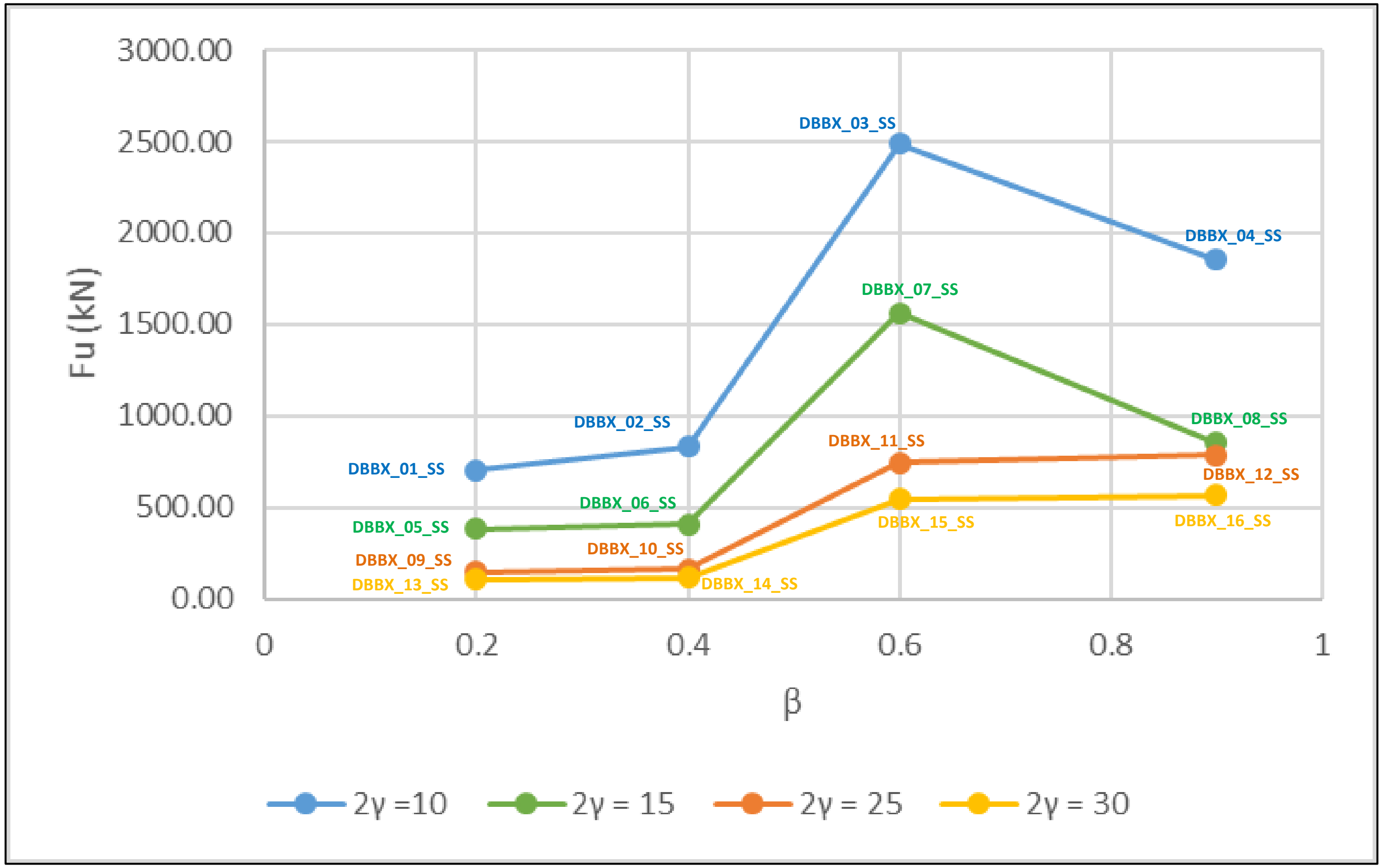

Figure 38 *Performance of β variation for all models under compression loading*

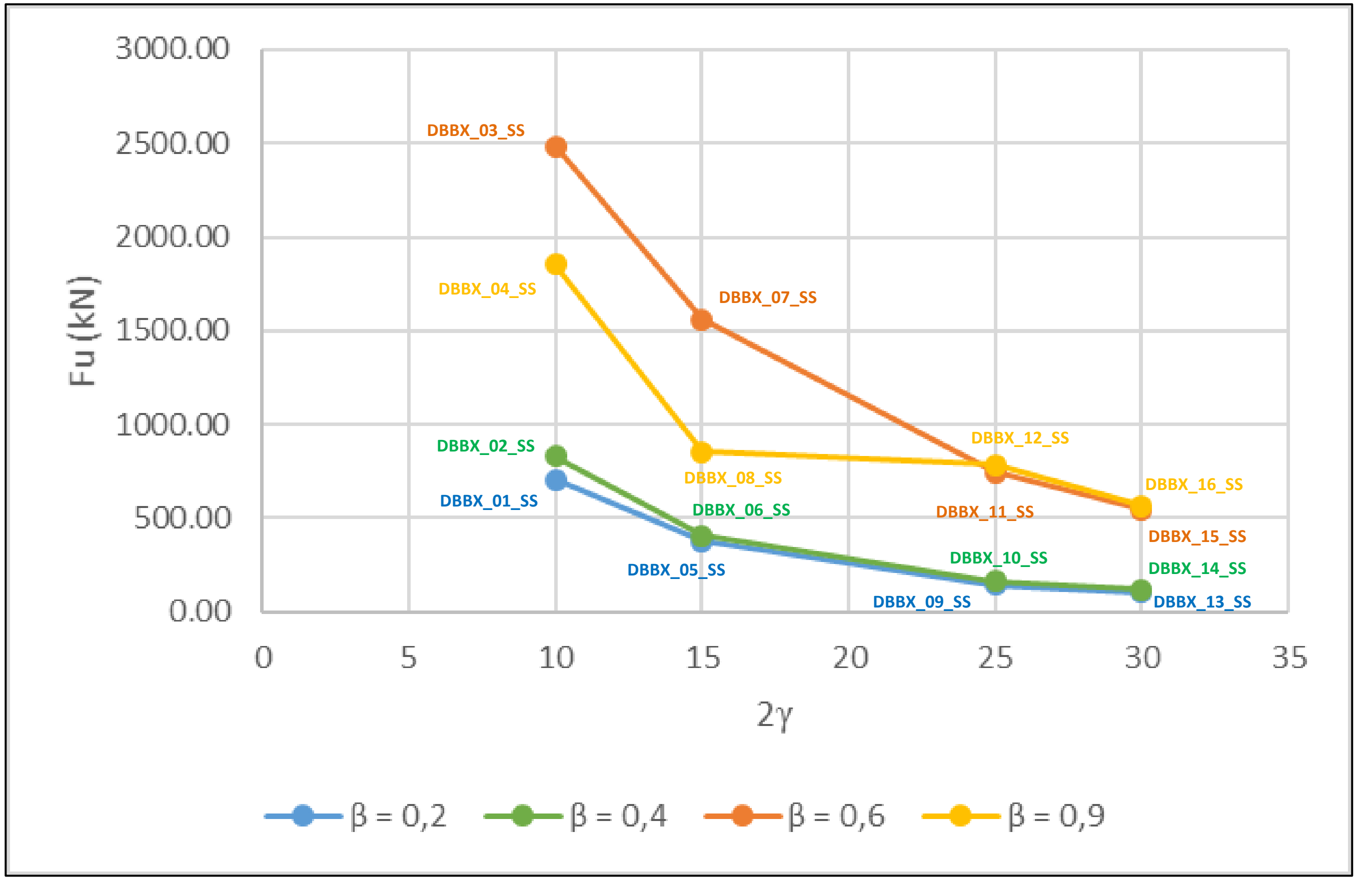

Figure 39 *Performance of 2γ variation for all models under compression loading*

As it is visible in *Figure 38* and *Figure 39*, results fo DBBX_04_SS and DBBX_08_SS which corresponds to {β=0,9;2γ=10} and {β=0,9;2γ=15} subjected to compression loading are not consistent with the overall analysis. Expected theoretical performance of the analysis for all the models is displayed in *Figure 40* (β dependence) and *Figure 41* (2γ dependence), where dashed line is the expected trend of the joint.

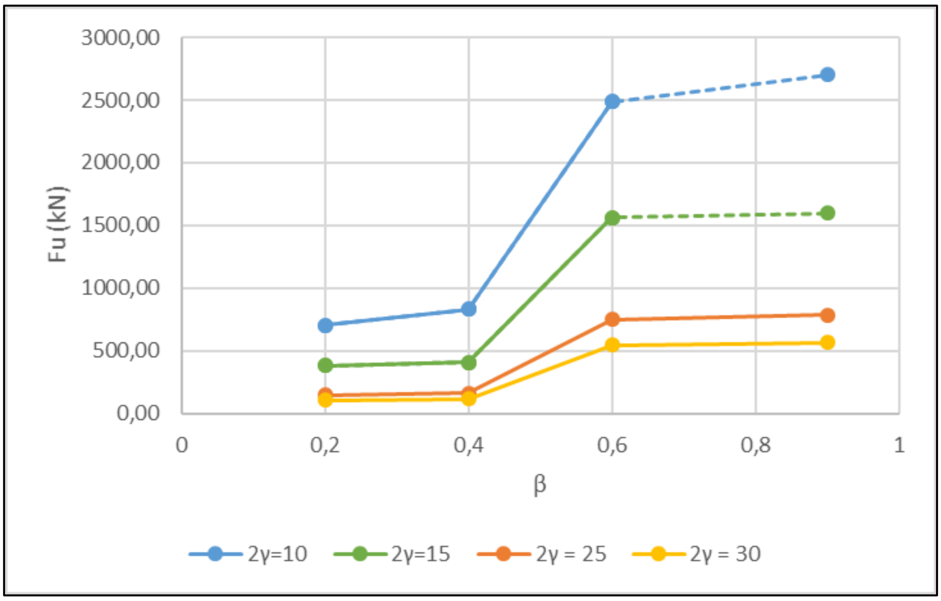

Figure 40 *Expected performance of β variation for all models under compression loading*

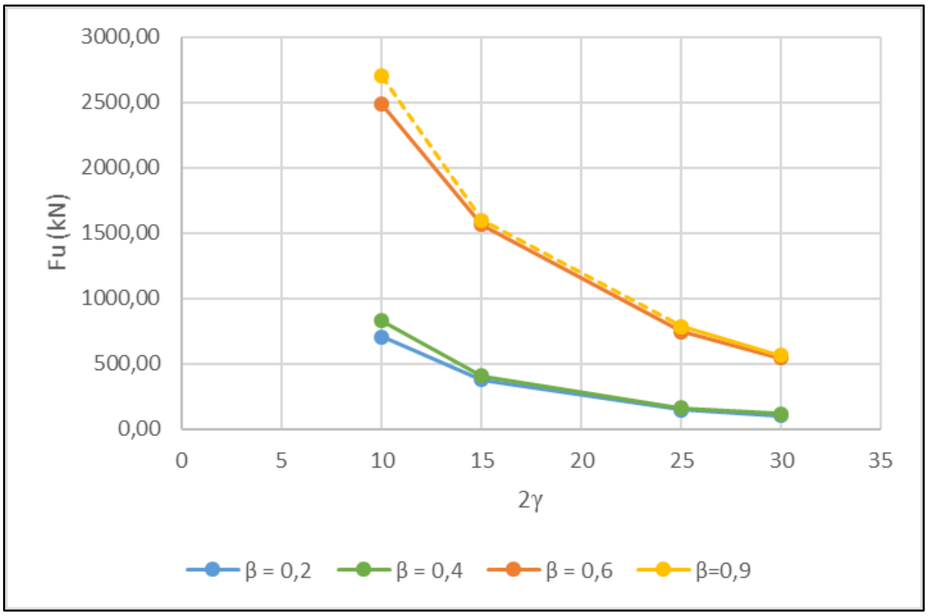

Figure 41 *Expected performance of 2γ variation for all models under compression loading*

5.2.2 Analysis of F_u-β under compression loading

This paragraph analyses design resistances dependence on β parameter for a fixed value of 2γ.

2γ=10

For a fixed 2γ=10, DBBX_01_SS, DBBX_02_SS, DBBX_03_SS and DBBX_04_SS are analysed. As it is displayed in *Figure 46*, for β=0,2 (b_1=30mm) and β=0,4 (b_1=60mm), design resistances obtained are close to both EN 1993-1-8 [3] as well as J.S. Owen et. al formulations and they are at the safety side. However, for β=0,6 (b_1=90mm) obtained results for design resistances are much higher than those of EN 1993-1-8 [3] as well as J.S. Owen et. al formulations, which might be explained because theoretical failure mode is different from the failure mode of the modelled joint. Thus, lower values of β are suitable to bibliography formulations.

As stated in "*5.2.1 Design resistance dependance on β and 2γ under compression loading*" results for DBBX_04_SS {β=0,9; 2γ=10} are not consistent with overall analysis, thus its design resistance should be higher than design resistance for DBBX_03_SS {β=0,6; 2γ=10}. Relative difference for those models is displayed in *Figure 42*.

2γ=15

Similar performance is obtained for a fixed value of 2γ=15 and results are displayed in *Figure 47*. Low values of parameter β derives to suitable results in comparison to bibliography formulation, whereas β=0,6 results in much higher design resistance than those of EN 1993-1-8 [3] as well as J.S. Owen et. al formulations, which might be explained because theoretical failure mode is different from the failure mode of the modelled joint.

As stated in "*5.2.1 Design resistance dependance on β and 2γ under compression loading*" results for DBBX_08_SS {β=0,9; 2γ=15} are not consistent with overall analysis, thus its design resistance should be higher than design resistance for DBBX_07_SS {β=0,6; 2γ=15}. Relative difference for those models is displayed in *Figure 43*.

2γ=25

For a constant value of 2γ=25, DBBX_09_SS, DBBX_10_SS, DBBX_11_SS and DBBX_12_SS are analysed. As it is displayed in *Figure 48*, for β=0,2 (b_1=30mm) and β=0,4 (b_1=60mm), design resistances obtained are close to both EN 1993-1-8 [3] as well as J.S. Owen et. al formulations and they are at the safety side. However, for β=0,6 (b_1=90mm) and β=0,9 (b_1=135mm), obtained results for design resistances are much higher than those of EN 1993-1-8 [3] as well as J.S. Owen et. al formulations, which might be explained because theoretical failure mode is different from the failure mode of the modelled joint. Thus, lower values of β are suitable to bibliography formulations.

Relative difference for those models is displayed in *Figure 44*.

2γ=30

Finally, DBBX_13_SS, DBBX_14_SS, DBBX_15_SS and DBBX_16_SS are analysed. As it is displayed in *Figure 49*, for β=0,2 (b_1=30mm) and β=0,4 (b_1=60mm), design resistances obtained are close to both EN 1993-1-8 [3] as well as J.S. Owen et. al formulations and they are at the safety side. However, for β=0,6 (b_1=90mm) and β=0,9 (b_1=135mm), obtained results for design resistances are much higher than those of EN 1993-1-8 [3] as well as J.S. Owen et. al formulations, which might be explained because theoretical failure mode is different from the failure mode of the modelled joint. Thus, lower values of β are suitable to bibliography formulations.

Relative difference for those models is displayed in *Figure 45*.

RELATIVE DIFFERENCES BETWEEN FORMULATIONS

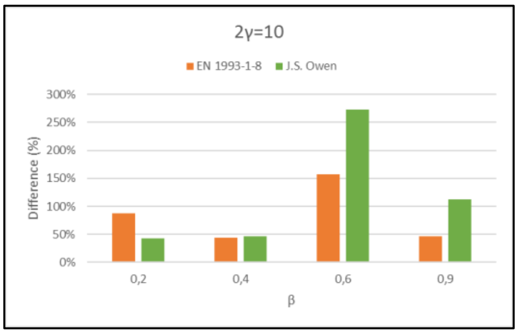

Figure 42 *Relative error design resistance in dependance on parameter β and constant parameter 2γ=10 under compression load*

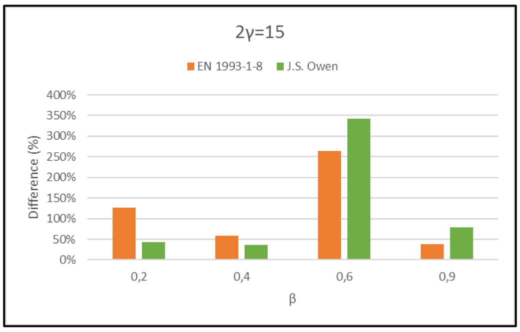

Figure 43 *Relative error design resistance in dependance on parameter β and constant parameter 2γ=15 under compression load*

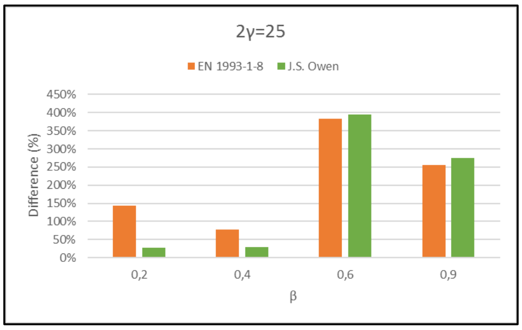

Figure 44 *Relative error design resistance in dependance on parameter β and constant parameter 2γ=25 under compression load*

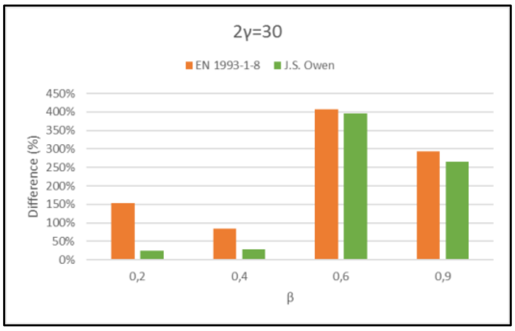

Figure 45 *Relative error design resistance in dependance on parameter β and constant parameter 2γ=30 under compression load*

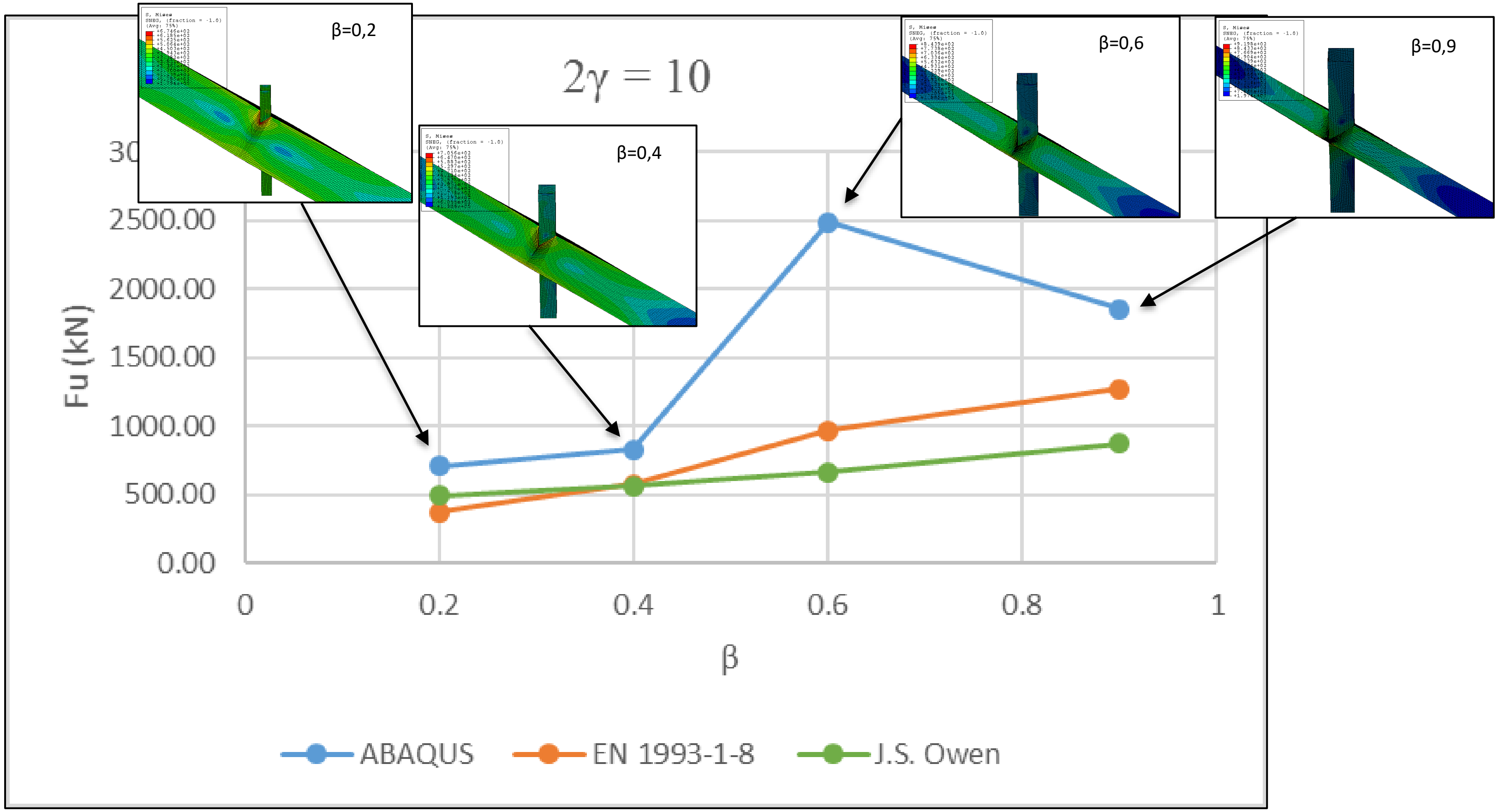

Figure 46 *Comparison of design resistances dependance on parameter β for 2γ=10 under compression loading*

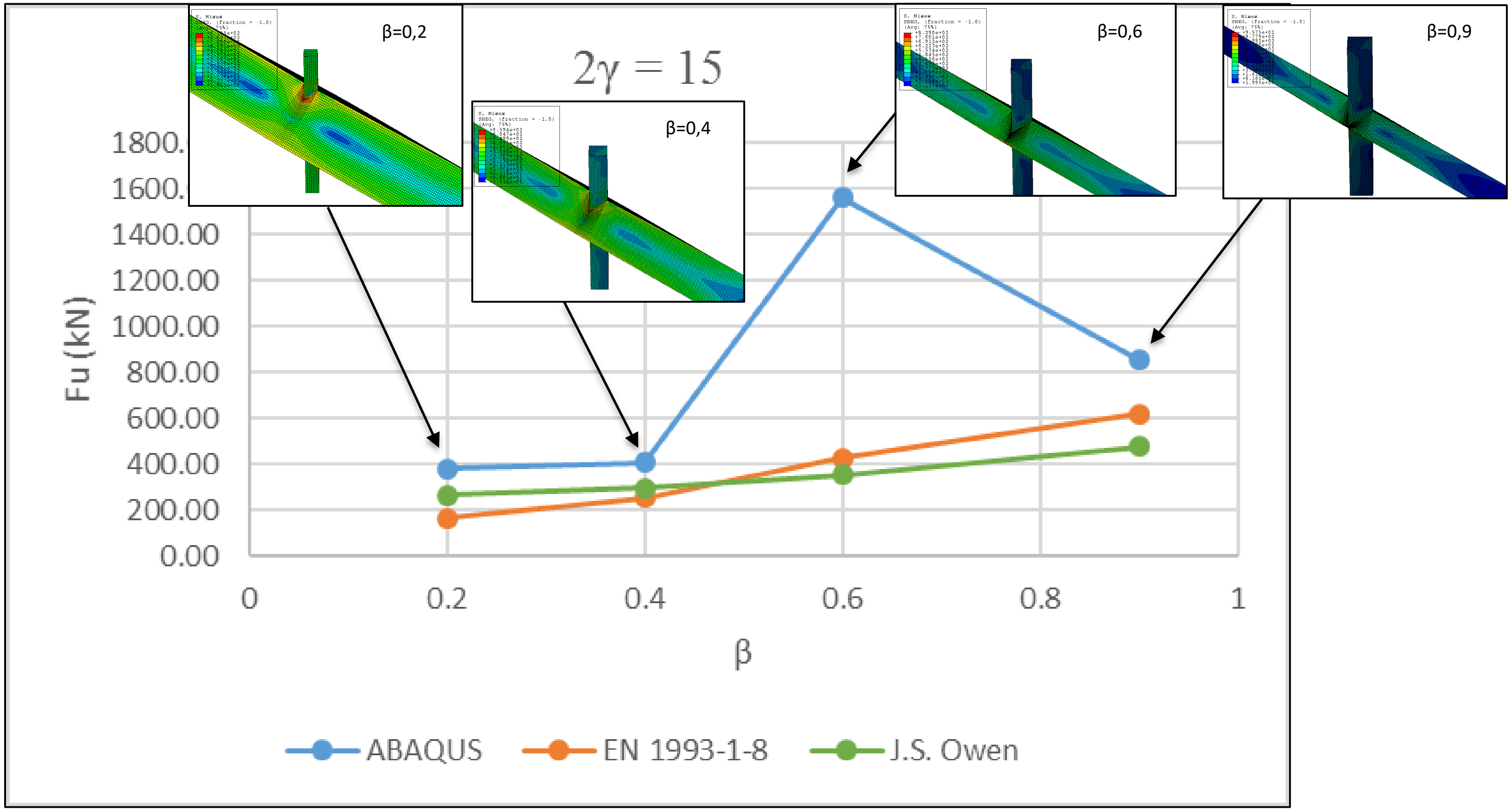

Figure 47 *Comparison of design resistances dependance on parameter β for 2γ=15 under compression loading*

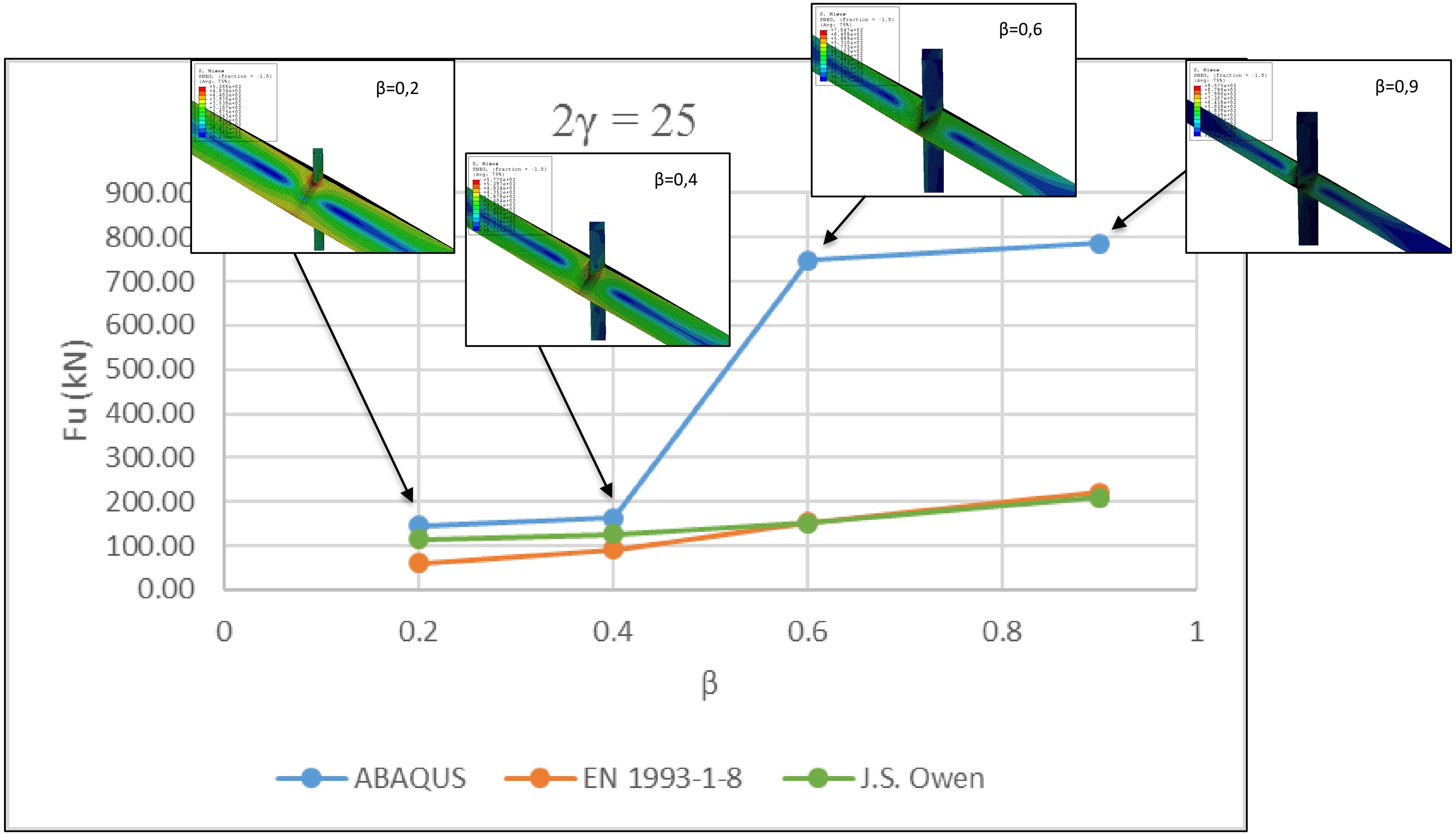

Figure 48 *Comparison of design resistances dependance on parameter β for 2γ=25 under compression loading*

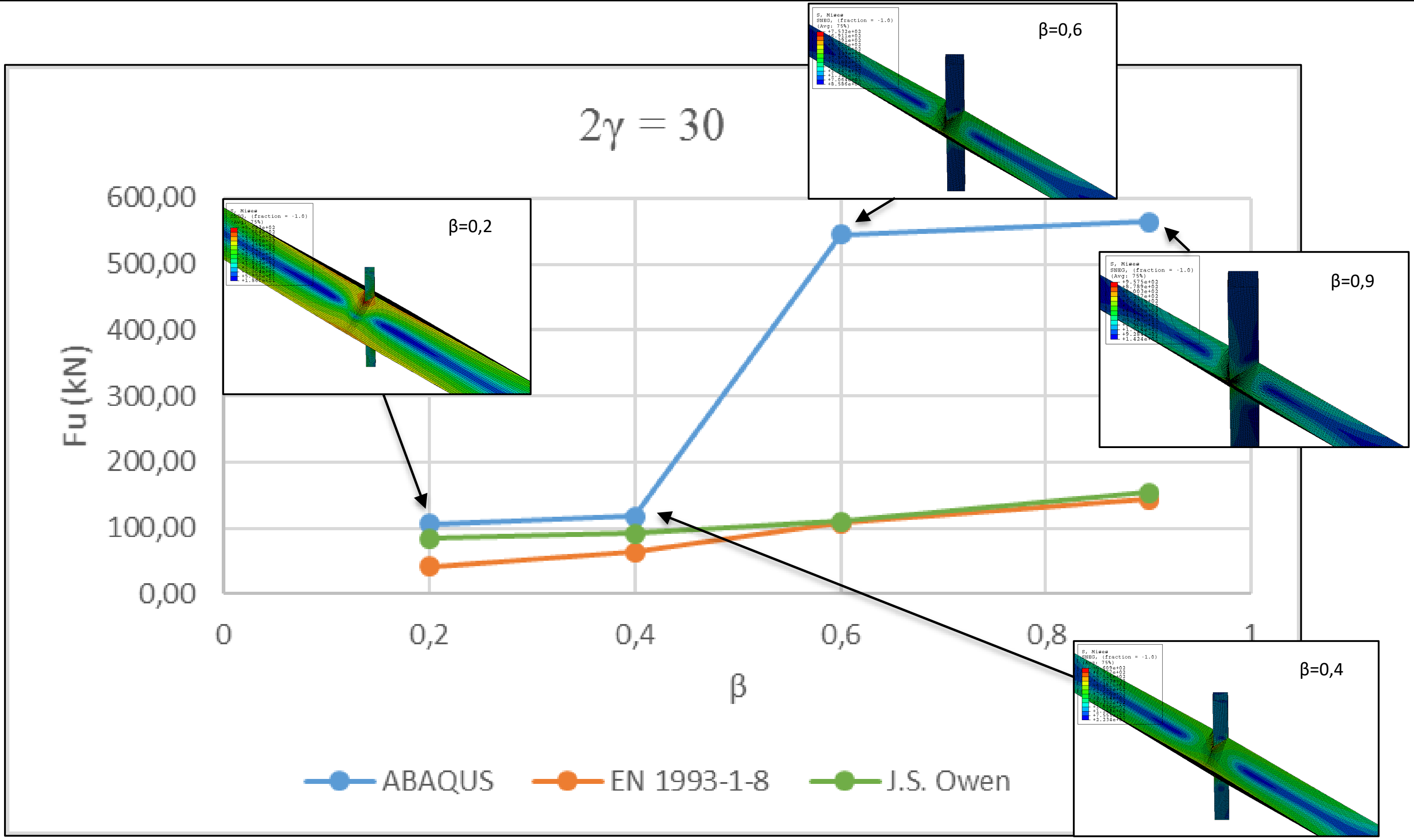

Figure 49 *Comparison of design resistances dependance on parameter β for 2γ=30 under compression loading*

5.2.3 Analysis of F_u-2γ under compression loading

This paragraph analyses design resistances dependance on 2γ parameter for a fixed value of β.

β=0,2

Design resistances for a constant parameter β=0,2, which corresponds to DBBX_01_SS, DBBX_05_SS_ DBBX_09_SS and DBBX_13_SS models, is displayed in *Figure 54*. As it is visible, curve trend is similar to curves obtained from EN 1993-1-8 [3] as well as owen formulations. Furthermore, relative difference between formulations concludes that 2γ dependance for β=0,2 of obtained results are set as being on the safety side.

Relative difference is displayed in *Figure 50*.

β=0,4

Design resistance for the particular case of β=0,4, which corresponds to DBBX_02_SS, DBBX_06_SS_ DBBX_10_SS and DBBX_14_SS models, is displayed in *Figure 55*. Similar performance results are achieved, thus not only curve trend is similar to curves obtained from EN 1993-1-8 [3] as well as owen formulations, but also safety side is met.

Relative difference is displayed in *Figure 51*.

β=0,6

For the particular case of β=0,6, models DBBX_03_SS, DBBX_07_SS, DBBX_11_SS and DBBX_15_SS are analysed and displayed in *Figure 56*. Results are consistent and trend is similar to bibliography formulations. Thus, design resistances are higher as expected and, therefore, safety side is met.

Relative difference is displayed in *Figure 52*.

β=0,9

Design resistances for a fixed value of β=0,9 are displayed in *Figure 57*, which corresponds to models DBBX_04_SS, DBBX_08_SS, DBBX_12_SS and DBBX_16_SS. As stated in previous paragraphs, results for DBBX_04_SS and DBBX_08_SS are not consistent with the overall analysis.

Relative difference is displayed in *Figure 53*.

RELATIVE DIFFERENCES BETWEEN FORMULATIONS

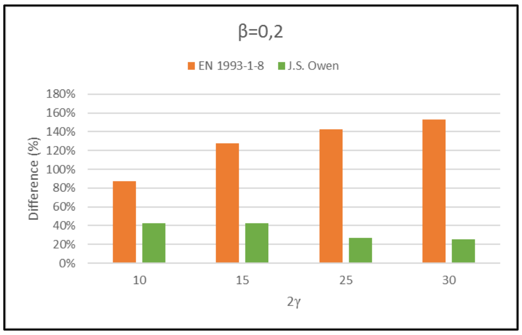

Figure 50 *Relative error design resistance in dependance on parameter 2γ and constant parameter β=0,2 under compression load*

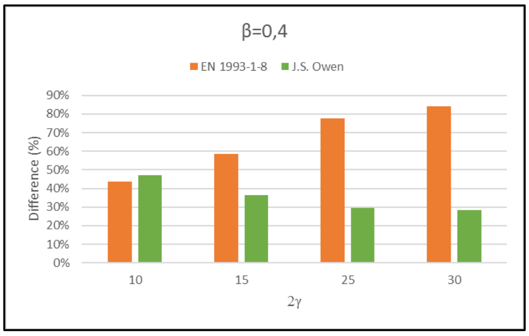

Figure 51 *Relative error design resistance in dependance on parameter 2γ and constant parameter β=0,4 under compression load*

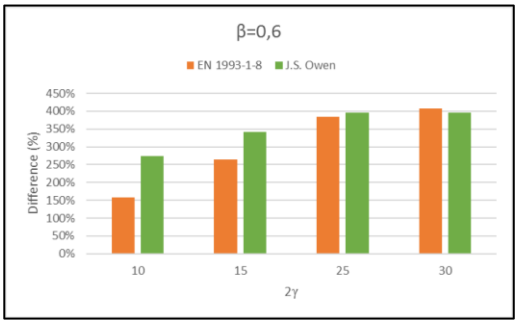

Figure 52 *Relative error design resistance in dependance on parameter 2γ and constant parameter β=0,6 under compression load*

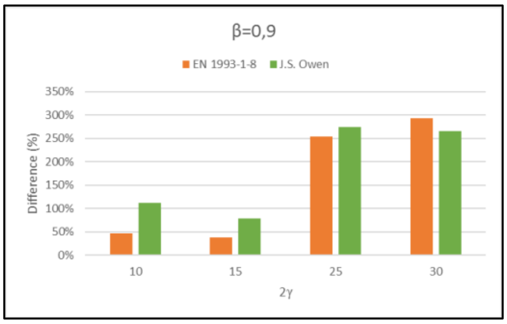

Figure 53 *Relative error design resistance in dependance on parameter 2γ and constant parameter β=0,9 under compression load*

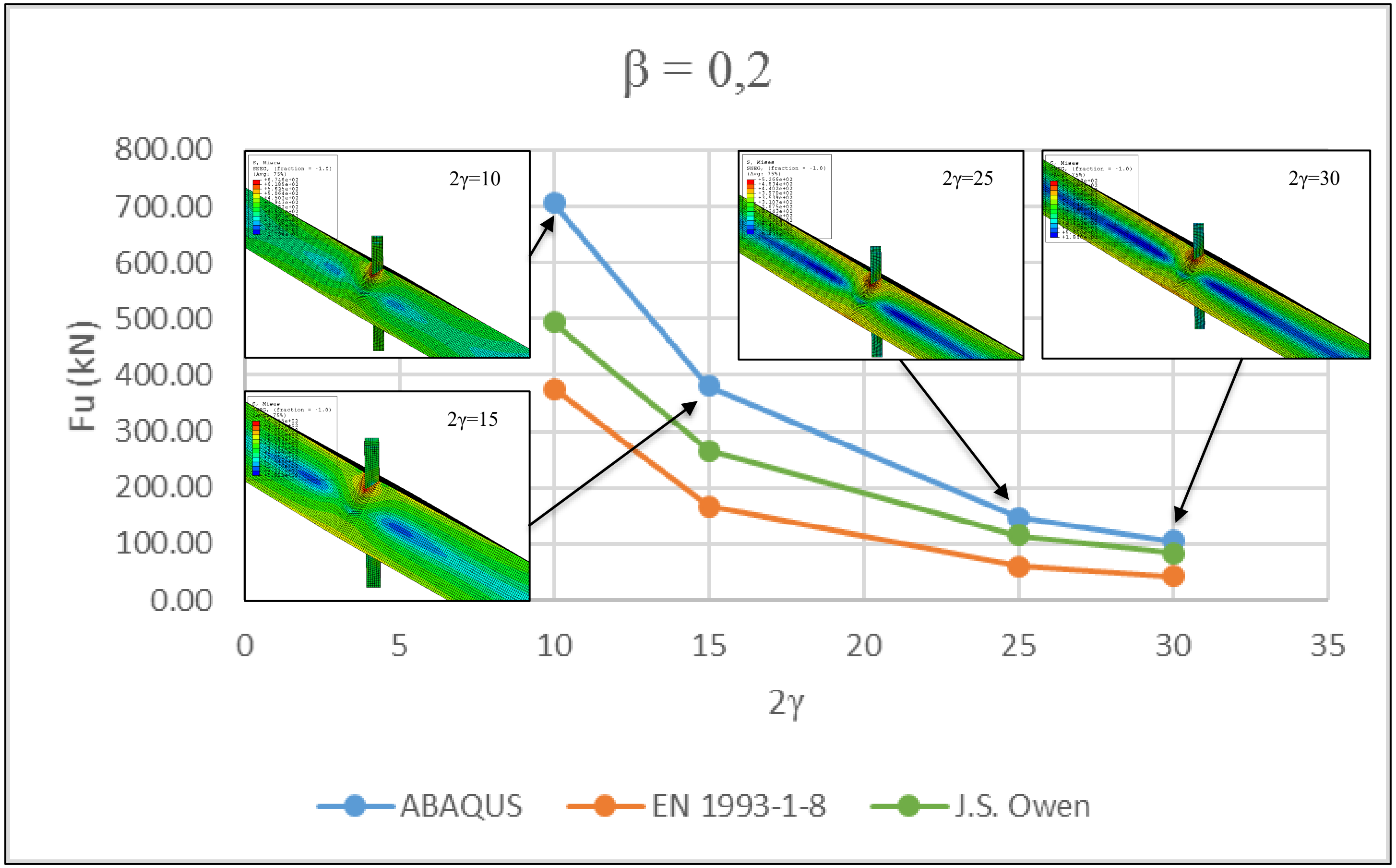

Figure 54 *Comparison of design resistances dependance on parameter 2γ for β=0,2 under compression loading*

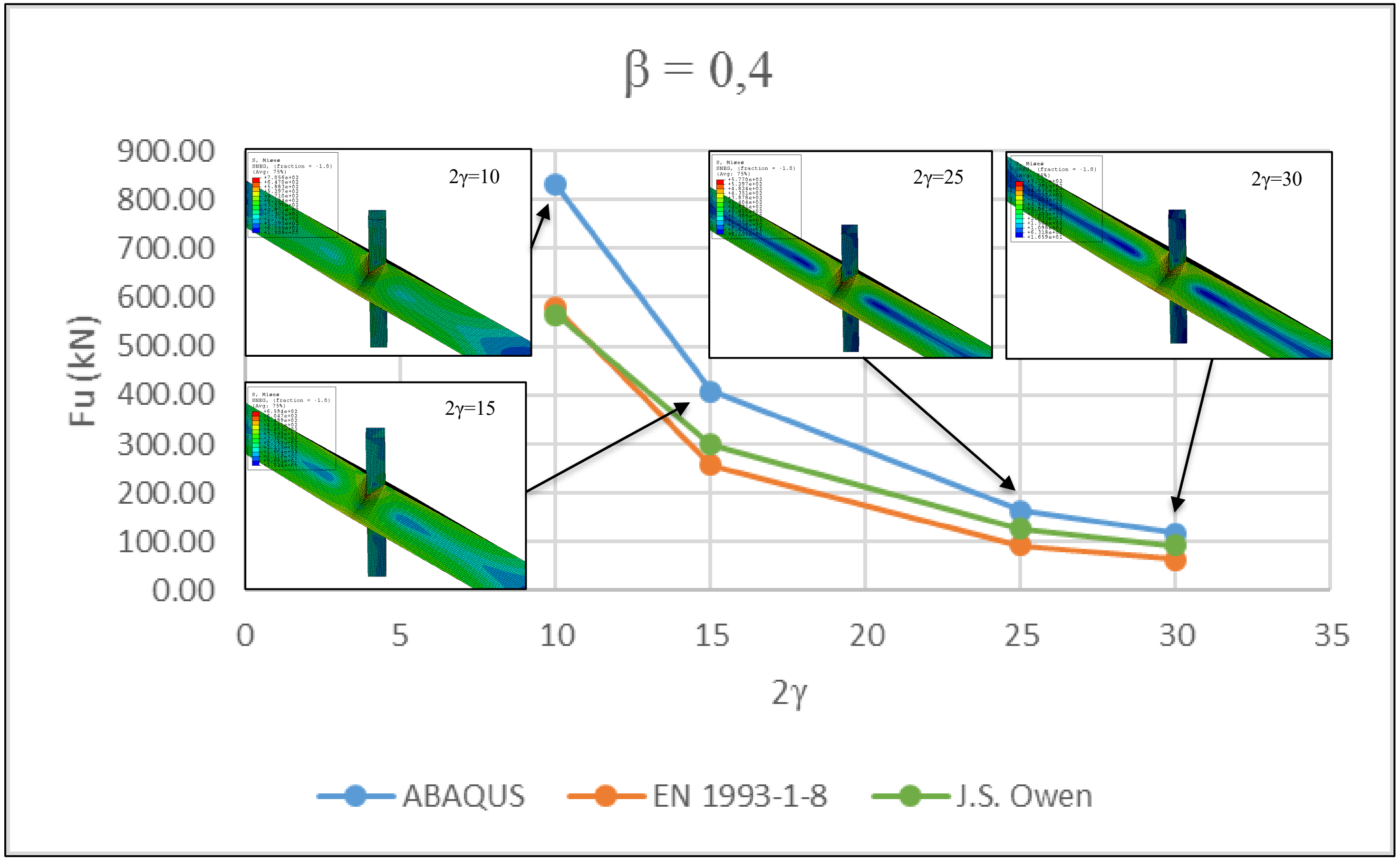

Figure 55 *Comparison of design resistances dependance on parameter 2γ for β=0,4 under compression loading*

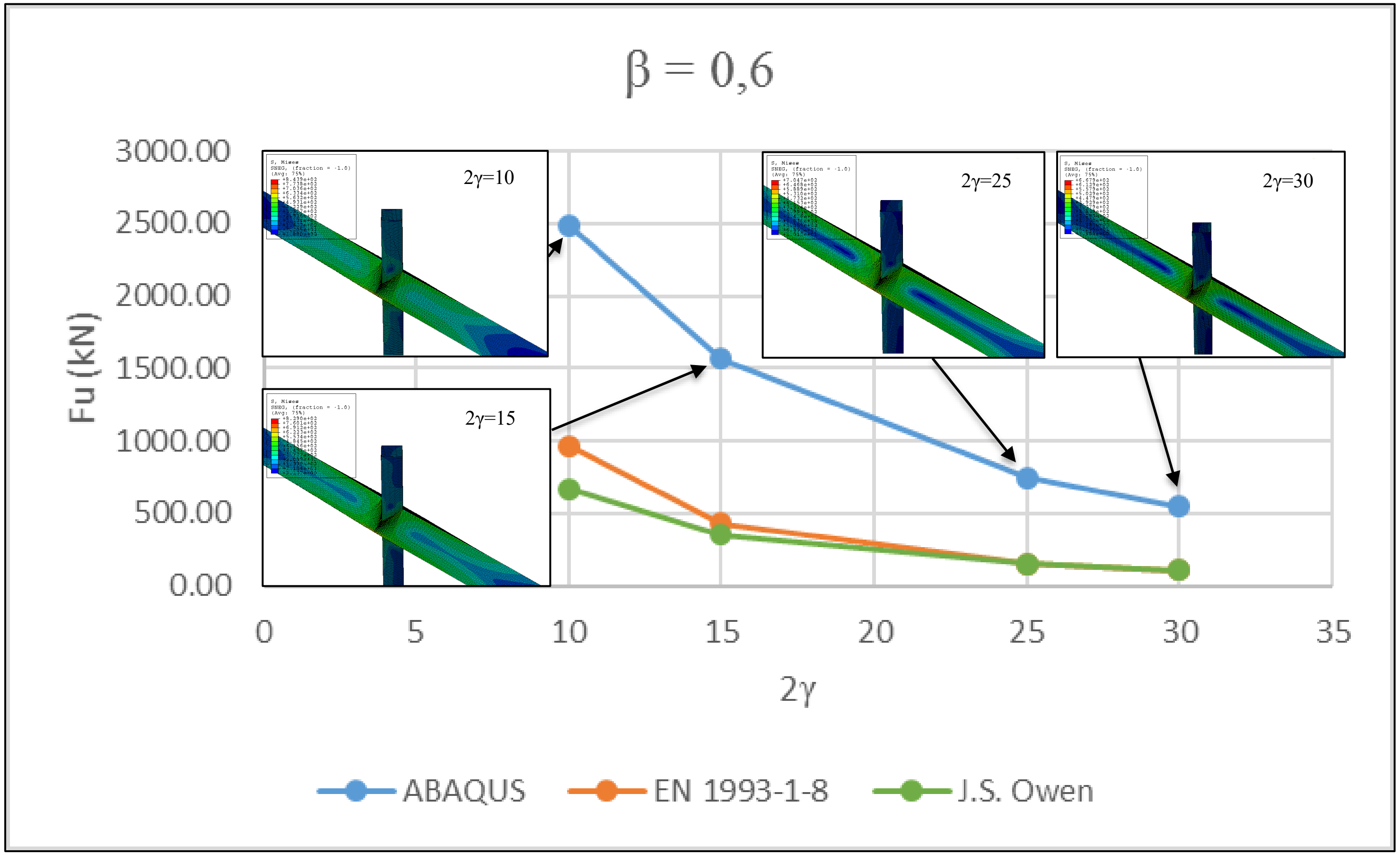

Figure 56 *Comparison of design resistances dependance on parameter 2γ for β=0,6 under compression loading*

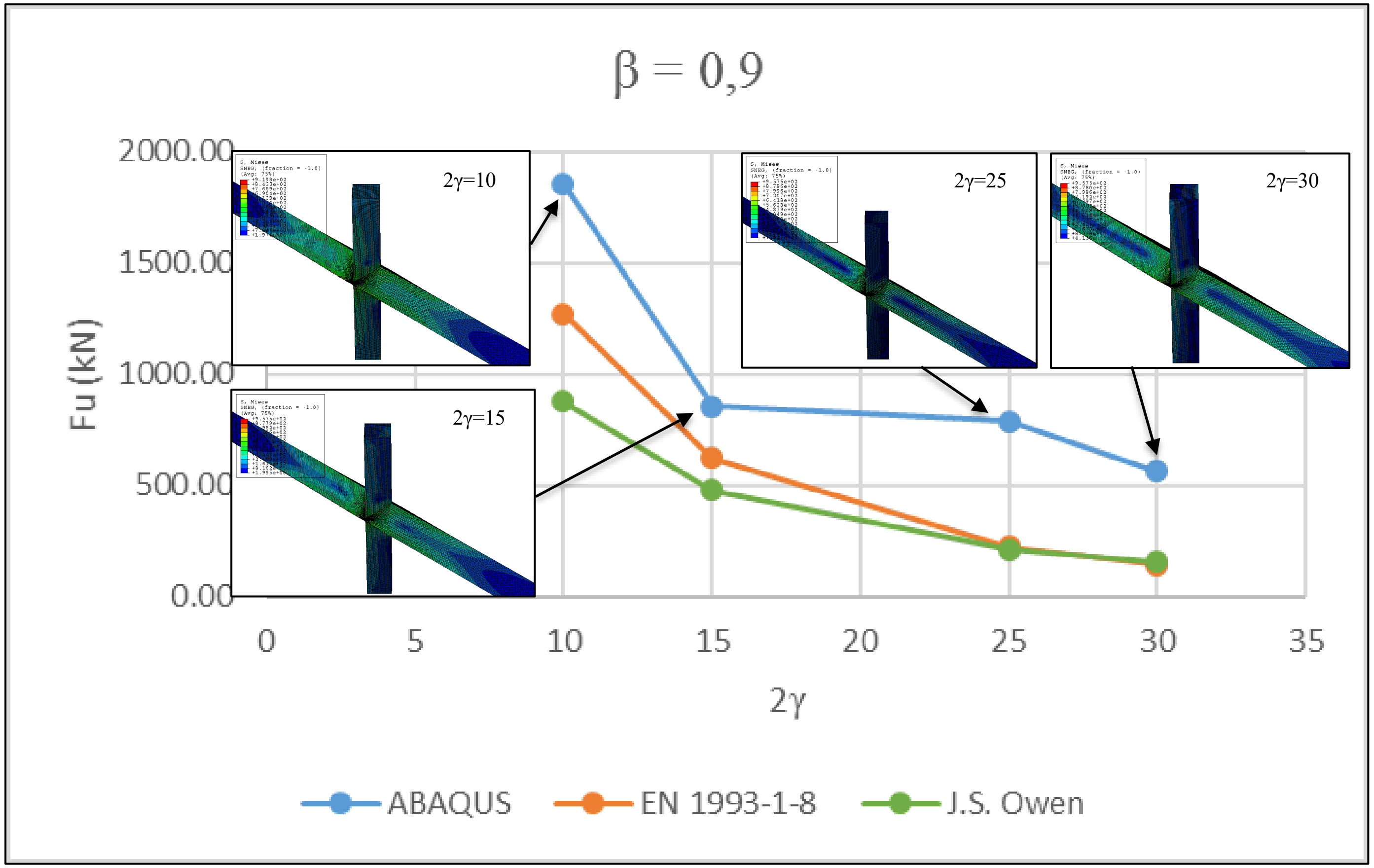

Figure 57 *Comparison of design resistances dependance on parameter 2γ for β=0,9 under compression loading*

5.2.4 Analysis of load-displacement curves under compression loading

One aspect that is equally important and is not visible in F_u-β and F_u-2γ curves is load-displacement performance of the joints.

5.2.4.1 Load-displacement dependance on β

As β increases (brace width increases), joint is able to resist higher loads, thus ultimate resistance is higher. If β increases, ultimate strength is achieved at higer values of displacement, thus increasing brace width implies achieving a more ductile joint. After ultimate resistance is achieved, load-displacement curves decreases slowly, almost constant.

Figure 58 displays load-displacement curves dependance on parameter β for a constant value of 2γ=10 as a representative performance of the joint. Load-displacement curves for all models are displayed in "*Appendix D. PARAMETRIC RESULTS*".

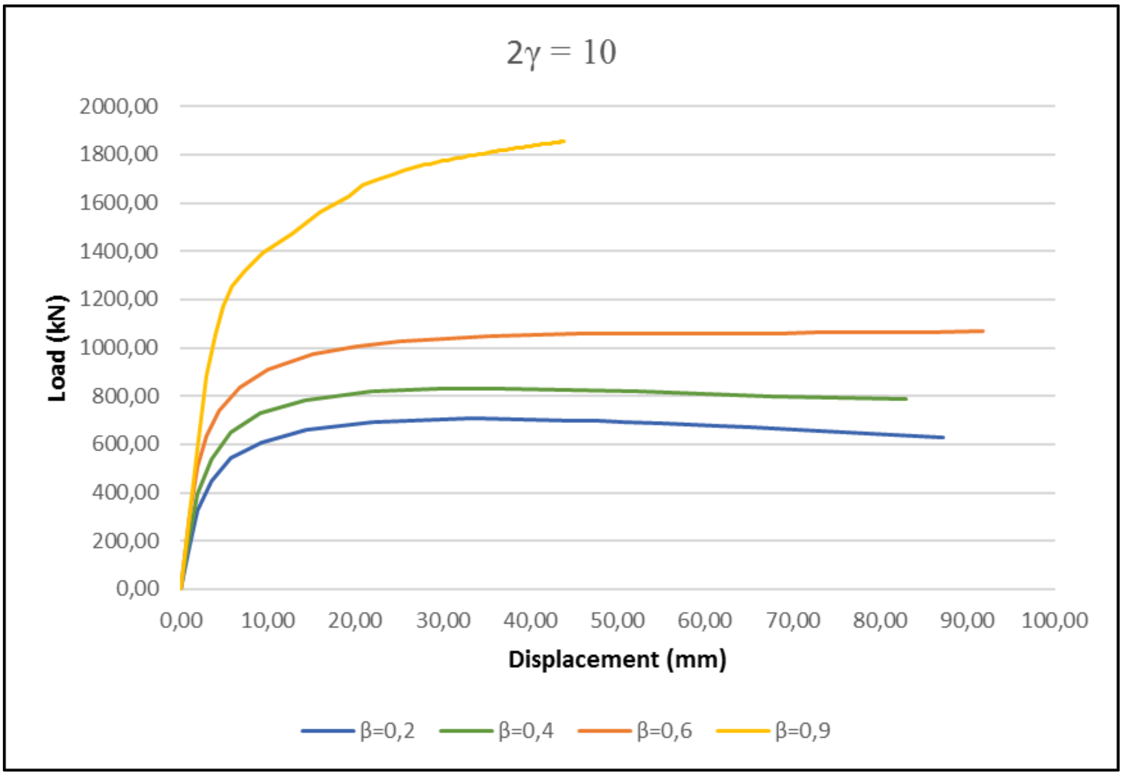

***Figure 58** Load-displacement curves for variation of parameter β for 2γ=10 under compression loading*

5.2.4.2 Load-displacement dependance on 2γ

As 2γ increseas, thickness of the chord decrease and, therefore, ultimate resistance decreases. On the one hand, for models with low values of 2γ i.e. DBBX_01_SS (2γ=10) and DBBX_05_SS (2γ=15); load decreases gradually after achieving ultimate resistance.

On the other hand, for models with high values of 2γ i.e. DBBX_09_SS (2γ=25) and DBBX_13_SS (2γ=30); load is almost constant after reaching ultimate strength. If 2γ increases, ultimate strength is achieved at lower values of displacement, thus decreasing thickness implies achieving a more brittle joint under compression loading.

Figure 59 shows load-displacement curves dependance on parameter 2γ for a constant value of β=0,2 as a representative performance. Load-displacement curves for all models are displayed in "*Appendix D. PARAMETRIC RESULTS*".

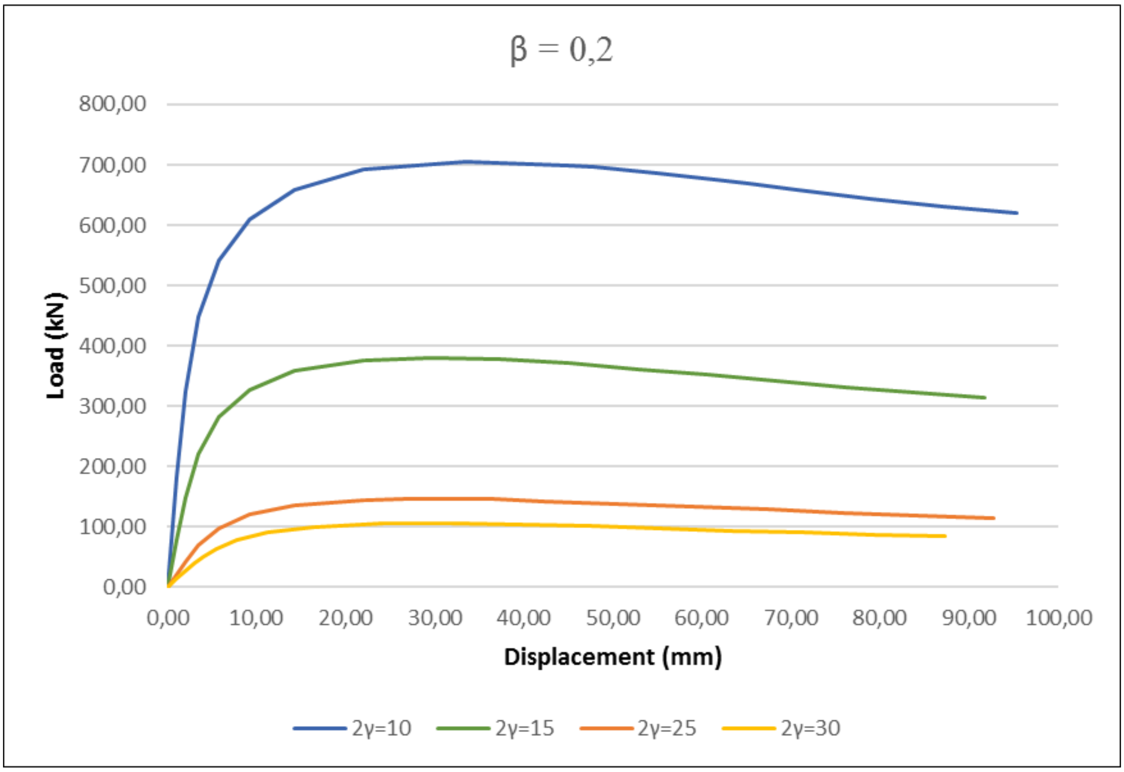

Figure 59 *Load-displacement curves for variation of parameter 2γ for β=0,2 under compression loading*

5.2.4.3 Failure modes

Compression in the brace derives to punching of the chord, which leads to the ultimate failure mode of the chord. Theoretical punching of the chord is explained in paragraph "*2.5.5 Failure modes for hollow section joints*" and is displayed in *Figure 60*, whereas *Figure 61* displays failure of a modelled diamond bird-beak joint under compression loading by means of the finite element method.

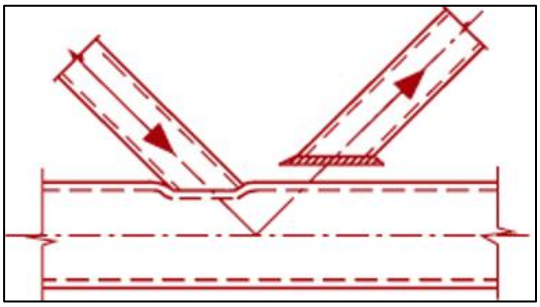

Figure 60 *Theoretical failure mode of punching of wall chord for diamond bird-beak joint under compression loading*

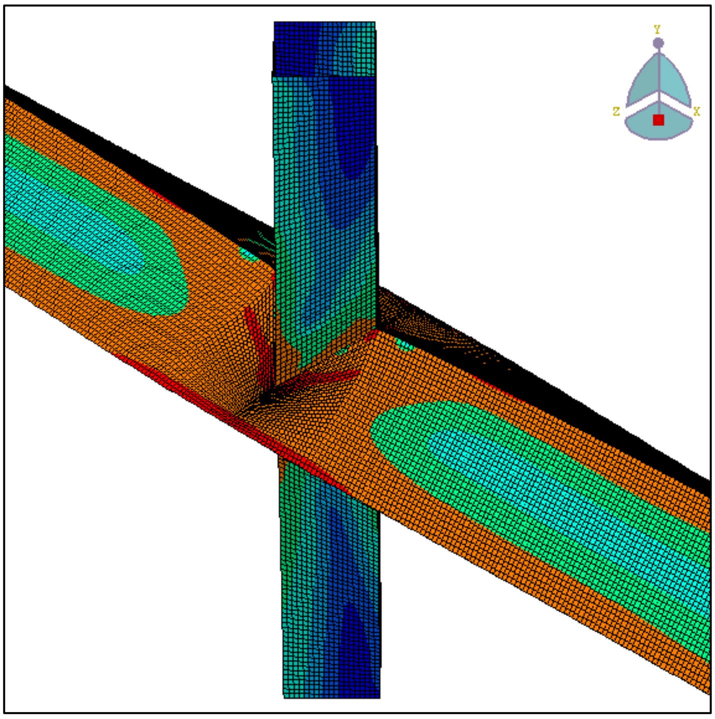

Figure 61 *Failure mode of punching of wall chord for diamond bird-beak joint under compression loading*

5.3 ANALYSIS OF RESULTS: TENSIILE LOADING

The same analysis of tensile loading results as compression results will be described in the current paragraph.

1) Overview analysis and summary of obtained results under tensile loading
2) Analysis of F_u-β curves of obtained results in the current thesis and comparison to EN 1993-1-8 [3] formulation as well as J.S. Owen empirically formulation in terms of the overall performance and relative error between different formulations with respect to ABAQUS results
3) Idem as previous point for F_u-2γ curve.
4) Analysis of Load-displacement curves of obtained results in this thesis for both β dependence as well as 2γ dependence and failure modes under tensile loading

5.3.1 Design resistance dependance on β and 2γ under tensile loading

Design resistance dependance on β and 2γ is displayed in *Table 19*. On the one hand, for a fixed column of *Table 19* i.e. a fixed value of parameter β, increasing 2γ means decreasing ultimate resistance. On the other hand, for a fixed row i.e. fixed value of parameter 2γ, increasing β means incrasing ultimate design resistance.

		β			
		0.2	**0.4**	**0.6**	**0.9**
2γ	**10**	DBBX_01_SS 1162.76 kN	DBBX_02_SS 1157.29 kN	DBBX_03_SS 3486.48 kN	DBBX_04_SS 4001.41 kN
	15	DBBX_05_SS 775.18 kN	DBBX_06_SS 1547.74 kN	DBBX_07_SS 2324.73 kN	DBBX_08_SS 2682.92 kN
	25	DBBX_09_SS 465.31 kN	DBBX_10_SS 929.17 kN	DBBX_11_SS 1394.78 kN	DBBX_12_SS 1742.20 kN
	30	DBBX_13_SS 387.74 kN	DBBX_14_SS 774.99 kN	DBBX_15_SS 1162.10 kN	DBBX_16_SS 1408.86 kN

Table 19 *Summary of the combined analysis for parameters β and 2γ under tensile loading*

However, results for DBBX_02_SS {β=0,4; 2γ=10} are not consitent with the overall analysis. This might be explained as a numerical analysis error within Abaqus calculation.

A summary of perfomance variation of parameter β is visible in *Figure 62*, whereas performance of parameter 2γ for all models is displayed in *Figure 63*.

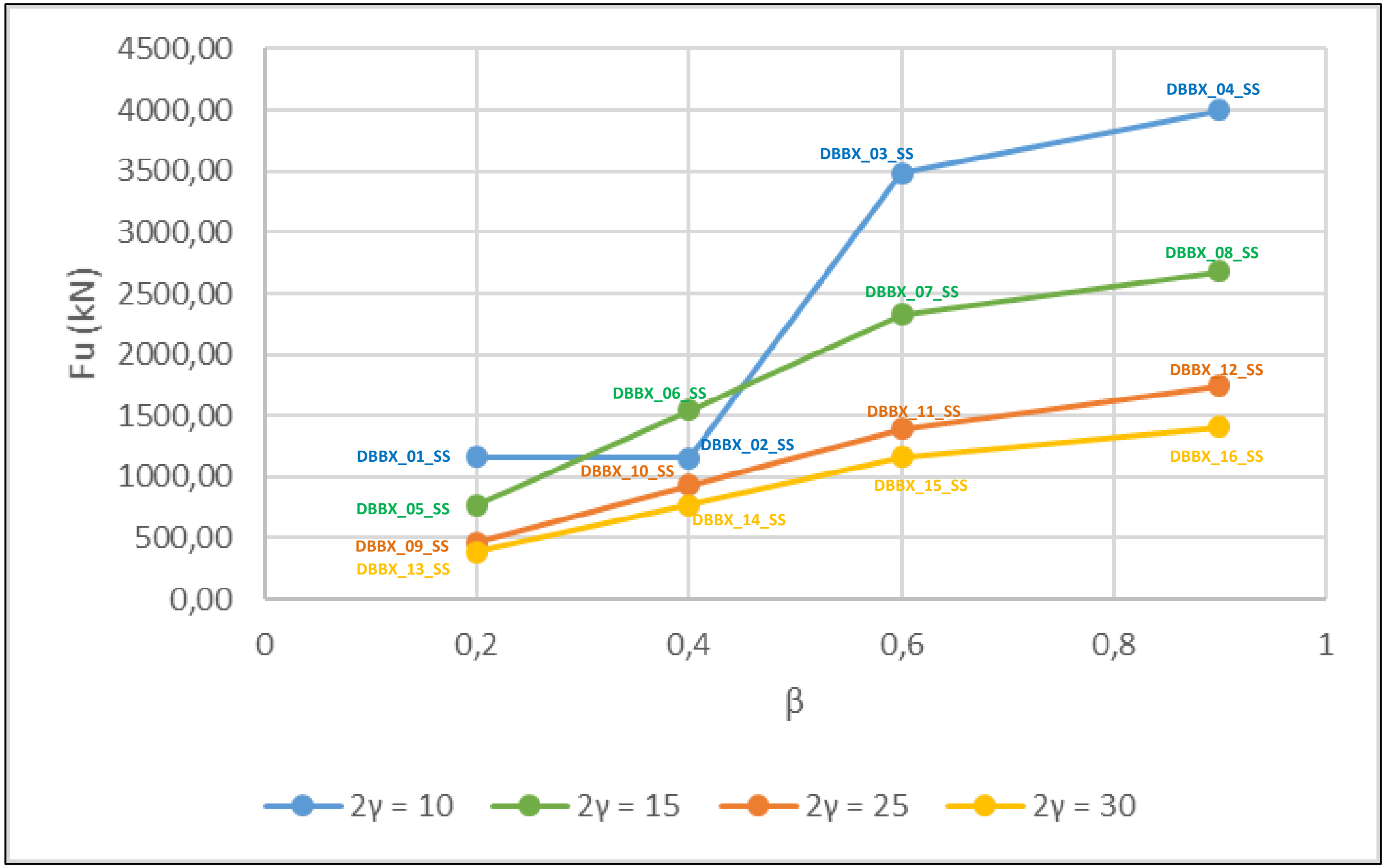

Figure 62 *Performance of β variation for all models under tensile loading*

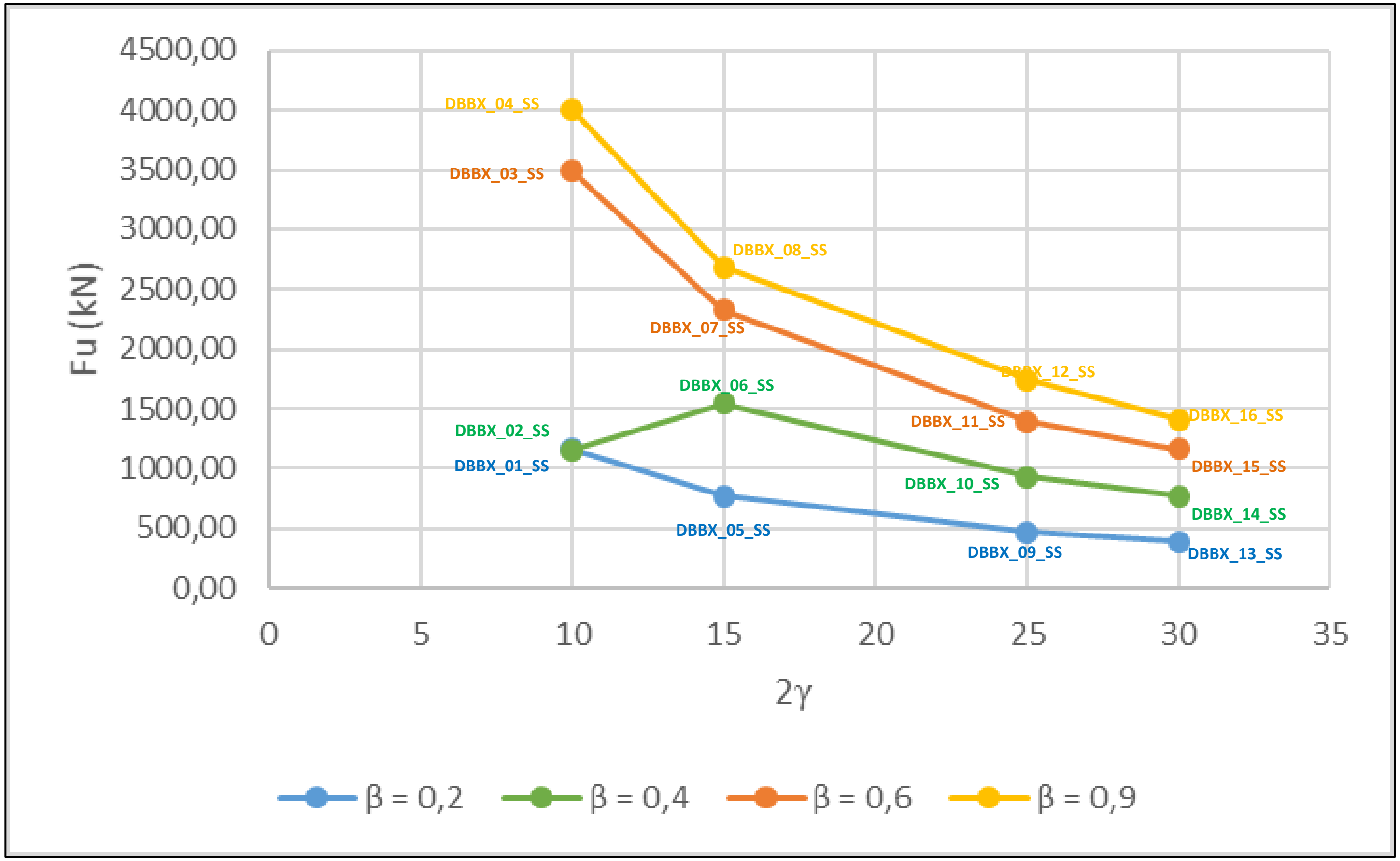

Figure 63 *Performance of 2γ variation for all models under tensile loading*

As it is visible in *Figure 62* and *Figure 63*, results of DBBX_02_SS, which corresponds to β=0,4 and 2γ=10, subjected to tensile loading are not consistent with the overall analysis. Expected theoretical performance of the analysis for all the models is displayed in *Figure 64* (β dependence) and *Figure 65* (2γ dependence), where dashed line is the expected trend of the joint.

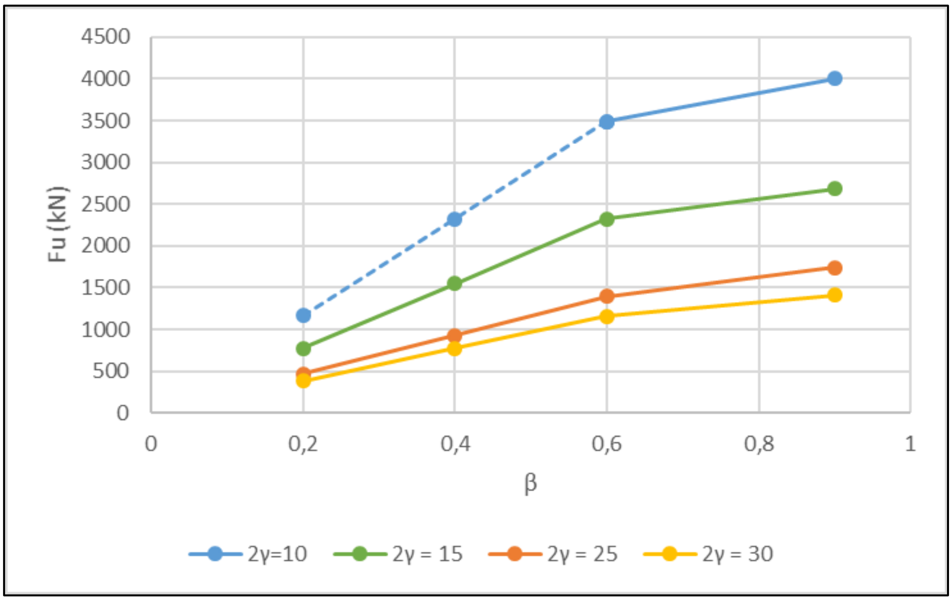

Figure 64 *Expected performance of β variation for all models under tensile loading*

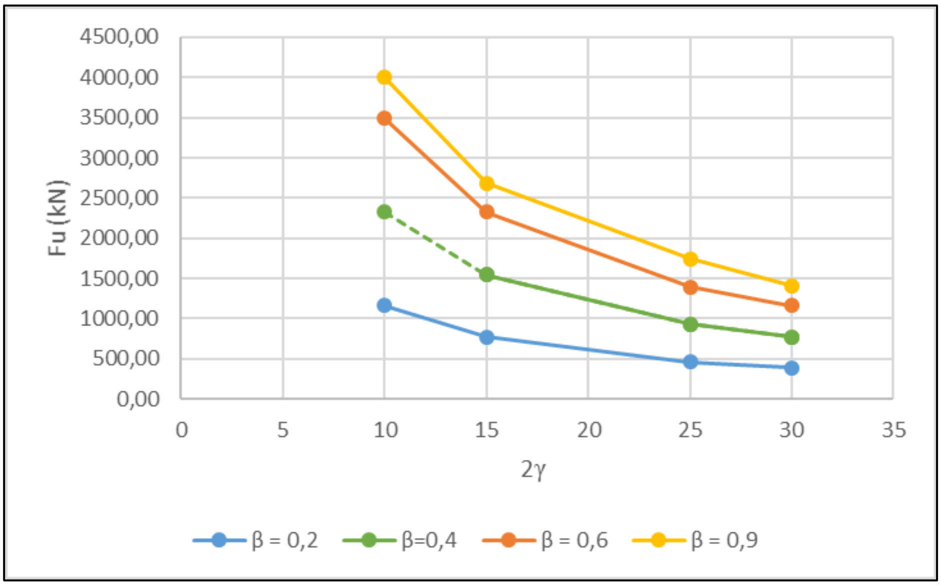

Figure 65 *Expected performance of 2γ variation for all models under tensile loading*

5.3.2 Analysis of F_u-β under tensile loading

This paragraph analyses design resistances dependance on β parameter for a fixed value of 2γ. It should be noted that, although the resistance of a joint with properly formed welds is generally higher under tension than under compression the design resistance of a joint according to European Normative is generally based on the resistance of the brace in compression to avoid the possible excessive local deformation or reduced rotation capacity or deformation capacity with which might otherwise occur. Therefore, design resistance of the modelled joint subjected to tensile loading might be largely higher than those of the theoretical formulation.

2γ=10

Design resistances for a constant parameter 2γ=10, which corresponds to DBBX_01_SS, DBBX_02_SS_ DBBX_03_SS and DBBX_04_SS models, are displayed in *Figure 70*. As it is visible, curve trend is similar to curves obtained from EN 1993-1-8 [3] as well as owen formulations. However, results for DBBX_02_SS are not consistent with the overall trend. Relative differences concludes that β dependance for 2γ=10 of obtained results are set as being on the safety side, which is displayed in *Figure 66*.

2γ=15, 2γ=25, 2γ=30

Results for models subjected to tensile loading for 2γ=15, 2γ=25 and 2γ=30 derives to a consistent trend and are displayed in *Figure 71*, *Figure 72* and *Figure 73*, respectively Therefore, they are discussed together in this paragraph.

Increasing parameter 2γ means increasing ultimate strength. Furthermore, obtained results within ABAQUS are much higher than those obtained to J.S. Owen et. al. and EN 1993-1-8 [3] formulations, with a high relative difference in all the cases. This might be explained because theoretical formulation is set for compression of the brace in order to avoid the possible excessive local deformation or reduced rotation capacity or deformation capacity with which might otherwise occur. Furthermore, theoretical design resistance that leads to a type of failure mode might be different from failure mode of the modelled joint as well.

Relative differences for 2γ=15, 2γ=25 and 2γ=30 is displayed in *Figure 67*, *Figure 68* and *Figure 69*, respectively.

RELATIVE DIFFERENCES BETWEEN FORMULATIONS

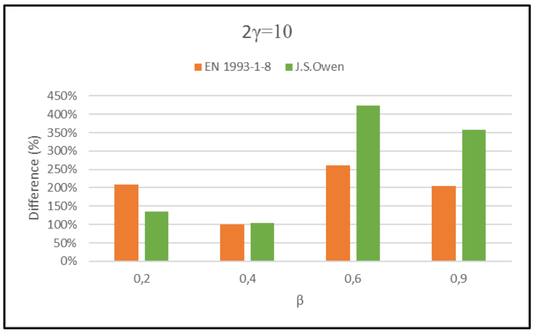

Figure 66 *Relative error design resistance in dependance on parameter β and constant parameter 2γ=10 under tensile load*

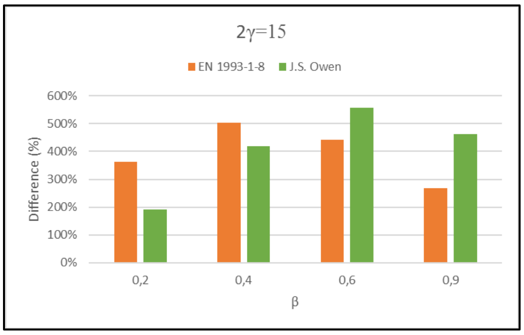

Figure 67 *Relative error design resistance in dependance on parameter β and constant parameter 2γ=15 under tensile load*

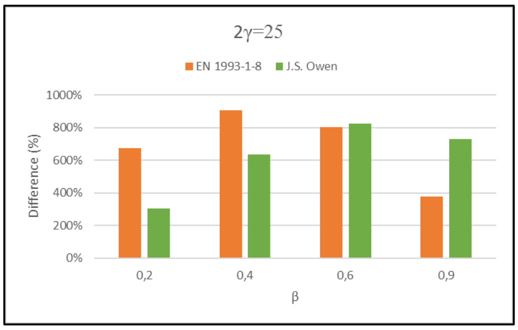

Figure 68 *Relative error design resistance in dependance on parameter β and constant parameter 2γ=25 under tensile load*

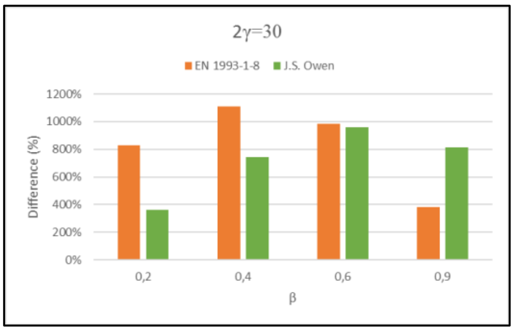

Figure 69 *Relative error design resistance in dependance on parameter β and constant parameter 2γ=30 under tensile load*

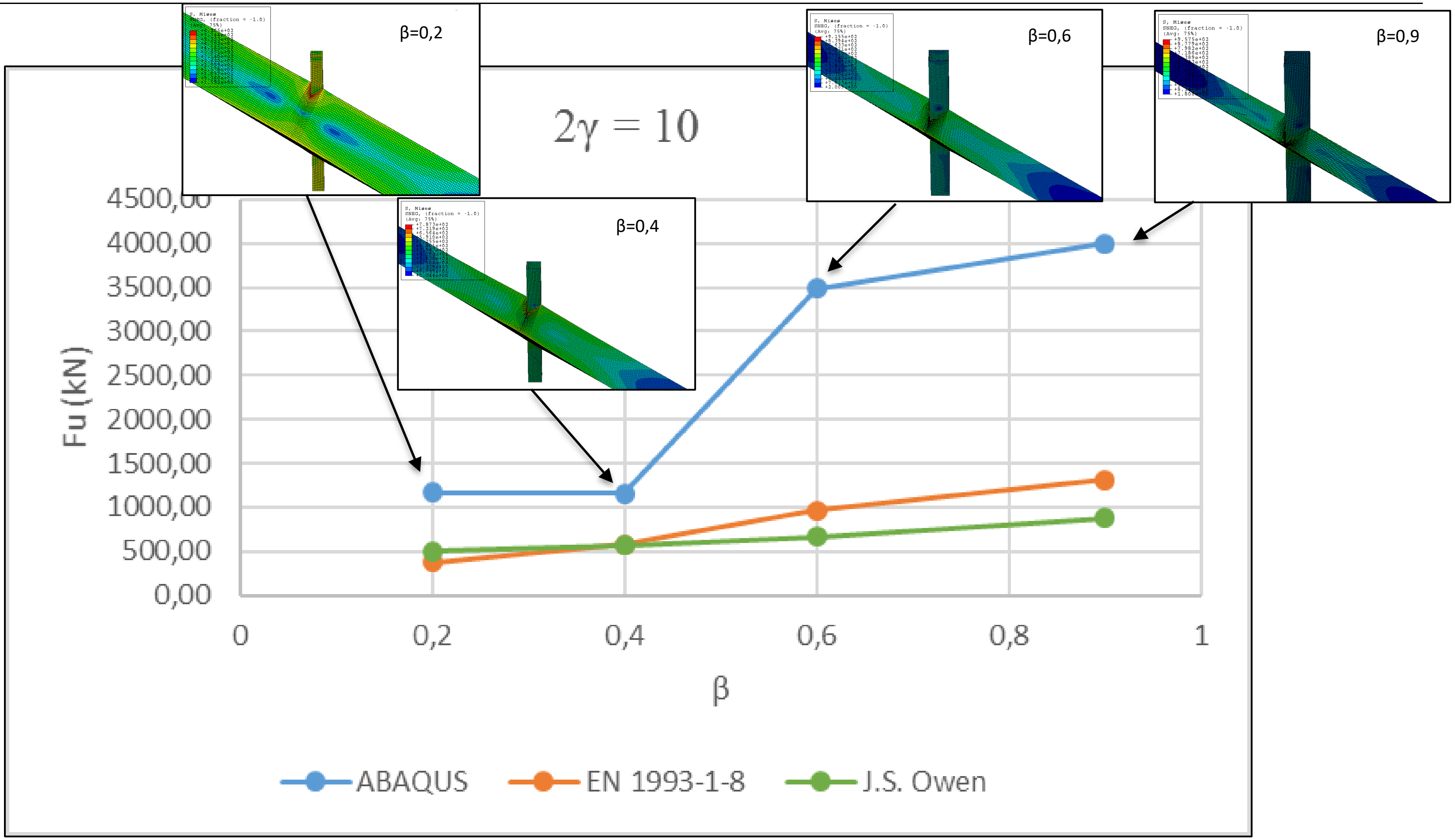

Figure 70 *Comparison of design resistances dependance on parameter β for 2γ=10 under tensile loading*

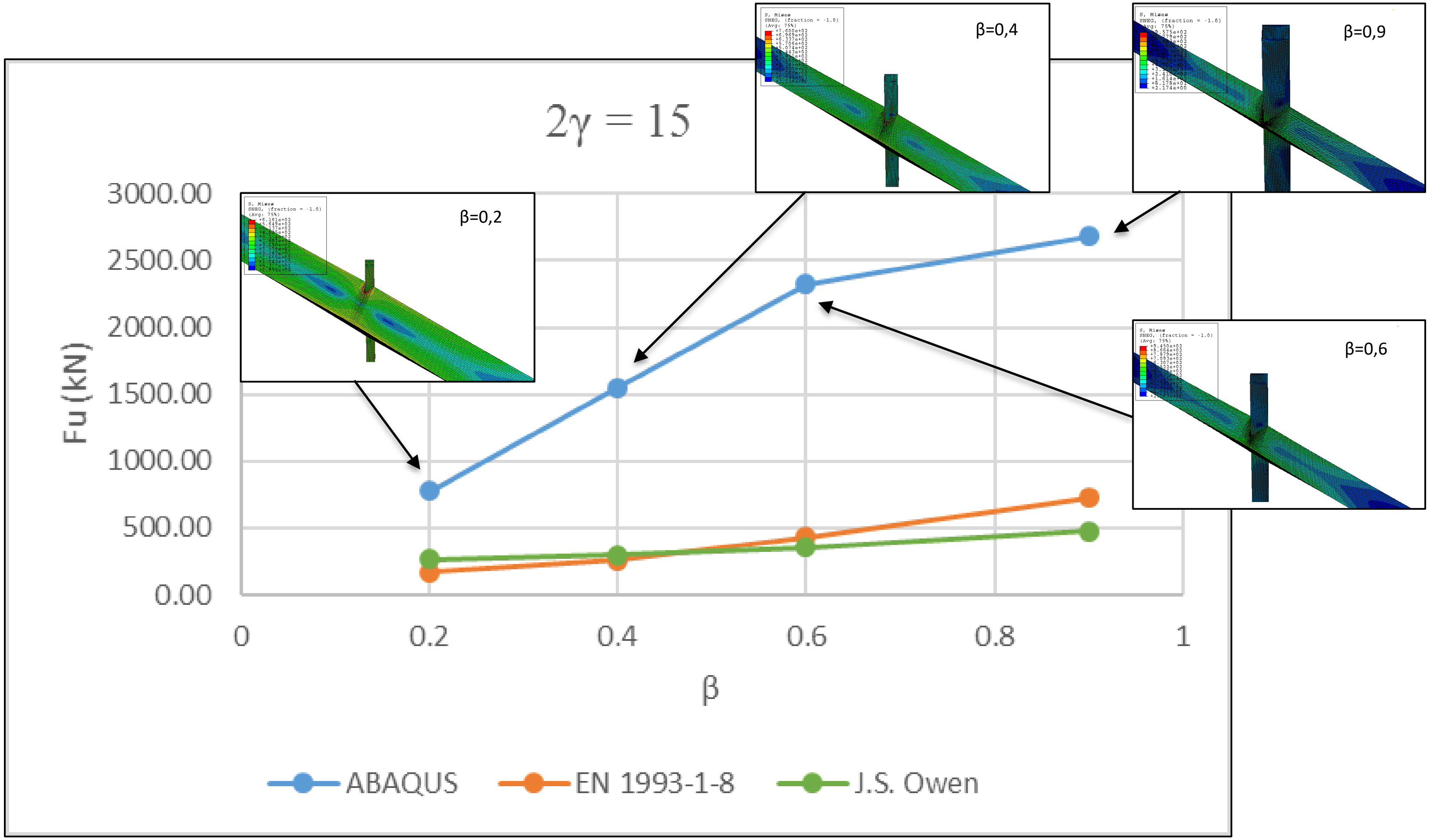

Figure 71 *Comparison of design resistances dependance on parameter β for 2γ=15 under tensile loading*

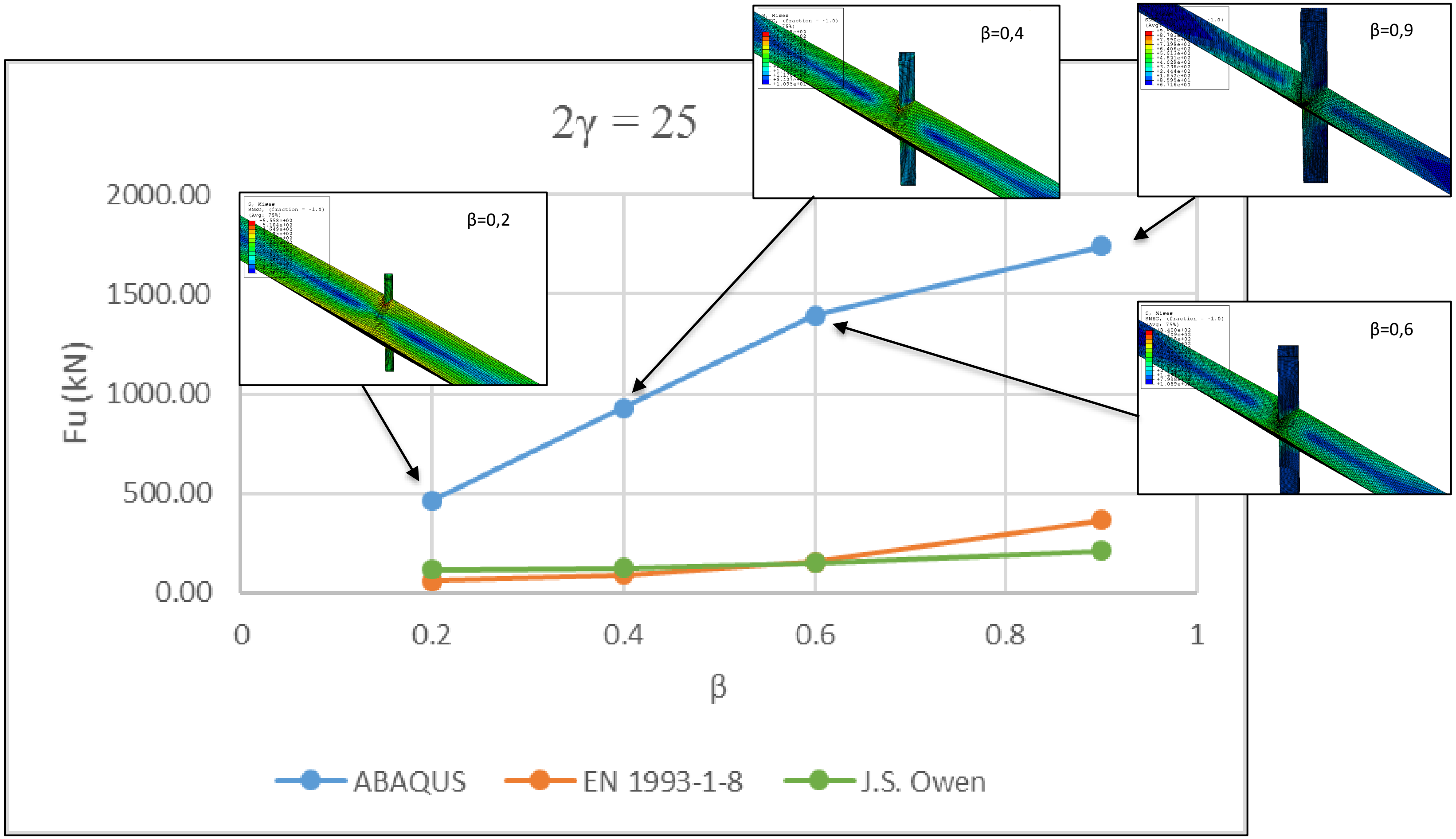

Figure 72 *Comparison of design resistances dependance on parameter β for 2γ=25 under tensile loading*

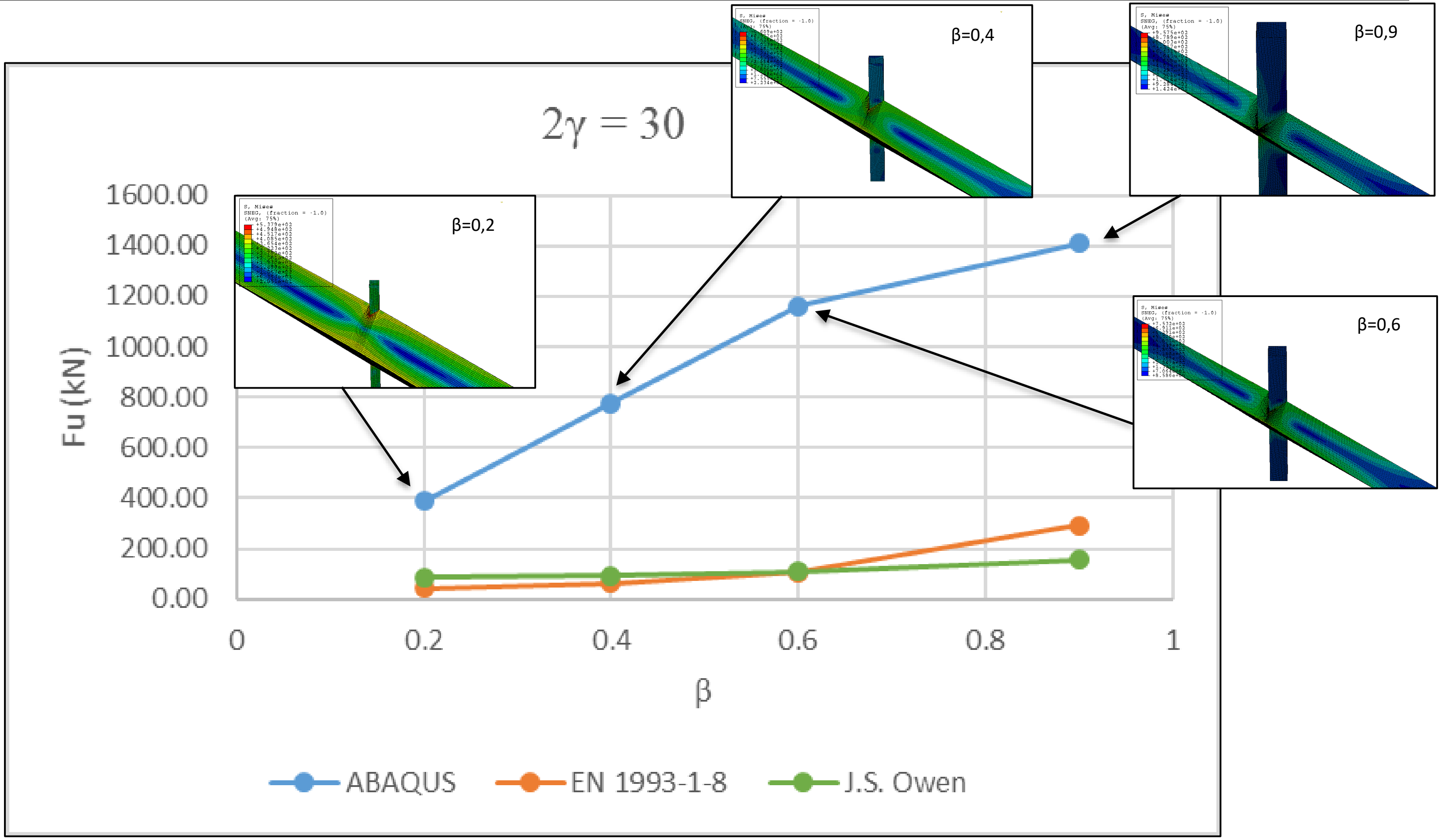

***Figure 73** Comparison of design resistances dependance on parameter β for 2γ=30 under tensile loading*

5.3.3 Analysis of F_u-2γ under tensile loading

This paragraph analyses design resistances dependance on β parameter for a fixed value of 2γ.

β=0,2

Design resistances under tensile loading for a constant parameter β=0,2, which corresponds to DBBX_01_SS, DBBX_05_SS_ DBBX_09_SS and DBBX_13_SS models, is displayed in *Figure 78*. As it is visible, curve trend is similar to curves obtained from EN 1993-1-8 as well as owen formulations. Furthermore, relative error concludes that 2γ dependance for β=0,2 of obtained results are set as being on the safety side. Relative difference is displayed in *Figure 74*.

β=0,4

Different results are achieved for the particular case of constant parameter β=0,4. For instance, for 2γ=10, ABAQUS results are close to bibliography formulations with a really low relative error, whereas for higher values of parameter 2γ ultimate resistance is much higher. As it has been stated in analysis of F_u-β, DBBX_02_SS is not consistent with the overall results. However, theoretical overall trend is achieved for parameter 2γ equal to 15, 25 and 30, but with much higher values. Relative difference is displayed in *Figure 75*.

β=0,6

Similar behaviour as β=0,2 is achieved for a constant value of parameter β=0,6, which is displayed in *Figure 80*. Relative error concludes that 2γ dependance for β=0,6 of obtained results are set as being on the safety side. Relative difference is displayed in *Figure 76*.

β=0,9

Finally, consistent results are obtained for a constant value of parameter β=0,9, which is displayed in *Figure 81*. Ultimate strength obtained when β=0,9 i.e. brace width is 135 mm, is the largest among all the models. Relative difference is displayed in *Figure 77*.

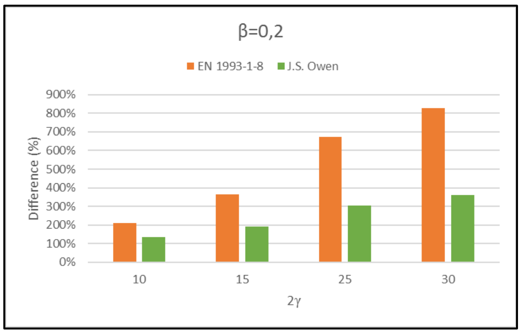

Figure 74 *Relative error design resistance in dependance on parameter 2γ and constant parameter β=0,2 under tensile load*

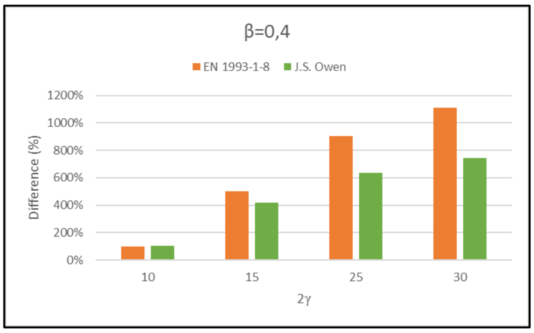

Figure 75 *Relative error design resistance in dependance on parameter 2γ and constant parameter β=0,4 under tensile load*

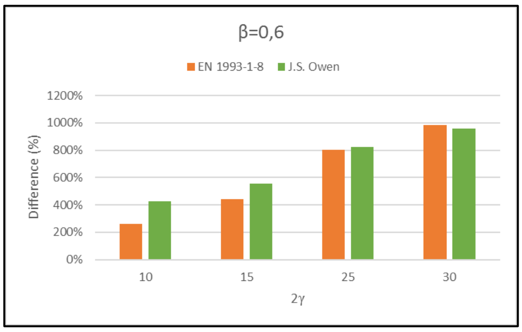

Figure 76 *Relative error design resistance in dependance on parameter 2γ and constant parameter β=0,6 under tensile load*

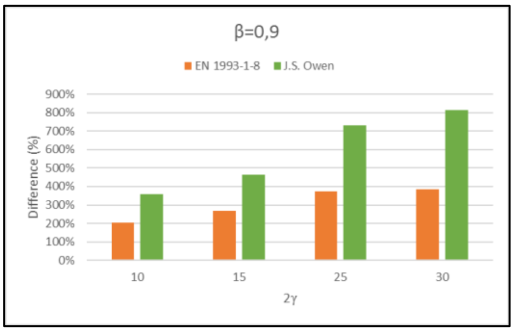

Figure 77 *Relative error design resistance in dependance on parameter 2γ and constant parameter β=0,9 under tensile load*

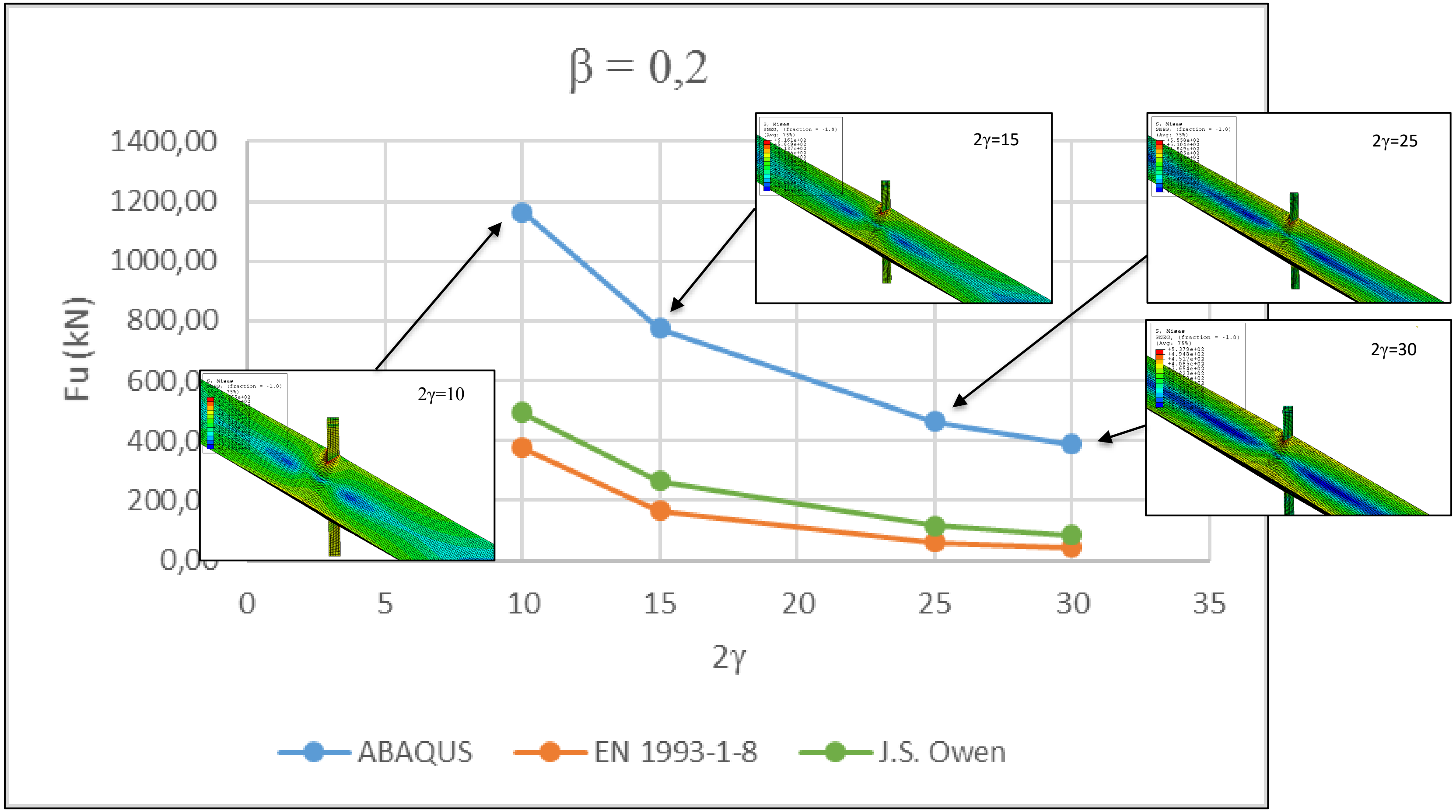

Figure 78 *Comparison of design resistances dependance on parameter 2γ for β=0,2 under tensile loading*

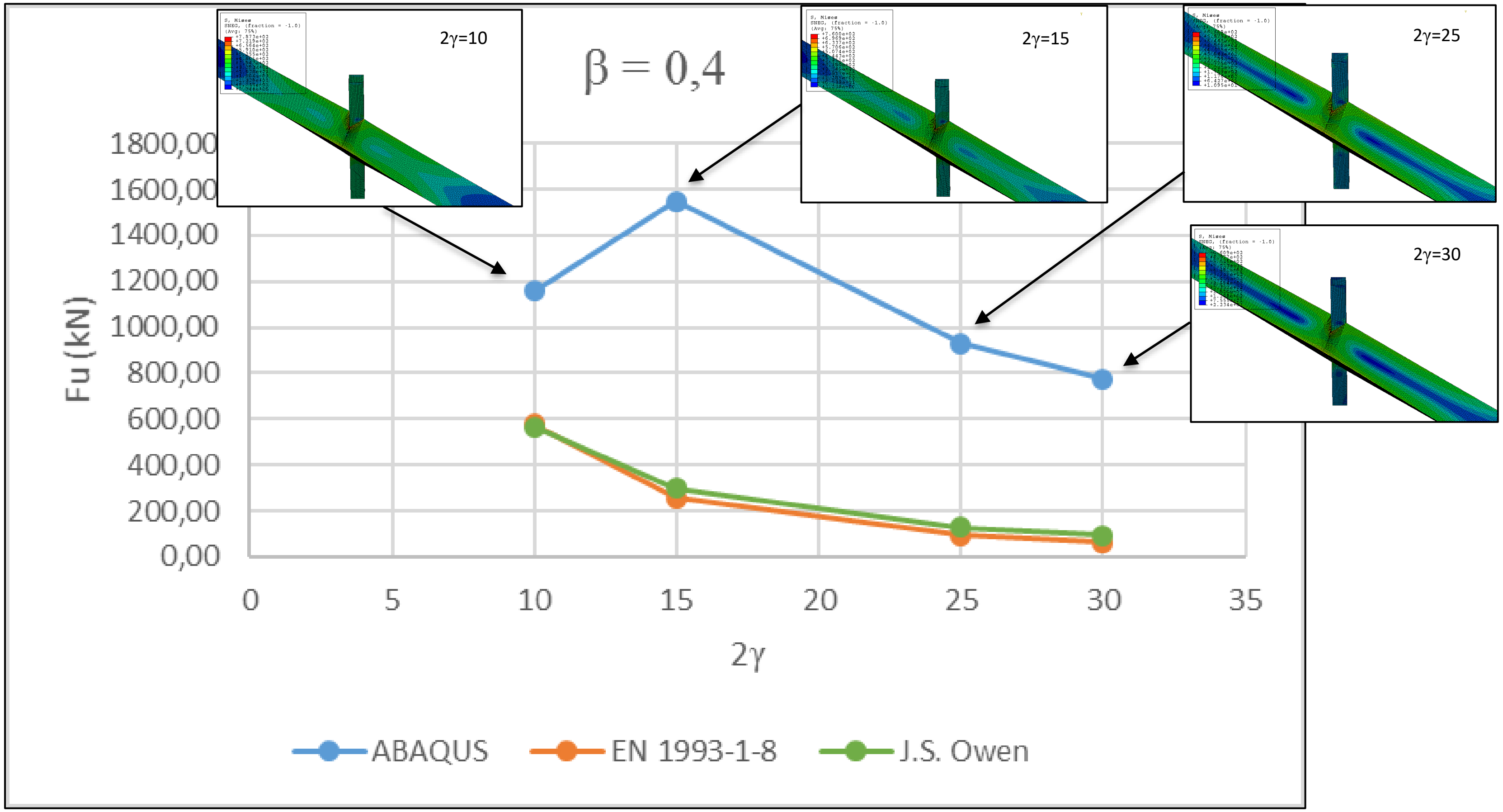

Figure 79 *Comparison of design resistances dependance on parameter 2γ for β=0,4 under tensile loading*

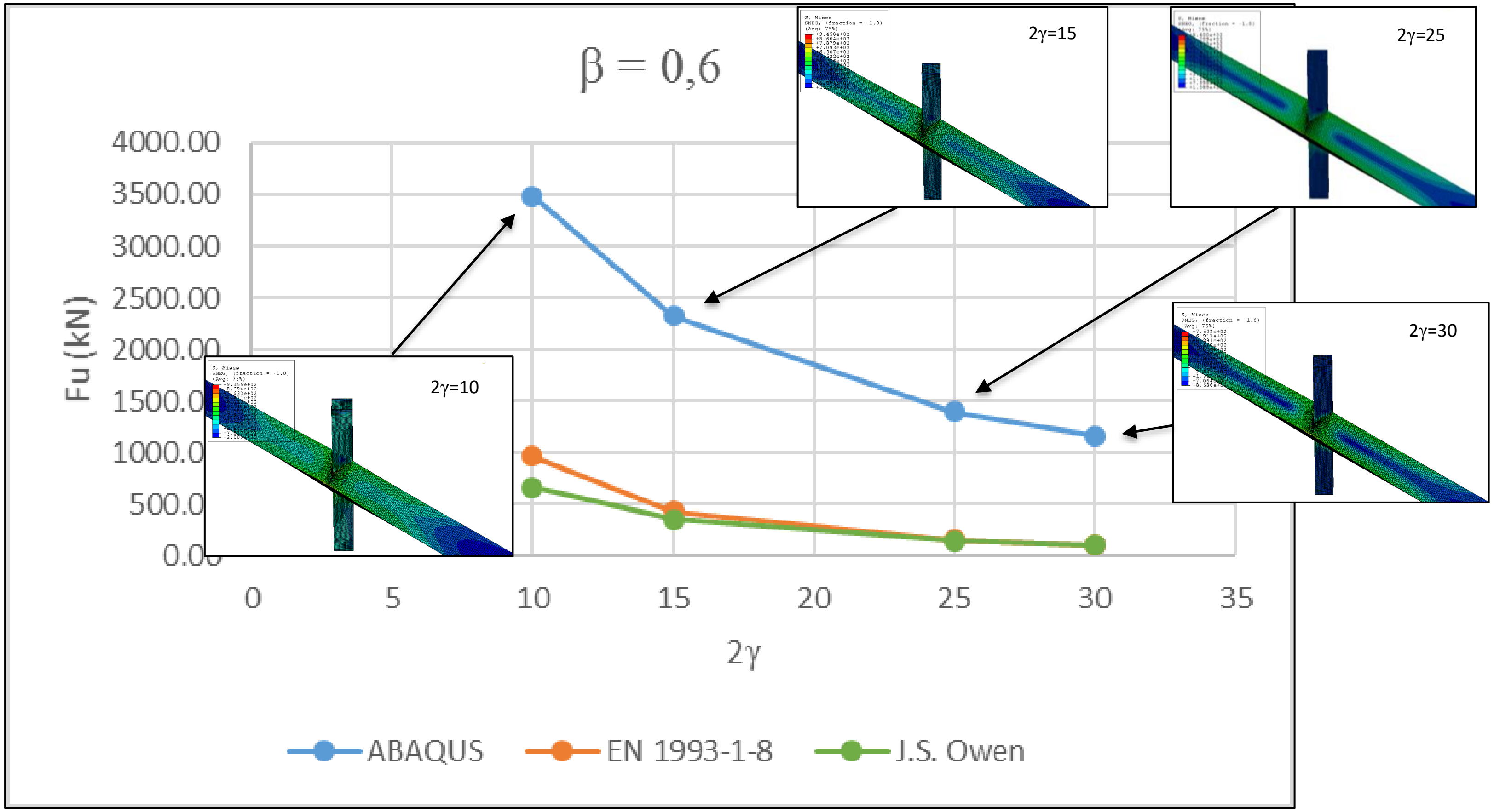

Figure 80 *Comparison of design resistances dependance on parameter 2γ for β=0,6 under tensile loading*

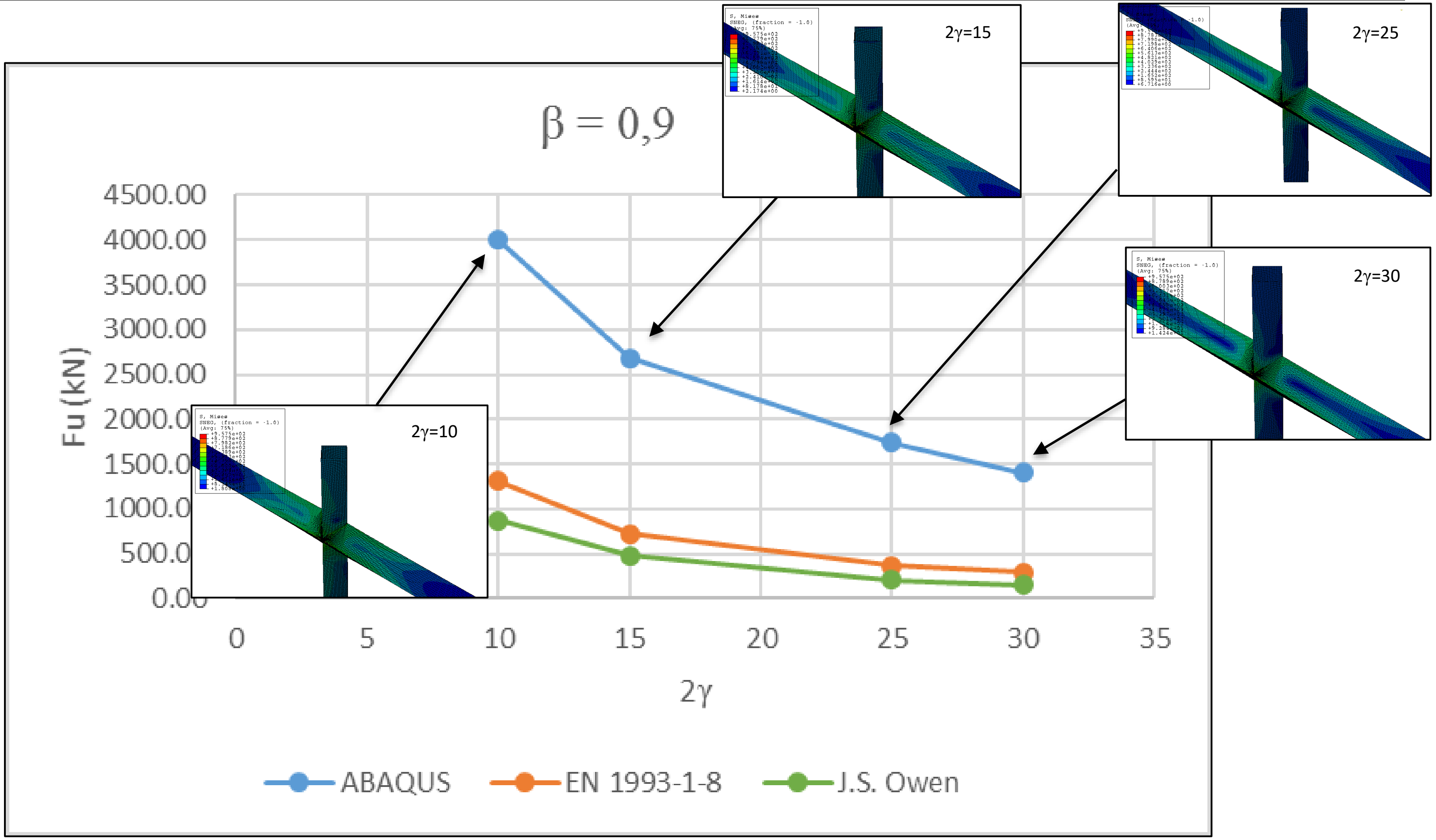

Figure 81 *Comparison of design resistances dependance on parameter 2γ for β=0,9 under tensile loading*

5.3.4 Analysis of load-displacement curves under tensile loading

As explained in the analysis of compression results, one aspect that is equally important and is not displayed in F_u-β and F_u-2γ curves is load-displacement performance of the joints, which allow to acknowledge ductility performance of the mdoels. Thus ultimate strength at high values of displacement means model is more ductile and ultimate strength at low values of displacement means model is more brittle.

5.3.4.1 Load-displacement dependance on β

For the particular case of tensile loading and constant parameter 2γ=15, variation of parameter β is displayed in *Figure 82* as a representative performance of the joint. Thus, as brace width increases, ultimate resistance increases as well. Furthermore, as β increases, ductility increases as well, which means ultimate strength is achieved at high values of displacement. Load-displacement curves for all models are displayed in "*Appendix D. PARAMETRIC RESULTS*".

A change in the slope of load-displacement curves might mean that there is a change in the failure mode. For instance, for β=0,2 there is no change in the load-displacement curve, thus failure occurs only in the brace. On the contrary, for higher values of β, there is coupling failure between chord and brace.

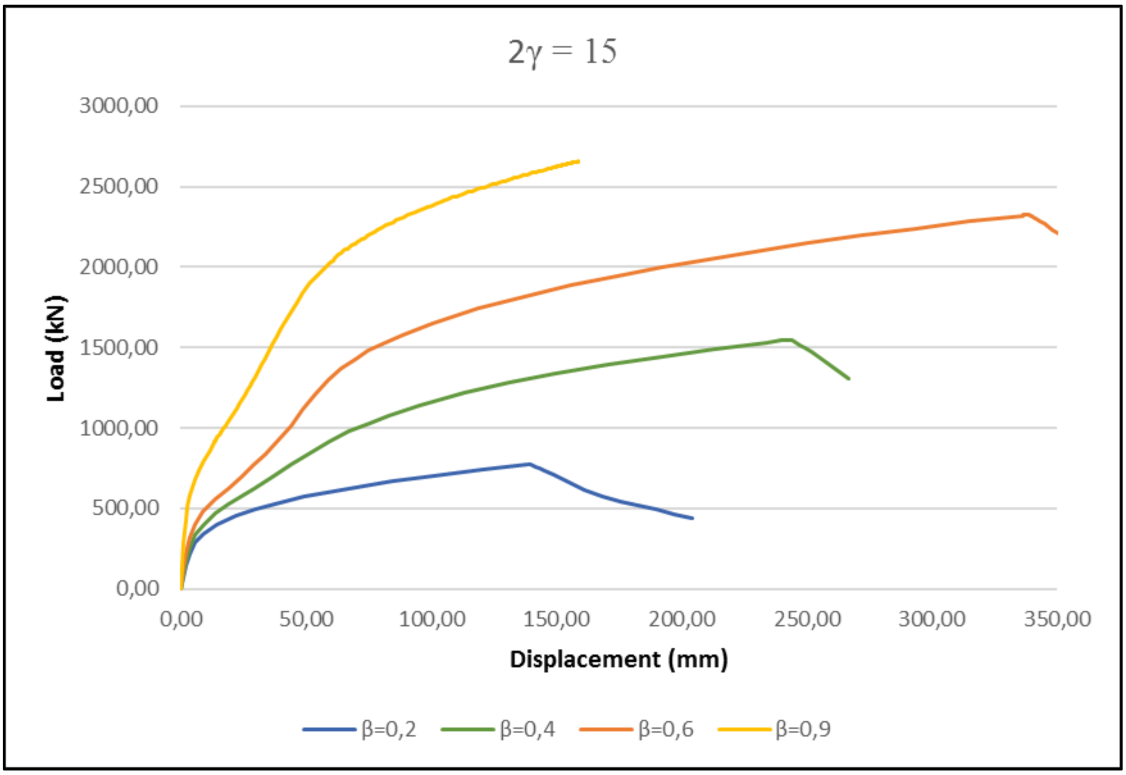

Figure 82 *Load-displacement curves for variation of parameter β for 2γ=15 under tensile loading*

5.3.4.2 Load-displacement dependance on 2γ

Similar performance as compression analysis is obtained for tensile loading analysis. As 2γ increases i.e. thickness decreases, ultimate resistance of the joint decreases as well. *Figure 83* displays models DBBX_01_SS (2γ=10), DBBX_05_SS (2γ=15), DBBX_09_SS (2γ=25) and DBBX_13_SS (2γ=30) as a representative performance for 2γ variation. On the contrary of β dependance, performance dependence on 2γ concludes that as 2γ increases, models are more ductile and ultimate strength is achieved at high values of displacement, whereas low values of parameter 2γ means models are more brittle, despite the fact they have higher ultimate resistance. Load- displacement curves for all models are displayed in "*Appendix D. PARAMETRIC RESULTS*".

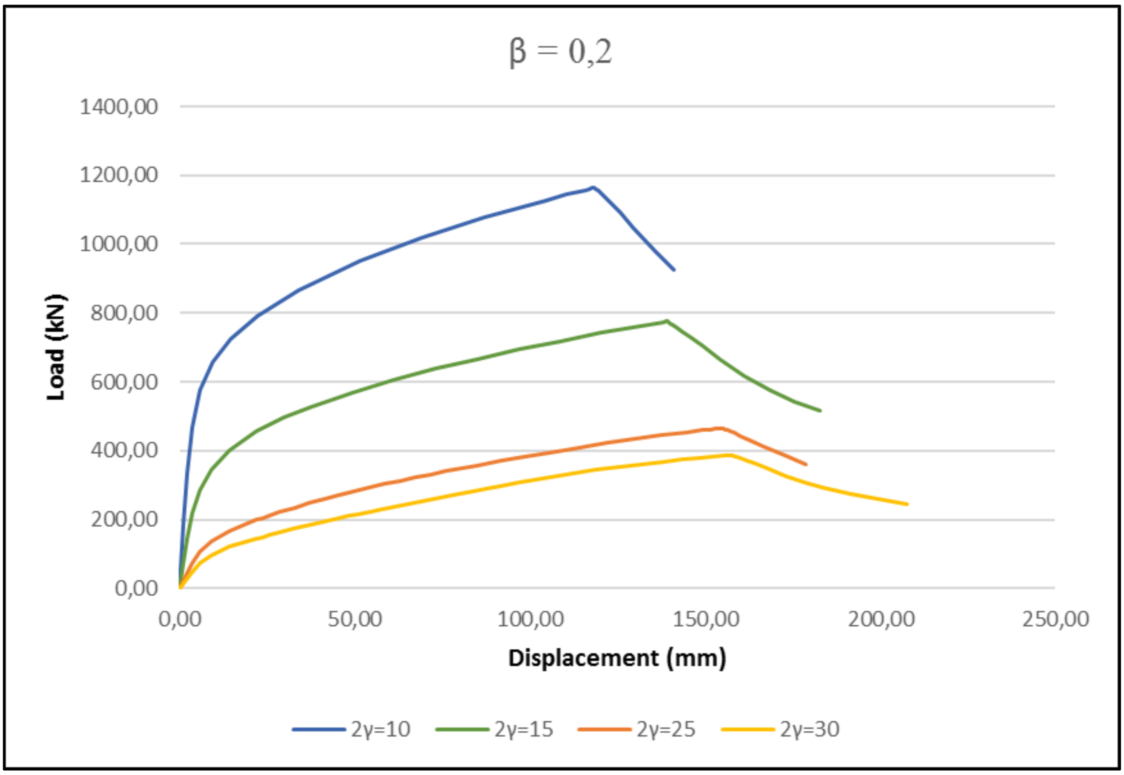

Figure 83 *Load-displacement curves for variation of parameter 2γ for β=0,2 under tensile loading*

5.3.4.3 Failure modes

Failure modes are analysed for two different cases in order to study the influence of brace width in failure. On the one hand, low values of parameter β (β=0,2) and, on the other hand, high values of β (β=0,6). β=0,9 case is not analysed since after 300 increments of calculation, joint has not achieved its ultimate strength.

5.3.4.3.1 Failure modes for β=0,2

Typical load-displacement curve for β=0,2 is displayed in *Figure 84*, where slope is constant i.e. there are not abrupt changes in curve's slope. Therefore, failure mode does not change as load increases.

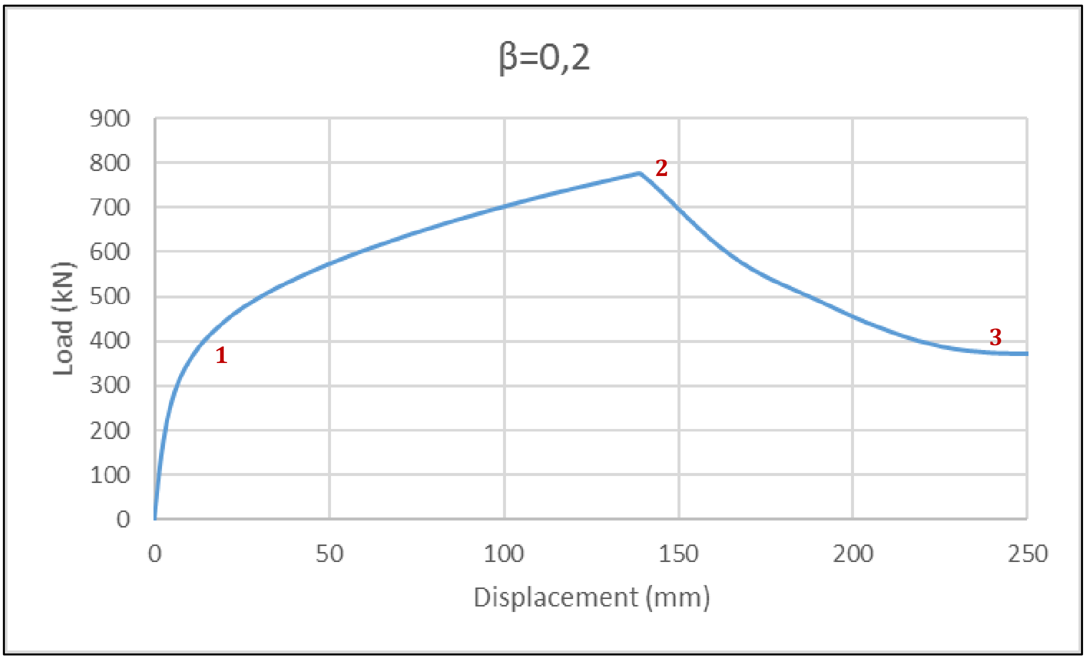

***Figure 84** Load-displacement curve for β=0,2 under tensile loading*

There are three important steps within load-displacement curve:

1) End of elastic phase, where only welded contour is being afected
2) Ultimate strength is achieved, which leads to failure. Brace is largely afected with high stresses and effective width is reduced.
3) Joint has already failed due to brace failure. However, stresses in the chord decreases

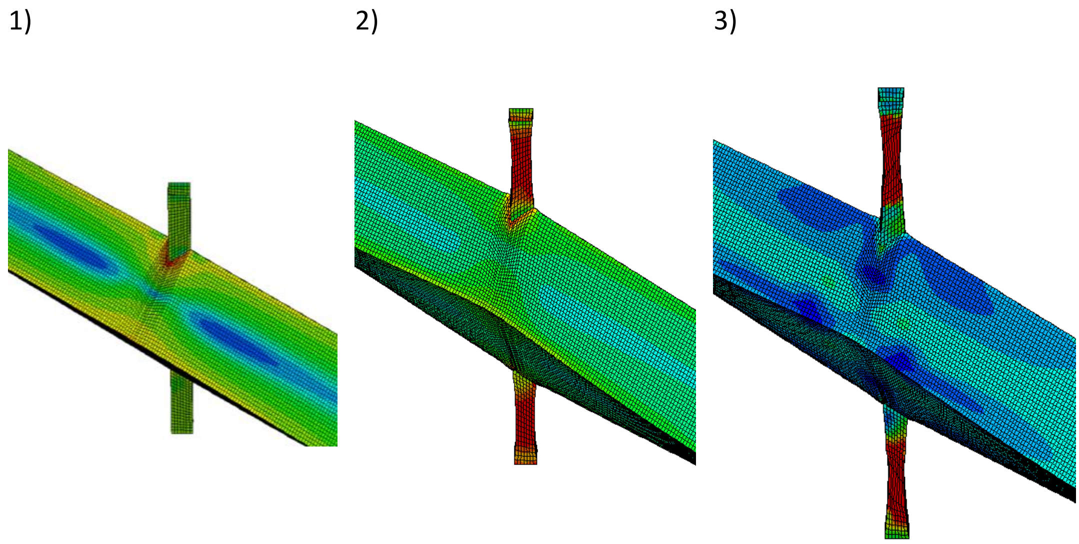

Figure 85 *Stages of deformed shape for β=0,2 under tensile loading*

Theoretical brace failure with reduced effective width is explained in paragraph "*2.5.5 Failure modes for hollow section joints*" and is displayed in *Figure 86*.

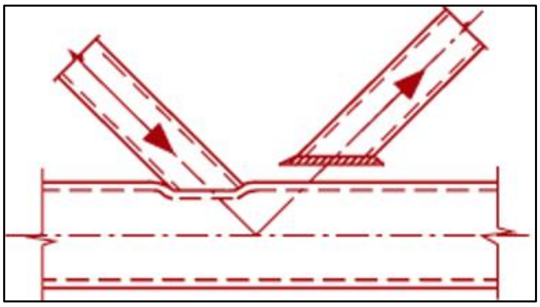

Figure 86 *Theoretical failure mode of brace failure with reduced effective width*

5.3.4.3.2 Failure modes for β=0,6

Typical load-displacement curve for β=0,6 is displayed in *Figure 87*. It is visible that the curve has different slopes before failure.

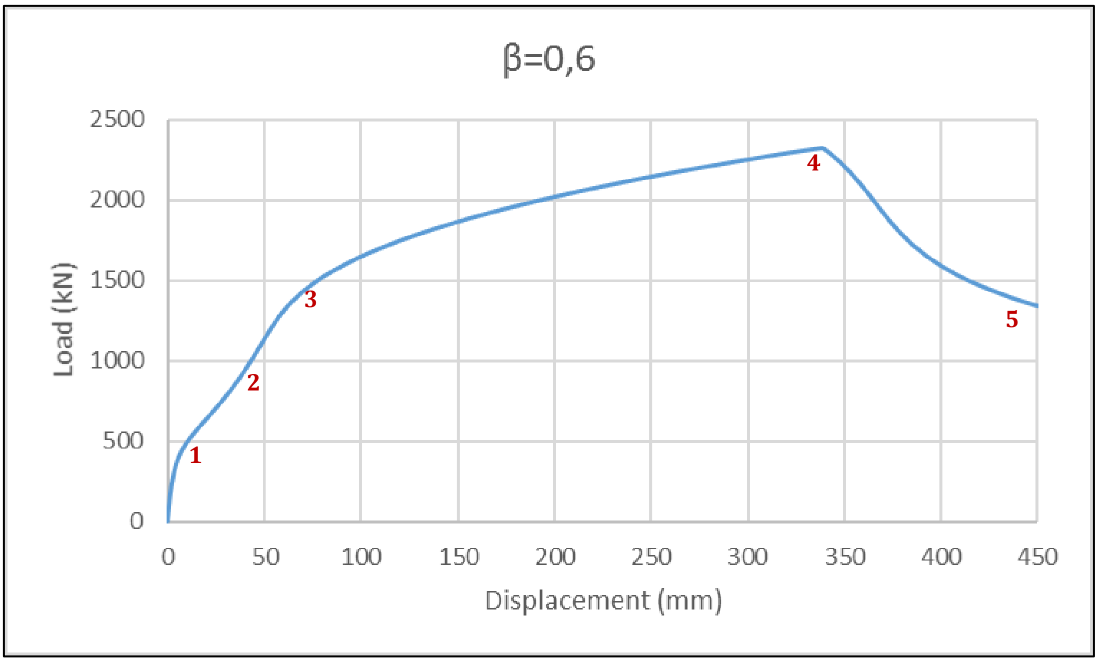

***Figure 87** Load-displacement curve for β=0,6 under tensile loading*

There are five important steps within load-displacement curve:

1) End of elastic phase, which not important stresses are visible
2) Chord face failure is starting to occur, which leads to chord plastification
3) Ultimate step of chord face failure. Chord is completely plastified. Afterwards, failure moves to brace
4) Failure mode is brace failure with reduced effective width. Ultimate design resistance is achieved.
5) Joint has already failed due to brace failure. Stresses in the chord decreases slowly

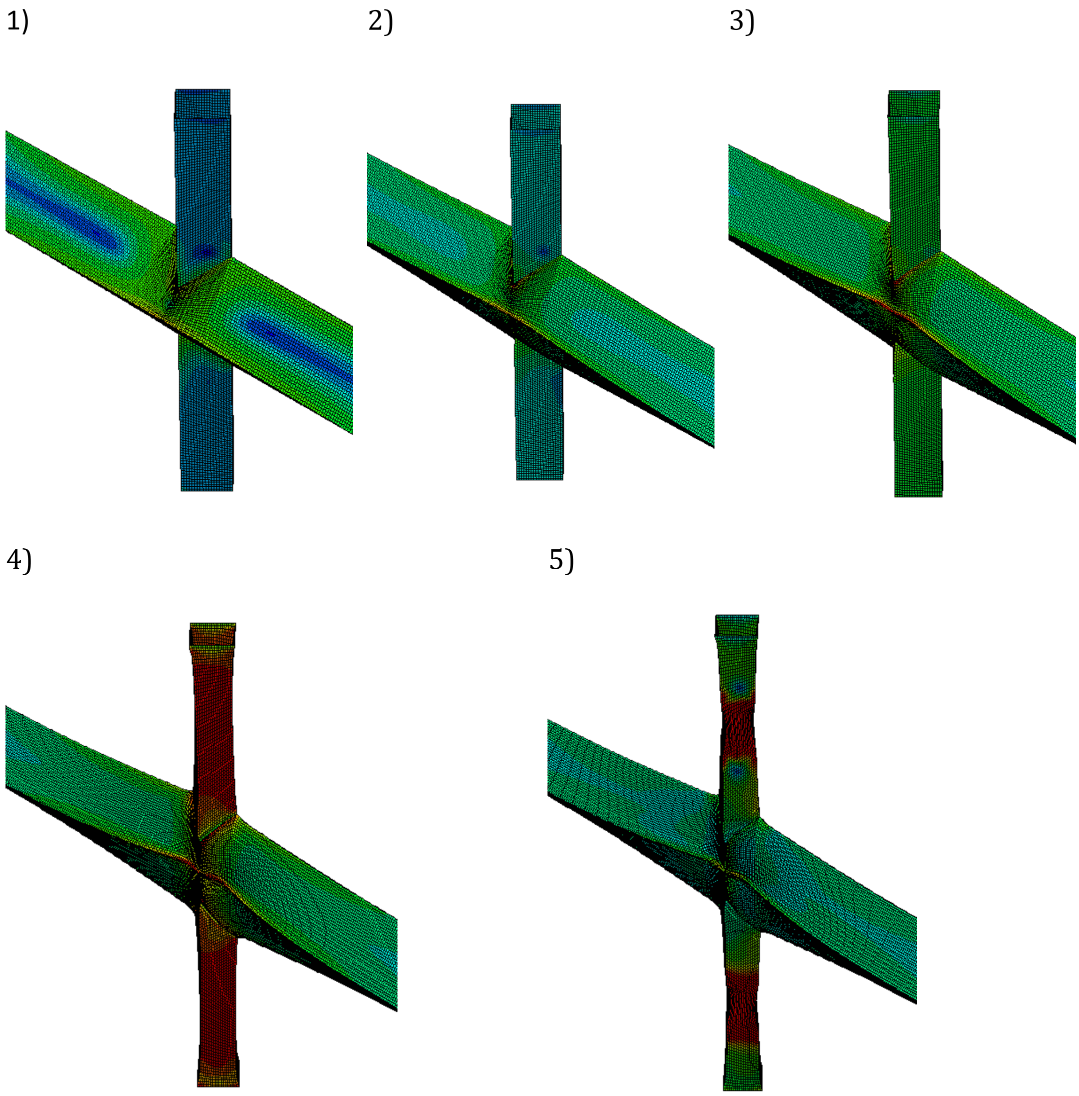

Figure 88 *Stages of deformed shape for β=0,6 under tensile loading*

Theoretical brace failure with reduced effective width and chord face failure are explained in paragraph "*2.5.5 Failure modes for hollow section joints*" and are displayed in *Figure 89*. In the particular case of high values of β there is coupling failure between chord and brace.

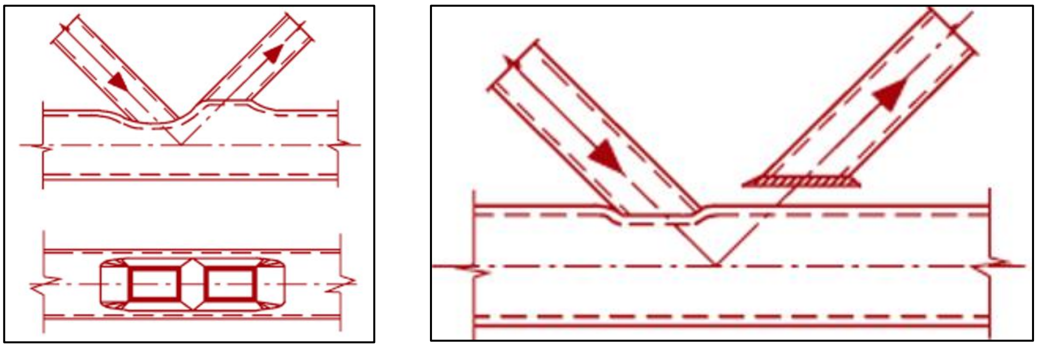

Figure 89 *Theoretical failure mode of chord face failure (left) and brace failure with reduced effective width (right)*

5.3.4.3.3 Specific analysis of failure modes for β=0,9 under tensile loading

Different failure modes are described in EN 1993-1-8 for β≥0,85. For the present thesis, design resistance for β≥0,9 has been considered as the minimum of different failure modes i.e. minimum value between chord face failure, chord side wall buckling, brace failure and punching shear.

Moreover, as it has been explained in "*2.5.5 Failure modes for hollow section joints*", the resistance of a joint with properly formed welds is generally higher under tension than under compression. However, the design resistance of a joint according to EN 1993-1-8 is generally based on the resistance of the brace in compression to avoid the possible excessive local deformation or reduced rotation capacity or deformation capacity with which might otherwise occur.

Therefore, minimum value of the design resistance of the European Normative might not be the actual design resistance that leads to failure mode of the modelled joint.

As it has been concluded within previous paragraphs, large differences have been obtained between modelled results and European Normative for β≥0,85. This fact might be due to theoretical failure mode stated in the normative is not the same as the actual failure mode of a modelled diamond bird-beak joints subjected to tensile loading.

JOINT	Chord face failure	Chord side wall buckling	Brace failure	Punching shear
	β≤0,85	β≥0,85	β≥0,85	0,85≤β≤(1-1/γ)
β=0.9 / 2γ=10	3471.55 kN	1764.00 kN	2016.00 kN	1309.43 kN
β=0.9 / 2γ=15	2074.91 kN	1036.00 kN	1148.00 kN	727.46 kN
β=0.9 / 2γ=25	2675.39 kN	554.40 kN	594.72 kN	366.64 kN
β=0.9 / 2γ=30	3176.09 kN	448.00 kN	476.00 kN	290.98 kN

Table 20 *Design resistances for β=0,9 for different failure modes according to EN 1993-1-8*

Results for β=0,9 for different failure modes are set in *Figure 90*. On the one hand, it is visible that the closer failure mode for 2γ=10 and 2γ=15 is chord face failure of the joint instead of punching shear, which is the minimum design resistance. On the other hand, for 2γ=25 and 2γ=30, theoretical design resistances that leads to chord face failure are higher than the modelled design resistances. Therefore, design resistance that leads to failure mode of modelled joint that is suitable with theoretical formulation for 2γ=25 and 2γ=30 is brace failure with reduced effective width.

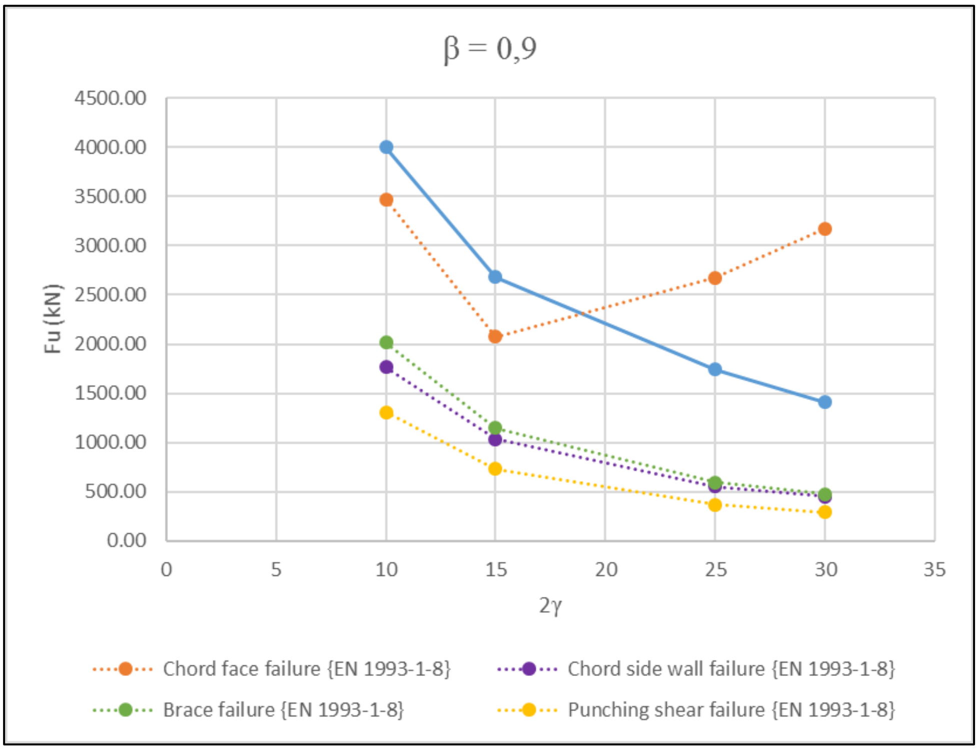

Figure 90 *Design resistances of EN 1993-1-8 for different failure modes in comparison to design resistances obtained within ABAQUS*

In conclusion, high values of thickness leads to chord face failure instead of theoretical failure modes of the European normative i.e. brace failure with reduced effective width, whereas low values of thickness leads to brace failure, which is consistent with theoretical failure mode of European Normative.

JOINT	ABAQUS	EN 1993-1-8	Failure mode
β=0.9 / 2γ=10	4001.41 kN	3471.55 kN	Chord face failure
β=0.9 / 2γ=15	2682.92 kN	2074.91 kN	Chord face failure
β=0.9 / 2γ=25	1742.20 kN	594.72 kN	Brace failure
β=0.9 / 2γ=30	1408.86 kN	476.00 kN	Brace failure

Table 21 *Design resistances of the actual failure modes of European Normative in comparison to modelled design resistances*

For instance, in the particular case of 2γ=10 and β=0,9, European Normative formulation states that failure mode should be punching shear taking into account the minimum value of design resistances. However, modelled results are closer to chord face failure value (*Figure 91*).

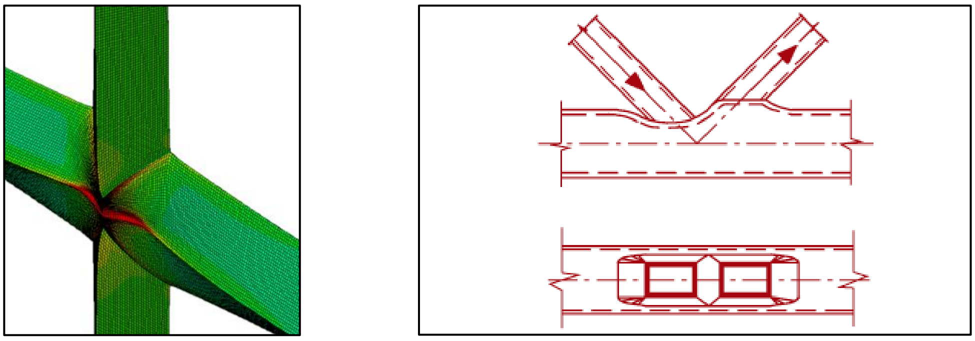

Figure 91 *Chord face failure of modelled joint for β=0.9 and 2γ=10 (left) and theoretical chord face failure (right)*

For the particular case of 2γ=30 and β=0,9, ultimate resistance that leads to failure mode of the joint is identical to failure mode explained in previous paragraph "*5.3.4.3.2 Failure modes for β=0,6*", which corresponds to brace failure with reduced effective width (*Figure 92*), instead of the minimum value of the design resistance that corresponds to punching shear failure.

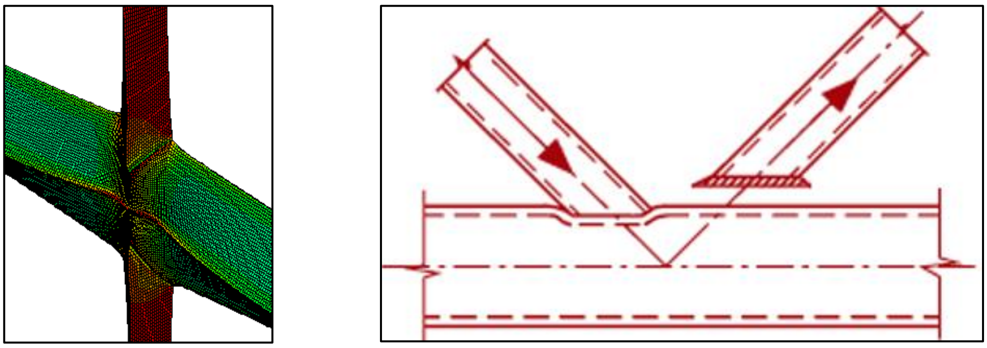

Figure 92 *Brace failure of modelled joint for β=0.9 and 2γ=30 (left) and theoretical brace failure with reduced effective width (right)*

5.4 COMPARISON OF CARBON STEEL AND STAINLESS STEEL

Once all the models have been analysed for both tensile and compression by means of curves F_u-β, F_u-2γ and P-δ, shall be of high importance to compare stainless steel results obtained in this thesis with carbon steel results of similar diamond bird-beak joints in order to understand behaviour of both cases and find advantages and disadvantages in using stainless steel against using carbon steel.

A. PEÑA and R. CHACÓN, in their article "*Structural analysis of diamond bird-beak joints subjected to compressive and tensile forces*" [7], studied several diamond bird-beak X-type joints of carbon steel. Thus, geometrical models that are exacly equal in their study in comparison to geometrical models in this thesis will be compared in terms of Load-Displacement curves.

They analysed three types of carbon steel of different yield strength each i.e. f_y=235 N/mm², f_y=275 N/mm² and f_y=460 N/mm². Since the material analysed in the current thesis is a stainless steel with a yield strength of 280 N/mm², it shall be compared to yield strength of 275 N/mm² since is the closer value. Young's modulus is slighltly different for both studies as well i.e. E=200000 N/mm² for this thesis, whereas E=210000 N/mm² for A. PEÑA and R. CHACÓN study.

Carbon steel and stainless steel models of both studies are linked in *Table 22*, where first column refers to models nomenclature in the article mentioned above. Comparison of carbon steel DBBX joints and stainless steel DBBX joints under compression loading and tensile loading will be carried out.

CARBON STEEL JOINT	STAINLESS STEEL JOINT	Geometric parameters					2γ	β
		Chord			Brace			
		L_0 (mm)	b_0 (mm)	t_0 (mm)	b_1 (mm)	t_1 (mm)		
DBBX_21	DBBX_05_SS	3000	150	10	30	10	15	0,2
DBBX_22	DBBX_06_SS	3000	150	10	60	10	15	0,4
DBBX_24	DBBX_08_SS	3000	150	10	135	10	15	0,9
DBBX_25	DBBX_09_SS	3000	150	6	30	6	25	0,2
DBBX_26	DBBX_10_SS	3000	150	6	60	6	25	0,4
DBBX_28	DBBX_12_SS	3000	150	6	135	6	25	0,9
DBBX_29	DBBX_13_SS	3000	150	5	30	5	30	0,2
DBBX_30	DBBX_14_SS	3000	150	5	60	5	30	0,4
DBBX_32	DBBX_16_SS	3000	150	5	135	5	30	0,9

Table 22 *Linked nomenclature and geometric parameters between carbon steel models by A. Peña and R. Chacón [7] and stainless steel models analysed in the current thesis*

The most important difference between carbon steel and stainless steel is visible in the stress-strain curve. Carbon steel stres-strain curve used within ABAQUS in the analysis by A. PEÑA and R. CHACÓN, as well as stainless steel stress-strain curve used in the present thesis, are displayed in *Figure 93*. It is visible that stainless steel does not reach a specific yield stress and displays a rounded curve. For high elongation percentages, i.e. elongation higher than approximately 4,5%, stainless steel achieves higher values of ultimate tensile strength due to its ductility.

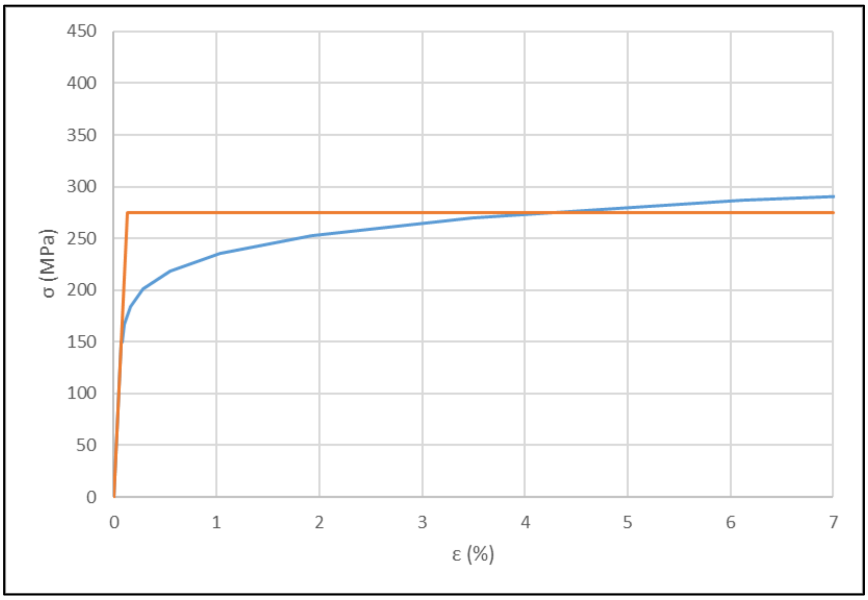

Figure 93 *Comparison of carbon steel and stainless steel stress-strain curves*

As expected, stainless steel models have higher ultimate strength due to their higher ductility, as it is clear from *Figure 94* to *Figure 102*.

On the one hand, in the particular case of compression loading and for lower values of β, ultimate strength for carbon steel is achieved at approximately 1/3 of the displacement that lead to ultimate strength for stainless steel. For instance, ultimate strength for carbon steel is achieved at approximately 10 mm of displacement, whereas for stainless steel is achieved at approximately 30 mm of displacement. This fact is visible in models for β=0,2 i.e. DBBX_05_SS, DBBX_09_SS and DBBX_13_SS (*Figure 94*, *Figure 97* and *Figure 100*, respectively); as well as in models for β=0,4 i.e. DBBX_06_SS, DBBX_10_SS and DBBX_14_SS (*Figure 95*, *Figure 98* and *Figure 101*, respectively). However, for higher values of β (β=0,9), which are models DBBX_08_SS, DBBX_12_SS and DBBX_16_SS (*Figure 96*, *Figure 99* and *Figure 102*, respectively), ultimate strength is achieved at much higher values of displacement.

Design resistances for carbon steel and stainless steel are listed in *Table 23*. Increment factor is approximately 1.3 for most of the models, which means stainless steel ultimate resistance is 30% higher than carbon steel. However, for the particular cases of {β=0,9 and 2γ=25} and { β=0,9 and 2γ=30}, increment factor is higher than 3.

	2γ	β	F_u Carbon steel	F_u Stainless steel	Increment factor
DBBX_05_SS	15	0,2	269,73	380,17	1,41
DBBX_06_SS	15	0,4	305,15	406,93	1,33
DBBX_08_SS	15	0,9	546,43	854,18	1,56
DBBX_09_SS	25	0,2	116,49	146,11	1,25
DBBX_10_SS	25	0,4	127,97	163,95	1,28
DBBX_12_SS	25	0,9	240,82	786,52	3,27
DBBX_13_SS	30	0,2	85,61	105,65	1,23
DBBX_14_SS	30	0,4	93,25	118,02	1,27
DBBX_16_SS	30	0,9	180,85	564,18	3,12

Table 23 *Design resistances comparison for stainless steel and carbon steel subjected to compression loading*

On the other hand, in the particular case of tensile loading, ultimate strength is higher than compression loading, as expected and consistent due to steel behaviour under tensile is much better than behaviour under compression. However, it is visible in figures from *Figure 94* to *Figure 102* that ultimate strength for stainless steel subjected to tensile loading is much more higher than carbon steel i.e. in most of the cases ultimate strength for stainless steel is more than double than ultimate strength for carbon steel, as it is visible in *Table 24* as well.

	2γ	β	F_u Carbon steel	F_u Stainless steel	Increment factor
DBBX_05_SS	15	0,2	324,43	775,18	2,39
DBBX_06_SS	15	0,4	654,02	1547,74	2,37
DBBX_08_SS	15	0,9	1435,37	2682,92	1,87
DBBX_09_SS	25	0,2	195,56	465,31	2,38
DBBX_10_SS	25	0,4	391,67	929,17	2,37
DBBX_12_SS	25	0,9	849,58	1742,20	2,05
DBBX_13_SS	30	0,2	163,60	387,74	2,37
DBBX_14_SS	30	0,4	325,75	774,99	2,38
DBBX_16_SS	30	0,9	704,30	1408,86	2,00

Table 24 *Design resistances comparison for stainless steel and carbon steel subjected to tensile loading*

β=0,2 / 2γ=15 (DBBX_21 vs DBBX_05_SS)

Compression

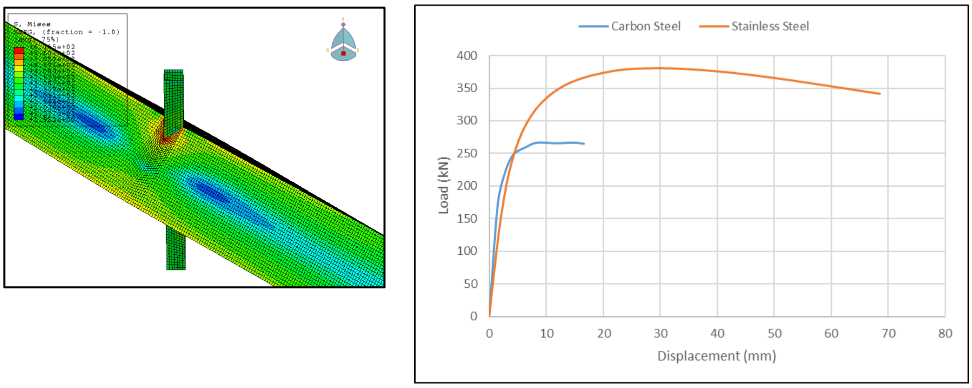

Tensile

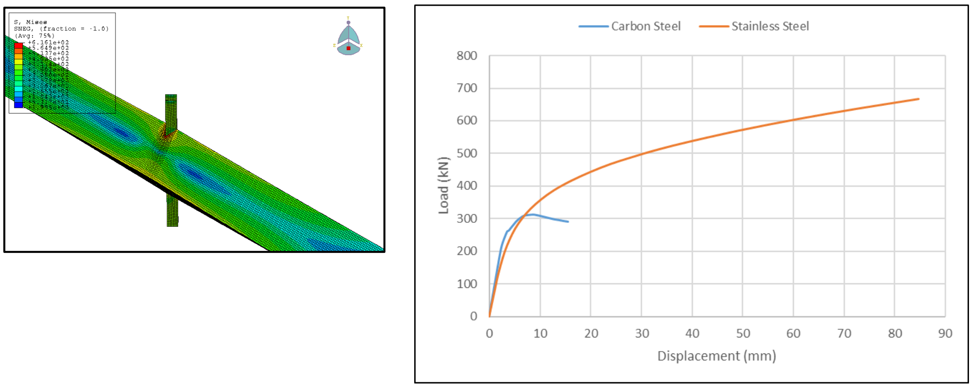

Figure 94 *Comparison of load-deformation curves for DBBX_21 (carbon steel) and DBBX_05_SS (stainless steel) under compression loading (up) and tensile loading (down)*

β=0,4 / 2γ=15 (DBBX_22 vs DBBX_06_SS)

Compression

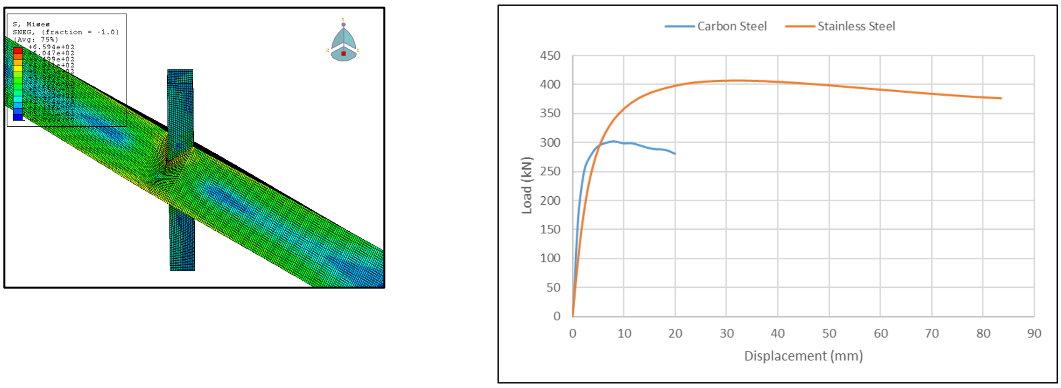

Tensile

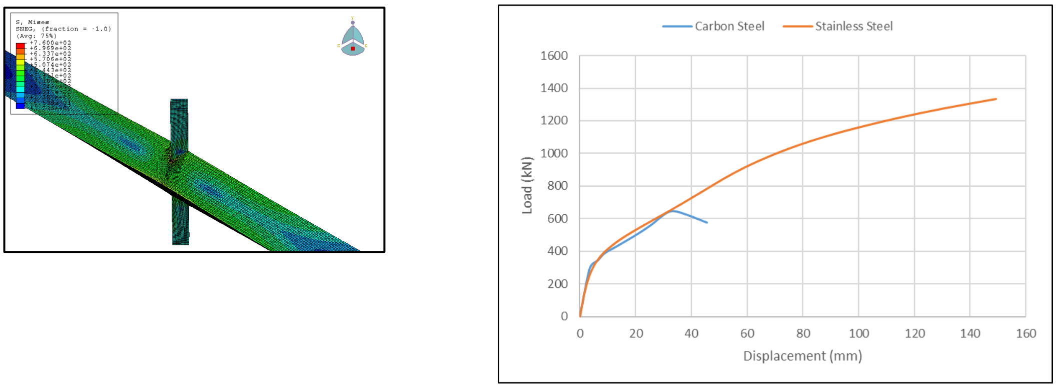

Figure 95 *Comparison of load-deformation curves for DBBX_22 (carbon steel) and DBBX_06_SS (stainless steel) under compression loading (up) and tensile loading (down)*

β=0,9 / 2γ=15 (DBBX_24 vs DBBX_08_SS)

Compression

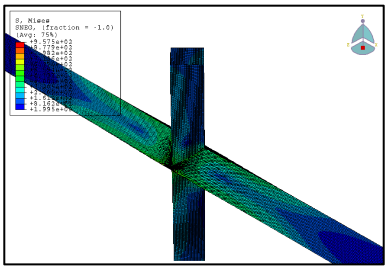

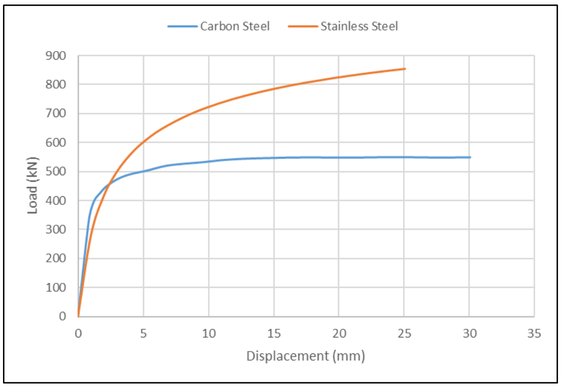

Tensile

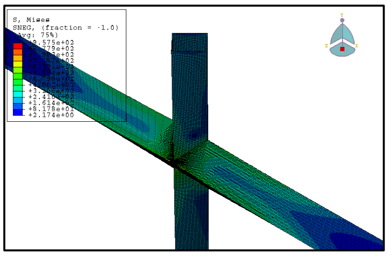

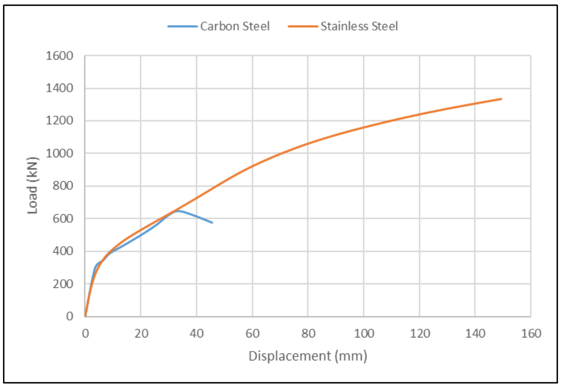

Figure 96 *Comparison of load-deformation curves for DBBX_24 (carbon steel) and DBBX_08_SS (stainless steel) under compression loading (up) and tensile loading (down)*

<u>β=0,2 / 2γ=25 (DBBX_25 vs DBBX_09_SS)</u>

Compression

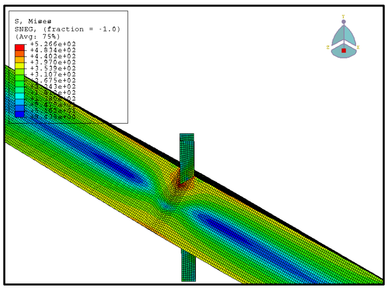

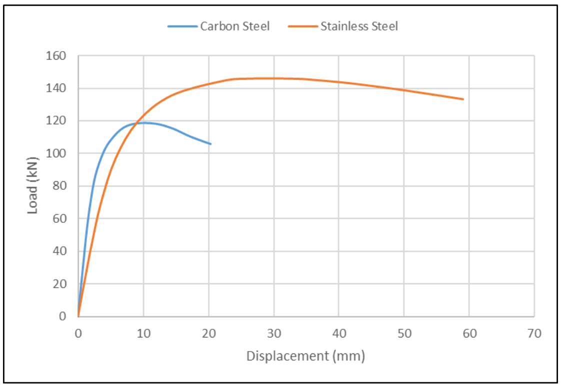

Tensile

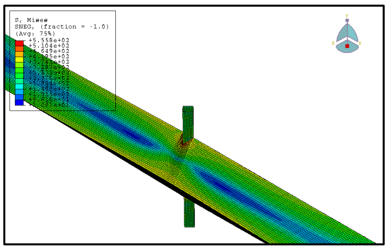

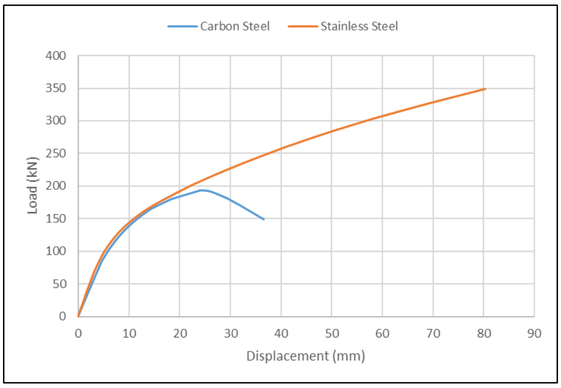

Figure 97 *Comparison of load-deformation curves for DBBX_25 (carbon steel) and DBBX_09_SS (stainless steel) under compression loading (up) and tensile loading (down)*

β=0,4 / 2γ=25 (DBBX_26 vs DBBX_10_SS)

Compression

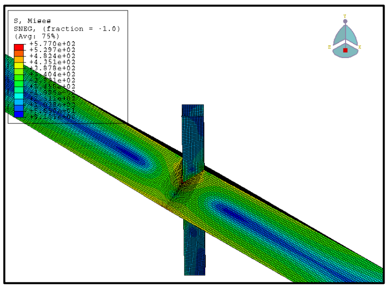

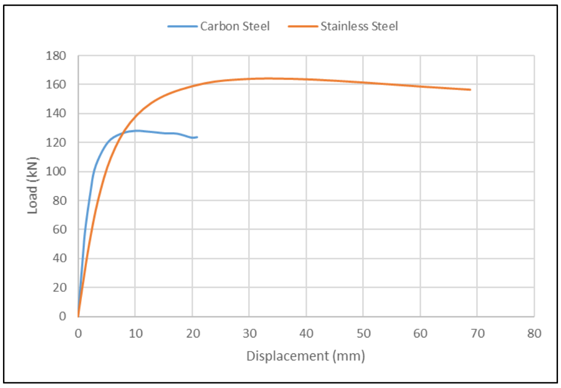

Tensile

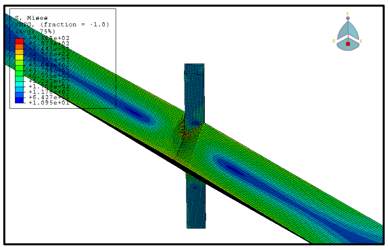

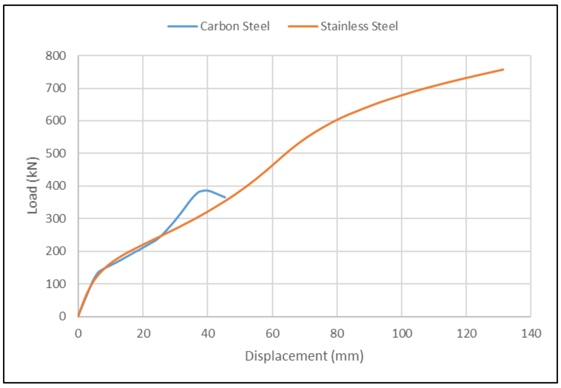

Figure 98 *Comparison of load-deformation curves for DBBX_26 (carbon steel) and DBBX_10_SS (stainless steel) under compression loading (up) and tensile loading (down)*

β=0,9 / 2γ=25 (DBBX_28 vs DBBX_12_SS)

Compression

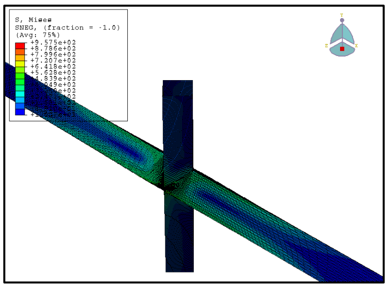

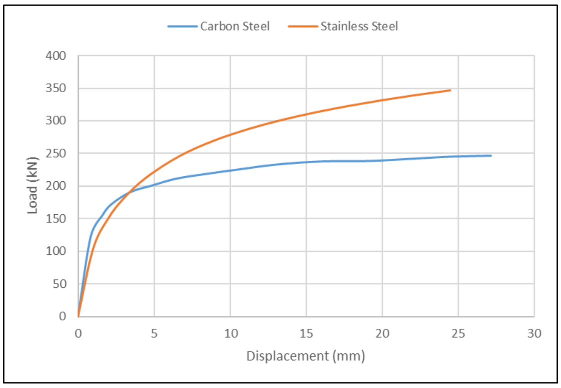

Tensile

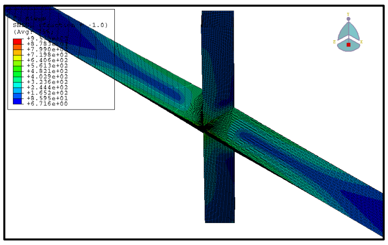

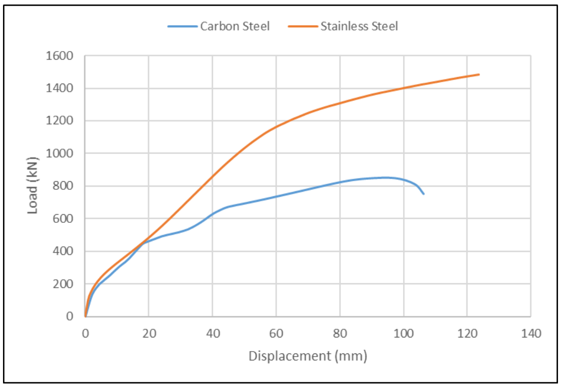

Figure 99 *Comparison of load-deformation curves for DBBX_28 (carbon steel) and DBBX_12_SS (stainless steel) under compression loading (up) and tensile loading (down)*

β=0,2 / 2γ=30 (DBBX_29 vs DBBX_13_SS)

Compression

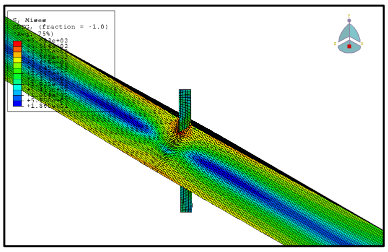

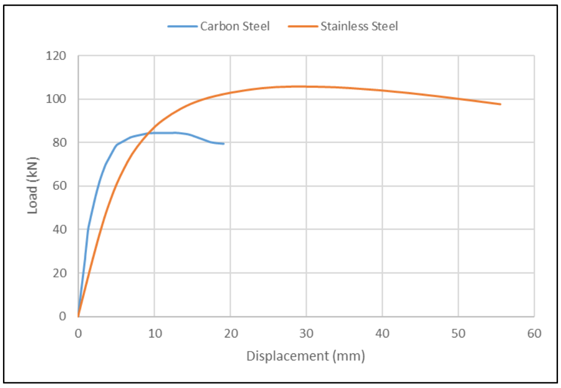

Tensile

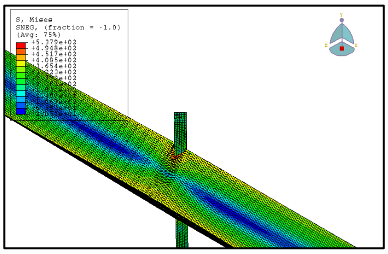

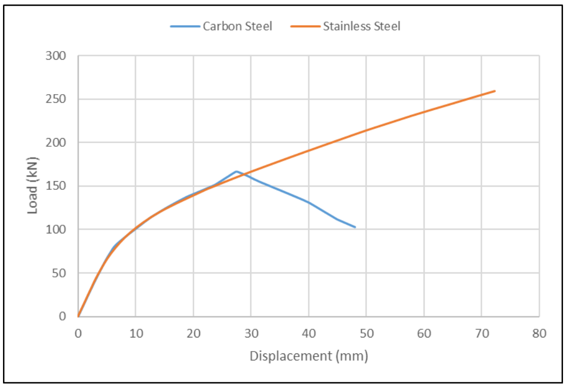

Figure 100 *Comparison of load-deformation curves for DBBX_29 (carbon steel) and DBBX_13_SS (stainless steel) under compression loading (up) and tensile loading (down)*

β=0,4 / 2γ=30 (DBBX_30 vs DBBX_14_SS)

Compression

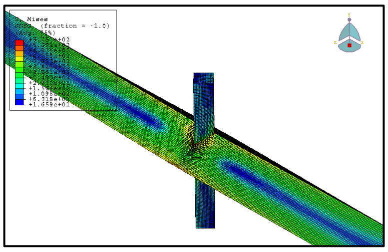

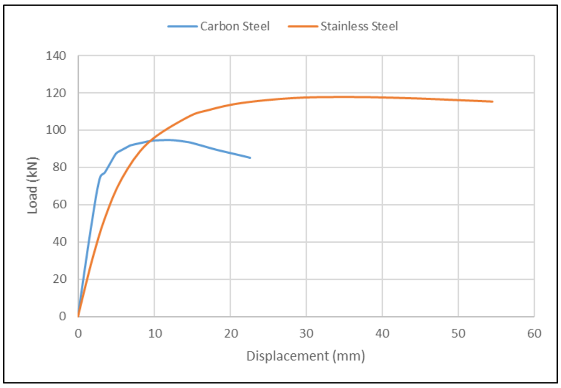

Tensile

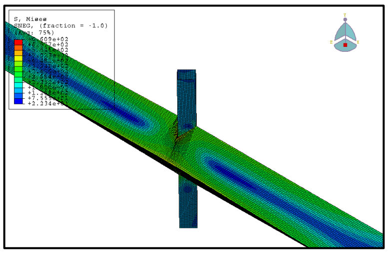

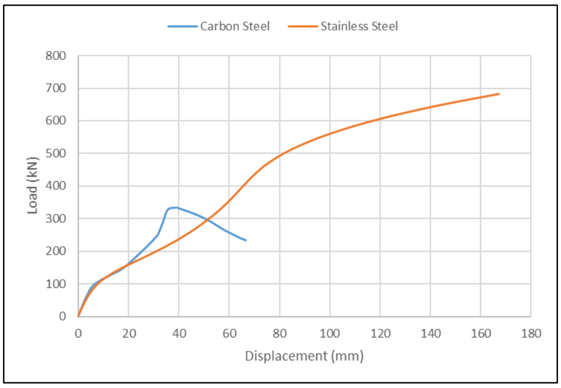

Figure 101 *Comparison of load-deformation curves for DBBX_30 (carbon steel) and DBBX_14_SS (stainless steel) under compression loading (up) and tensile loading (down)*

<u>β=0,9 / 2γ=30 (DBBX_32 vs DBBX_16_SS)</u>

Compression

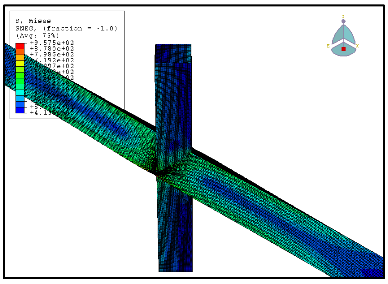

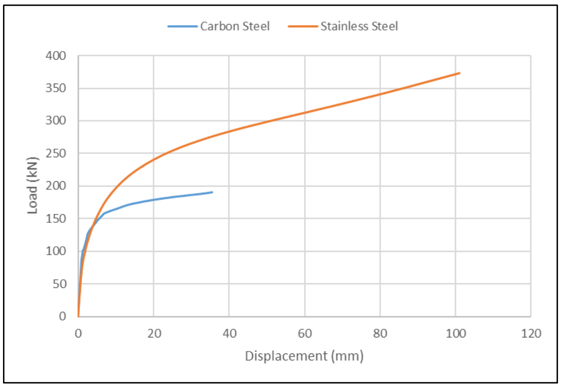

Tensile

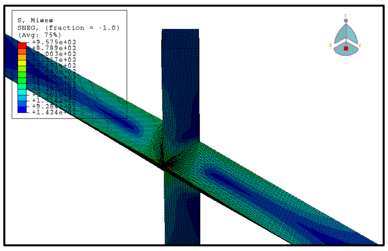

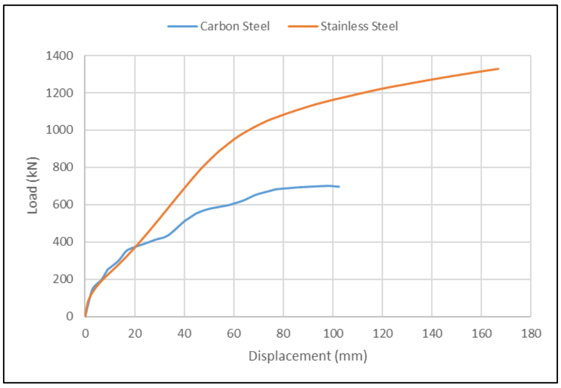

Figure 102 *Comparison of load-deformation curves for DBBX_32 (carbon steel) and DBBX_16_SS (stainless steel) under compression loading (up) and tensile loading (down)*

6. CONCLUSIONS

6.1 SUMMARY OF THE THESIS

The main objective of the current thesis has been to analyse hollow secion joints taking into account stainless steel material by means of a parametric study. In particular, several models of diamond bird-beak X-type (DBBX) joints have been modelled and calculated within ABAQUS, which is a high resolution finite element method software.

As stated in "*1. INTRODUCTION*" paragraph, there are some studies and articles analysing tubular hollow section joints in carbon steel under all kinds of loading assumptions i.e. tensile loading, compression loading, and both in-plane bending and out-of-plane bending. Furthermore, all types of joints have been analysed and studied throughtout recent history.

This thesis has been an attempt to study a specific X-type of diamond bird-beak joint under axial tensile and axial compression loading for a stainless steel material. Results obtained by means of the finite element method within ABAQUS will be compared to analytical formulation obtained by J.S. Owen et. al. in their article *"The influence of member orientation on the resistance of cross joints in square RHS construction" [6]* as well as the European Normative formulation EN 1993-1-8 [3].

First of all, tubular hollow section of joints as well as the most important characteristics of stainless steel have been largely explained in "*2. STATE OF THE ART*" paragraph, which are the most important tools for being able to carry out this study. Afterwards, finite elements method as well as modelling procedure within ABAQUS is explained and detailed in "*3. THE FINITE ELEMENT METHOD*".

As mentioned before, the main objective of the current thesis is to carry out a parametric analysis of a diamond bird-beak X-type joint, which is explained in "*4. PARAMETRIC STUDY OF DBB-X JOINTS*". Variation of two dimensionless parameters are considered: $\beta = b_1/b_0$ (relation between brace width and chord width) and $2\gamma = b_0/t_0$ (relation between chord width and chord thickness).

On the one hand, as stated in Owen et. al., parameter β ranges from 0.2 to 0.9. In the particular case of this thesis, β is taken as 0.2, 0.4, 0.6 and 0.9, which have been obtained from mantaining constant chord width and varying brace width for values 30 mm, 60 mm, 90mm and 135 mm, respectively. On the other hand, in the Owen et. al.'s article 2γ is ranged between 9.4 to 35.3. In this thesis, 2γ values are: 10, 15, 25 and 30, which are obtained from varying thickness for values 15 mm, 10 mm, 6 mm and 5 mm, respectively. Thus, the total number of models is 16, which are analysed under compression loading as well as tensile loading, which leads to a total amount of 32 different cases.

Finally, results have been analysed and discussed in the last paragraph of the thesis called "*5. ANALYSIS OF RESULTS*". Results are mainly analised and studied by three different points of view: design resistance dependance on β parameter (F_u-β); design resistance dependance on 2γ parameter (F_u-2γ); and load-displacement analysis. Furthermore, as mentioned before, results have been compared to J.S. Owen formulation as well as EN 1993-1-8 [3] formulation.

6.2 CONCLUSIONS OF THE STUDY

As mentioned before, 16 models have been analysed under compression as well as tensile loading and their design resistances have been compared to European Normative EN 1993-1-8 [3] and J.S. Owen article [6]. Also, stainless steel models have been compared to identical geometry models, but calculated in carbon steel material. Conclusions of the results obtained in the overall thesis are listed below:

Conclusions of results under axial compression loading

First of all, design resistance (F_u) dependance on parameter β concludes that as β increases, ultimate resistance increases as well. Moreover, β dependance states that for low values of β, results are similar to those of bibliography formulation and, therefore, they are suitable to analyse stainless steel joints taking into account these geometrical characteristics. Results for {β=0.9; 2γ=10} and {β=0.9; 2γ=15} are not consistent with the overall analysis.

Moreover, design resistance (F_u) dependance on parameter 2γ concludes that increasing parameter 2γ (reducing brace thickness) for a fixed value of β means decreasing ultimate resistance. Design resistance curves states that, as before, {β=0.9; 2γ=10} and {β=0.9; 2γ=15} are not consistent with the overall analysis.

Finally, conclusions for load-displacement curves states that as β increases (brace width increases), ultimate resistance increases as well and as 2γ increases (brace thickness decreases), design resitance decreases, which is consistent with previous conclusions. Moreover, load-displacement curves allows to acknowledge ductility performance. Thus, if β increases, ductility incrases and ultimate strength is achieve at higher values of displacement. However, if parameter 2γ increases (thickness decreases), ultimate strength decreases and models are less ductile i.e. models are more brittle and ultimate strength is achieved at lower values of displacement.

It is important to highlight that for compression loading, punching on the chord is the principal failure mode.

Conclusions of results under axial tensile loading

First of all, design resistance (F_u) dependance on parameter β concludes that as β increases, ultimate resistance increases as well. Furthermore, it is visible that modelled results in this thesis derive to a much higher ultimate resistance in comparison to design resistance of mentioned bibliography, which might be explained because EN 1993-1-8 is generally based on the resistance of the brace in compression to avoid the possible excessive local deformation or reduced rotation capacity or deformation capacity with which might otherwise occur. It is important to note that results for {β=0.4, 2γ=10} are not consistent with the overall analysis.

Analysis of design resistance (F_u) dependence on parameter 2γ for mdoels subjected to axial tensile loading concludes that increasing parameter 2γ for a fixed value of β means decreasing ultimate resistance. Thus, decreasing thickness means decreasing ultimate resistance. It is visible that modelled results in this thesis derive to a much higher ultimate resistance in comparison to design resistance of mentioned bibliography. As before, results for {β=0.4, 2γ=10} are not consistent with the overall analysis.

Finally, conclusions for load-displacement curves states that as β increases (brace width increases), ultimate resistance increases as well and as 2γ increases (brace thickness decreases), design resitance decreases, which is consistent with previous conclusions. Moreover, load-displacement curves allows to acknowledge ductility performance. Thus, if β increases, ductility incrases and ultimate strength is achieve at higher values of displacement. However, if parameter 2γ increases (thickness decreases), ultimate strength decreases but models are still more ductile, therefore ultimate strength is achieved at higher displacement for higher values of 2γ.

Principal failure mode for low values of β is brace failure with reduced effective width, whereas for high values of β there is coupling failure between chord face failure and brace failure. It should be important to note that for β=0.9, high values of thickness leads to chord face failure instead of theoretical failure modes of the European normative i.e. brace failure with reduced effective width, whereas low values of thickness leads to brace failure, which is consistent with theoretical failure mode of European Normative.

Conclusions of comparison between carbon steel and stianless steel

Stainless steel results of diamond bird-beak joints show a much higher ultimate strength than identical carbon steel geometry models, as expected. On the one hand, in the particular case of compression loading and for lower values of β, ultimate strength for carbon steel is achieved at approximately 1/3 of the displacement that lead to ultimate strength for stainless steel. Furthermore, ultimate strength for stainless steel is about 1.3 times of the design resistance for carbon steel. On the other hand, ultimate resistance under tensile loading for stainless steel is more than double of design resistance for carbon steel for most of the cases. This might be explained due to stainless steel ductility is higher than carbon steel's.

6.3 FUTURE SCOPE AND PERSPECTIVES

This thesis is a parametric study to understand the failure modes of a stainless steel diamond bird-beak X-type joint (DBBX) subjected to compression and tensile forces. This paragraph highlights some perspectives in order to enlarge this study.

First of all, despite the fact that this thesis concludes with great advantages of stainless steel joints against traditional carbon steel joints when the joint is subjected to axial forces due to its ductility, it shall be of high interest to study all the models but subjected to in-plane bending as well as out-of-plane bending in order to acknowledge their performance.

Furthermore, different types or grades of stainless steel should be studied in order to acknowledge their differences. For instance, different yield stresses might be considered in future studies. Also, this study has been carried out for a X-type welded planar joint with 90º angles between brace and chord. It shall be interesting to study joints with diagonal elements as well as different joint configurations (T, Y, N, K or KT) and/or study a spatial 3D joint, with braces in the transversal axis in order to realistically approach truss configuration.

Stress concentration factors should be of high interest to study as well in further research of stainless steel diamond bird beak-joints in order to compare results with literature of stress concentration factors of diamond bird-beak joints.

Finally, it is worth pointing out that the database of results provided herein is based upon an experimentally validated numerical model which assumes perfect match between solids. Further research detailing the effect of welding might improve and enlarge conclusions of this thesis by including the potential failure mode which involves the welding toes.

Bibliography

NORMATIVES

[1] EN 1993-1-1:2005, Eurocode 3: Design of steel structures. Part 1-1: General rules and rules for buildings

[2] EN 1993-1-4:2006, Eurocode 3: Design of steel structures. Part 1-4: General rules – Supplementary rules for stainless steel

[3] EN 1993-1-8:2005, Eurocode 3: Design of steel structures. Part 1-8: Design of joints

[4] EN 1993-1-9:2005, Eurocode 3: Design of steel structures. Part 1-9: Fatigue

MANUALS

[5] Abaqus Standar user's manual, version 6.12

ARTICLES

[6] J.S. OWEN, G. DAVIES, R.B. KELLY "The influence of member orientation on the resistance of cross joints in square RHS construction" Journal of Constructional Steel Research 57 (2001) 253-278

[7] A. PEÑA, R. CHACÓN "Structural analysis of diamond bird-beak joints subjected to compressive and tensile forces" Journal of Constructional Steel Research 98 (2014) 158-166

[8] Y. CHEN, R. FENG, J. WANG "Behaviour of bird-beak square hollow X-joints under out-of-plane bending" Journal of Constructional Steel Research 106 (2015) 234-245

[9] Y. CHEN, R. FENG, J. WANG "Behaviour of bird-beak square hollow X-joints under in-plane bending" Thin-Walled Structures 86 (2015) 94-107

[10] L. TONG, G. XU, D. YAN, XL ZHAO "Fatigue tests and design of diamond bird-beak SHS T-joints under axial loading in brace" Journal of Constructional Steel Research 118 (2016) 49-59

[11] L. TONG, G. XU, Y. LIU, D. YAN, XL. ZHAO "Finite elements analysis and formulae for stress concentration factors of diamond bird-beak SHS T-joints" Thin-Walled Structures 86 (2015) 108-120

[12] B. CHENG, Q. QIAN, XL. ZHAO "Numerical investigation on stress concentration factors of square bird-beak SHS T-joints subject to axial forces" Thin-Walled Structures 94 (2015) 435-445

[13] Y. CHEN, J. WANG "Numerical study and design equations of square and diamond bird-beak SHS T-joints under axial compression" Thin-Walled Structures 97 (2015) 215-224

[14] Y. CHEN, J. YANG, K. HU "Parametric study and formulae of SCFs for positive large eccentricity CHS N-joints" Journal of Constructional Steel Research 120 (2016) 117-131

[15] J. YANG, Y. CHEN, K. HU "Stress concentration factors of negative large eccentricity tubular N-joints under axial compressive loading in vertical brace" Thin-Walled Structures 96 (2015) 359-371

[16] Y. CHEN, Y. WU, X. RUAN, R. FENG "Tests of SHS brace-H-shaped chord X-joints under in-plane bending" Thin-Walled Structures 97 (2015) 171-185

[17] I. ARRAYAGO, E. REAL, L. GARDNER "Description of stress-strain curves for stainless steel alloys" Materials & Design 87(2015) 540-552

[18] A.D. CHRISTITSAS, D.T. PACHOUMIS, C.N. KALFAS, E.G. GALOUSSIS "FEM analysis of conventional and square bird-beak SHS joint subject to in-plane bending moment — experimental study" Journal of Constructional Steel Research 63 (2007) 1361-1372

[19] L. TONG, Y. FU, Y. LIU, X.L. ZHAO "Stress concentration factors of diamond bird-beak SHS T-joints under brace loading" Thin-Walled Structures 74 (2014) 201-212

[20] B. CHENG, C. LI, Y, LOU, X.L. ZHAO "SCF of bird-beak SHS X-joints under asymmetrical brace axial forces" Thin-Walled Structures 123 (2018) 57-69

BOOKS

[21] J. WARDENIER, J.A. PACKER, X.L. ZHAO, G.J. VAN DER VEGTE "Hollow sections in structural applications" Staal Bouwen met CIDECT (2010)

APPENDICES

A. GEOMETRY OF MODELS

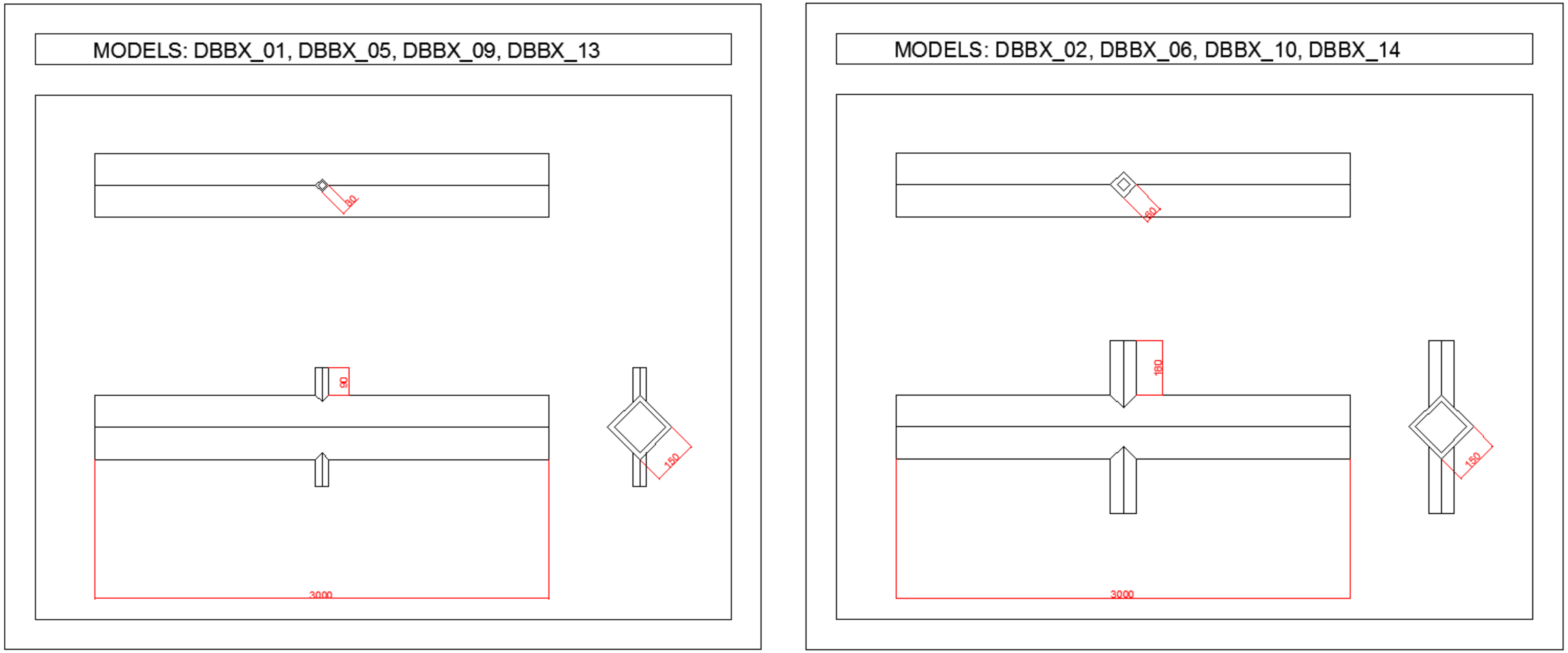

Figure 103 *Geometry of models. Brace widht of 30 mm (left) and brace width of 60 mm (right)*

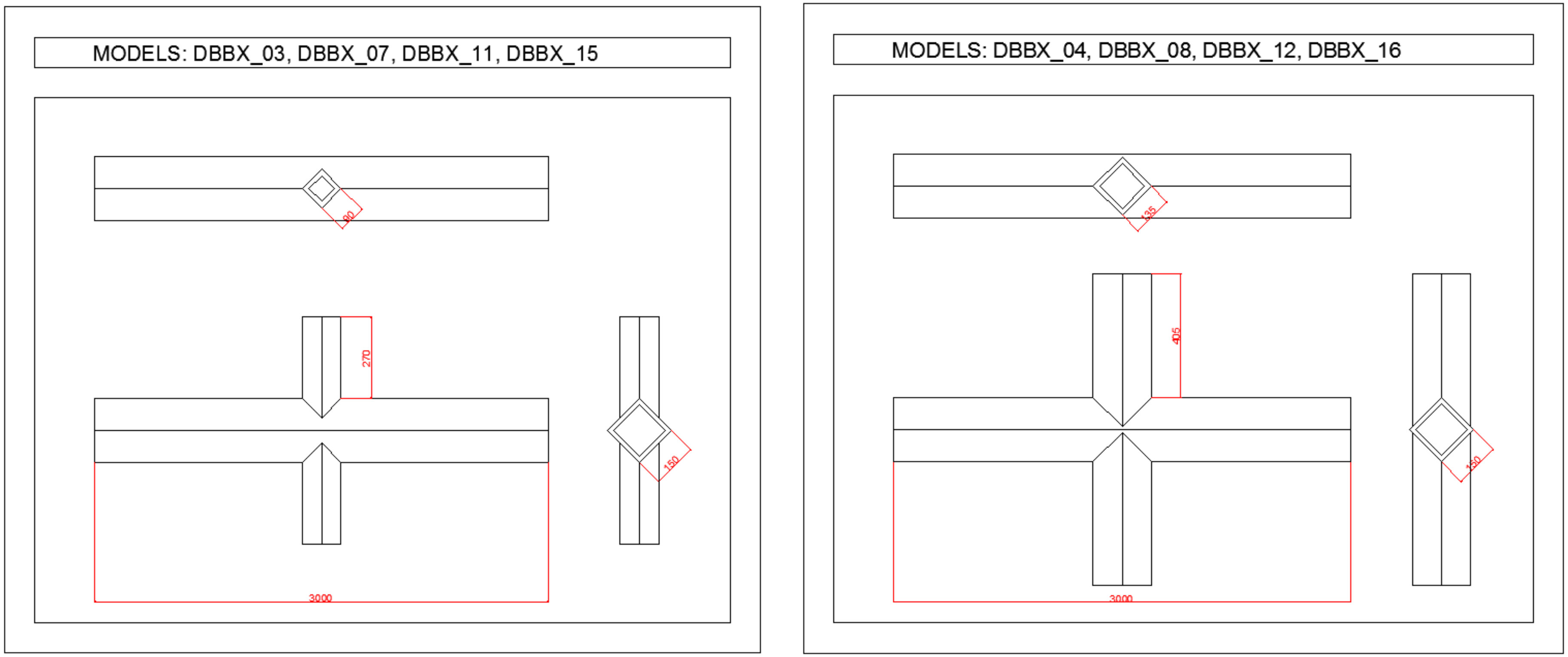

Figure 104 *Geometry of models. Brace widht of 90 mm (left) and brace width of 135 mm (right)*

B. DESIGN RESISTANCES

B.1 DESIGN RESISTANCES ACCORDING TO EN 1993-1-8

<table>
<tr><th>Type of joint</th><th colspan="2">Design resistance [$i = 1$]</th></tr>
<tr><td rowspan="8">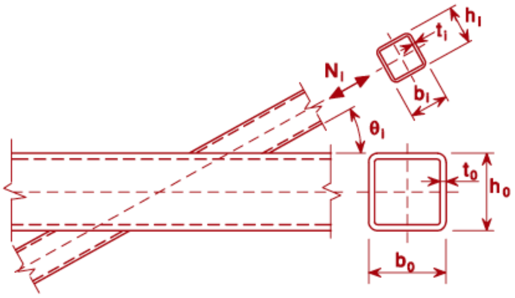
</td><td>Chord face failure</td><td>$\beta \leq 0{,}85$</td></tr>
<tr><td colspan="2">$N_{i,Rd} = \frac{k_n f_{y0} t_0^2}{(1-\beta)\sin\theta_1}\left(\frac{2\eta}{\sin\theta_1} + 4\sqrt{1-\beta}\right) / \gamma_{M5}$</td></tr>
<tr><td>Chord side wall buckling [1)]</td><td>$\beta = 1{,}0$ [2)]</td></tr>
<tr><td colspan="2">$N_{i,Rd} = \frac{f_b t_0}{\sin\theta_i}\left(\frac{2h_i}{\sin\theta_1} + 10t_0\right) / \gamma_{M5}$</td></tr>
<tr><td>Brace failure</td><td>$\beta \geq 0{,}85$</td></tr>
<tr><td colspan="2">$N_{i,Rd} = f_{yi} t_i (2h_i - 4t_i + 2b_{eff}) / \gamma_{M5}$</td></tr>
<tr><td>Punching shear</td><td>$0{,}85 \leq \beta \leq (1 - 1/\gamma)$</td></tr>
<tr><td colspan="2">$N_{i,Rd} = \frac{f_{y0} t_0}{\sqrt{3}\sin\theta_1}\left(\frac{2h_i}{\sin\theta_1} + 2b_{e,p}\right) / \gamma_{M5}$</td></tr>
<tr><td colspan="3">[1)] For X joints with $\theta < 90°$ use the smaller of this value and the design shear resistance of the chord side walls given for K and N gap joints in Table 7.12.
[2)] For $0{,}85 \leq \beta \leq 1{,}0$ use linear interpolation between the value for chord face failure at $\beta = 0{,}85$ and the governing value for chord side wall failure at $\beta = 1{,}0$ (side wall buckling or chord shear).</td></tr>
<tr><td colspan="3">For circular braces, multiply the above resistances by $\pi/4$, replace b_1 and h_1 by d_1 and replace b_2 and h_2 by d_2.</td></tr>
<tr><td rowspan="3">For tension:
$f_b = f_{y0}$

For compression:
$f_b = \chi f_{y0}$ (T and Y joints)
$f_b = 0{,}8\,\chi f_{y0} \sin\theta_i$ (X joints)

where χ is the reduction factor for flexural buckling obtained from EN 1993-1-1 using the relevant buckling curve and a normalized slenderness $\overline{\lambda}$ determined from:
$\overline{\lambda} = 3{,}46 \frac{\left(\frac{h_0}{t_0} - 2\right)\sqrt{\frac{1}{\sin\theta_i}}}{\pi\sqrt{\frac{E}{f_{y0}}}}$</td><td colspan="2">$b_{eff} = \frac{10}{b_0/t_0}\frac{f_{y0}t_0}{f_{yi}t_i} b_i$ but $b_{eff} \leq b_i$</td></tr>
<tr><td colspan="2">$b_{e,p} = \frac{10}{b_0 t_0} b_i$ but $b_{e,p} \leq b_i$</td></tr>
<tr><td colspan="2">For $n > 0$ (compression): $k_n = 1{,}3 - \frac{0{,}4n}{\beta}$
but $k_n \leq 1{,}0$
For $n \leq 0$ (tension): $k_n = 1{,}0$</td></tr>
</table>

***Table 25** Design axial resistances of welded T, X and Y joints between RHS braces and RHS chords (EN 1993-1-8 Table 7.11 [3])*

JOINT	Chord face failure		Chord side wall buckling		Brace failure		Punching shear	
	β≤0,85		β≥0,85		β≥0,85		0,85≤β≤(1-1/γ)	
	Tension	Compression	Tension	Compression	Tension	Compression	Tension	Compression
	$N_{i,Rd,TENS}$	$N_{i,Rd,COMP}$	$N_{i,Rd,TENS}$	$N_{i,Rd,COMP}$	$N_{i,Rd,TENS}$	$N_{i,Rd,COMP}$	$N_{i,Rd,TENS}$	$N_{i,Rd,COMP}$
DBBX_01_SS	376.24	376.24	NA	NA	NA	NA	NA	NA
DBBX_02_SS	577.33	577.33	NA	NA	NA	NA	NA	NA
DBBX_03_SS	965.45	965.45	NA	NA	NA	NA	NA	NA
DBBX_04_SS	Linear interpolation		1764.00	1270.08	2016.00	2016.00	1309.43	1309.43
DBBX_05_SS	167.22	167.22	NA	NA	NA	NA	NA	NA
DBBX_06_SS	256.59	256.59	NA	NA	NA	NA	NA	NA
DBBX_07_SS	429.09	429.09	NA	NA	NA	NA	NA	NA
DBBX_08_SS	Linear interpolation		1036.00	621.60	1148.00	1148.00	727.46	727.46
DBBX_09_SS	60.20	60.20	NA	NA	NA	NA	NA	NA
DBBX_10_SS	92.37	92.37	NA	NA	NA	NA	NA	NA
DBBX_11_SS	154.47	154.47	NA	NA	NA	NA	NA	NA
DBBX_12_SS	Linear interpolation		554.40	221.76	594.72	594.72	366.64	366.64
DBBX_13_SS	41.80	41.80	NA	NA	NA	NA	NA	NA
DBBX_14_SS	64.15	64.15	NA	NA	NA	NA	NA	NA
DBBX_15_SS	107.27	107.27	NA	NA	NA	NA	NA	NA
DBBX_16_SS	Linear interpolation		448.00	143.36	476.00	476.00	290.98	290.98

Table 26 *Design axial resistances of DBBX different models according to EN 1993-1-8*

B.2 DESIGN RESISTANCES ACCORDING TO J.S. OWEN

Design resistances according to J.S. Owen are obtained from following formulation:

$$F_{u1} = \frac{f_{y0}}{1000}\left(\frac{f_{y0}}{275}\right)^{0.8} \frac{(6.06 - 5.6\beta + 11.4\beta^2)(0.6 + 1.97\sqrt{\beta})t_0^2}{\frac{t_0}{b_0}(6.06 - 5.6\beta + 11.4\beta^2) + \frac{1}{3}(0.6 + 1.97\sqrt{\beta})} \qquad \textbf{\textit{Eq. 16}}$$

JOINT	F_{u1} (kN)
DBBX_01_SS	494,33
DBBX_02_SS	564,45
DBBX_03_SS	665,58
DBBX_04_SS	875,41
DBBX_05_SS	266,01
DBBX_06_SS	298,47
DBBX_07_SS	353,54
DBBX_08_SS	477,34
DBBX_09_SS	115,18
DBBX_10_SS	126,68
DBBX_11_SS	150,82
DBBX_12_SS	209,95
DBBX_13_SS	84,26
DBBX_14_SS	92,09
DBBX_15_SS	109,81
DBBX_16_SS	154,35

Table 27 *Design axial resistances of DBBX joints according to J.S. Owen formulation*

C. VON MISES

C.1 COMPRESSION

DBBX_01_SS_C

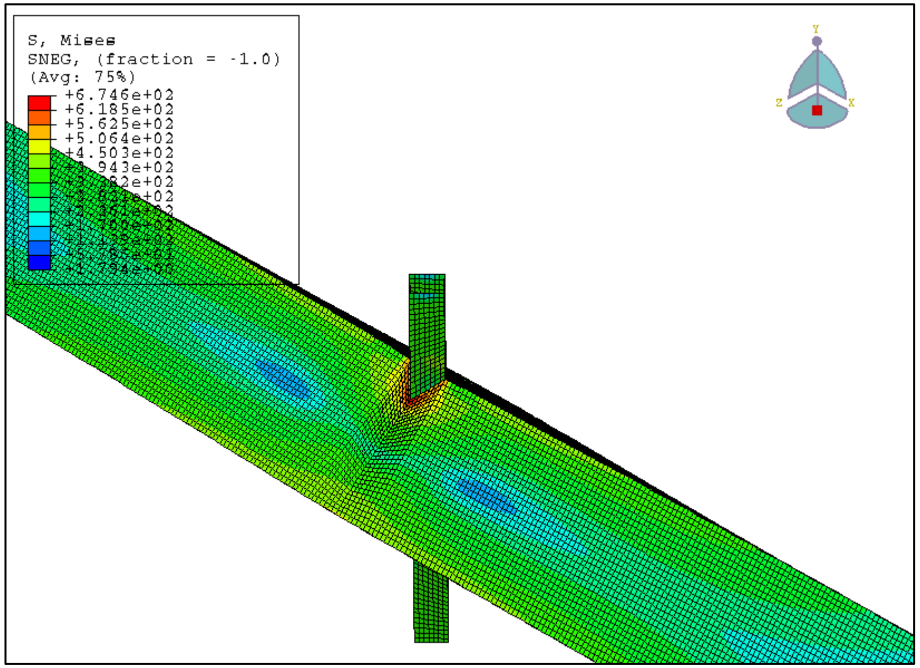

DBBX_02_SS_C

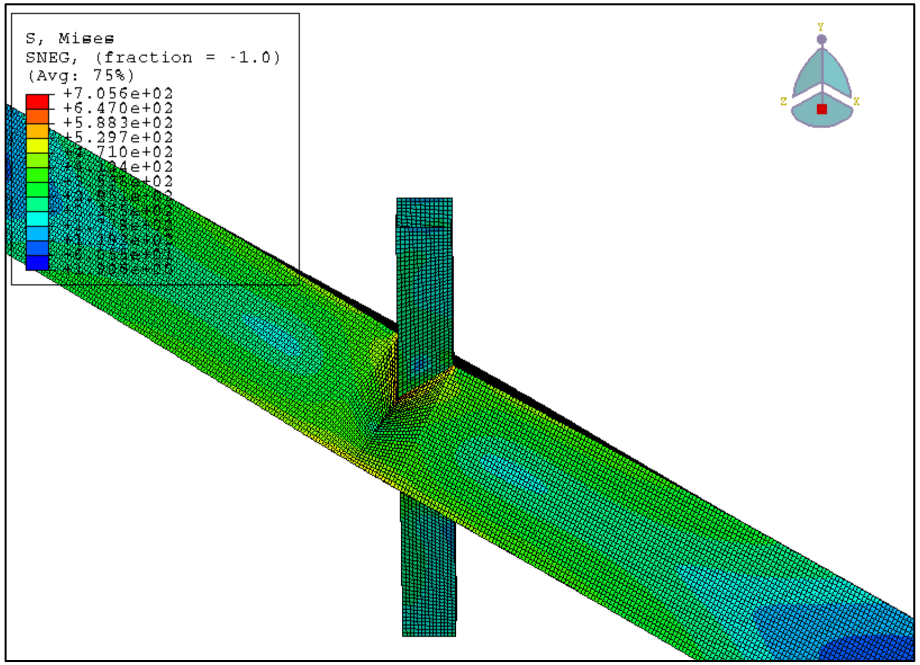

Figure 105 *Von Mises stresses for DBBX_01_SS (left) and DBBX_02_SS (right) under compression loading*

DBBX_03_SS_C

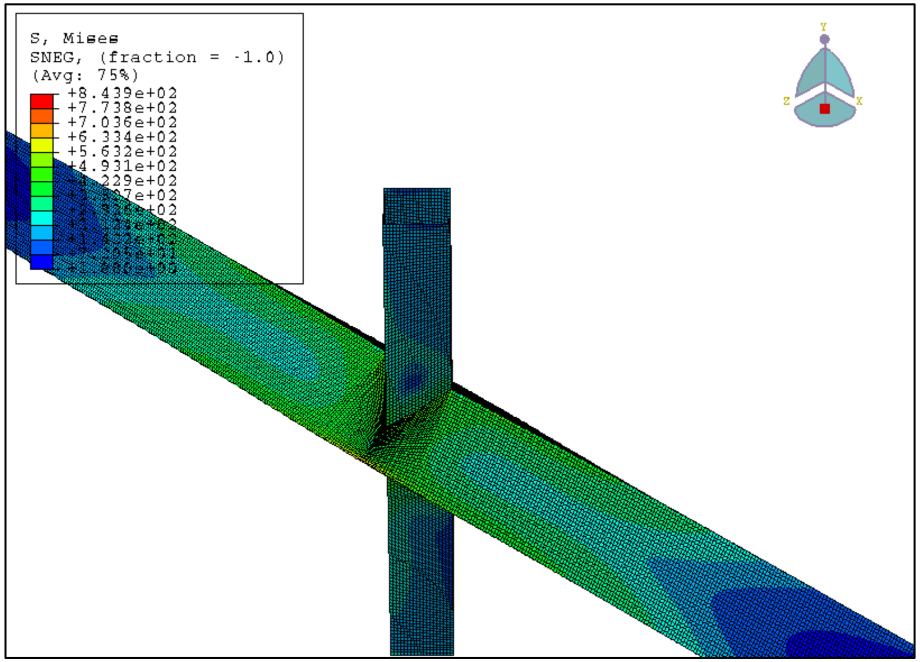

DBBX_04_SS_C

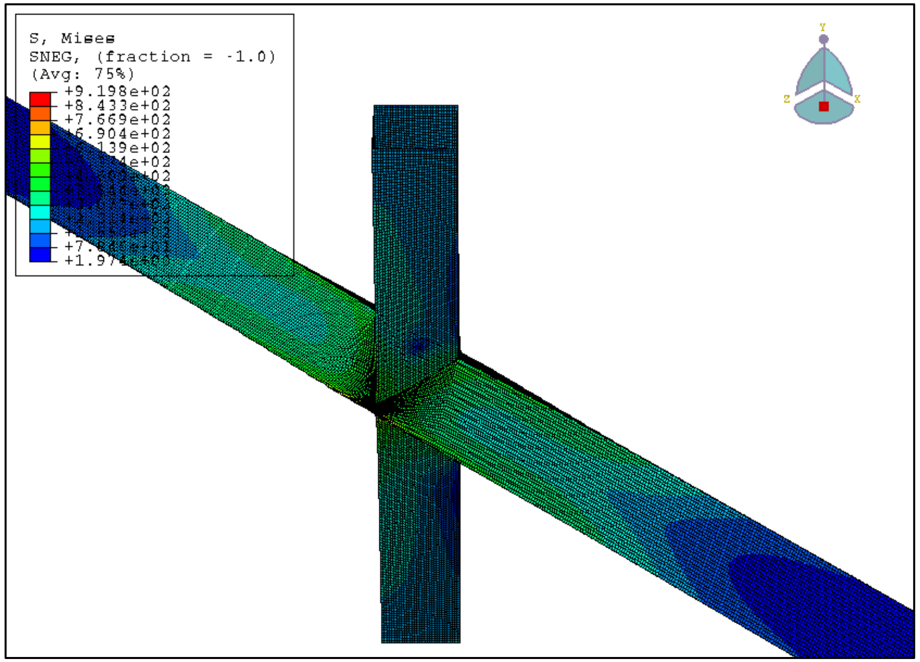

Figure 106 *Von Mises stresses for DBBX_03_SS (left) and DBBX_04_SS (right) under compression loading*

DBBX_05_SS_C

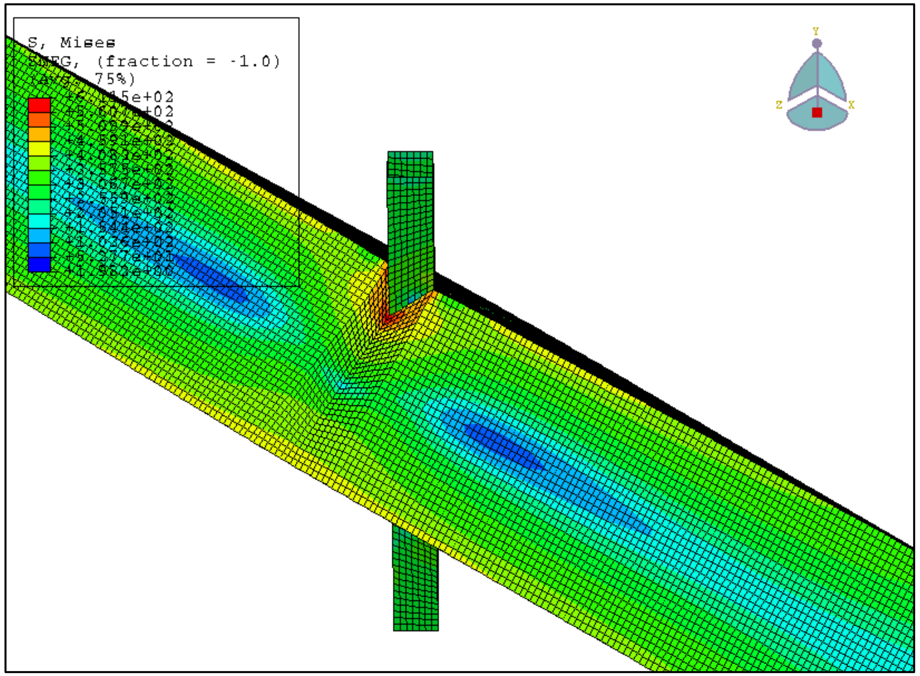

DBBX_06_SS_C

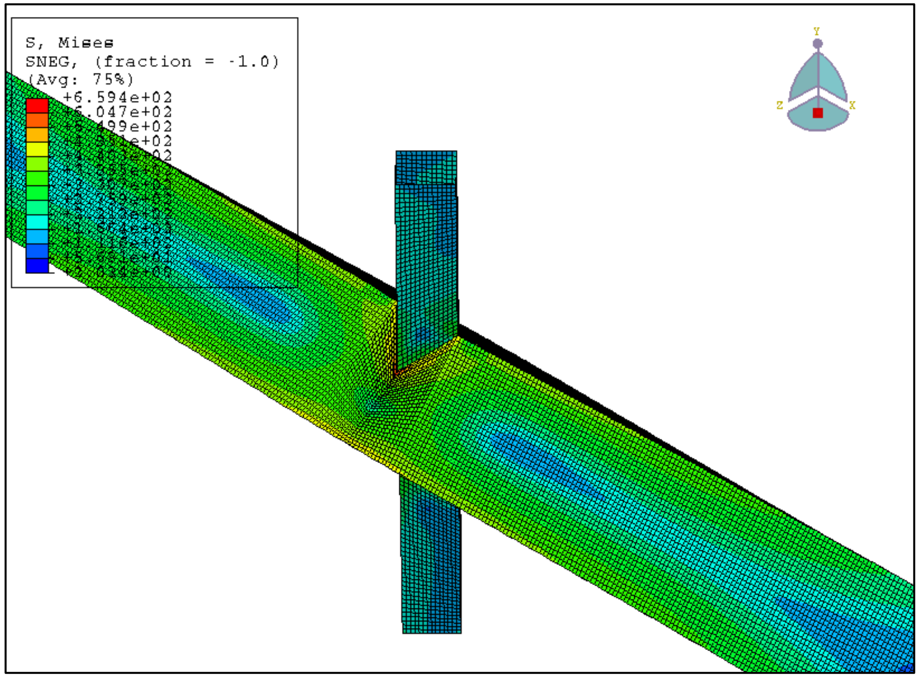

Figure 107 *Von Mises stresses for DBBX_05_SS (left) and DBBX_06_SS (right) under compression loading*

DBBX_07_SS_C DBBX_08_SS_C

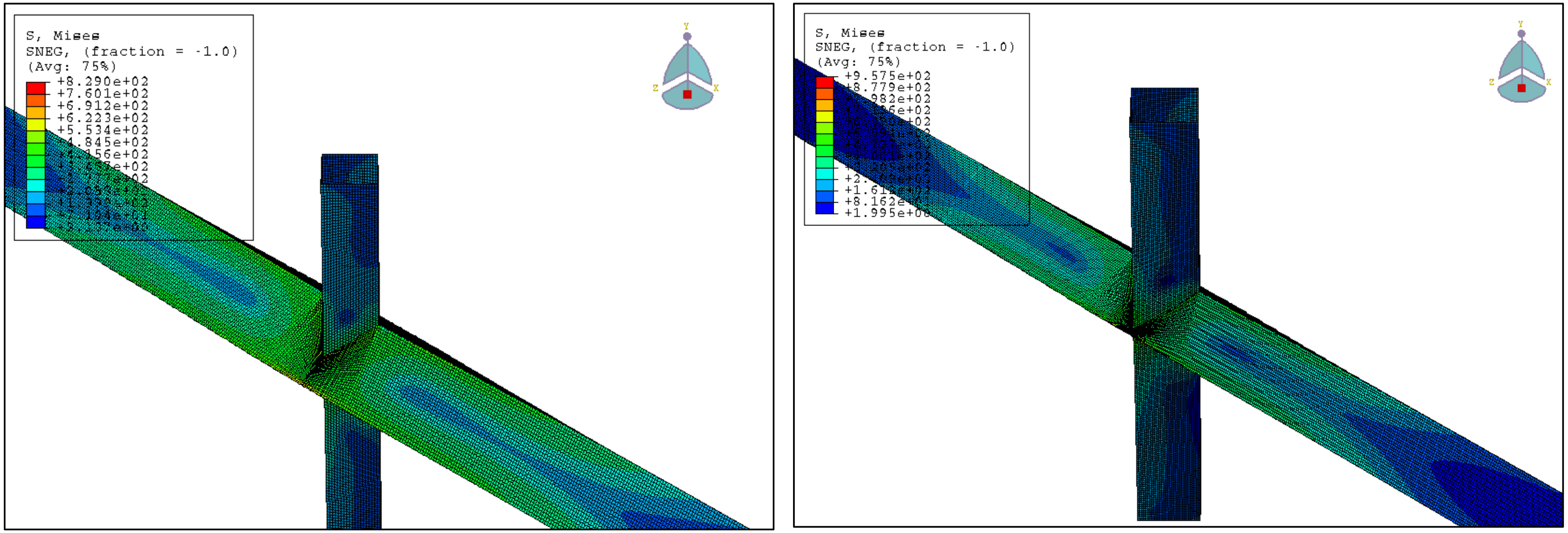

Figure 108 *Von Mises stresses for DBBX_07_SS (left) and DBBX_08_SS (right) under compression loading*

DBBX_09_SS_C

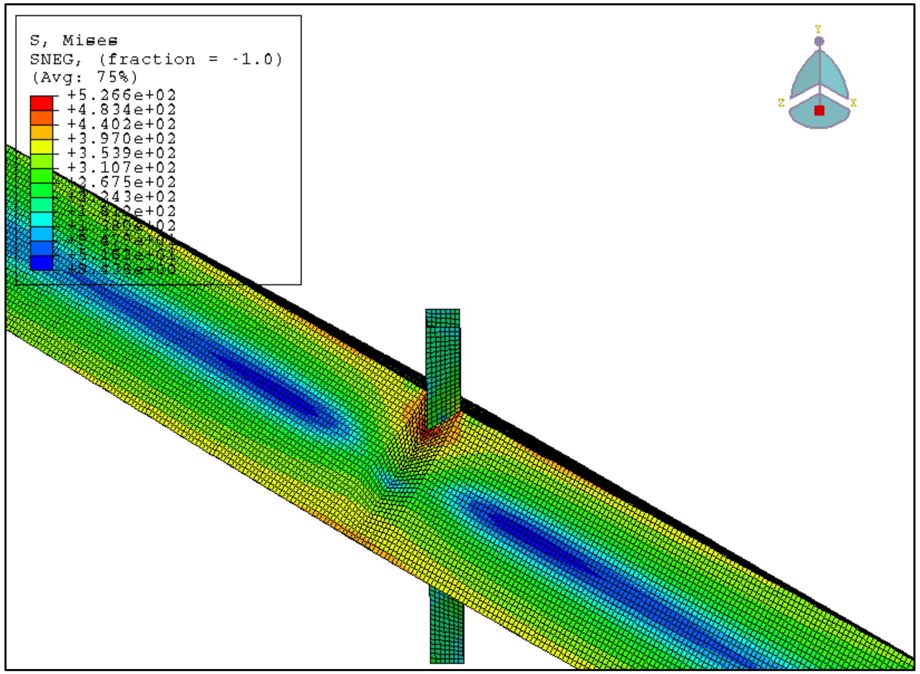

DBBX_10_SS_C

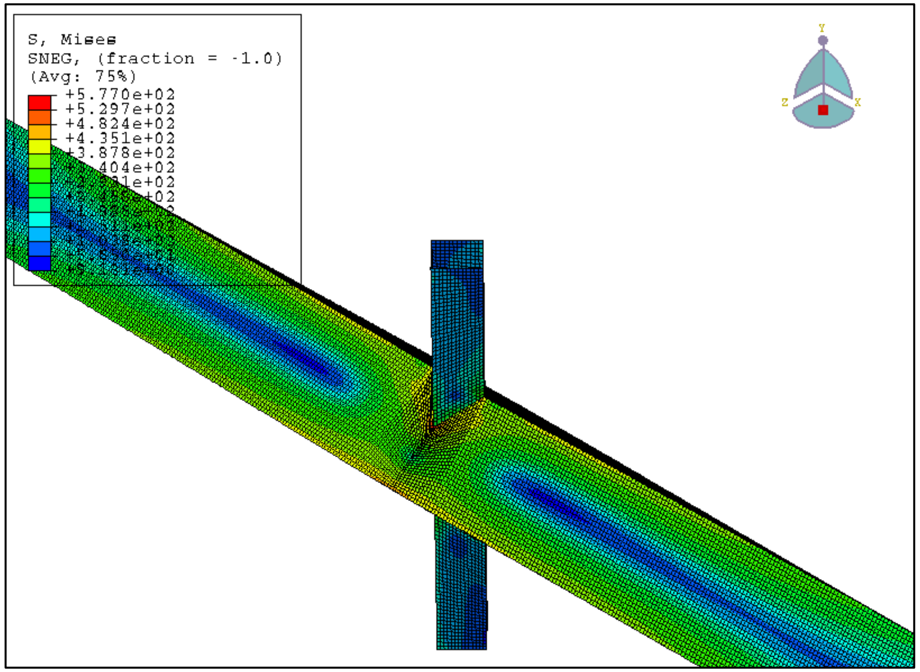

Figure 109 *Von Mises stresses for DBBX_09_SS (left) and DBBX_10_SS (right) under compression loading*

DBBX_11_SS_C DBBX_12_SS_C

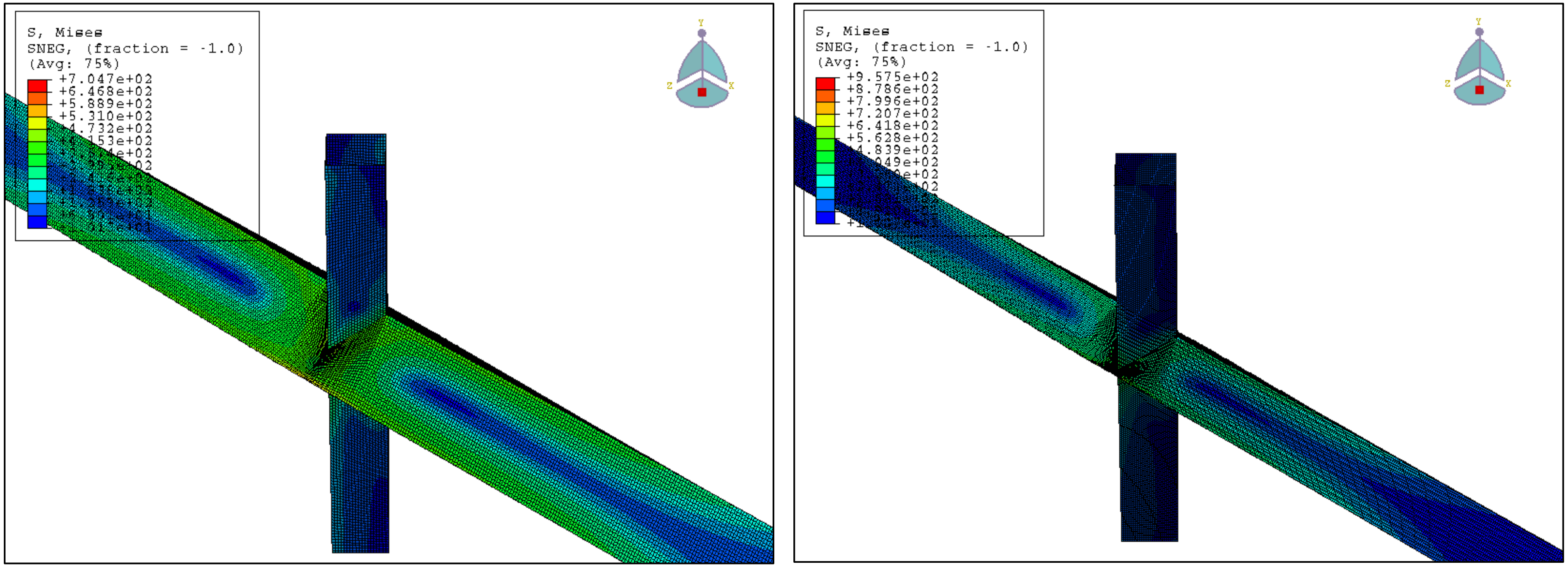

Figure 110 *Von Mises stresses for DBBX_11_SS (left) and DBBX_12_SS (right) under compression loading*

DBBX_13_SS_C

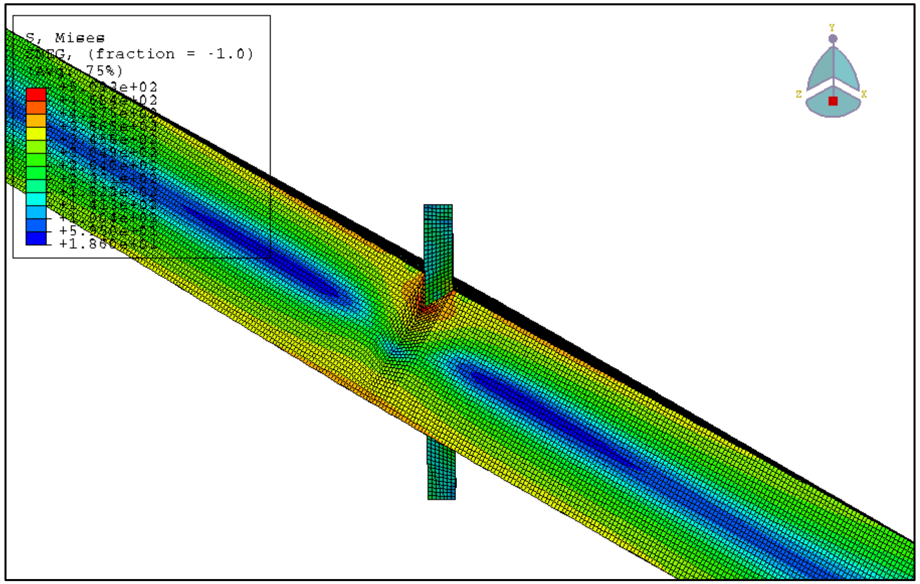

DBBX_14_SS_C

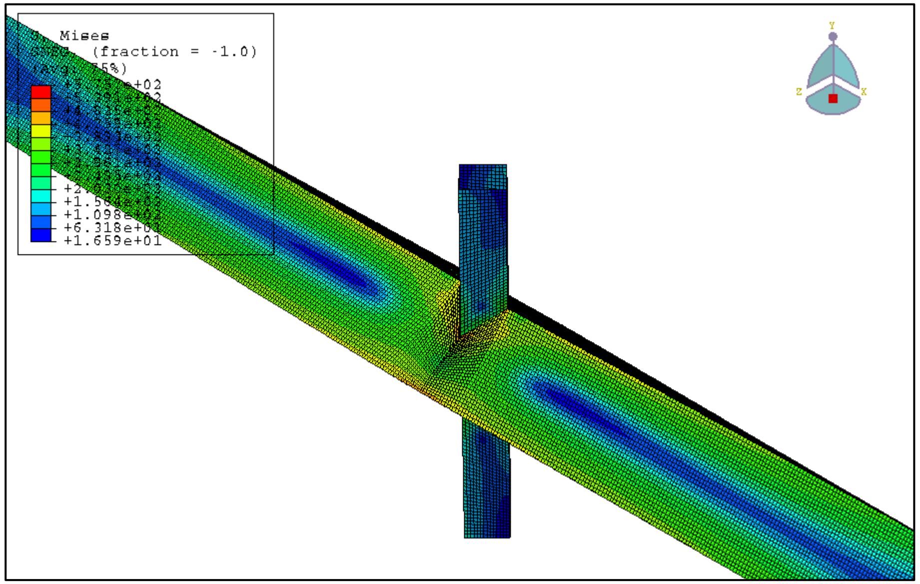

Figure 111 *Von Mises stresses for DBBX_13_SS (left) and DBBX_14_SS (right) under compression loading*

DBBX_15_SS_C

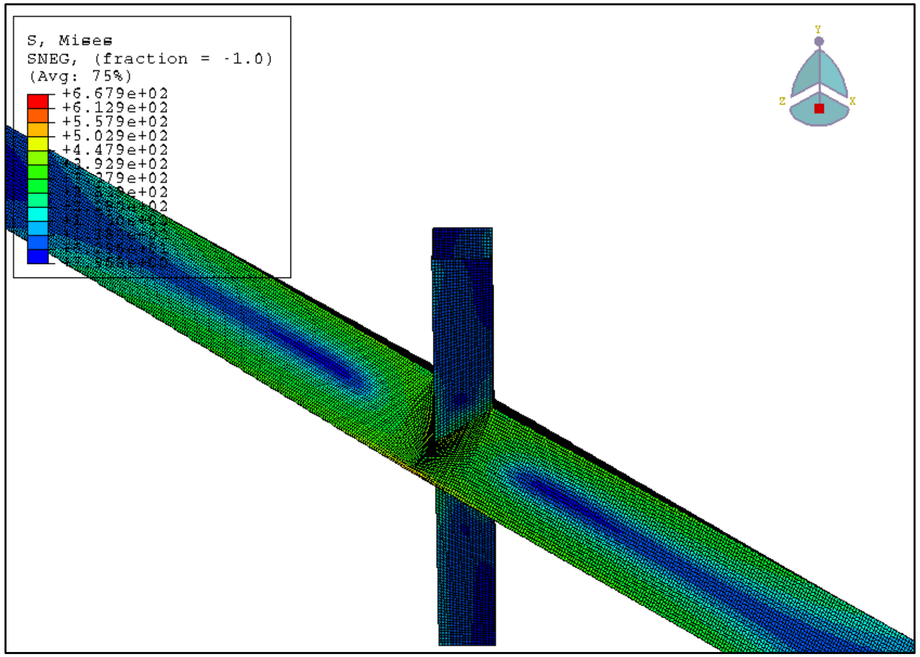

DBBX_16_SS_C

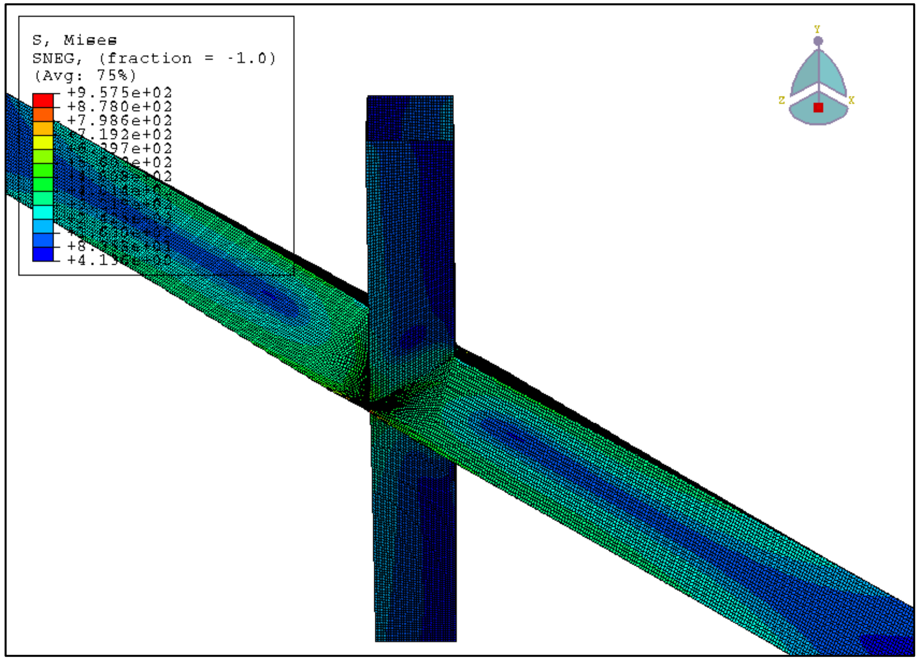

Figure 112 *Von Mises stresses for DBBX_15_SS (left) and DBBX_16_SS (right) under compression loading*

C.2 TENSION

DBBX_01_SS_T

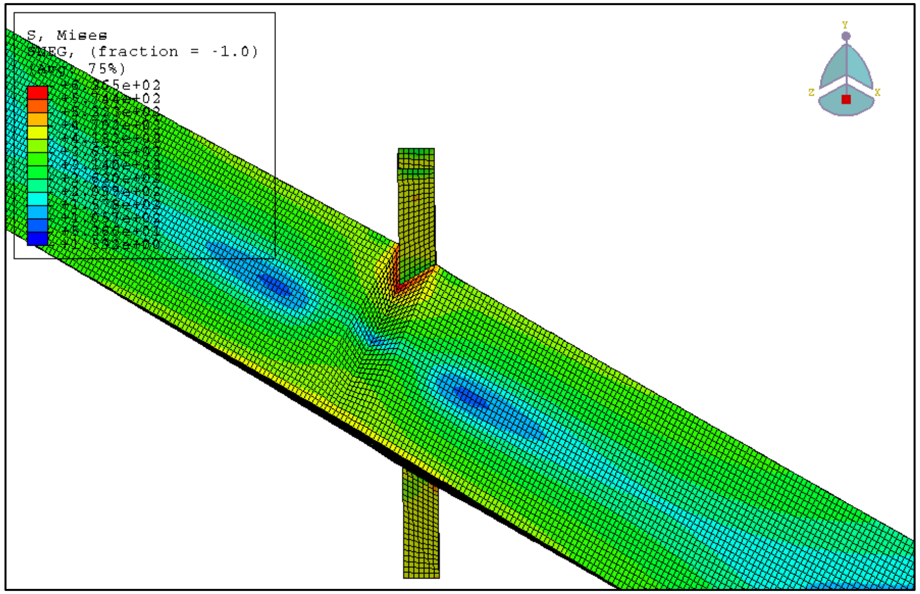

DBBX_02_SS_T

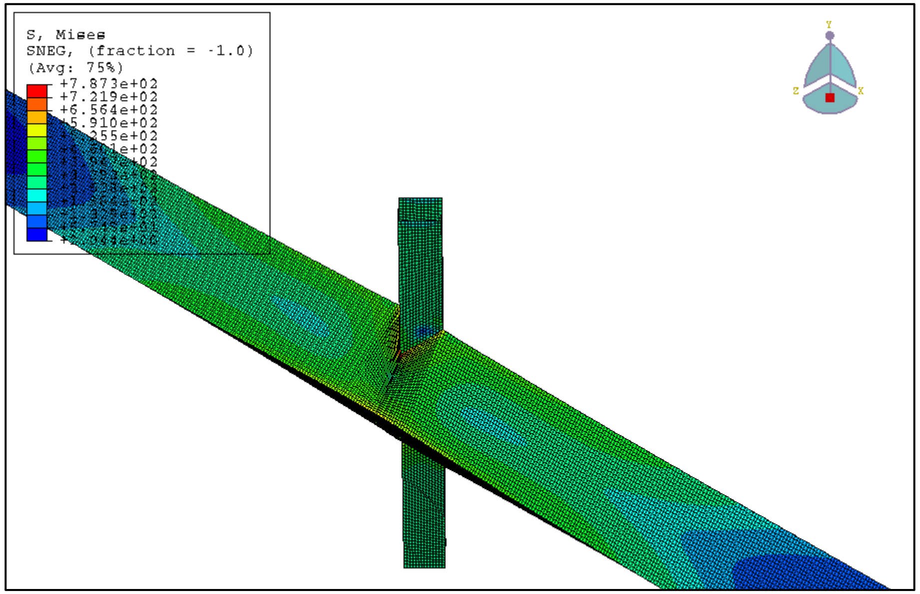

Figure 113 *Von Mises stresses for DBBX_01_SS (left) and DBBX_02_SS (right) under tensile loading*

DBBX_03_SS_T

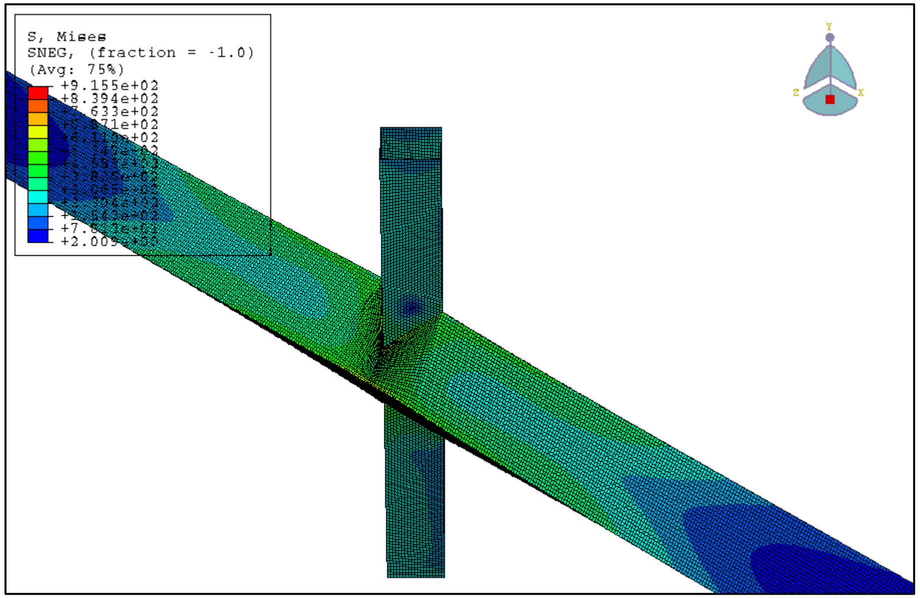

DBBX_04_SS_T

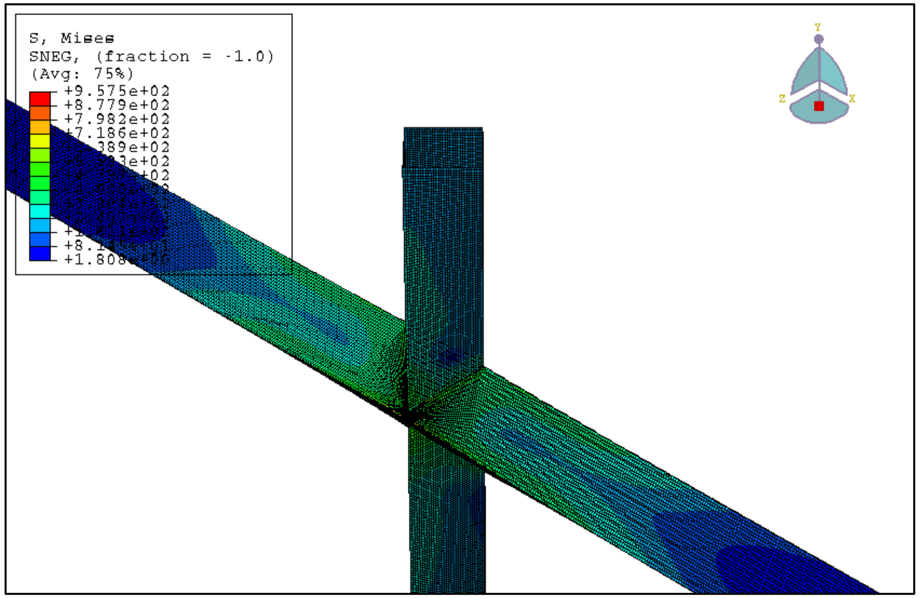

Figure 114 *Von Mises stresses for DBBX_03_SS (left) and DBBX_04_SS (right) under tensile loading*

DBBX_05_SS_T DBBX_06_SS_T

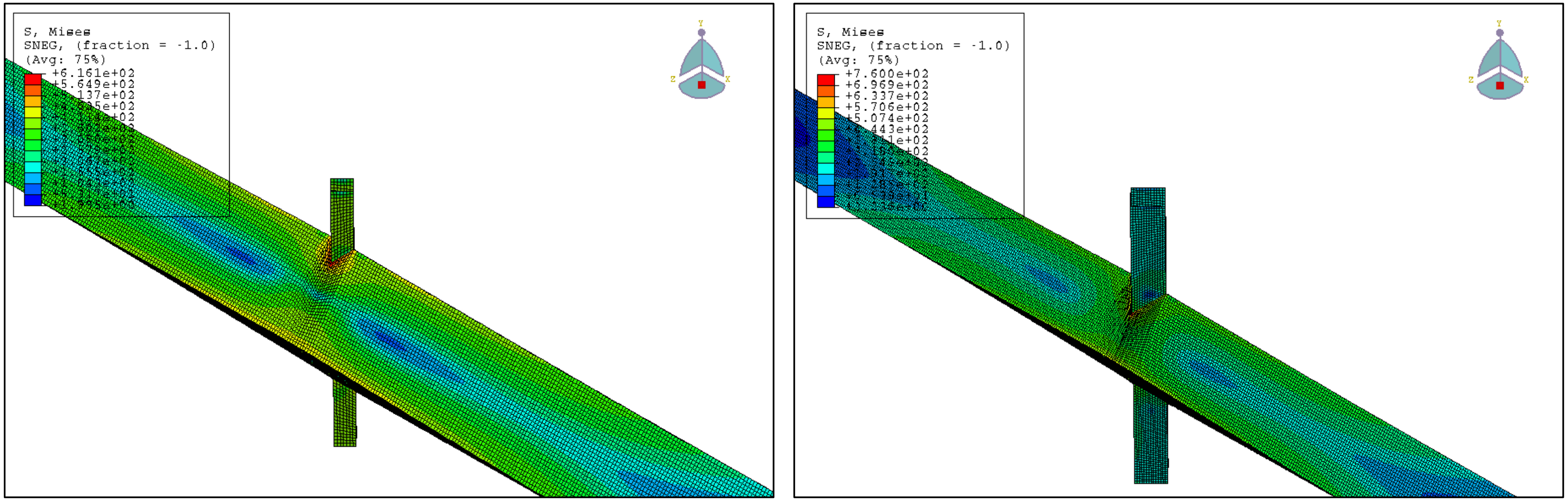

Figure 115 *Von Mises stresses for DBBX_05_SS (left) and DBBX_06_SS (right) under tensile loading*

DBBX_07_SS_T

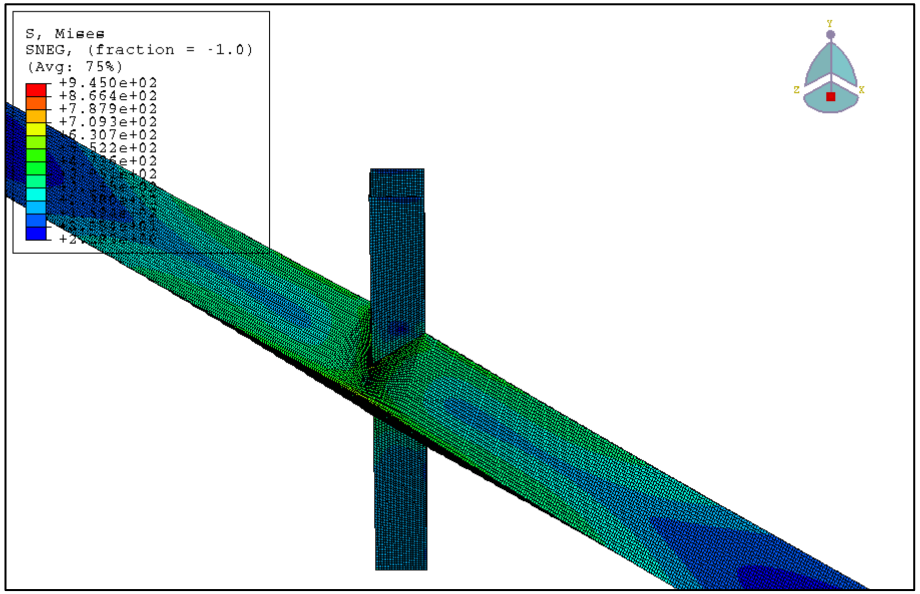

DBBX_08_SS_T

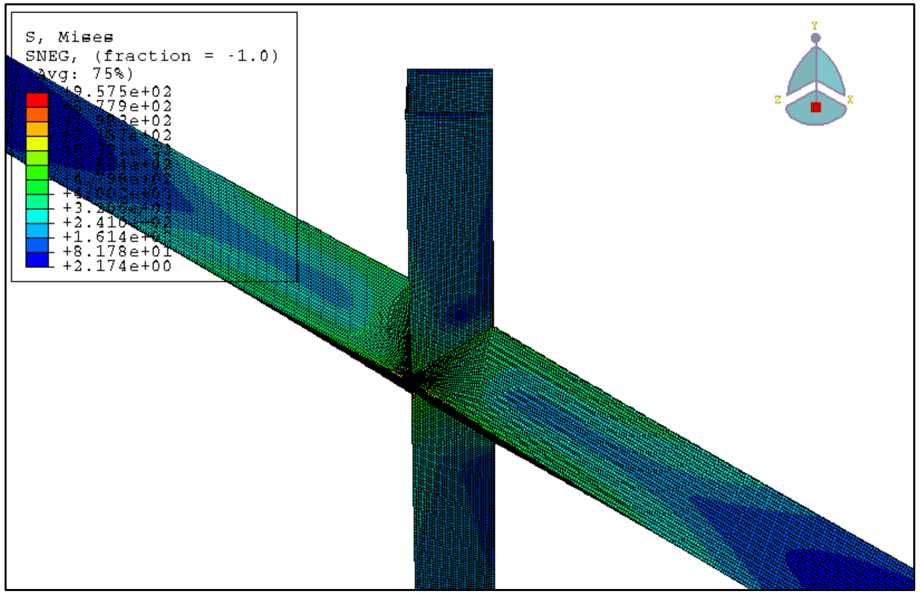

Figure 116 *Von Mises stresses for DBBX_07_SS (left) and DBBX_08_SS (right) under tensile loading*

DBBX_09_SS_T

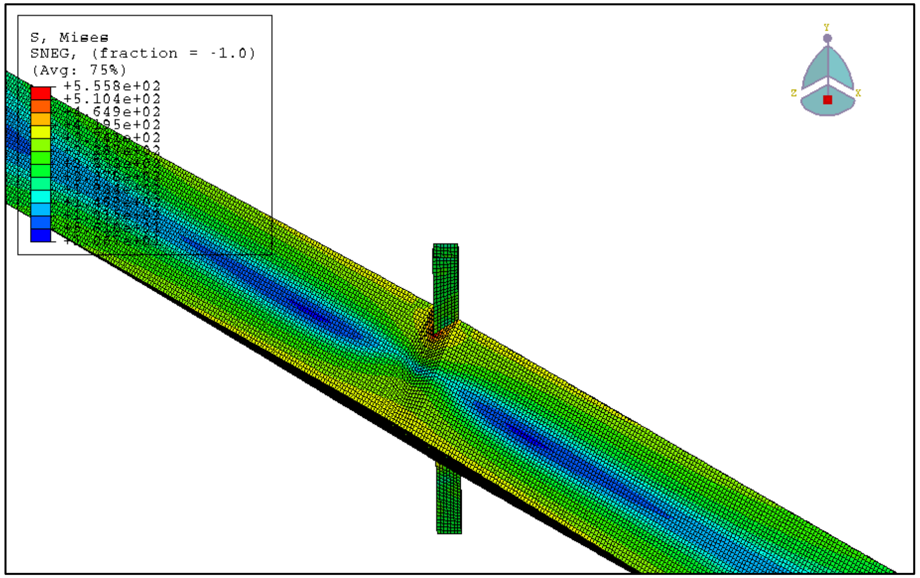

DBBX_10_SS_T

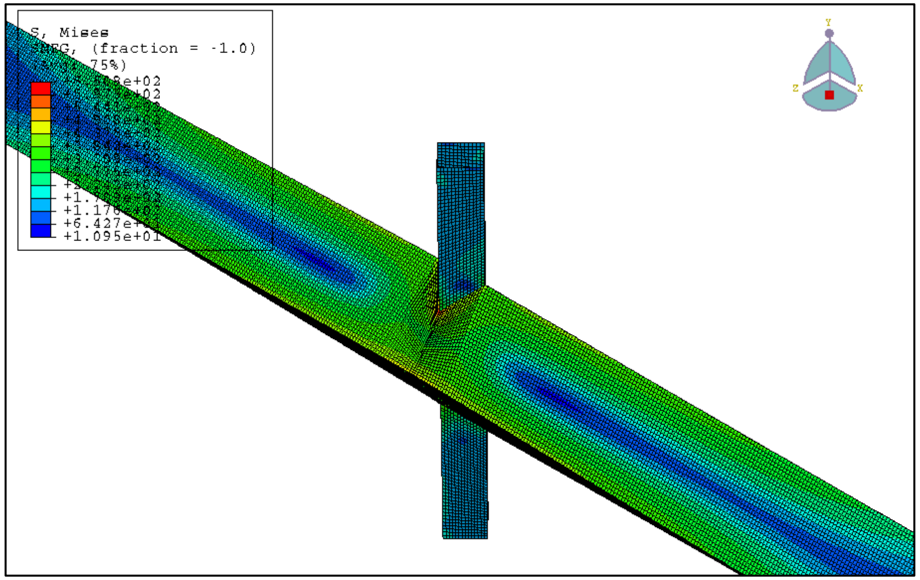

Figure 117 *Von Mises stresses for DBBX_09_SS (left) and DBBX_10_SS (right) under tensile loading*

DBBX_11_SS_T

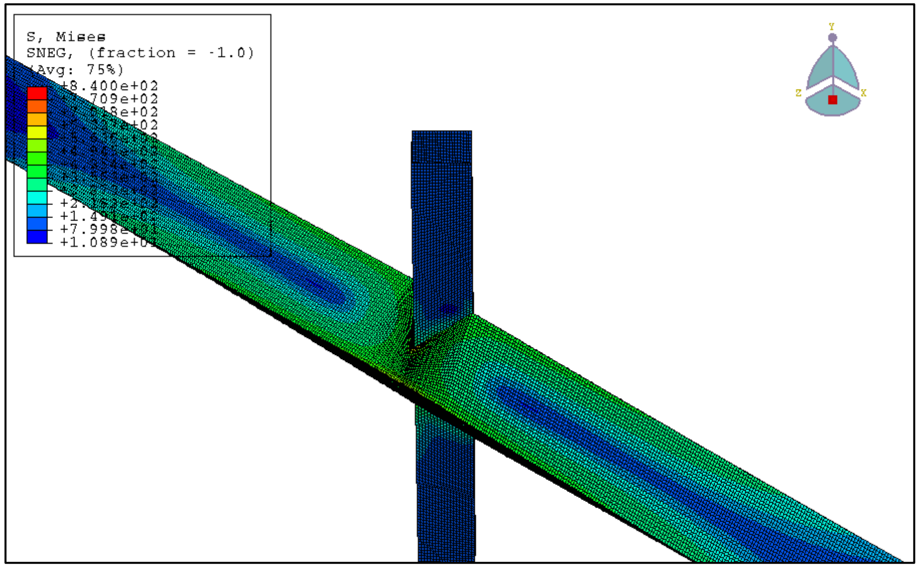

DBBX_12_SS_T

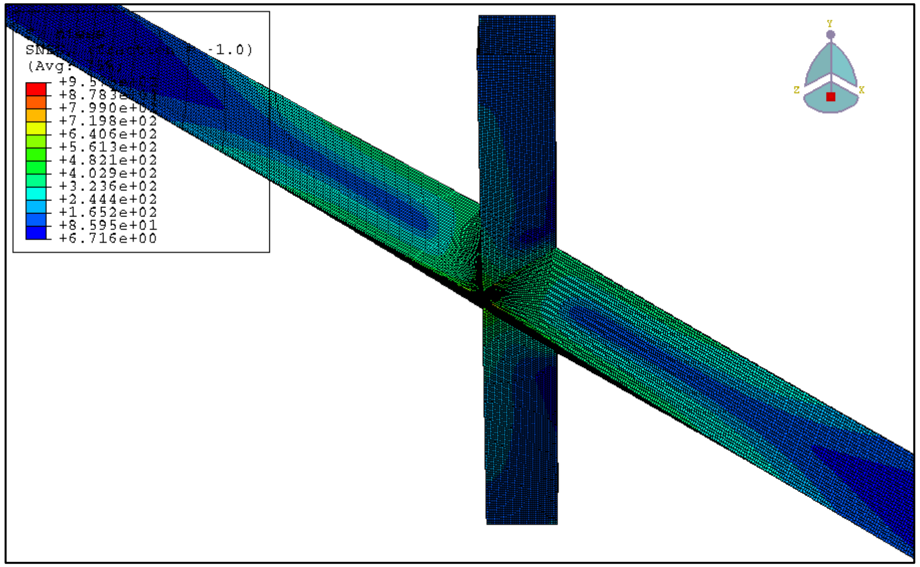

Figure 118 *Von Mises stresses for DBBX_11_SS (left) and DBBX_12_SS (right) under tensile loading*

DBBX_13_SS_T

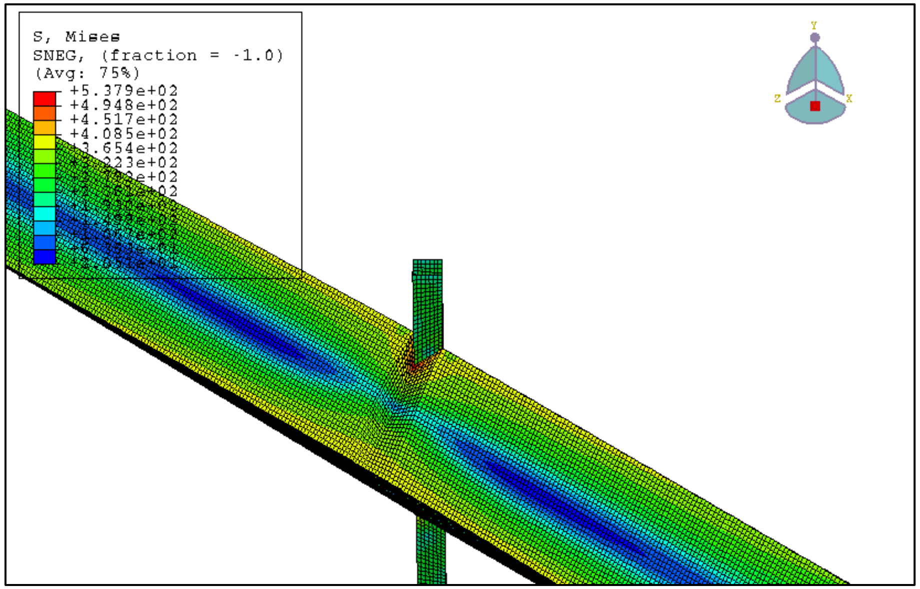

DBBX_14_SS_T

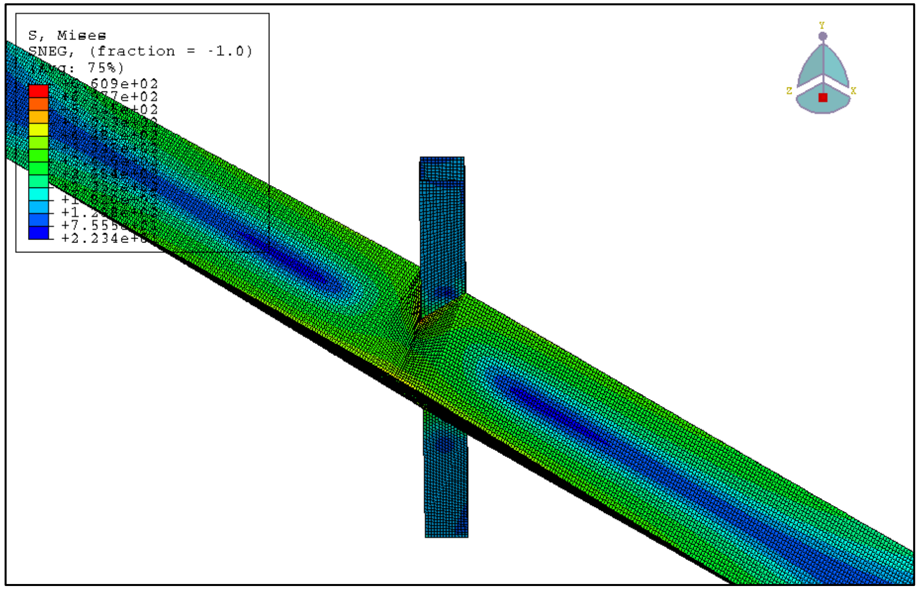

Figure 119 *Von Mises stresses for DBBX_13_SS (left) and DBBX_14_SS (right) under tensile loading*

DBBX_15_SS_T DBBX_16_SS_T

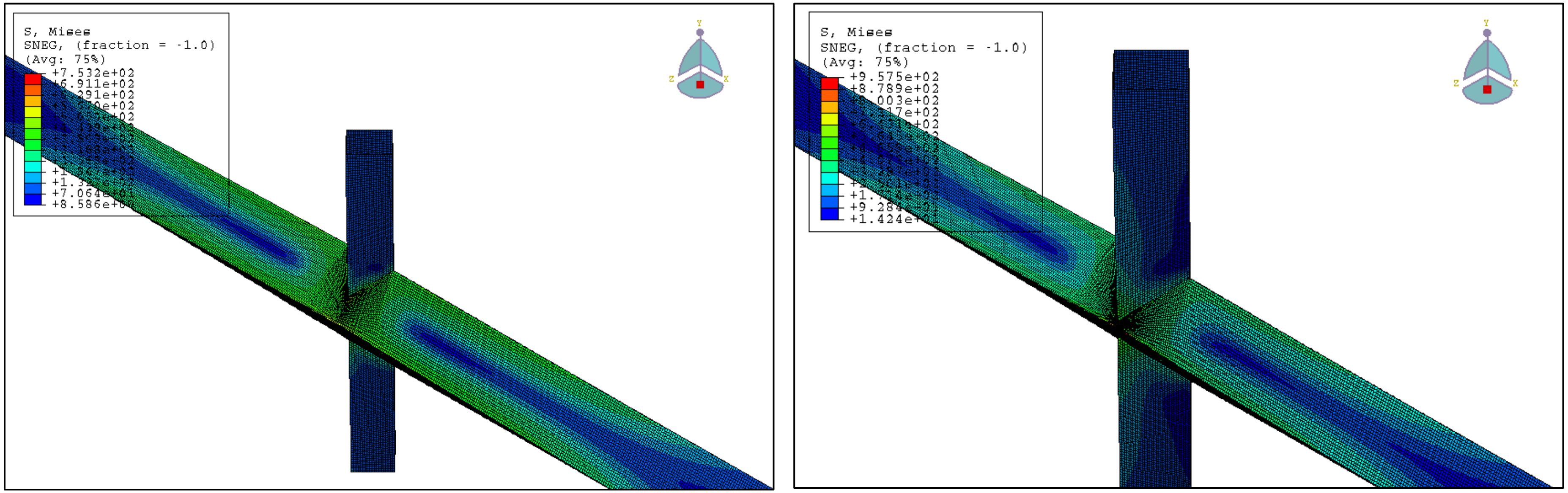

Figure 120 *Von Mises stresses for DBBX_15_SS (left) and DBBX_16_SS (right) under tensile loading*

D. PARAMETRIC RESULTS

D.1COMPRESSION LOADING

D.1.1 Variation of parameter β

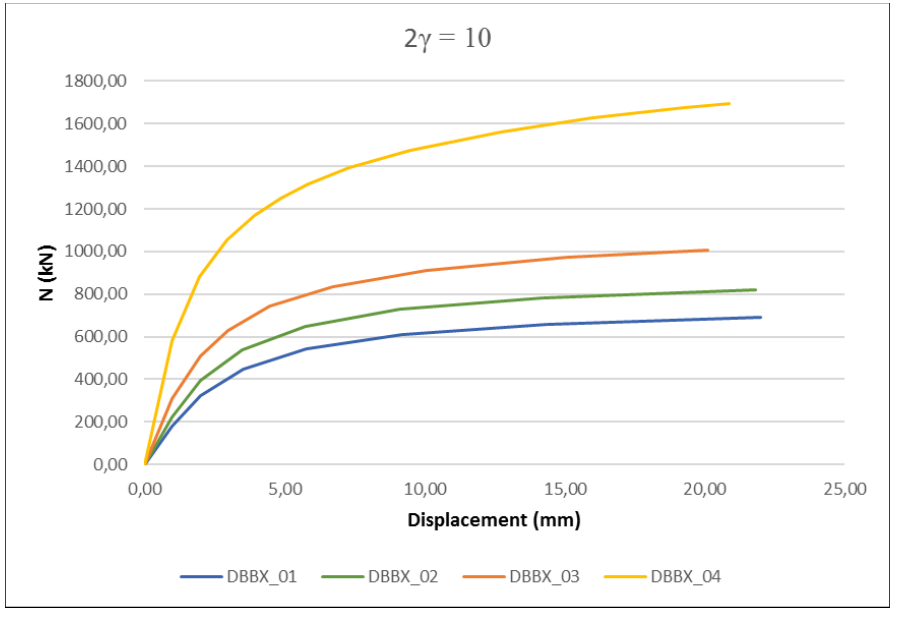

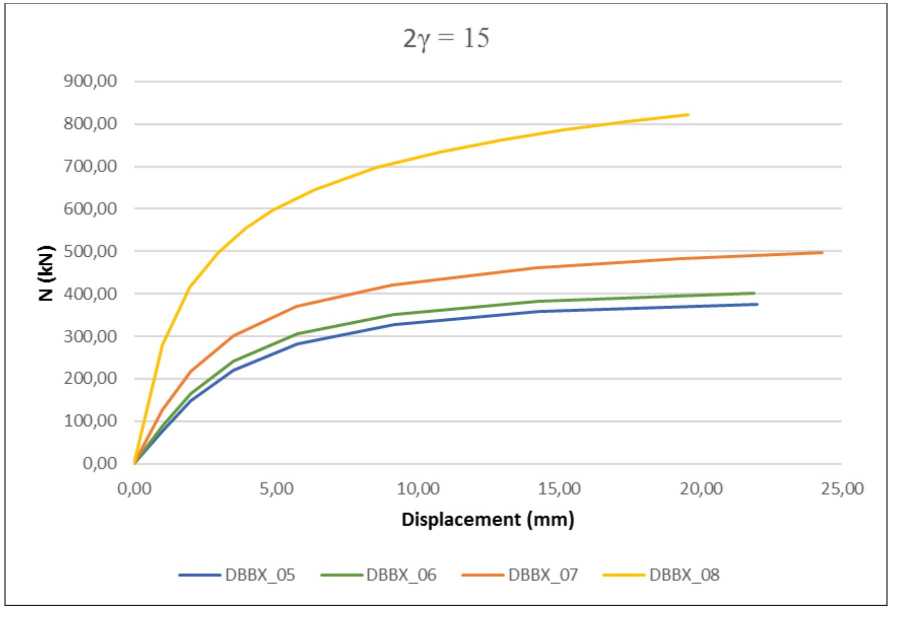

Figure 121 *Load-displacement curves for variation of parameter β for 2γ=10 (left) and for 2γ=15 (right) under compression loading*

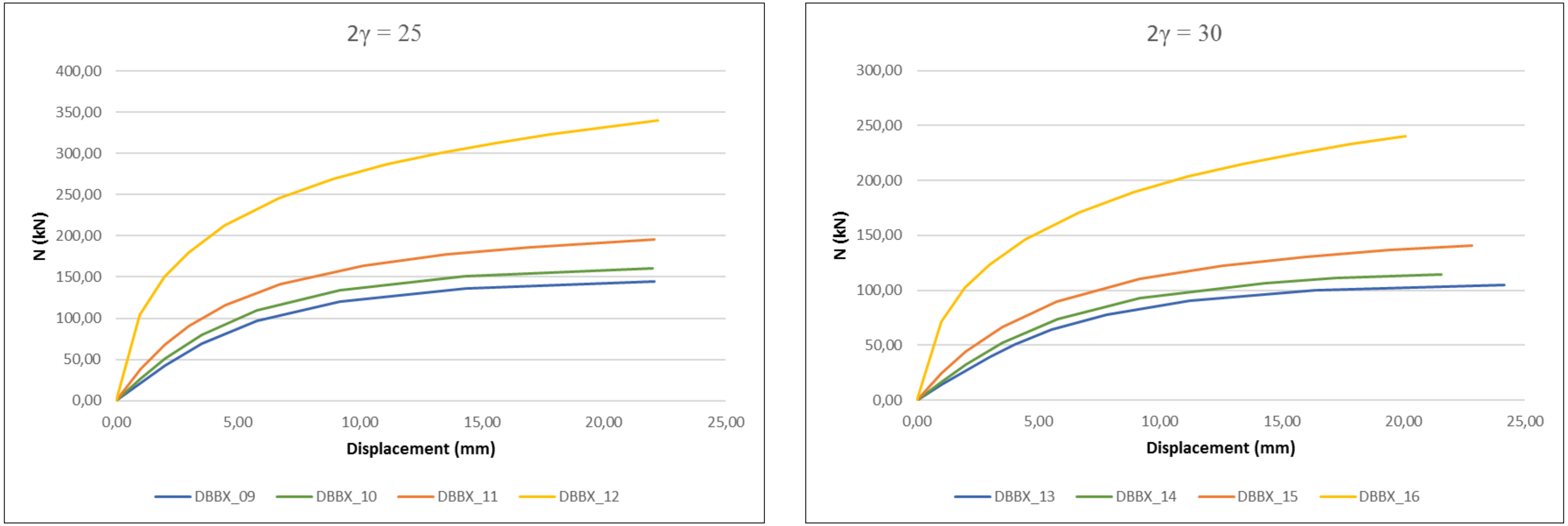

Figure 122 *Load-displacement curves for variation of parameter β for 2γ=25 (left) and for 2γ=30 (right) under compression loading*

D.1.2 Variation of parameter 2γ

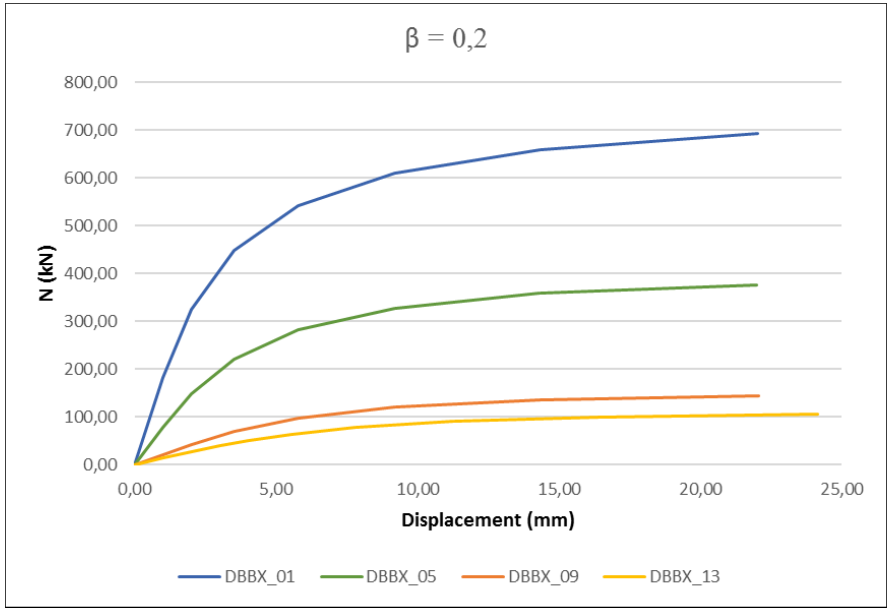

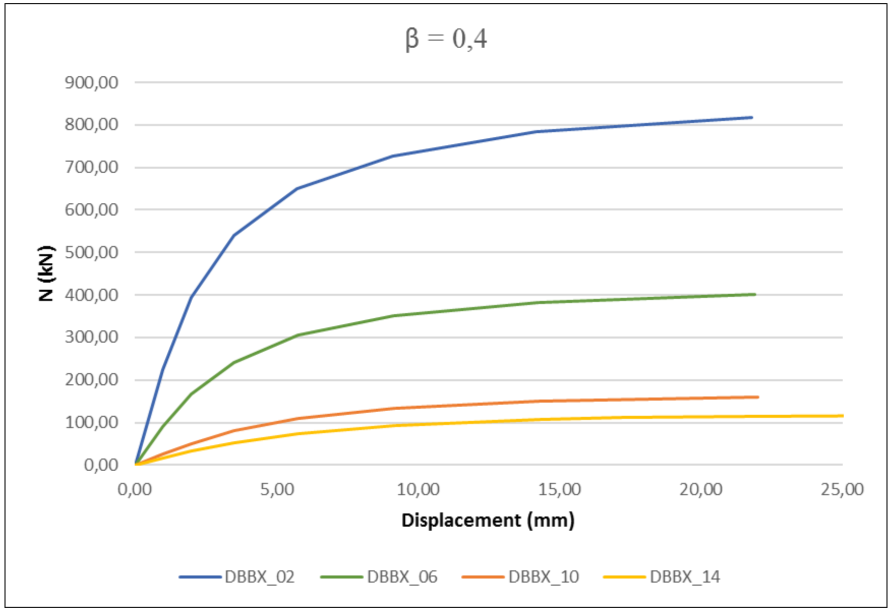

Figure 123 *Load-displacement curves for variation of parameter 2γ for β=0,2 (left) and for β=0,4 (right) under compression loading*

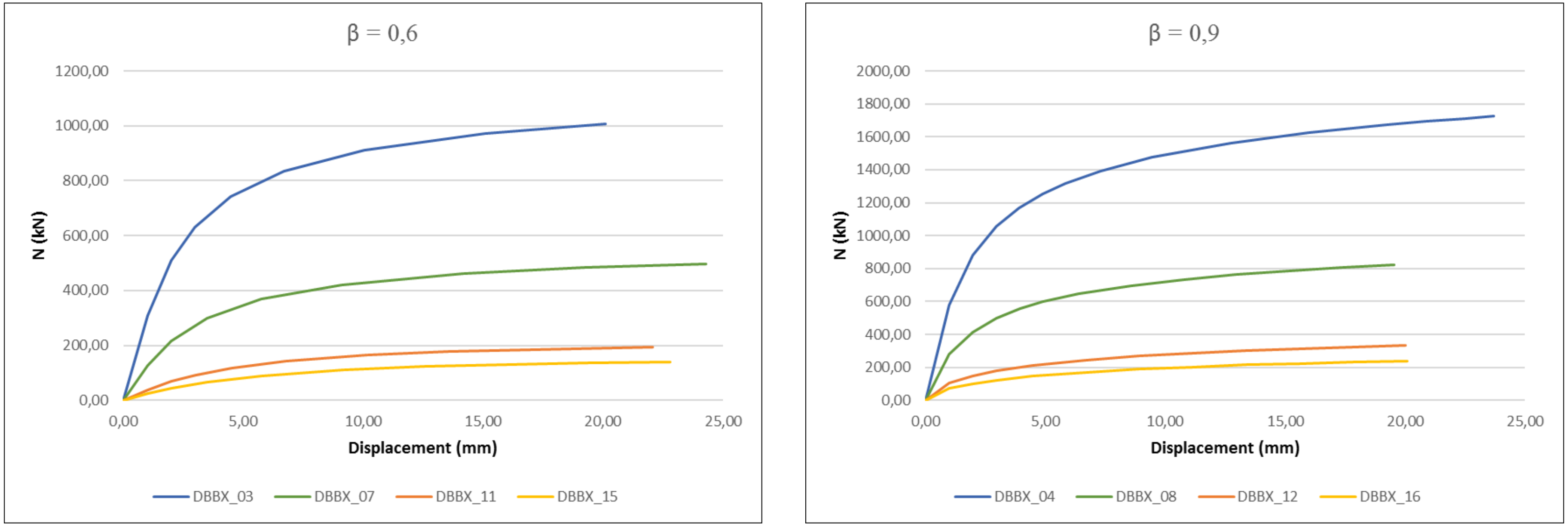

Figure 124 *Load-displacement curves for variation of parameter 2γ for β=0,6 (left) and for β=0,9 (right) under compression loading*

D.1.3 Compression loading numerical results

DBBX_01		DBBX_02		DBBX_03		DBBX_04		DBBX_05		DBBX_06		DBBX_07		DBBX_08	
Displ (mm)	React (kN)	Displ (mm)	React (kN)	Displ (mm)	React (kN)	Displ (mm)	React (kN)	Displ (mm)	React (kN)	Displ (mm)	React (kN)	Displ (mm)	React (kN)	Displ (mm)	React (kN)
0,00	0,00	0,00	0,00	0,00	0,00	0,99	0,00	0,00	0,00	0,00	0,00	0,00	0,00	0,00	0,00
1,00	181,69	1,00	225,31	1,00	307,71	1,97	580,00	1,00	77,72	1,00	89,90	1,00	127,65	1,00	280,49
2,00	324,82	2,00	394,44	2,00	508,59	2,95	882,97	2,00	148,17	2,00	165,87	2,00	217,14	1,98	416,16
3,51	449,06	3,50	540,04	2,99	631,57	3,91	1055,44	3,51	221,25	3,50	242,04	3,50	300,67	2,96	497,81
5,78	542,15	5,75	649,09	4,48	742,11	4,88	1169,54	5,77	282,33	5,76	305,11	5,74	369,69	3,94	554,97
9,19	609,05	9,12	727,56	6,71	834,53	5,85	1252,50	9,18	327,46	9,15	351,08	9,11	421,76	4,91	597,96
14,32	658,84	14,19	783,38	10,05	911,13	7,29	1316,71	14,30	358,45	14,24	382,68	14,16	461,15	6,37	646,19
22,00	692,89	21,79	817,96	15,07	972,66	9,46	1391,36	22,00	376,41	21,89	401,59	19,22	482,84	8,57	697,46
33,51	706,12	29,41	828,94	20,09	1006,74	12,72	1474,57	29,71	380,17	29,56	406,93	24,29	496,20	10,76	734,54
45,02	698,96	37,04	829,57	25,12	1027,28	15,97	1562,44	37,43	377,34	37,25	406,22	29,37	504,68	12,95	763,30
47,90	695,73	44,67	824,88	30,15	1040,14	19,23	1625,51	45,17	370,67	44,95	402,48	34,45	510,17	15,15	786,49
50,79	692,08	52,32	817,57	35,19	1048,29	20,86	1673,80	52,92	361,66	52,66	397,20	39,53	513,73	17,34	805,81
55,11	685,80	59,97	809,05	40,23	1053,40	22,48	1694,04	60,68	351,47	60,38	391,39	44,62	515,97	19,54	822,11
61,60	675,06	67,62	800,45	45,27	1056,54	23,71	1712,32	68,45	341,00	68,11	385,74	49,71	517,31	21,73	836,14
65,25	668,73	75,28	792,59	50,31	1058,38	24,62	1724,82	76,22	330,92	75,84	380,68	54,81	518,15	22,28	839,34
70,73	658,93	82,94	785,87	55,36	1059,42	25,31	1733,66	84,01	321,69	83,58	376,64	59,91	518,79	22,83	842,48
78,95	644,09	90,60	781,02	60,41	1059,99	25,83	1739,99	91,80	313,74	91,33	374,11	65,02	519,41	23,38	845,53
87,17	630,66	98,27	779,11	65,46	1060,40	26,34	1744,59	99,59	307,41	99,08	373,65	70,13	520,15	23,93	848,47
95,40	619,55	105,93	781,01	68,30	1060,77	26,86	1749,06	107,38	303,27	106,83	375,66	75,23	521,18	24,48	851,33

DBBX_01		DBBX_02		DBBX_03		DBBX_04		DBBX_05		DBBX_06		DBBX_07		DBBX_08	
Displ (mm)	React (kN)	Displ (mm)	React (kN)	Displ (mm)	React (kN)	Displ (mm)	React (kN)	Displ (mm)	React (kN)	Displ (mm)	React (kN)	Displ (mm)	React (kN)	Displ (mm)	React (kN)
103,63	611,33	113,60	787,20	72,56	1061,46	27,37	1753,41	115,18	301,64	114,59	380,43	80,34	522,62	25,03	854,11
111,87	606,63	121,27	798,10	78,96	1063,14	27,89	1757,62	122,98	302,92	122,35	388,28	85,46	524,58	25,04	854,13
124,21	607,10	128,94	814,17	85,35	1066,10	28,41	1761,74	130,78	307,48	130,11	399,01	90,57	527,19	25,04	854,15
136,56	619,12	136,61	834,82	91,75	1070,55	28,92	1765,75	142,47	319,51	137,87	412,15	95,68	530,54	25,04	854,16
139,65	624,57	144,28	859,64	98,15	1076,98	29,44	1769,67	145,40	323,93	145,62	427,47	100,80	534,70	25,04	854,18
142,74	630,57	151,95	888,36	104,54	1085,91	29,95	1773,50	148,32	328,66	153,38	444,69	105,91	539,76	25,04	854,18
147,37	640,59	159,61	921,06	110,94	1097,61	30,47	1777,24	152,71	336,35	161,12	463,56	111,02	545,76	25,04	854,18
154,32	658,53	167,27	957,49	117,34	1112,28	30,99	1780,89	159,30	349,55	168,86	484,02	116,14	552,73	25,04	854,18
161,27	680,78	174,93	997,26	123,73	1129,96	31,50	1784,47	165,88	365,20	176,59	506,17	121,25	560,66	25,04	854,18
168,22	707,07	182,58	1040,22	130,12	1150,59	32,02	1787,95	172,47	383,46	184,31	530,01	128,91	574,06	25,04	854,18
175,19	735,37	190,22	1086,19	136,51	1174,05	32,54	1791,36	179,05	403,23	192,03	555,47	136,57	589,42	25,04	854,18
182,16	765,40	197,86	1134,53	142,90	1200,18	33,05	1794,70	185,64	423,37	199,74	582,35	144,23	606,57	25,04	854,18
189,13	796,46	209,31	1209,89	149,28	1228,73	33,57	1797,97	192,22	443,85	207,45	610,49	151,88	625,59	25,04	854,18
196,11	828,43	220,77	1287,68	155,65	1259,79	34,09	1801,18	198,80	297,93	215,15	639,70	159,52	646,62	25,04	854,18
203,08	861,25	232,26	1364,72	162,02	1293,47	34,60	1804,33	0,00	0,00	222,87	669,79	167,15	669,86	25,04	854,18
210,05	894,46	243,82	1441,36	168,39	1329,88	35,12	1807,42	0,00	0,00	230,61	700,57	174,77	695,41	25,04	854,18
217,00	927,92	255,41	1516,19	174,74	1369,23	35,64	1810,44	0,00	0,00	238,39	731,89	182,37	723,26	25,04	854,18
223,90	961,43	267,06	1590,32	181,09	1411,59	36,02	1813,41	0,00	0,00	246,26	763,48	189,96	753,51	25,04	854,18
225,60	969,60	269,96	1608,56	187,43	1456,99	36,41	1815,60	0,00	0,00	254,22	794,75	197,52	786,08	25,04	854,18
0,00	0,00	272,84	1626,53	193,75	1505,34	36,80	1817,77	0,00	0,00	266,25	839,51	205,07	820,77	25,04	854,18

DBBX_01		DBBX_02		DBBX_03		DBBX_04		DBBX_05		DBBX_06		DBBX_07		DBBX_08	
Displ (mm)	React (kN)	Displ (mm)	React (kN)	Displ (mm)	React (kN)	Displ (mm)	React (kN)	Displ (mm)	React (kN)	Displ (mm)	React (kN)	Displ (mm)	React (kN)	Displ (mm)	React (kN)
0,00	0,00	277,13	1652,73	200,07	1556,47	37,19	1819,91	0,00	0,00	275,78	872,65	212,58	857,30	25,04	854,18
0,00	0,00	281,37	1677,86	(...)	(...)	(...)	(...)	0,00	0,00	281,84	892,72	(...)	(...)	25,04	854,18
0,00	0,00	285,54	1701,80	295,06	2354,80	43,30	1852,11	0,00	0,00	286,64	908,03	313,94	1437,84	25,04	854,18
0,00	0,00	291,63	1734,69	302,01	2387,00	43,35	1852,36	0,00	0,00	290,81	920,80	319,17	1459,88	25,04	854,18
0,00	0,00	297,54	1763,98	308,77	2413,58	43,41	1852,61	0,00	0,00	294,52	931,78	324,23	1478,60	25,04	854,18
0,00	0,00	303,27	1789,91	315,36	2435,25	43,46	1852,86	0,00	0,00	297,90	941,48	329,13	1494,50	25,04	854,18
0,00	0,00	308,87	1812,66	321,81	2452,68	43,52	1853,11	0,00	0,00	0,00	0,00	333,92	1508,23	25,04	854,18
0,00	0,00	314,31	1832,22	328,16	2466,19	43,57	1853,36	0,00	0,00	0,00	0,00	338,64	1520,21	25,04	854,18
0,00	0,00	319,58	1848,67	334,40	2475,84	43,63	1853,61	0,00	0,00	0,00	0,00	343,31	1530,60	25,04	854,18
0,00	0,00	327,05	1867,17	340,56	2482,06	43,68	1853,86	0,00	0,00	0,00	0,00	347,93	1539,53	25,04	854,18
0,00	0,00	334,02	1879,46	346,64	2484,84	43,73	1854,11	0,00	0,00	0,00	0,00	352,51	1547,09	25,04	854,18
0,00	0,00	340,47	1885,59	352,63	2484,38	43,78	1854,36	0,00	0,00	0,00	0,00	357,05	1553,29	25,04	854,18
0,00	0,00	346,46	1886,01	358,56	2481,02	43,78	1854,54	0,00	0,00	0,00	0,00	361,53	1557,98	25,04	854,18
0,00	0,00	352,11	1881,86	364,42	2474,71	43,78	1854,57	0,00	0,00	0,00	0,00	365,95	1560,96	25,04	854,18
0,00	0,00	357,52	1873,16	370,22	2465,69	43,78	1854,58	0,00	0,00	0,00	0,00	370,29	1562,32	25,04	854,18
0,00	0,00	362,79	1860,33	375,98	2454,11	43,78	1854,58	0,00	0,00	0,00	0,00	374,57	1562,01	25,04	854,18

Table 28 *Numerical results for compression loading. Models from DBBX_01_SS to DBBX_08_SS*

DBBX_09		DBBX_10		DBBX_11		DBBX_12		DBBX_13		DBBX_14		DBBX_15		DBBX_16	
Displ (mm)	React (kN)	Displ (mm)	React (kN)	Displ (mm)	React (kN)	Displ (mm)	React (kN)	Displ (mm)	React (kN)	Displ (mm)	React (kN)	Displ (mm)	React (kN)	Displ (mm)	React (kN)
0,00	0,00	0,00	0,00	0,00	0,00	0,00	0,00	0,00	0,00	0,00	0,00	0,00	0,00	0,00	0,00
1,00	21,53	1,00	26,36	1,00	38,50	1,00	104,02	1,00	13,80	1,00	16,77	1,00	24,56	1,00	71,36
2,00	42,42	2,00	50,74	2,00	68,35	1,98	150,14	2,00	27,26	2,00	32,55	2,00	44,32	1,99	102,25
3,51	69,55	3,51	80,16	3,00	90,92	2,97	180,14	3,00	39,91	3,51	52,60	3,50	66,38	2,98	122,89
5,77	97,13	5,77	109,63	4,50	116,27	4,45	212,47	4,01	51,01	5,77	74,21	5,76	89,50	4,46	145,98
9,19	119,81	9,17	133,85	6,76	141,72	6,67	245,88	5,52	64,29	9,18	93,22	9,16	110,46	6,69	170,98
14,33	135,68	14,30	150,68	10,15	163,96	8,89	269,18	7,80	78,11	14,31	106,91	12,56	122,68	8,91	189,23
22,07	144,55	22,01	160,69	13,55	177,05	11,11	286,81	11,22	90,48	17,21	111,02	15,97	130,63	11,14	203,40
26,44	146,11	29,75	163,86	16,96	185,93	13,33	300,88	16,38	99,78	21,56	114,80	19,39	136,42	13,37	214,95
33,02	146,05	37,51	163,95	22,07	195,05	15,56	312,65	24,15	105,00	28,11	117,38	22,81	140,84	15,60	224,61
36,72	145,13	45,30	162,58	27,19	201,45	17,78	322,78	31,96	105,65	34,68	118,02	26,24	144,33	17,84	232,98
42,29	142,98	53,10	160,58	32,32	206,08	20,00	331,64	39,81	104,03	41,27	117,62	29,67	147,13	20,07	240,36
50,66	138,58	60,92	158,43	37,46	209,36	22,23	339,51	47,68	101,14	47,88	116,68	33,10	149,40	22,31	246,93
59,06	133,44	68,75	156,45	42,60	211,71	24,46	346,59	55,57	97,63	54,50	115,53	36,54	151,24	24,55	252,81
67,47	128,15	76,59	154,89	47,76	213,39	26,69	353,11	63,48	93,92	61,13	114,37	39,98	152,72	25,11	254,18
75,89	123,12	84,43	153,95	52,91	214,66	28,92	359,10	71,42	90,27	67,76	113,35	43,43	153,93	25,67	255,54
84,33	118,64	92,29	153,84	58,08	215,69	31,15	364,71	79,36	86,93	74,41	112,61	46,88	154,91	26,51	257,52
92,78	114,94	100,15	154,76	63,25	216,67	33,38	369,95	87,31	84,06	81,06	112,19	50,33	155,75	27,77	260,39
101,23	112,26	108,01	156,90	68,42	217,70	35,62	374,87	0,00	0,00	87,72	112,18	53,79	156,49	29,66	264,45
109,69	110,86	115,88	160,33	73,59	218,86	37,85	379,52	0,00	0,00	94,39	112,67	57,25	157,18	31,55	268,28

DBBX_09		DBBX_10		DBBX_11		DBBX_12		DBBX_13		DBBX_14		DBBX_15		DBBX_16	
Displ	React	Displ	React	Displ	React	Displ	React	Displ	React	Displ	React	Displ	React	Displ	React
(mm)	(kN)	(mm)	(kN)	(mm)	(kN)	(mm)	(kN)	(mm)	(kN)	(mm)	(kN)	(mm)	(kN)	(mm)	(kN)
118,14	110,98	123,76	164,98	78,77	220,21	40,09	383,98	0,00	0,00	101,05	113,73	60,71	157,85	33,44	271,90
126,61	112,79	131,63	170,74	83,95	221,82	42,33	388,27	0,00	0,00	107,73	115,44	64,17	158,54	35,34	275,37
135,07	116,40	139,50	177,40	89,13	223,71	44,57	392,40	0,00	0,00	114,40	117,77	67,63	159,25	38,18	280,27
143,53	121,77	147,37	184,79	94,32	225,93	46,81	396,38	0,00	0,00	121,08	120,72	71,10	160,01	41,03	284,88
152,00	128,74	155,23	192,74	99,50	228,49	49,05	400,24	0,00	0,00	127,76	124,25	74,56	160,83	43,88	289,25
0,00	0,00	163,08	201,25	104,69	231,42	51,29	404,01	0,00	0,00	134,44	128,27	78,03	161,72	46,72	293,48
0,00	0,00	170,93	210,34	109,88	234,72	53,54	407,73	0,00	0,00	141,11	132,70	81,50	162,70	49,58	297,56
0,00	0,00	178,76	220,07	115,06	238,38	55,78	411,39	0,00	0,00	147,78	137,47	84,97	163,76	52,43	301,57
0,00	0,00	0,00	0,00	120,25	242,40	58,02	415,01	0,00	0,00	154,45	142,51	88,45	164,91	55,28	305,53
0,00	0,00	0,00	0,00	121,55	243,48	60,27	418,58	0,00	0,00	161,11	147,79	91,92	166,16	58,14	309,46
0,00	0,00	0,00	0,00	122,84	244,58	63,64	423,93	0,00	0,00	167,76	153,31	95,39	167,51	61,00	313,37
0,00	0,00	0,00	0,00	124,79	246,24	67,01	429,27	0,00	0,00	174,40	159,05	98,87	168,96	63,86	317,31
0,00	0,00	0,00	0,00	127,70	248,81	70,39	434,62	0,00	0,00	181,00	165,06	102,34	170,52	66,72	321,28
0,00	0,00	0,00	0,00	130,62	251,46	73,76	440,03	0,00	0,00	187,57	171,48	105,82	172,20	69,58	325,28
0,00	0,00	0,00	0,00	133,53	254,21	77,14	445,50	0,00	0,00	193,82	177,85	109,29	173,99	72,44	329,34
0,00	0,00	0,00	0,00	137,90	258,47	80,52	451,05	0,00	0,00	198,77	182,94	112,77	175,88	75,31	333,46
0,00	0,00	0,00	0,00	142,26	262,94	83,90	456,70	0,00	0,00	202,44	186,68	116,24	177,89	78,17	337,63
0,00	0,00	0,00	0,00	146,63	267,61	87,28	462,46	0,00	0,00	205,33	189,55	119,72	179,99	81,04	341,87
0,00	0,00	0,00	0,00	150,98	272,49	90,66	468,29	0,00	0,00	207,67	191,83	123,19	182,21	83,91	346,17
0,00	0,00	0,00	0,00	155,34	277,58	94,05	474,19	0,00	0,00	209,62	193,64	126,66	184,52	86,78	350,54

DBBX_09		DBBX_10		DBBX_11		DBBX_12		DBBX_13		DBBX_14		DBBX_15		DBBX_16	
Displ (mm)	React (kN)	Displ (mm)	React (kN)	Displ (mm)	React (kN)	Displ (mm)	React (kN)	Displ (mm)	React (kN)	Displ (mm)	React (kN)	Displ (mm)	React (kN)	Displ (mm)	React (kN)
0,00	0,00	0,00	0,00	(...)	(...)	(...)	(...)	0,00	0,00	211,29	195,11	(...)	(...)	(...)	(...)
0,00	0,00	0,00	0,00	297,72	651,43	238,03	712,80	0,00	0,00	212,74	196,28	293,00	475,80	252,39	564,15
0,00	0,00	0,00	0,00	303,28	668,83	243,11	724,96	0,00	0,00	214,03	197,22	297,40	486,47	254,07	564,18
0,00	0,00	0,00	0,00	308,87	683,90	248,21	736,57	0,00	0,00	215,21	197,99	301,84	496,27	255,67	562,32
0,00	0,00	0,00	0,00	314,49	696,92	253,31	747,67	0,00	0,00	216,30	198,62	306,29	505,14	257,17	558,56
0,00	0,00	0,00	0,00	320,13	708,32	258,43	758,29	0,00	0,00	217,33	199,14	310,74	513,02	258,66	553,00
0,00	0,00	0,00	0,00	325,78	718,27	263,56	768,25	0,00	0,00	218,30	199,58	315,22	520,03	260,14	546,05
0,00	0,00	0,00	0,00	331,44	726,61	268,73	777,17	0,00	0,00	219,66	200,07	319,71	526,12	261,61	538,30
0,00	0,00	0,00	0,00	337,10	733,43	273,99	783,88	0,00	0,00	221,56	200,56	324,21	531,34	263,07	530,26
0,00	0,00	0,00	0,00	342,75	738,83	275,28	785,15	0,00	0,00	223,34	200,91	328,70	535,73	264,52	522,40
0,00	0,00	0,00	0,00	348,38	742,92	276,57	786,09	0,00	0,00	225,04	201,17	333,19	539,32	265,98	514,99
0,00	0,00	0,00	0,00	353,97	745,77	277,82	786,52	0,00	0,00	226,67	201,40	337,64	542,14	267,43	508,26
0,00	0,00	0,00	0,00	359,37	747,20	279,05	786,34	0,00	0,00	228,99	201,67	341,94	544,04	268,88	502,30
0,00	0,00	0,00	0,00	364,29	747,25	280,84	784,57	0,00	0,00	231,22	201,98	345,81	544,64	271,05	494,47
0,00	0,00	0,00	0,00	368,20	745,98	282,59	781,39	0,00	0,00	233,37	202,37	349,01	543,32	273,22	488,15

Table 29 *Numerical results for compression loading. Models from DBBX_09_SS to DBBX_16_SS*

D.2 TENSILE LOADING

D.2.1 Variation of parameter β

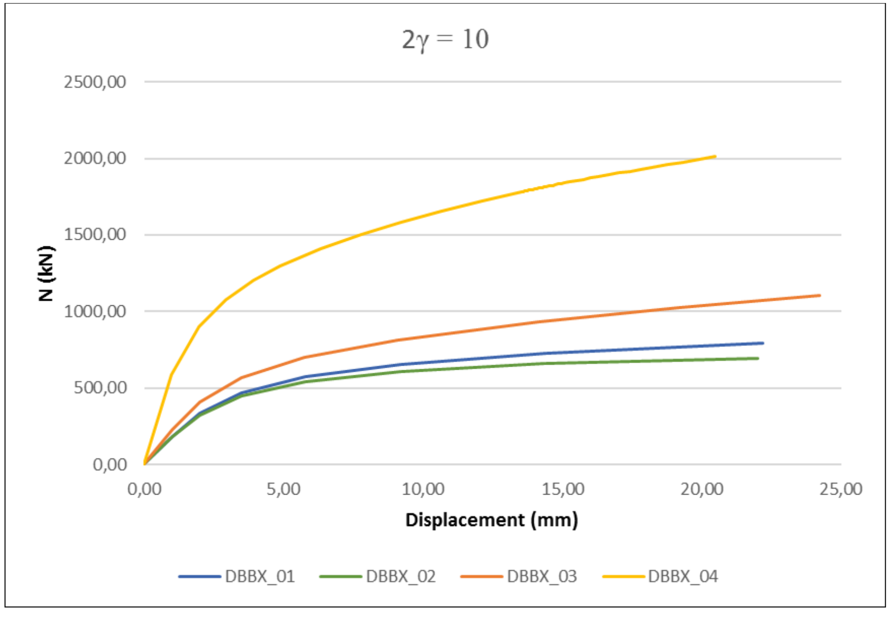

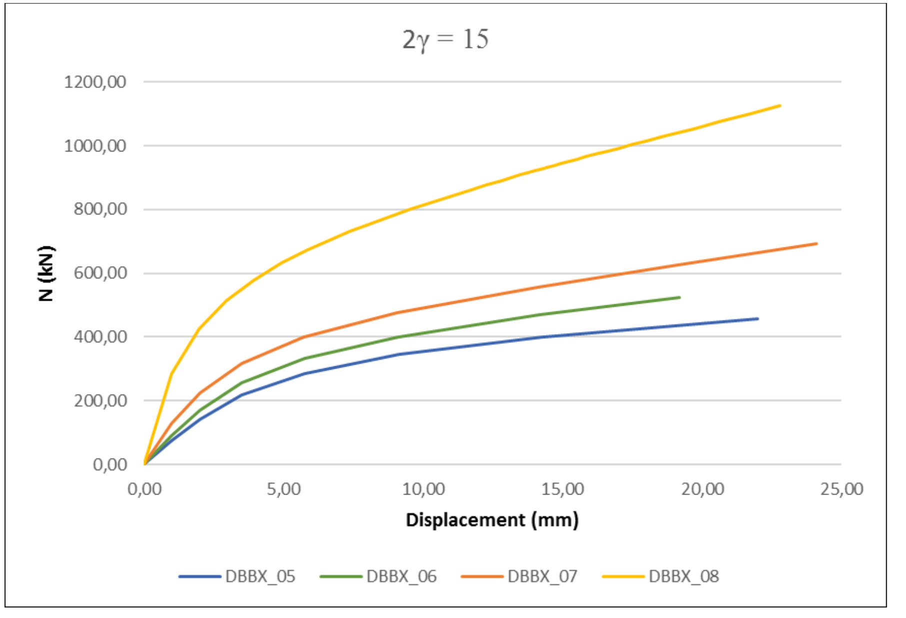

Figure 125 *Load-displacement curves for variation of parameter β for 2γ=10 (left) and for 2γ=15 (right) under tensile loading*

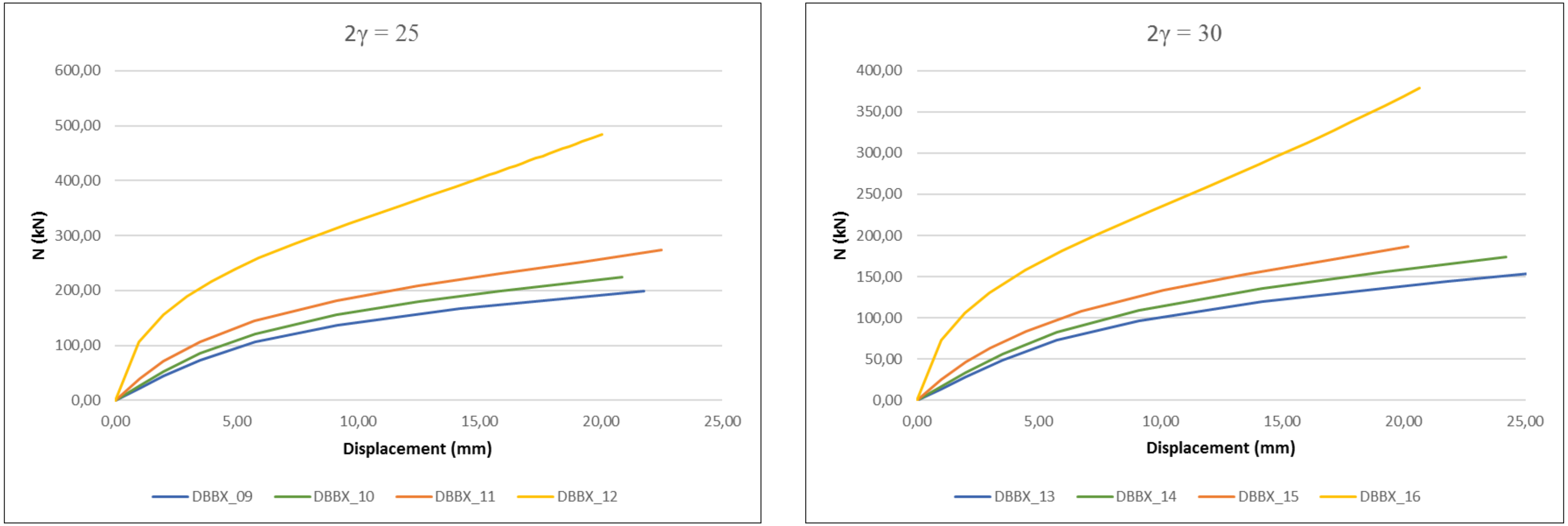

Figure 126 *Load-displacement curves for variation of parameter β for 2γ=25 (left) and for 2γ=30 (right) under tensile loading*

D.2.2 Variation of parameter 2γ

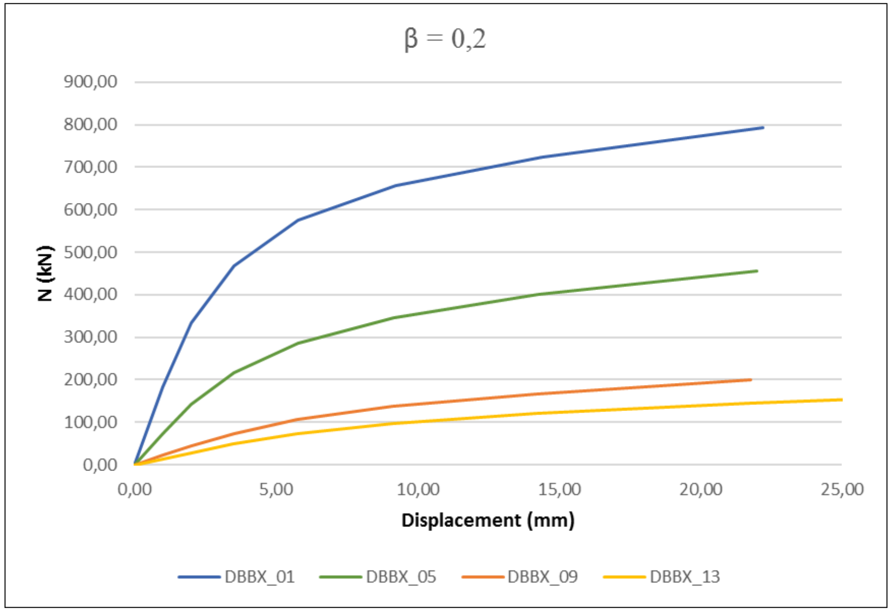

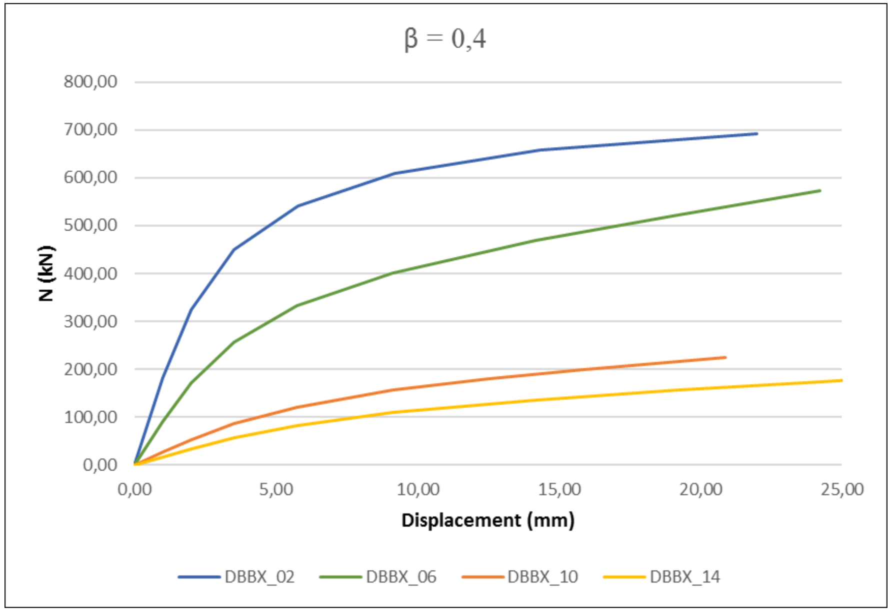

Figure 127 *Load-displacement curves for variation of parameter 2γ for β=0,2 (left) and for β=0,4 (right) under tensile loading*

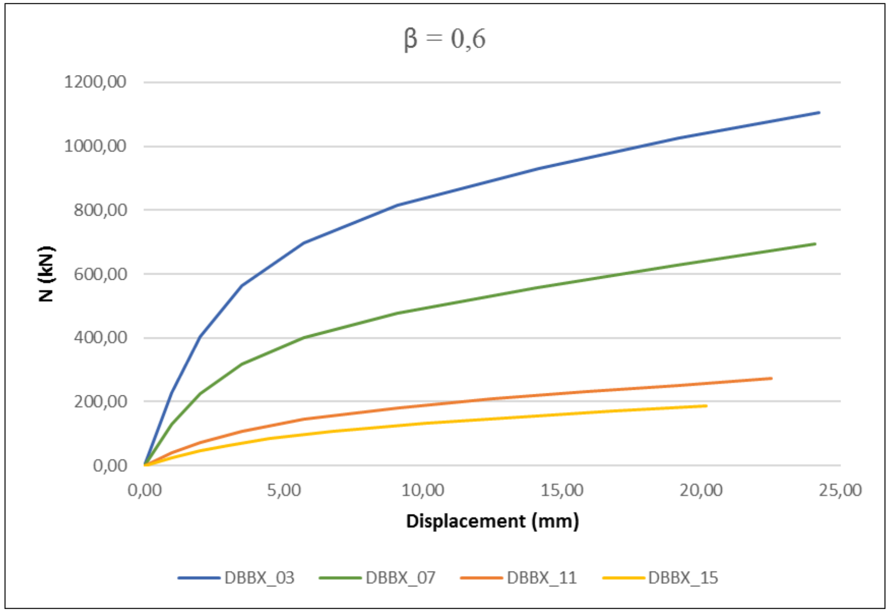

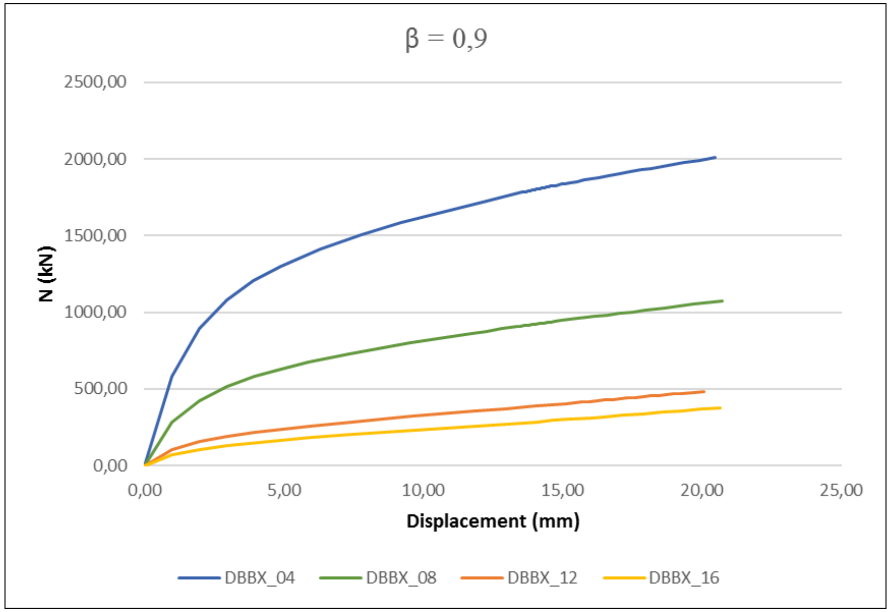

Figure 128 *Load-displacement curves for variation of parameter 2γ for β=0,6 (left) and for β=0,9 (right) under tensile loading*

D.2.3 Tensile loading numerical results

DBBX_01		DBBX_02		DBBX_03		DBBX_04		DBBX_05		DBBX_06		DBBX_07		DBBX_08	
Displ (mm)	React (kN)	Displ (mm)	React (kN)	Displ (mm)	React (kN)	Displ (mm)	React (kN)	Displ (mm)	React (kN)	Displ (mm)	React (kN)	Displ (mm)	React (kN)	Displ (mm)	React (kN)
0.00	0.00	0.00	0.00	0.00	0.00	0.00	0.00	0.00	0.00	0.00	0.00	0.00	0.00	0.00	0.00
1.00	184.11	1.00	121.28	1.00	311.91	1.00	585.00	1.00	73.73	1.00	91.51	1.00	129.92	1.00	283.95
2.00	332.95	2.00	214.81	2.00	521.62	1.98	895.95	2.00	142.55	2.00	171.45	2.00	224.24	1.98	425.22
3.51	467.34	3.50	299.11	3.48	704.84	2.95	1078.25	3.50	216.93	3.50	255.50	3.49	316.85	2.96	513.75
5.78	574.45	5.74	368.85	5.71	855.75	3.91	1203.77	5.76	284.91	5.75	332.20	5.73	400.72	3.93	578.79
9.22	655.91	9.11	429.96	9.05	992.42	4.88	1299.40	9.16	344.72	9.12	400.50	9.08	476.84	4.91	630.58
14.41	724.76	14.15	491.49	14.04	1136.23	6.33	1411.94	14.26	400.59	14.16	468.76	14.10	557.03	5.88	674.02
22.21	792.94	19.18	539.77	21.51	1311.40	7.77	1503.64	21.98	455.93	19.19	523.06	19.10	625.42	7.34	729.31
33.93	866.79	24.22	582.55	28.97	1477.90	9.21	1583.07	29.75	496.03	24.21	572.37	24.09	692.52	9.53	799.41
51.54	950.38	31.80	640.61	36.44	1649.90	10.66	1654.36	37.56	528.73	29.22	620.31	29.06	763.01	11.71	861.74
69.17	1018.02	39.45	692.15	43.97	1822.35	12.10	1720.06	49.32	570.17	36.70	693.22	34.02	839.63	12.25	876.55
86.80	1076.20	47.17	737.31	51.65	1978.28	13.54	1781.36	61.11	605.90	44.18	769.56	38.96	923.63	12.80	891.19
104.45	1127.73	58.87	793.52	59.47	2107.83	13.56	1782.12	72.93	637.87	51.73	846.88	43.91	1015.24	13.34	905.48
110.50	1144.22	70.66	839.77	67.39	2209.90	13.58	1783.05	84.77	666.93	59.43	916.99	48.86	1112.61	13.48	908.97
113.90	1153.11	82.49	879.47	79.33	2340.59	13.61	1783.98	96.63	693.72	67.27	977.75	53.89	1209.35	13.62	912.50
115.81	1157.97	100.29	930.55	91.31	2451.14	13.64	1785.37	108.50	718.76	75.18	1031.27	59.03	1298.00	13.75	916.01
116.89	1160.66	121.16	980.60	103.31	2543.28	13.69	1787.45	120.39	741.95	83.15	1078.08	64.30	1368.60	13.89	919.47
117.50	1162.11	142.07	1023.10	121.35	2665.94	13.74	1789.52	138.23	774.44	95.15	1138.37	69.63	1428.10	14.02	922.86
117.84	1162.76	162.99	1059.99	139.40	2771.78	13.79	1791.58	138.70	775.18	113.20	1214.82	75.00	1477.74	14.16	926.21

DBBX_01		DBBX_02		DBBX_03		DBBX_04		DBBX_05		DBBX_06		DBBX_07		DBBX_08	
Displ (mm)	React (kN)	Displ (mm)	React (kN)	Displ (mm)	React (kN)	Displ (mm)	React (kN)	Displ (mm)	React (kN)	Displ (mm)	React (kN)	Displ (mm)	React (kN)	Displ (mm)	React (kN)
118.35	1161.97	183.92	1092.72	157.46	2866.21	13.84	1793.62	139.16	774.88	131.29	1279.21	80.38	1523.45	14.30	929.53
118.86	1158.84	204.86	1120.93	178.62	2965.14	13.89	1795.64	139.61	772.75	149.39	1334.94	88.48	1578.88	14.43	932.83
119.38	1154.86	225.81	1146.94	199.77	3055.39	13.94	1797.63	140.06	770.19	170.59	1392.19	100.65	1652.62	14.57	936.11
120.14	1148.18	231.04	1152.55	220.94	3137.00	13.99	1799.61	140.73	765.99	191.80	1443.71	118.94	1743.04	14.70	939.37
121.30	1137.25	233.99	1155.61	242.11	3214.10	14.04	1801.58	141.74	759.21	213.01	1489.67	137.25	1818.50	14.91	944.27
123.02	1119.75	235.65	1157.29	263.28	3285.02	14.10	1803.54	143.26	748.52	234.22	1532.51	155.57	1885.43	15.21	951.39
125.62	1092.16	238.13	1151.37	284.46	3351.61	14.15	1805.49	145.53	731.78	239.53	1542.35	173.89	1944.95	15.52	958.42
129.50	1049.23	240.61	1135.82	305.63	3415.72	14.20	1807.43	148.94	705.78	242.51	1547.74	192.22	1999.34	15.83	965.43
135.33	985.11	243.10	1118.77	326.80	3473.89	14.25	1809.36	154.05	666.61	244.21	1544.21	210.55	2049.66	16.13	972.42
141.16	926.68	245.58	1100.57	327.13	3474.72	14.30	1811.29	161.23	616.13	245.88	1530.90	228.89	2095.76	16.59	982.87
0.00	0.00	248.06	1081.31	327.47	3475.57	14.35	1813.21	168.41	574.75	247.56	1516.41	250.36	2147.48	17.05	993.01
0.00	0.00	251.79	1050.34	327.80	3476.43	14.42	1816.09	175.59	542.53	249.23	1501.11	271.83	2194.77	17.51	1003.21
0.00	0.00	257.37	1000.09	328.29	3477.70	14.50	1818.96	182.78	516.77	251.75	1476.67	293.31	2239.73	17.97	1013.56
0.00	0.00	265.75	924.08	329.04	3479.61	14.58	1821.79	189.96	491.75	255.52	1436.79	314.78	2282.70	18.65	1029.13
0.00	0.00	274.13	859.98	330.15	3482.46	14.65	1824.54	197.14	465.54	261.17	1370.95	336.24	2321.23	19.68	1052.69
0.00	0.00	282.51	810.05	331.82	3486.34	14.73	1827.26	204.33	440.78	266.83	1303.39	336.58	2321.78	20.71	1076.72
0.00	0.00	290.89	769.84	331.91	3486.44	14.84	1831.33	211.51	419.64	272.48	1240.34	336.92	2322.34	21.74	1100.94
0.00	0.00	299.27	736.34	331.98	3486.48	14.96	1835.33	218.70	401.03	280.96	1160.06	337.26	2322.90	22.77	1125.95
0.00	0.00	307.65	709.87	332.05	3486.29	**(...)**	**(...)**	225.88	387.16	289.45	1097.42	337.76	2323.72	23.80	1151.61
0.00	0.00	316.03	687.73	332.12	3485.83	153.62	4001.24	233.06	378.46	297.93	1047.63	338.51	2324.73	24.83	1177.71

DBBX_01		DBBX_02		DBBX_03		DBBX_04		DBBX_05		DBBX_06		DBBX_07		DBBX_08	
Displ (mm)	**React (kN)**	**Displ (mm)**	**React (kN)**	**Displ (mm)**	**React (kN)**	**Displ (mm)**	**React (kN)**	**Displ (mm)**	**React (kN)**	**Displ (mm)**	**React (kN)**	**Displ (mm)**	**React (kN)**	**Displ (mm)**	**React (kN)**
0.00	0.00	324.42	664.04	332.22	3484.66	153.62	4001.25	240.24	373.78	306.42	1005.39	339.06	2323.39	**(...)**	**(...)**
0.00	0.00	332.80	640.17	332.38	3481.98	153.63	4001.27	247.43	371.99	314.90	969.41	339.48	2320.39	164.90	2679.14
0.00	0.00	341.18	623.99	332.60	3477.01	153.63	4001.28	254.61	372.33	323.39	940.53	339.90	2316.97	164.97	2679.41
0.00	0.00	349.57	610.33	332.95	3468.83	153.63	4001.29	261.79	374.28	331.87	917.11	340.54	2311.56	165.05	2679.69
0.00	0.00	357.95	597.52	333.46	3455.79	153.63	4001.30	268.97	377.48	340.36	895.04	341.49	2303.04	165.13	2679.96
0.00	0.00	366.33	586.22	334.22	3435.12	153.64	4001.31	276.16	381.60	348.85	866.37	342.91	2289.62	165.20	2680.23
0.00	0.00	374.71	575.93	335.37	3402.10	153.64	4001.33	283.34	386.32	357.35	839.19	345.05	2268.20	165.28	2680.51
0.00	0.00	383.09	565.25	336.88	3355.12	153.64	4001.34	290.52	391.26	365.84	823.06	348.27	2233.19	165.36	2680.78
0.00	0.00	391.46	546.74	338.39	3304.07	153.64	4001.35	297.71	395.70	374.33	810.21	351.48	2194.99	165.43	2681.06
0.00	0.00	393.56	541.55	339.89	3248.60	153.65	4001.36	304.88	397.54	382.82	797.80	354.69	2153.60	165.51	2681.33
0.00	0.00	395.65	535.85	341.39	3188.39	153.65	4001.37	312.07	392.70	391.31	784.64	357.90	2109.16	165.59	2681.60
0.00	0.00	397.75	529.80	342.88	3123.43	153.65	4001.38	319.25	387.18	399.79	766.73	361.11	2062.04	165.66	2681.88
0.00	0.00	399.84	523.82	344.38	3054.25	153.65	4001.40	326.42	384.74	408.28	739.69	364.33	2013.04	165.74	2682.15
0.00	0.00	401.93	518.15	345.86	2982.27	153.66	4001.41	333.58	384.14	416.76	715.93	369.14	1938.08	165.82	2682.42
0.00	0.00	405.08	510.47	347.35	2909.59	153.66	4001.41	335.38	383.97	425.25	699.33	373.96	1866.39	165.89	2682.70
0.00	0.00	409.79	500.81	348.84	2838.52	153.66	4001.41	337.18	384.06	433.74	688.89	378.78	1801.24	165.97	2682.97

Table 30 *Numerical results for tensile loading. Models from DBBX_01_SS to DBBX_08_SS*

DBBX_09		DBBX_10		DBBX_11		DBBX_12		DBBX_13		DBBX_14		DBBX_15		DBBX_16	
Displ (mm)	React (kN)	Displ (mm)	React (kN)	Displ (mm)	React (kN)	Displ (mm)	React (kN)	Displ (mm)	React (kN)	Displ (mm)	React (kN)	Displ (mm)	React (kN)	Displ (mm)	React (kN)
0.00	0.00	0.00	0.00	0.00	0.00	0.00	0.00	0.00	0.00	0.00	0.00	0.00	0.00	0.00	0.00
1.00	21.92	1.00	26.92	1.00	39.35	1.00	106.07	1.00	14.05	1.00	17.14	1.00	25.13	1.00	73.04
2.00	43.94	2.00	52.82	2.00	71.07	1.98	155.39	2.00	28.27	2.00	33.95	2.00	46.17	1.99	106.49
3.50	73.70	3.50	85.56	3.50	106.69	2.97	189.10	3.50	48.55	3.50	56.35	3.00	63.24	2.98	129.98
5.76	106.22	5.75	121.19	5.74	144.52	3.96	215.96	5.75	72.62	5.75	82.43	4.50	84.14	4.46	157.87
9.14	137.44	9.12	155.77	9.11	181.47	4.94	238.80	9.13	96.82	9.12	109.15	6.74	108.06	5.94	181.08
14.20	167.28	12.49	179.55	12.47	207.83	5.93	258.93	14.20	120.17	14.17	135.44	10.11	133.35	7.42	201.73
21.77	198.79	15.85	198.75	15.83	230.39	7.40	285.75	21.75	144.50	19.19	155.71	13.48	152.49	9.64	230.27
23.66	205.62	20.87	223.99	19.17	252.03	9.61	321.55	23.63	149.73	24.20	174.22	16.84	169.45	11.86	258.00
25.55	212.21	25.87	247.89	22.51	274.28	11.82	355.25	25.51	154.80	29.18	192.75	20.19	186.23	14.07	286.28
28.37	221.65	30.85	272.07	24.39	287.51	12.92	371.97	28.33	162.14	34.14	212.14	23.53	203.96	14.62	293.53
32.61	235.13	35.81	297.59	27.19	308.57	14.02	388.81	32.54	172.65	39.08	233.10	26.86	223.45	15.17	300.92
36.86	247.97	40.74	324.98	31.40	343.57	15.12	405.77	38.83	187.82	43.99	256.14	30.19	245.23	16.00	312.15
41.11	260.29	45.66	354.81	35.58	383.13	15.40	410.02	45.13	202.60	48.87	281.73	35.16	282.67	16.47	318.53
45.39	271.84	50.55	387.71	39.75	427.40	15.67	414.31	46.70	206.25	53.72	310.60	40.10	326.03	17.17	328.22
49.69	282.95	55.42	424.31	43.90	476.74	15.95	418.62	48.27	209.91	58.55	343.68	45.01	375.50	17.86	338.05
54.02	293.35	60.30	465.05	48.03	531.02	16.22	422.95	50.63	215.28	63.38	381.81	49.91	430.60	18.56	348.02
58.35	303.56	65.28	508.04	52.16	589.24	16.50	427.28	54.21	222.92	68.34	423.15	54.79	490.22	19.26	358.09
62.72	313.04	70.45	547.02	56.31	649.94	16.77	431.63	57.78	230.52	73.55	459.65	59.72	553.10	19.96	368.24
67.10	322.40	75.76	579.72	60.53	710.27	17.05	435.99	61.38	237.77	78.93	488.04	64.78	614.39	20.65	378.52

DBBX_09		DBBX_10		DBBX_11		DBBX_12		DBBX_13		DBBX_14		DBBX_15		DBBX_16	
Displ (mm)	React (kN)	Displ (mm)	React (kN)	Displ (mm)	React (kN)	Displ (mm)	React (kN)	Displ (mm)	React (kN)	Displ (mm)	React (kN)	Displ (mm)	React (kN)	Displ (mm)	React (kN)
71.50	331.42	81.14	607.87	64.86	765.76	17.32	440.37	65.00	244.81	84.37	511.54	70.06	665.20	21.35	388.93
75.92	340.16	86.55	630.54	69.36	809.28	17.60	444.73	68.63	252.03	89.83	530.67	75.49	703.97	22.04	399.39
80.35	348.91	94.70	660.87	73.92	845.94	17.87	449.08	72.30	259.14	95.30	548.00	81.00	732.39	22.74	409.96
84.81	357.42	106.95	698.26	78.53	874.12	18.15	453.45	76.01	266.69	100.79	562.80	86.52	757.68	23.43	420.66
91.53	370.10	119.22	729.39	83.15	900.04	18.42	457.85	79.75	274.67	106.27	576.75	92.05	777.88	24.13	431.44
98.28	382.57	131.50	756.91	90.11	931.81	18.70	462.27	83.53	282.57	114.51	595.35	97.59	796.47	24.82	442.23
105.07	394.58	143.78	781.31	100.56	972.90	18.97	466.73	87.34	290.59	126.87	619.98	103.14	814.09	25.52	453.12
111.87	406.12	156.06	803.60	111.02	1006.91	19.24	471.21	91.17	298.21	145.42	651.50	108.69	829.25	26.21	464.13
122.09	422.13	174.49	833.62	121.49	1037.62	19.66	477.94	96.94	309.10	167.13	683.18	117.01	850.31	26.90	475.19
137.45	443.79	196.07	865.37	131.97	1065.17	20.07	484.66	105.62	324.00	188.86	710.78	129.51	879.38	27.94	491.82
144.84	453.52	217.65	893.62	147.69	1102.09	20.48	491.46	118.66	343.54	210.58	735.28	148.26	916.66	28.98	508.49
149.00	458.69	239.23	919.90	163.42	1135.56	20.89	498.34	138.25	367.97	232.31	758.08	167.02	949.83	30.02	525.27
151.34	461.48	244.63	925.90	179.15	1165.95	21.30	505.30	143.15	373.49	237.74	763.39	185.79	979.50	31.06	542.11
152.66	463.01	247.66	929.17	202.76	1207.56	21.92	515.91	148.05	378.83	245.88	770.99	207.77	1011.25	32.10	559.02
154.64	465.24	249.38	925.04	235.52	1258.58	22.84	531.90	155.40	386.26	250.47	774.99	229.76	1040.02	33.14	575.93
154.75	465.31	251.08	916.10	268.30	1304.94	23.76	548.28	155.83	386.66	250.72	774.89	251.75	1066.96	34.17	592.85
154.91	465.18	252.78	906.51	301.08	1346.60	24.69	565.00	156.41	387.22	250.96	774.25	273.74	1091.88	35.21	609.76
155.06	464.78	254.49	896.41	333.85	1384.62	26.07	590.54	156.66	387.45	251.20	773.34	295.74	1115.15	36.25	626.66
155.22	464.29	256.19	885.86	342.04	1393.01	28.14	629.54	157.03	387.74	251.56	771.88	317.74	1137.68	37.29	643.51
155.46	463.48	258.75	869.20	342.48	1393.45	30.21	669.13	157.24	387.56	252.11	769.58	339.72	1157.80	38.33	660.36

DBBX_09		DBBX_10		DBBX_11		DBBX_12		DBBX_13		DBBX_14		DBBX_15		DBBX_16	
Displ (mm)	React (kN)	Displ (mm)	React (kN)	Displ (mm)	React (kN)	Displ (mm)	React (kN)	Displ (mm)	React (kN)	Displ (mm)	React (kN)	Displ (mm)	React (kN)	Displ (mm)	React (kN)
155.81	462.17	262.58	842.70	342.91	1393.87	32.28	708.90	157.44	387.04	252.92	765.99	340.07	1158.10	39.88	685.40
156.33	460.09	266.41	815.30	343.35	1394.28	34.35	748.78	157.65	386.45	254.14	760.35	340.42	1158.39	41.45	710.30
157.13	456.81	270.25	788.02	343.99	1394.77	36.42	788.58	157.96	385.48	255.97	751.43	340.76	1158.68	43.01	734.99
158.31	451.69	276.00	749.22	344.02	1394.78	38.49	828.31	158.43	383.94	257.81	742.06	341.28	1159.11	44.58	759.41
160.09	443.73	284.62	699.40	344.05	1394.78	(...)	(...)	159.13	381.53	259.64	732.32	342.05	1159.76	46.15	783.22
162.76	431.36	293.25	660.11	344.07	1394.76	239.01	1741.34	160.17	377.76	262.38	717.01	343.21	1160.72	46.55	788.95
166.77	412.39	301.87	629.08	344.10	1394.71	239.06	1741.43	161.75	371.90	266.51	692.83	344.94	1162.05	46.94	794.44
172.78	384.98	310.50	604.31	344.13	1394.63	239.11	1741.51	164.10	362.79	270.63	668.17	345.04	1162.09	47.34	799.99
178.78	361.00	319.13	582.85	344.15	1394.53	239.21	1741.69	167.64	348.76	274.75	644.10	345.18	1162.10	47.73	805.40
184.79	341.09	327.76	563.39	344.18	1394.39	239.26	1741.77	172.95	328.06	280.93	610.77	345.31	1161.97	(...)	(...)
193.81	317.90	336.40	548.24	344.21	1394.24	239.31	1741.86	178.25	309.33	287.11	582.25	345.45	1161.68	212.53	1408.53
202.83	298.50	345.03	536.67	344.23	1394.05	239.36	1741.95	183.56	293.19	293.29	558.27	345.66	1160.96	212.64	1408.69
211.84	278.05	353.65	524.03	344.26	1393.84	239.41	1742.03	191.52	273.61	302.57	528.60	345.96	1159.64	212.75	1408.85
220.86	258.69	362.29	505.43	344.28	1393.61	239.46	1742.12	199.48	258.89	311.84	505.48	346.43	1157.53	212.78	1408.85
229.88	241.85	370.93	488.22	344.31	1393.36	239.51	1742.20	207.45	245.67	321.12	486.24	347.12	1154.21	212.78	1408.86

***Table 31** Numerical results for tensile loading. Models from DBBX_09_SS to DBBX_16_SS*

E. CROSS-SECTION CLASSIFICATION

Tubular sections

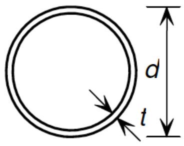

Class	Section in bending Up to 240 CHS	Section in compression
1	$d/t \leq 50\varepsilon^2$	$d/t \leq 50\varepsilon^2$
2	$d/t \leq 70\varepsilon^2$	$d/t \leq 70\varepsilon^2$
3	$d/t \leq 280\varepsilon^2$ **NOTE:** For $d > 240$ mm and $d/t > 280\varepsilon^2$ see EN 1993-1-6.	$d/t \leq 90\varepsilon^2$ **NOTE:** For $d/t > 90\varepsilon^2$ see EN 1993-1-6.

$\varepsilon = \left[\frac{235}{f_y}\frac{E}{210\,000}\right]^{0,5}$	Grade	1.4301	1.4401	1.4462
	f_y (N/mm^2)	210	220	460
	ε	1,03	1,01	0,698

Table 32 *Maximum width-to-thickness ratios for compression parts for stainless steel (EN 1993-1-4 Talbe 5.2 [2])*

				d/t		Cross section class	
JOINT	**ε**	**$50*\varepsilon^2$**	**$70*\varepsilon^2$**	**Chord**	**Brace**	**Chord**	**Brace**
DBBX_01_SS	0.938	43.963	61.548	10	2	Class 1	Class 1
DBBX_02_SS	0.938	43.963	61.548	10	4	Class 1	Class 1
DBBX_03_SS	0.938	43.963	61.548	10	6	Class 1	Class 1
DBBX_04_SS	0.938	43.963	61.548	10	9	Class 1	Class 1
DBBX_05_SS	0.938	43.963	61.548	15	3	Class 1	Class 1
DBBX_06_SS	0.938	43.963	61.548	15	6	Class 1	Class 1
DBBX_07_SS	0.938	43.963	61.548	15	9	Class 1	Class 1
DBBX_08_SS	0.938	43.963	61.548	15	13.5	Class 1	Class 1
DBBX_09_SS	0.938	43.963	61.548	25	5	Class 1	Class 1
DBBX_10_SS	0.938	43.963	61.548	25	10	Class 1	Class 1
DBBX_11_SS	0.938	43.963	61.548	25	15	Class 1	Class 1
DBBX_12_SS	0.938	43.963	61.548	25	22.5	Class 1	Class 1
DBBX_13_SS	0.938	43.963	61.548	30	6	Class 1	Class 1
DBBX_14_SS	0.938	43.963	61.548	30	12	Class 1	Class 1
DBBX_15_SS	0.938	43.963	61.548	30	18	Class 1	Class 1
DBBX_16_SS	0.938	43.963	61.548	30	27	Class 1	Class 1

Table 33 *Cross section classification of each model according to EN 1993-1-4*

F. STAINLESS STEEL CODE

Stainless steel used in the current thesis is an austenitic elasto-plastic material with the following code for stress-strain curve obtained by means of the CodeSkulptor web site (www.codeskulptor.org).

```
####################################
####################################
####################################
####################################
####################################
####################################
# Ecuación constitutiva de austenitico
####################################
####################################
#####para ABAQUS .inp###############
####################################
####################################
####################################
####################################
####################################

import math

#Introducir sigma0,2-(MPa)

sig02=325.0

#Introducir E-(MPa)

E=200000.0

#Introducir sigmaE-(MPa)

sig05=280.0

#Introducir fin rama lineal

lin=150.0
#Cálculos
```

```
n=math.log(4,10)/math.log((sig02/sig05),10)
E02=E/(1+0.002*n*E/sig02)
sigu=sig02/(0.20+185*sig02/E)
m=1+2.8*sig02/sigu
epu=(1-sig02/sigu)

sig03=sig02+(sig02-lin)/10
print "n=",n
print "E02=",E02
print "sigu=",sigu
print "m=",m
print "epu=",epu
print "***************   Material  ****************"
print "*Material, name=InoxAustenitic,sigma02="+str(sig02)
print "*Elastic"
print str(E)+",0.3"
print "*Plastic"
print str(lin)+",0.0"
vecaux1=range(int(lin),int(sig02),(int(sig02)-int(lin))/10)
vecaux1.pop(10)
vecaux1.append(int(sig02))
vecaux2=range(int(sig02),int(sigu),int((int(sigu)-int(sig02))/10))
#print vecaux1
#print vecaux2
def p1(x):
   return ((x/E)+0.002*math.pow((x/sig02),n))
vecaux3=map(p1,vecaux1)
#print vecaux3
#print map(p1,vecaux1)
def p2(x):
   ep02=0.002+sig02/E
   return                    ((x-sig02)/E02)+(epu-ep02-(sigu-sig02)/E02)*(((x-sig02)/(sigu-
sig02))**m)+ep02
vecaux4=map(p2,vecaux2)
#print vecaux4
#print map(p2,vecaux2)
def p3(x,y):
```

```
    return x*(1+y)
vecaux5=map(p3,vecaux1,vecaux3)
vecaux6=map(p3,vecaux2,vecaux4)
#print vecaux5
#print vecaux6
def p4(x,y):
    return math.log(1+x)-y/E
vecaux7=map(p4,vecaux3,vecaux5)
vecaux8=map(p4,vecaux4,vecaux6)
#print vecaux7
#print vecaux8
for i in range(10):
    print str(float(vecaux5[i]))+","+str(float(vecaux7[i]))
for i in range(11):
    print str(float(vecaux6[i]))+","+str(float(vecaux8[i]))
```

G. CONVERGENCE ANALYSIS

G.1 LOAD-DISPLACEMENT RESULTS FOR EACH MESH SIZE

2 mm		3 mm		5 mm		10 mm		15 mm		20 mm	
Displ (mm)	React (kN)	Displ (mm)	React (kN)	Displ (mm)	React (kN)	Displ (mm)	React (kN)	Displ (mm)	React (kN)	Displ (mm)	React (kN)
0.00	0.00	0.00	0.00	0.00	0.00	0.00	0.00	0.00	0.00	0.00	0.00
1.00	36.30	1.00	36.36	1.00	36.48	1.00	36.77	1.00	37.02	1.00	37.19
2.00	65.31	2.00	65.45	2.00	65.85	2.00	66.60	2.00	67.54	2.00	68.23
2.25	70.75	2.25	70.92	2.25	71.41	2.57	78.69	2.57	80.09	3.51	97.70
2.50	75.68	2.50	75.87	2.50	76.45	3.41	92.97	3.41	95.11	5.76	122.74
2.75	80.26	2.75	80.41	2.88	83.26	4.68	108.60	4.68	111.32	9.13	137.46
3.00	84.50	3.00	84.65	3.44	92.17	6.58	122.98	6.58	126.48	12.51	141.67
3.25	88.45	3.25	88.64	4.28	103.03	8.47	129.00	9.42	135.26	15.90	144.17
3.50	92.16	3.50	92.39	5.13	111.18	10.37	132.17	12.27	138.84	21.01	147.99
3.76	95.63	3.88	97.52	5.97	117.59	12.28	134.42	15.13	141.03	26.14	152.02
4.01	98.82	4.26	101.97	7.23	123.81	14.19	136.03	19.44	144.19	31.29	156.42
4.26	101.72	4.63	105.87	9.13	128.01	17.06	138.10	23.76	147.41	36.46	161.04
4.51	104.37	5.01	109.34	11.02	130.64	21.37	141.20	28.10	150.90	41.65	165.18
4.76	106.81	5.57	113.90	12.93	132.46	25.71	144.58	32.45	154.74	46.86	168.84
5.01	109.07	6.13	117.73	14.83	133.78	30.06	148.43	36.81	158.53	52.08	172.16
5.26	111.16	6.69	120.60	17.70	135.67	34.43	152.54	39.27	160.57	57.32	174.92
5.51	113.11	7.26	122.53	20.57	137.69	38.80	156.34	42.97	163.42	62.58	177.31
5.76	114.92	7.82	123.96	23.45	139.81	43.19	159.37	45.05	164.94	67.84	179.52
6.01	116.58	8.38	125.11	26.33	142.14	47.59	161.54	48.18	167.05	73.12	181.67
6.26	118.08	8.94	126.11	29.22	144.64	52.01	163.23	52.89	169.65	78.41	183.94
6.51	119.34	9.79	127.41	32.12	147.14	56.43	164.70	55.55	170.81	83.71	186.27
6.76	120.38	10.64	128.57	35.02	149.66	63.09	166.59	59.53	172.35	89.02	188.71
7.01	121.27	11.48	129.61	35.74	150.22	69.76	168.39	65.53	174.61	94.33	191.41
7.26	122.03	12.33	130.52	36.47	150.84	76.46	170.22	71.54	176.77	99.66	194.31
7.51	122.70	13.18	131.26	37.56	151.66	78.14	170.67	77.57	179.07	104.99	197.25
7.76	123.29	14.03	131.83	37.83	151.84	79.81	171.14	83.61	181.53	110.33	200.30
8.13	124.10	14.88	132.36	38.10	152.03	82.33	171.86	89.66	184.17	115.67	203.47
8.51	124.82	15.73	132.96	38.51	152.30	83.74	172.26	95.73	186.99	123.70	208.61
8.88	125.47	15.95	133.05	38.92	152.56	84.54	172.48	101.80	189.95	131.74	213.86
9.26	126.09	16.00	133.07	39.33	152.80	85.73	172.79	107.89	193.10	139.77	219.23

Table 34 *Load-displacement results for different mesh sizes*

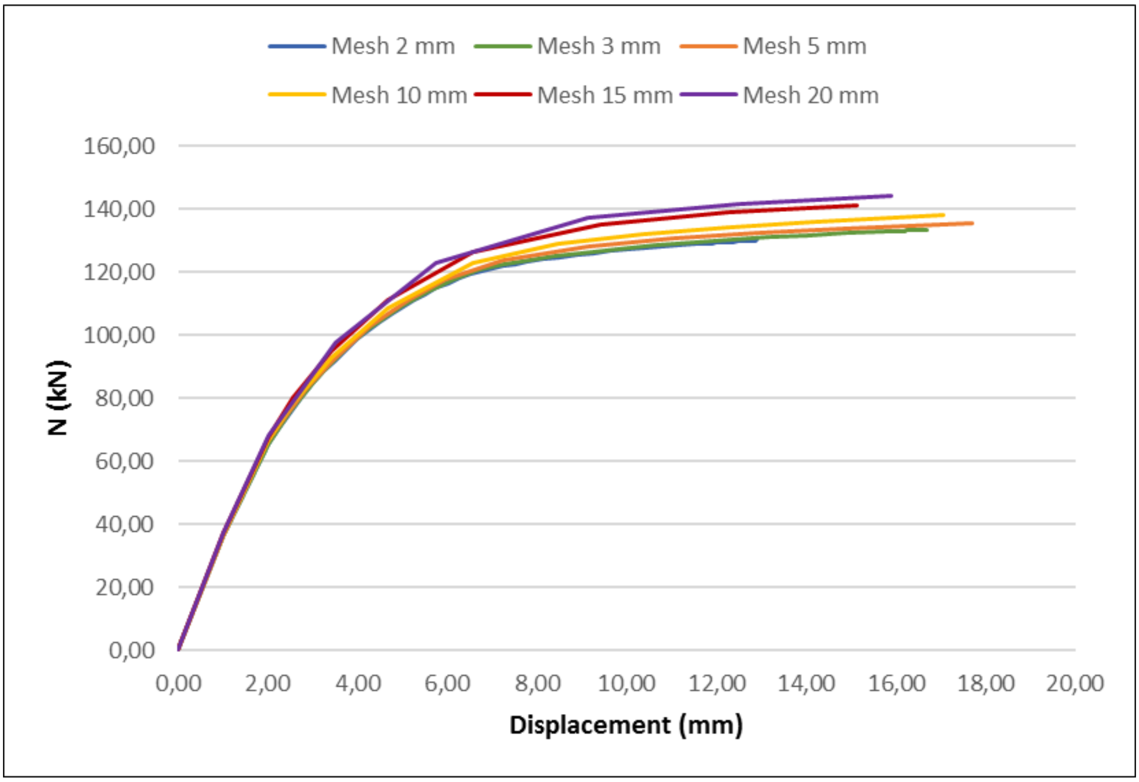

Figure 129 *Load-deformation curves for different mesh sizes*

G.2 JOB TIME SUMMARY AND PROBLEM SIZE

Mesh 20 mm		Mesh 15 mm	
JOB TIME SUMMARY		**JOB TIME SUMMARY**	
USER TIME (SEC)	529.35	USER TIME (SEC)	818.46
SYSTEM TIME (SEC)	22.76	SYSTEM TIME (SEC)	28.42
TOTAL CPU TIME (SEC)	552.11	TOTAL CPU TIME (SEC)	846.88
WALLCLOCK TIME (SEC)	569	WALLCLOCK TIME (SEC)	872
PROBLEM SIZE		**PROBLEM SIZE**	
NUMBER OF ELEMENTS	1881	NUMBER OF ELEMENTS	2936
NUMBER OF NODES	1907	NUMBER OF NODES	2962
NUMBER OF NODES DEFINED BY THE USER	1907	NUMBER OF NODES DEFINED BY THE USER	2962
TOTAL NUMBER OF VARIABLES IN THE MODEL	11442	TOTAL NUMBER OF VARIABLES IN THE MODEL	17772

Table 35 *Job time summary and problem size for mesh size 20 mm (left) and 15 mm (right)*

Mesh 10 mm		Mesh 5 mm	
JOB TIME SUMMARY		**JOB TIME SUMMARY**	
USER TIME (SEC)	2071.2	USER TIME (SEC)	3027.8
SYSTEM TIME (SEC)	62.78	SYSTEM TIME (SEC)	70.94
TOTAL CPU TIME (SEC)	2134	TOTAL CPU TIME (SEC)	3098.8
WALLCLOCK TIME (SEC)	2254	WALLCLOCK TIME (SEC)	3133
PROBLEM SIZE		**PROBLEM SIZE**	
NUMBER OF ELEMENTS	7192	NUMBER OF ELEMENTS	27990
NUMBER OF NODES	7252	NUMBER OF NODES	28113
NUMBER OF NODES DEFINED BY THE USER	7252	NUMBER OF NODES DEFINED BY THE USER	28113
TOTAL NUMBER OF VARIABLES IN THE MODEL	43512	TOTAL NUMBER OF VARIABLES IN THE MODEL	168678

Table 36 *Job time summary and problem size for mesh size 10 mm (left) and 5 mm (right)*

Mesh 3 mm		Mesh 2 mm	
JOB TIME SUMMARY		**JOB TIME SUMMARY**	
USER TIME (SEC)	22684	USER TIME (SEC)	70316.19
SYSTEM TIME (SEC)	571.57	SYSTEM TIME (SEC)	570.81
TOTAL CPU TIME (SEC)	23256	TOTAL CPU TIME (SEC)	70887
WALLCLOCK TIME (SEC)	23502	WALLCLOCK TIME (SEC)	71187
PROBLEM SIZE		**PROBLEM SIZE**	
NUMBER OF ELEMENTS	77617	NUMBER OF ELEMENTS	176683
NUMBER OF NODES	77804	NUMBER OF NODES	176920
NUMBER OF NODES DEFINED BY THE USER	77804	NUMBER OF NODES DEFINED BY THE USER	176920
TOTAL NUMBER OF VARIABLES IN THE MODEL	466824	TOTAL NUMBER OF VARIABLES IN THE MODEL	1061520

Table 37 *Job time summary and problem size for mesh size 3 mm (left) and 2 mm (right)*

Mesh size (mm)	Number of elements	Time CPU (s)	Load (kN) (at 7 mm)	Error (kN)	Relative error (%)
2	176683	70887	120.8014	-	0.00%
3	77617	23256	121.2852	0.4838	0.40%
5	27990	3098.8	123.0032	2.2018	1.82%
10	7192	2134	124.5703	3.7689	3.12%
15	2936	846.88	127.5204	6.719	5.56%
20	1881	552.11	130.7149	9.9135	8.21%

Table 38 *Summary of convergence analysis*

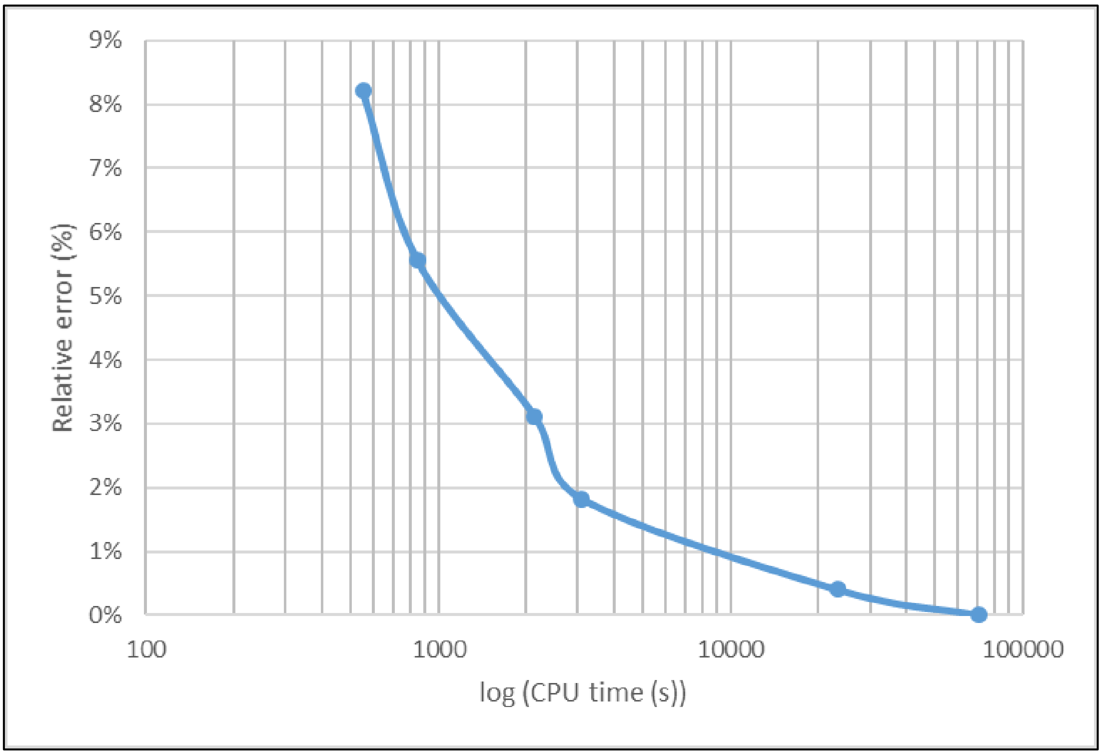

Figure 130 Graphical representation of relative error of reaction load to calculation CPU time in logaritmic scale

G.3 MESH SIZES

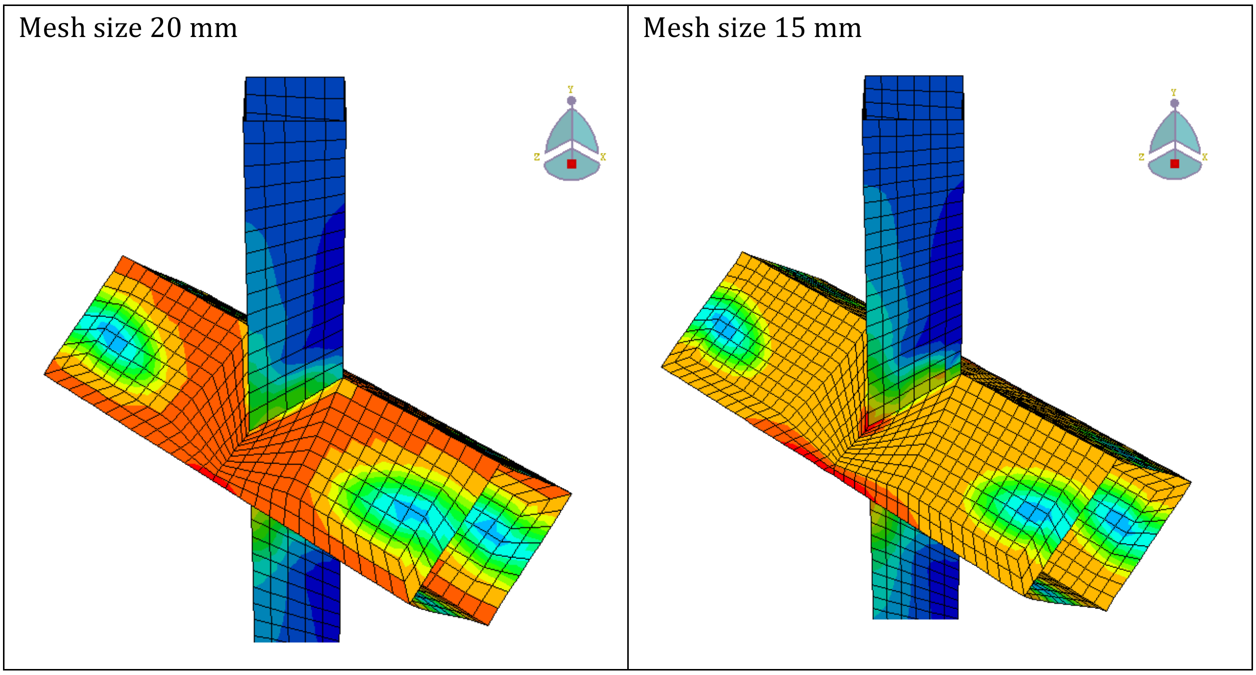

Figure 131 Graphical representation of mesh size 20 mm (left) and mesh size 15 mm (right)

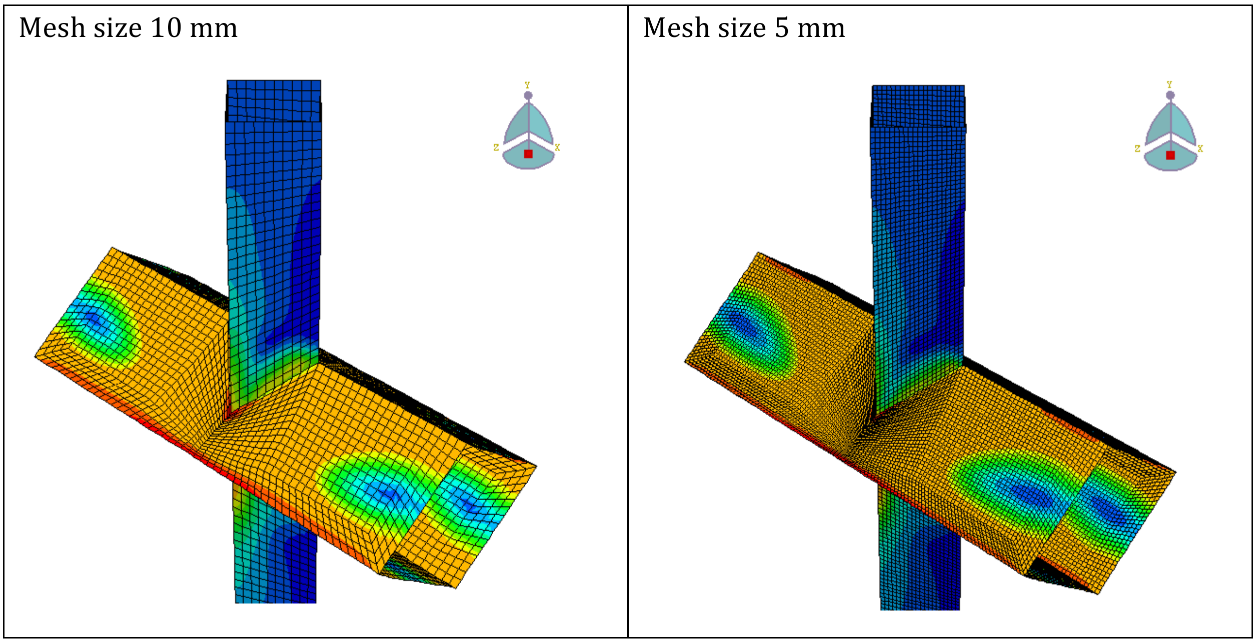

Figure 132 Graphical representation of mesh size 10 mm (left) and mesh size 5 mm (right)

Mesh size 3 mm	Mesh size 2 mm
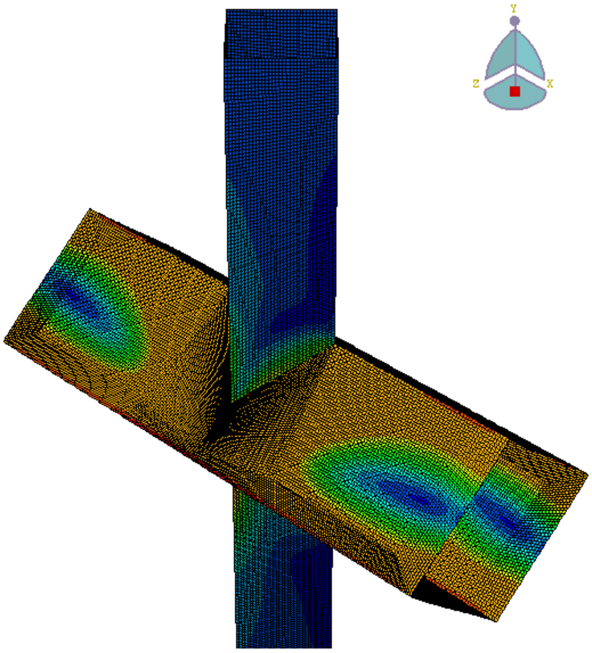	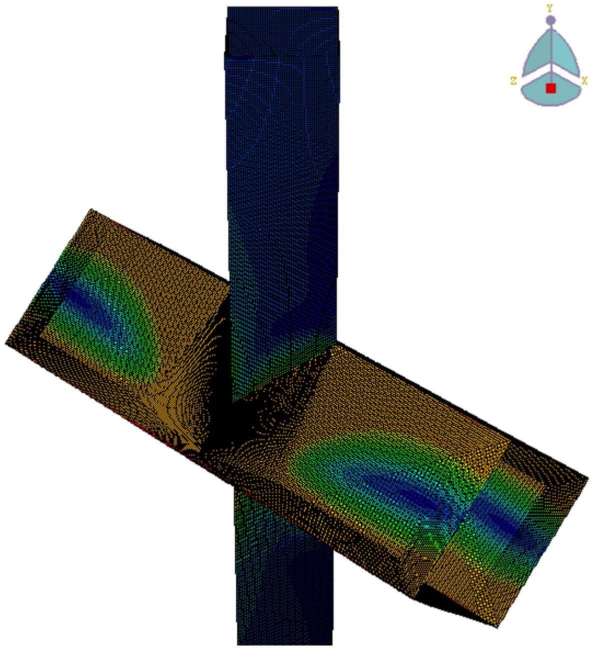

Figure 133 Graphical representation of mesh size 3 mm (left) and mesh size 2 mm (right)